Two-photon spectra of Rydberg states of alkaline-earth atoms (strontium and barium)

Thesis

UNRESTRICTED

Two-photon spectra of Rydberg states of alkaline-earth atoms (strontium and barium)

A thesis submitted for the Degree of

Doctor of Philosophy

The Open University, UK

GEORGE PHILIP

B.Sc. (Special); M. Sc; M.E. (El. Engg.)

External Supervisor **PROFESSOR JEAN-PATRICK CONNERADE**
The Blackett Laboratory,
Imperial College, London

Internal Supervisor **PROFESSOR DEREK RICHARDS**
The Open University
Milton Keynes, UK

Submission date: 7 May 2008
Date of award: 17 Nov. 2008

March 2008

Dedicated to
The Memory of:

My beloved father
VARKEY PHILIP PANICKASSERIL

My beloved mother
ANNAMMA PHILIP PANICKASSERIL

And My beloved sister
ACCAMMA PHILIP PANICKASSERIL

Declaration for Personal work

Except where stated otherwise, this thesis is the result of my own work and contains nothing which is the outcome of work done in collaboration. This thesis has not been submitted in whole or in part for the award of any degree or diploma at this or any other university.

George Philip

Kerala- India

March 31, 2008

Abstract

The even-parity spectra of strontium and barium are very complex due to strong perturbation by several doubly excited configurations and this also increases discrepancies between theory and experiment in accurate level assignment and energy level and atomic structure data, particularly for the spectra of highly excited atoms and their behaviour in external fields and collisional processes which are of fundamental importance in the emerging applications in physics of cold atoms, quantum computing, precision atomic clocks and in the crossed-field problem.

This thesis presents results from an experimental study to improve and extend the previously published observations in the two-photon spectra of the high-lying Rydberg states of SrI and BaI placed under a variety of test conditions such as external fields, collisions etc. Orthogonal excitation of a novel atomic jet in a purpose-built heat-pipe setup using a Xenon Chloride excimer laser pumped tunable narrow bandwidth dye laser and high sensitivity space-charge ionization in thermionic diode with complimentary optical detection was used for measurements.

Presented are the two-photon spectra covering the dye laser wavelength (air) range of 460 – 425 nm for strontium and 495 – 467 nm for barium by which the $J = 0,2$ even-parity Rydberg series and autoionizing resonances just above the ionization limits labeled as; $(4d^2+5p^2)\ ^1D_2$ in strontium and $5d5f\ ^1P_1$ in barium were observed.

Original new energy level values are presented with substantial extension to the data in the literature for even-parity Rydberg series:
Sr I: $5sns\ ^1S_0$ $(12 < n < 46)$, $5snd\ ^3D_2$ $(9 < n < 47)$ and $5snd\ ^1D_2$ $(9 < n < 82)$
Ba I: $6sns\ ^1S_0$ $(13 < n < 68)$, $6snd\ ^3D_2$ $(11 < n < 46)$ and $6snd\ ^1D_2$ $(11 < n < 88)$

New observation of certain anomalies including a Stark shift reversal effect and zero-field thermionic diode detection with remarkable sensitivity preserving all spectral features of Rydberg states is also presented. Controlled configuration mixing by exploiting electric field and collisions has allowed new observations for the two-photon forbidden odd-parity Rydberg series of SrI:
$5s^2\ ^1S_0 \rightarrow 5snp\ ^1P_1^o$ $(32 < n < 46)$ and $5s^2\ ^1S_0 \rightarrow 5snf\ ^1F_3^o$ $(29 < n < 44)$

Extensive study of collision involving Rydberg atoms with neutral rare gas atoms has allowed to obtain new data for shift and broadening rates for Sr I series: $5sns\ ^1S_0$ and $5snd\ ^{1,3}D_2$ in the perturbed region which clearly exhibit Ramsauer effect. Collisional evolution of a remarkably broad resonance, labeled as $4d^2\ ^1G_4$, also exhibiting Ramsauer effect, is presented besides new level data for strontium $4d^2\ ^3P_J$ states accessed by two distinct processes- direct two-photon excitation and single-photon sequential excitation.

Furthermore, the thesis presents the results of a novel experimental technique involving time-resolved gated pulsed field detection technique (GPT) employed for the first time to examine the time decay of Rydberg atoms yielding their effective lifetimes.

ACKNOWLEDGMENTS

Professor Jean- Patrick Connerade had been extremely generous, despite his heavy responsibilities in Imperial College, at Euro-science and many others, in consenting to find time to take the responsibility as my External Supervisor. I am deeply indebted to Professor Connerade for the constant inspiration besides the excellent guidance and supervision of my thesis research ever since he arranged the external registration at the Open University and motivated me to the Ph.D programme.

I was fortunate to have Professor Derek Richards as my Internal Supervisor at the Open University. I am extremely grateful to Professor Richards for giving me much encouragement and support in sustaining my registration and completing the Thesis. I would like to express my heartfelt gratitude to Professor Richards and Dr. Mick Bromilow for their sympathetic considerations and constantly encouraging me during the period of my illness. I am also deeply indebted to Professor Richards and Dr. Bromilow for their profound encouragement and support during my visit to the Open University for attending the thesis defense oral examination.

I was privileged to receive, at a time of great hardship, financial support which included expenses incurred on my journey and stay as the Open University guest in Milton Keynes and a few quarterly registration fee waiver by the hospitality of the Department of Mathematics & Computing. I am, indeed, extremely thankful to the Open University for the extremely valuable financial support.

It is a great pleasure for me to take this opportunity to express my most sincere thanks to Dr. Jonathan Underwood who was always willing to offer very valuable guidance and suggestions in my thesis research. Also, I wish to place on record my profound appreciation for Ms.Tracy Johns, Ms. Kathryn Reeves and several members of the Research School at the Open University for their great enthusiasm in giving me prompt administrative support as an external student.

It is a great pleasure to express my gratitude to Kuwait University for inviting me to join the new reconstruction of the laser laboratory in the Department of Physics. I wish to extend my most sincere thanks to Dr. Yacob Makdisi for all help and encouragement during my stay at Kuwait University. I am sincerely thankful to the Physics Department Machine Shop for technical assistance in constructing the experimental setup. I also wish to acknowledge many interesting discussions with Dr. E. Davis and Dr. Mustafa Marafie.

I owe much also to my wife Rachel and my sons Philip and Jacob who have always been very encouraging despite deprivation of time for them due to my much extended preoccupation with the thesis project. Special thanks are to be extended to Philip who assisted me with the preparation of several diagrams.

Preface

The Rydberg states of the alkaline-earth atoms had been under extensive investigation for the past several decades, both in theory and experiment, for the characterization of both bound and autoionizing series and doubly-excited states. Theoretical calculations of the energy levels of the alkaline-earth atoms had been successfully carried out by the well-known Multi-Channel Quantum Defect Theory (MQDT) and the eigen-channel R-Matrix methods first formulated during the early seventies and extensively developed in the nineties. However, the gap between theory and accurate experimental data still remains significant, despite the wealth of experimental data reported in the multi-photon processes of atoms and hence there exists considerable need for reliable experimental data, especially for the perturbed bound states of the alkaline-earth atoms in which the different regions of the principal quantum number with different quantum defects behave quite distinctly. The need for reliable experimental investigation is also important for the spectra of the autoionizing states which not only interact with each other, like the bound states, producing energy level perturbations, but also interact with the continuum states producing spectral features which are difficult to characterize theoretically.

Contemporary studies of spectra of Rydberg atoms in external fields have also revived the interest in the spectroscopy of alkaline-earth atoms, especially in crossed electric and magnetic fields, in the quest for the observation transitions from a state of quantum order to a semi-classical state of chaos. In this context observations of n- and ℓ-mixing in barium with distinct features of pure diamagnetic spectrum have already been reported. Besides the crossed-field problem, the spectroscopy of Rydberg states of these heavy alkaline –earth atoms is becoming increasingly

important because of its relevance in the applications in precision atomic clocks, experimental realization of low temperatures (below 1μK) by laser cooling in magneto-optical traps and in Bose-Einstein Condensation (BEC) setups. Electric field effect in Rydberg atom also is of great importance in future quantum computing.

Much of the experimental study involving the highly excited states of these atoms became feasible after the advent of efficient tunable lasers. Using laser excitation the outer most electron(s) of the alkaline-earth atoms can be raised to a specific excited state(s) because of the excellent wavelength match for photo-excitation and this also provides an excellent opportunity to probe the independent particle and many-body effects and correspondence principle limit of quantum mechanics. The spectra of the Rydberg atoms which have several exaggerated properties which scale with the principal quantum number (exceptionally large size, extreme sensitivity to external fields and environment, enhanced collision probabilities, large orbital lifetime, large dipole moment and polarizabilities etc.) also exhibit other properties- presence of Rydberg series converging to different ionization thresholds, autoionization states and electron-electron correlation effects etc. which make them extremely attractive for observing such effects. Two-photon absorption provides excellent opportunity for excitation to the even-parity states which cannot otherwise be possible from the ground state due to parity and selection rules. Both odd and even-parity states of strontium and barium can be accessible with remarkable resolution by selective excitation using present day tunable lasers in the visible.

I was motivated by the importance of improving and extending the spectral data existing in the literature for the even-parity Rydberg states of the alkaline-earth

atoms and I was delighted in developing some new experimental methods in two-photon spectroscopy of the highly excited atoms placed in external fields and collisions. I decided to select strontium and barium as the candidates for the experimental investigation principally because these atoms were never studied before in Kuwait University where I had made the measurements. The experimental schemes I had developed (novel and efficient techniques using entirely indigenous resources and in-house fabrication as substitutes for expensive and complex commercial experimental facilities) and the original new findings from the study of a complex experimental problem, some of which have been already published and some are under preparation for publication in peer-reviewed journals, are presented in this Ph. D. thesis.

This Ph. D thesis which presents the important results from a complex experimental investigation I had undertaken, involving two-photon spectroscopy of Rydberg states of strontium and barium, as already mentioned, is organized in to six chapters. Rydberg atoms with different ranges of principal quantum number n were generated by resonant transverse excitation of a novel atomic jet using narrow bandwidth tunable dye laser pumped by a xenon chloride excimer laser and detected by a modified field ionization technique. Optical detection was also used as complimentary to ionization detection.

Chapter1 (Introduction) briefly reviews the historical development of multi-photon processes. Chapters 3, 4 and 5 are given special introduction subsections summarizing the progress in the respective areas of study.

Chapter2 is devoted to a description of the instrumentation and the design and development of novel methods of measurement techniques which were

employed to obtain reliable data some of which are new extensions to the existing data in NIST while others are entirely new.

Chapter 3, with its various subsections, is devoted to present new results obtained from two-photon spectroscopy of the bound and autoionizing transitions in strontium and barium with attempts for their interpretation besides theoretical concepts involved.

Chapter 4 gives a survey of the Rydberg atom collisions with ground state neutral rare gas atoms. Results are presented for the broadening and shift rates of important region for the even-parity Rydberg transitions in Sr and Ba.

Chapter 5 attempts to present some of the effects observed by external electric fields which are essentially based on Stark effect and the change in energy level structure and mixing of states leading to forbidden transitions.

Finally, *Chapter 6* concludes the thesis by attempting to project some future experimental challenges motivated by the new observations in this thesis.

Below is a partial citation of articles I had published from the original results I had obtained from the study reported in the Thesis.

1. Appl. Phys. B 90,407 (2008)

2. Rev. Sc. Instrum.78,13101 (2007)

3. Optics Commun. 279, 141(2007)

4. Opt. Commun. 266, 253(2006)

5. J. Phys. B At. Mol. Opt. Phys. 34 (2001) 521

March 2008
The Open University, UK

George Philip-
Varkey Philip Panickasseril

CONTENTS

Chapter 3
Spectroscopy of Rydberg Atoms

Figure Captions

Chapter 1

Chapter 2

Chapter 3

Fig. 3.15 (b) Two-photon spectrum of Sr I in the wavelength range 443.6 nm $\rightarrow$ 476.8 nm recorded with detector bias set to zero. Singlet–triplet swap over around n = 16 can be seen clearly. (*Opt. Commun.* **279,** 141, 2007)

Fig. 3.15 (c) Two-photon spectrum of Sr I showing highly excited states for the laser two-photon wavelength range indicated. Strong single-photon resonances to the doubly excited states can be seen in the spectrum taken with 20 mbar Ar buffer and +4.8 volt bias for the thermionic detector.

Fig. 3.15 (d) Two-photon spectrum of Sr I showing highly excited states for the laser two-photon wavelength range indicated. Single-photon resonances to the doubly excited states are all quenched in the spectrum taken with 20 mbar Ar buffer and zero volt bias for the thermionic detector. The baseline shift near the series limit is an experimental artifact.

Fig. 3.16 (a) Two-photon spectrum of Sr I with 40 mbar He showing 5sns $^1S_0$ and the forbidden $^1P_1$ and $^1F_3$ series. Detection by +9 volt DC

Fig.3.16 (b) Two-photon spectrum of Sr I @ (40 mbar He + 60 mbar Ar) showing 5s(n+1)s $^1S_0$ members on the blue wing of 5snd $^1D_2$ members. Forbidden 5snp $^1P_1$ and 5snf $^1F_3$ series are also seen. Detection by +9 volt DC (*Opt. Commun.* **279,** 141, 2007)

Fig. 3.17 Relative signal strength for the two-photon transitions to 5sns $^1S_0$ Rydberg states at two compositions of the buffer gas

Fig. 3.18 Signal intensity variation with n for allowed $^3D_2$ (decay) and forbidden $^1P_1$ and $^1F_3$ (growth) transitions in Sr I.

Fig. 3.19 Quantum defect plots for Sr I. Fluctuations are seen around perturbing transitions

Fig. 3.20 Experimental quantum defects plotted against energy relative to the continuum threshold.

Fig.3.21, Energy Level diagram of Ba I for the energy range 34000 cm^{-1}- first threshold.

Fig.3.22 Two-photon spectrum of Ba I showing the J = 0,2 even-parity 6sns $^1S_0$ and 6snd $^{1,3}D_2$ Rydberg members

Fig. 3.23 Two-photon spectrum of Ba I showing the J = 0, 2 Rydberg series. Effect of collision on 5d7d $^1D_2$ is seen (He buffer)

Fig. 3.24 A well-resolved two-photon spectrum of Ba I showing the

Fig.3.38 (b) .Two-photon spectrum of Sr I showing the $(4d^2 + 5p^2)\ ^1D_2$ autoionizing resonance just above the first ionization threshold (10 mbar Ar buffer and 2 μJ dye laser energy/pulse, +7 volt detector bias). Note that the continuum above threshold which approaches zero remains nearly flat over a wide range and the relative strength of single-photon resonances improves with a different buffer gas composition.

Fig. 3.39 Two-photon spectrum of Ba I showing the ionization threshold and the autoionizing level labeled as 5d5f $^1P_1$. Single-photon resonances also are observed which are due to sequential excitation from the $6s6p\ ^1P_1$ intermediate level. (This is the same spectrum shown in Fig. 3.25 in Page 126 of the Thesis. Because of its relevance it is repeated here).

Fig. 3.40(a) Schematic of the experimental geometry for transverse excitation of an atomic jet

Fig. 3.40(b) Schematic of the Timing Sequence for GPT

Fig. 3.41 (a) Two-photon spectrum of Sr I taken with the GPT with +2.5 V pulse height, 0.5ms width

Fig. 41 (b) Two-photon spectrum of Sr I taken with a thermionic diode detector biased with a DC voltage

Fig.3.41(c) Two-photon spectrum of Sr I 5s*n*d $^1D_2$ Rydberg series with GPT showing $4d^2\ ^1G_4$ interloper

Fig. 3.42 (a) Growth of intensity ratio of adjacent Rydberg members as a function of gate delay time establishing GPT

Fig. 3.42 (b). Time evolution of Sr I, 5s14d $^{1,3}D_2$ Rydberg states probed using GPT

Fig. 3.43 (a) Time decay of Sr I 5s*n*s $^1S_0$ states probed by GPT. Continuous curves are the $\exp(-t/\tau_{eff})$ fit to the experimental data

Fig. 3.43 (b) Time decay of Sr I- 5s*n*d $^1D_2$ states probed by GPT. Continuous curves are the $\exp(-t/\tau_{eff})$ fit to the experimental data

Fig. 3.44 Power law fit for experimental data of lifetime of heavily perturbed 5s*n*s $^1S_0$ and 5s*n*d 3d $^3D_2$ Rydberg series of Sr I.

Fig. 3.45 Effect of buffer gas collisions on time evolution of Sr I Rydberg states

Chapter 4

Chapter 5

List of Tables

Table 3.8
Energy level values for the two-photon forbidden Sr I $5s^2\ ^1S_0 \rightarrow 5snf\ ^1F_3$ Rydberg series (*Opt. Commun.* **279**,141, 2007)

Table 3.9
Observed two-photon excitations to the bound $J = 0$, even-parity $6s^2\ ^1S_0 \rightarrow 6sns\ ^1S_0$ Rydberg series

Table3.10
THESIS *Extension of two-photon excitations to the bound $J = 0$, even-parity Ba I $6s^2\ ^1S_0 \rightarrow 6sns\ ^1S_0$ Rydberg series

Table 3.11
Two-photon excitations to the Ba I $6s^2\ ^1S_0 \rightarrow 6snd\ ^1D_2$ Rydberg series

Table 3.12
**THESIS Extension of the two-photon excitations to the Ba I $6s^2\ ^1S_0 \rightarrow 6snd\ ^1D_2$ Rydberg series

Table 3.13
Experimental effective lifetime τ_{eff} of the $5sns\ ^1S_0$ Rydberg series of Sr I from GPT

Table 3.14
Experimental effective lifetime τ_{eff} of the $5snd\ ^1D_2$ Rydberg series of Sr I from GPT

Table 3.15
Experimental effective lifetime τ_{eff} of the $5snd\ ^3D_2$ Rydberg series of Sr I from GPT

Table 3.16
Experimental lifetime τ_{eff} of the high-lying members of the $5snd\ ^1D_2$ Rydberg series of Sr I from GPT

Table 4. 1
Polarizability and Scattering length *
He, Ne, Ar and Xe

Table 4. 2 Pressure shift rates – Xe
Sr I $5sns\ ^1S_0$ ($15 < n < 20$)

Chapter 1

Introduction

1.1 Rydberg Atoms

Named after the Swedish scientist, Johannes Robert Rydberg (8th November 1854-28th December 1919) for his discovery of a formula in 1888 that has become a logo of atomic spectroscopy, the Rydberg atom is an excited atom with one or more electrons in excited state (s) with very high principal quantum number(s). These atoms have *n*-dependent extraordinary properties compared to atoms in the ground state or low lying states (Stebbings and Dunning 1983, Friedrich 1991, Gallagher 1994, Lebedev and Biegman 1998, Connerade 1998) which make them extremely attractive in the study of topics of fundamental importance in atomic physics. Classically, a Rydberg atom in many respects behaves like a highly excited hydrogen atom with the outer electron in a spatially extended orbit, far outside the atomic core consisting of the nucleus and all the inner electrons. Johannes Rydberg established a simple relationship between the spectrum of hydrogen and those of many-electron atoms and the Rydberg formula contains a term characteristic of the hydrogen atom in which the electron moves in the Coulomb field far away from the core. The Rydberg formula was devised to predict the wavelengths of photons emitted by electronic transitions in an atom. The energy spectrum of the hydrogen

atom is given by the Rydberg formula: $E_n = I - \frac{Z^2 R}{(n)^2}$ and for a many-electron atom the energy levels E_n are given by a modified Rydberg relation replacing the principal quantum number n by an effective principal quantum number $n^* = n - \mu$. The simplest case of the non-hydrogenic Rydberg atom is one with a single valence electron like in an alkali atom. Thus the energy E_{nl} of such an atom in the highly excited state with principal quantum number n can be written as,

$$E_{nl} = I - \frac{Z^2 R}{(n^*)^2} \qquad (1.1)$$

The 'quantum defect' μ accounts for the non-hydrogenic core of the many-electron atom. R is the Rydberg constant. I is the ionization threshold and Z is the effective nuclear charge. $Z = 1$ for a neutral atom. The quantum defect has a weak dependence on the principal quantum number but it is strongly dependent on the orbital quantum number ℓ. The Rydberg constant (recent value $R_\infty = 109737.31568549\ cm^{-1}$) whose precision has been improved continuously is expressed in terms of the fundamental physical quantities: electronic mass m_e and charge e, speed of light c and the Planck's constant h by the relation:

$$R_\infty = \frac{m_e e^4}{(4\pi\varepsilon_0)^2 2\hbar^2 c} \qquad (1.2)$$

$$R_\infty = 109737.31568549 cm^{-1} \qquad (1.3)$$

The infinity Rydberg constant in energy form is: $(hc \times R_\infty) = 13.6056923\ \text{eV}$.

The Rydberg constant for any atom of mass M can be written as:

$$R_M = \frac{R_\infty}{\left(1 + \frac{m_e}{M}\right)} \qquad (1.4)$$

Rydberg atoms of very high principal quantum number are observed in the interstellar space, especially for the characteristic microwave radiation at 2.4 GHz with a very long lifetime corresponding to the transition $n = 109 \rightarrow n = 108$ in hydrogen. In the laboratory, Rydberg atoms are produced by direct excitations and by dielectronic recombination processes forming autoionizing states which subsequently decay to bound Rydberg states. In laboratories the maximum value of the principal quantum number observed is around 500 where as in interstellar space it is beyond 1000 (Lebedev and Beigman 1998).

Early motivation for the study of Rydberg atoms came from the opportunities offered by these atoms with several exaggerated properties which scale as the principal quantum number n and other properties. The radius of the Rydberg atom scales as n^2 and the size scales as n^4. Therefore, the diamagnetic effect which scales as the area of the orbit can be easily studied using Rydberg atoms whereas these effects cannot be detected in ground state atoms. The effect of an applied electric field on a Rydberg atom, the Stark effect is of fundamental importance in the study of Rydberg atoms. The outer electron in a Rydberg atom is in a large orbit far from the ionic core and feels an effective Coulomb potential ($1/r$ potential somewhat similar to a hydrogen atom) due to the ionic core consisting of the nucleus and the inner filled electron shells. The outer electron is loosely bound to the nucleus and the influence of the external field becomes comparable or larger than that of the internal atomic field (which varies as n^{-4}) leading to ionization. Whereas the Coulomb field felt by the valence electron in a ground state atom is $\geq 10^9$ volt/cm, the corresponding field experienced by an electron excited to a Rydberg state with principal quantum number $n = 20$ is only 10^3 volt/cm which is easy to be achieved in the laboratory. This opens up a new class of experiments using high intensity lasers to study multi-

photon ionization of atoms and the highly nonlinear response of atoms in a laser field (Mansfray and Manus 1991). Significant deviation from the simple Coulomb potential arises because of multi-electron excitations in many-electron atoms with comparable orbital radii of the excited electrons and polarization of the ionic core by penetration of the excited electron orbit, thereby modifying the $1/r$ Coulomb potential with an anisotropic $1/(r^3)$ dipole term that causes an angular correlation between excited electrons. In external magnetic field Rydberg atoms allow the study of Landau quantization of the free or quasi-free electron. In combined electric and magnetic fields one observes interesting phenomena involving the existence of quasi bound states near the Stark saddle point of the potential surface by trapping of the outer electron at large radial distance from the core (Fauth *et al* 1987). Application of a unidirectional pulsed field to a Rydberg atom causes adiabatic evolution of the electron orbit in to a field-perturbed orbit and the threshold field for ionization becomes sensitive to the shape and size of the pulse besides the pulse duration (Jones *et al* 1993, Frey *et al* 1996, Tannian *et al* 1998).

Selective excitation of Rydberg atoms with low angular momentum (ℓ) states in to high angular momentum ($\ell \approx n$) states has been achieved by a well-known method (Richards 1984) involving adiabatically switching ON, rotating through 90^0 and suddenly switching OFF of an electric field. This method is also used with reversing the field (Yamoda *et al* 2005). Systematic dependence of the excitation energy E_n on principal quantum number n also provides an opportunity for scaled energy spectroscopy (Zhan *et al* 2001, Liu *et al* 2002).

1.2 Important Properties of Rydberg Atoms

The important properties of Rydberg atoms are summarized below:

1. Very large physical size with radius of the orbit scaling as $r_n \propto n^2$. Rydberg atoms are known with diameters reaching 0.01mm corresponding to 100,000 times the diameter of atoms in the ground state;
2. Very small ionization potential $I_n \propto 1/n^2$;
3. Very low orbital speed $v_n \propto 1/n$;
4. Very large radiative lifetime $T_n \propto n^3$ due to very large orbital period (decided by the Kepler frequency of the Rydberg electron): typical lifetime of a lower excited state is of the order of 10 ns; there are Rydberg atoms with lifetime exceeding 1 s;
5. Energy spacing between successive members decreases as n^{-3}: $\{E_{n+1} - E_n = 2R_y/n^3\}$
6. Extreme sensitivity to external electric and magnetic fields and perturbation;
7. Large polarizability which scales as n^7. Rydberg atoms may be strongly polarized by relatively small electric fields.

Typically, for a Rydberg atom with principal quantum number $n = 30$ (very common in laboratory experiments), values of the properties are:

Size (diameter) – 1000 Å

Binding energy ~ 0.01 eV; Lifetime ~ 30 μs.

Transition energy between adjacent levels $\Delta E \sim 0.001$ eV ~ 10 cm^{-1}

Due to its large size, the internal structure of the ionic core is of not much consequence and the dominant interaction is the Coulomb interaction between the ionic core and the nearly-free Rydberg electron as illustrated in figures 1.1 and 1.2.

Table 1.1 gives an overview of selected important properties of the Rydberg atoms.

Table 1.1

Characteristic physical properties of neutral (Z = 1) Rydberg atom (Lebedev and Biegman 1998)

Physical property	**Formula**	**Unit**	**Value for n = 10**	**Value for n = 100**	**Value for n = 1000**
Radius r_n	$a_0 n^2/Z$	metre	5.3×10^{-9}	5.3×10^{-7}	5.3×10^{-5}
Geometric -al area S_n	$\pi(a_0 n^2/Z)^2$	$(\text{metre})^2$	8.8×10^{-17}	8.8×10^{-13}	8.8×10^{-9}
Ionization Potential I_n	$R_y Z^2/n^2$	eV	13.6×10^{-2}	13.6×10^{-4}	13.6×10^{-6}
Orbital speed v_n	$Z\, v_0/n$	metre/s	2.18×10^5	2.18×10^4	2.18×10^3

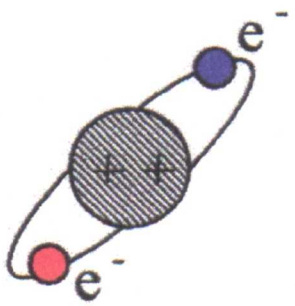

Fig.1.1 Classical picture of the ground state alkaline-earth atom with two ms^2 valence electrons and core

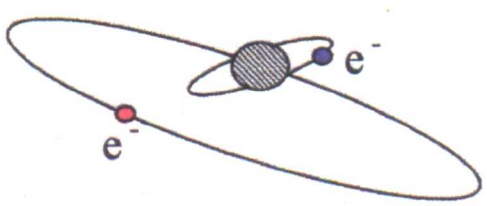

Fig.1.2 Classical illustration of the Rydberg state of the alkaline-earth atom

The spectra of Rydberg atoms with two or more valence electrons (for example, the alkaline-earth atoms with two electrons outside a closed shell) have several peculiar properties: the presence of Rydberg series converging to different ionization thresholds, autoionizing states and electron-electron correlation effects which make them extremely interesting to study such effects. The deviations from the hydrogenic potential for the Rydberg atom occur under conditions of double excitation when a second electron also is excited to a state with energy close to the state of the first electron, whereby, the orbits of the two excited electrons become correlated (radial correlation). Moreover, the polarization of the ionic core leads to a dipole potential which causes an angular correlation between the two valence electrons (Connerade 1998).

The spectroscopy of the high Rydberg states of the alkaline-earth atoms have undergone rapid advancement since the advent of highly efficient tunable lasers (Gallagher 1994, Connerade 1998) and, recently, there has been a revival of interest in the Rydberg states of heavy alkaline-earth atoms (strontium and barium) because of their emerging importance in the physics of cold atoms (Chu *et al* 1998, Robinson *et al* 2000), applications in precision atomic clocks and quantum computing (Ryabtsev *et al* 2005) and in the crossed-field problem (Elliot *et al* 1995, Connerade *et al* 1997, Rao *et al* 2001, Connerade *et al* 2005). Both the odd- and the even-parity high Rydberg states of these atoms became easily accessible with remarkable resolution by selective excitation from the ground state $ms^2\ ^1S_0$ (m = 5 and 6 for strontium and barium respectively) using tunable laser sources in the visible region. Two-photon excitation from the ground states of these atoms produces even-parity spectra whereas single-photon transitions produce odd-parity states.

Alkaline-earth atoms display singlet and triplet manifolds and therefore, inter-combination transitions can be observed in the spectra of these atoms. The first three excited states in strontium and barium, the ^3P_J manifold ($J = 0, 1, 2$) lie in the optical region for excitation (for example the excitation energies for strontium $^3P_{0,1,2}$ are 1.78 eV, 1.80 eV and 1.85 eV respectively). The transition to $^3P_1$ from the ground state $^1S_0$ is spin-forbidden and the transitions to the states $^3P_0$ and $^3P_2$ from the ground state $^1S_0$ are electric dipole forbidden. These ^3P_J manifolds are important for applications in the physics of cold atoms and in precision atomic clocks. The study of inelastic collisions of slow electrons with strontium atom (Smirnov 2001) is important for the development of electron pumped metal vapour lasers with transitions in the infrared region (λ = 6.45 μm, 3.0665 μm, 3.0111 μm). The exaggerated properties of Rydberg atoms, huge size, long lifetime and large dipole moments etc. make them ideal candidates also for experiments to study collective phenomena like evolution to ultra-cold plasma. Singlet-triplet inter-combination transitions in strontium offer an excellent route for quantum degenerate system for realization of the Bose-Einstein Condensation (BEC) (Isoya and Katori 2000) and cold collisions (Derevianko 2001).

For an atom, the classical limit for excitation leads to states with energy spacing between adjacent levels so small as to behave like continuum states of the classical particle. Rydberg atoms with one electron excited to an electronic state with very large principal quantum number in strong electrical and magnetic fields is an ideal experimental paradigm to study the quantum mechanical properties of a classically chaotic system (Connerade 1998).

The alkaline-earth atoms had played a very vital role for the development of atomic physics because of the experimental convenience these two-electron systems offer to obtain accurate theoretical and experimental data. Also these systems have the experimental convenience to simulate a three-body Coulomb system with highly correlated electron motion. The famous experiment by Madden and Codling in 1963 opened the way to initiate the studies looking for the experimental realization of electron-electron correlation using the doubly-excited states of alkaline-earth atoms.

In view of the various applications mentioned above, the study of the Rydberg states of the heavy alkaline-earth atoms still continues to be an interesting field of research in laser spectroscopy (Aymar *et al* 1996). Accurate level designation of many-electron atom is difficult due to configuration interaction and splitting of terms due to spin-orbit interactions. Reliable experimental data are required to extend the understanding of the structure of the many-electron atoms for which the well-known multi-channel quantum defect theory (MQDT) has difficulties in adequately describing the perturbations due to compact doubly excited configurations: mp^2 and $(m\text{-}1)d^2$ (m = 5 and 6 for strontium and barium respectively, as mentioned earlier). Strontium with the electronic structure $1s^2\ 2s^2\ 2p^6\ 3s^2\ 3p^6\ 3d^{10}\ 4s^2\ 4p^6\ 5s^2$ has the filled 3d-shell, unlike the lighter alkaline-earth atoms, magnesium and calcium. The valence state of strontium, $5s^2$, with two identical s-electrons has also a very complicated atomic structure. Like in strontium the atomic structure of barium is complicated by the presence of several doubly-excited perturbations: the J = 2 even-parity $6snd$ $^{1,3}D_2$ spectra of neutral barium are very complex with several perturbers such as $5d7d\ ^3D_2$, $5d7d\ ^1D_2$, $5d8s\ ^3D_2$, $5d8s\ ^1D_2$, $6p^2\ ^1D_2$. Hence adequate experimental data are required for accurate interpretation of the spectra of these heavy alkaline-earth atoms (Aymar 1984).

Reliable experimental data for the atomic structure of the two-electron atoms were lagging behind the theoretical calculations until the development of spectroscopy using monochromatic synchrotron radiation and multi-photon excitation using tunable lasers. Compared to synchrotron radiation which gives only $^1P_1$ excitations from the ground state, $ms^2\ ^1S_0$, multi-photon excitation using lasers offers possibilities of exciting levels with different angular momenta in a controlled manner. Selective multi-photon excitation starting from a known state such as the ground state through a specified path decided by the frequency and polarization of the exciting laser photon became a reality. Two-photon absorption (TPA) refers to the simultaneous absorption of two photons of equal frequencies to excite an atom or molecule to an excited state. Such an idea was first proposed by Goppert-Mayer in 1931 and it was experimentally verified first by Werner Kaiser *et al* in 1961, after the laser was invented, and later by Abella (1962) and Peticolas (1963). Whereas the probability of single-photon excitation grows linearly with photon density, the probability of two-photon excitation grows as the square of the intensity of the laser and, therefore, two-photon transitions become stronger with increasing exciting laser intensity. For single-photon transitions, the electric dipole transitions are the strongest and transitions are possible between terms of the same multiplicity and inter- combination transitions are forbidden.

The alkaline-earth atoms (Mg, Ca, Sr and Ba) had played the most important role in the understanding of the energy level structure of multi-electron atoms. This is because of the opportunity provided by these atoms with ionization potentials lying within the convenient energy range for two-photon excitation by efficient tunable dye lasers operating in the visible region of the spectrum.

The advancement in multi-photon absorption processes by tunable lasers also stimulated the development of efficient detection techniques for Rydberg atoms. At present there are several methods available with varying sensitivity and selectivity for either detection of photons or the detection of charge (electron or ions) with signals proportional to the number of Rydberg atoms. Among the optical detection methods, spectrally resolved fluorescence emission measurement with monochromator/optical multi-channel analyzer or photomultiplier is the widely used technique. However, fluorescence detection suffers from low efficiency and poor signal-to-noise ratios due to low quantum efficiency and weakness of fluorescence intensity, which scales as n^{-6} at high principal quantum numbers. Field ionization and space charge amplification techniques are the most efficient and most widely used techniques, which are also state selective. Mainly sensitive and reliable ionization detection methods were employed for the measurements reported in this thesis. Optical detection which provides complimentary information was also used.

References -Chapter 1 (alphabetical order)

1. Abella I.D
Phys. Rev. Lett. **9**, 453 (1962)

2 Aymar M
Phys. Rep. **110**, 163 (1984)

3 Aymar M., Greene C.H. and Luc-Koenig E
Rev. Mod. Phys. **68**, 1015 (1996)

4 Chu S., Cohen-Tannoudji C. and Phillips W.D
Rev. Mod. Phys.**70**, 685 (1998)

5 Connerade J._ P
"*Highly Excited Atoms*" (Cambridge University Press, Cambridge, 1998)

6 Connerade J._ P., Droungas G., Karapanagioti N.E. and Zhan M.S
J. Phys. B: At. Mol. Opt. Phys. **30**, 2047 (1997)

7 Connerade J._P., Hogan S. and Abdullah A.M
J. Phys. B: At. Mol. Opt. Phys. **38**, S141 (2005)

8 Derevianko A
Phys.Rev. Lett **87**, 023002 (2001)

9 Elliot R.J., Dounias G. and Connerade J._P
J. Phys. B: At. Mol. Opt. Phys. **28**, L537 (1995)

10 Fauth M., Walther H. and Werner E
Z. Phys. D. **7**, 293 (1987)

11 Frey M.T., Dunning F.B., Reinhold C.O. and Burgdofer J
Phys. Rev. A **53**, R2929 (1996)

12 Friedrich H
"*Theoretical Atomic Physics*" (Springer Verlag- Berlin, 1991)

13 Gallagher T.F
"*Rydberg Atoms*" (Cambridge University Press, Cambridge, 1994)

14 Goppert-Mayer M
Ann Phys. **9**, 273 (1931)

15 Ido T., Isova Y. and Katori H
Phys. Rev. A **61**, 061403 (2000)

16 Jones R.R., You D. and Bucksbaum P.H
Phys. Rev. Lett. **70**, 1236(1993)

17 Lebedev V.S and Biegman I..I
"*Physics of Highly Excited Atoms and Ions*"
(Springer –Verlag, Berlin 1991)

18 Liu X.J., Cao J.W., Zhan M.S. and Connerade J._P
J. Phys. B: At. Mol. Opt. Phys. **35**, 2069 (2002)

19 Madden R.P. and Codling K
Phys. Rev. Lett. **10**, 516 (1963)

20 Mainfray G. and Manus C
Rep. Prog. Phys. **54**, 1333 (1991)

21 Peticolas W.L., Goldsborough J.P. and Rieckhoff K.E
Phys. Rev. Lett. **10**, 43 (1963)

22 Rao J., Delande D. and Taylor K.T
J. Phys. B: At. Mol. Opt. Phys. **34**, L391 (2001)

23 Richards D
J. Phys. B: At. Mol. Opt. Phys. **17**, 1221 (1984)

24 Ryabtsev I.I., Tretyakov D.B. and Beterov I.I
J. Phys. B: At. Mol. Opt. Phys. **38**, S421 (2005)

25 Smirnov Y.M
Doklady Physics **46**, 232 (2001)

26 Stebbings R.F and Dunning F.B
"(Eds.) *Rydberg States of Atoms and Molecules*"
(Cambridge University Press, Cambridge, 1983)

27 Tannian B.E., Popple R.A., Dunning F.B., Yoshida S., Reinhold C.O. and Burgdofer J
J. Phys. B: At. Mol. Opt. Phys. **31**, L 455 (1998)

28 Werner Kaiser W. and Garret C.G.B
Phys. Rev. Lett. 7, 229 (1961)

29 Yamada S., Funahashi H., Shibata M., Kominato K., KishimotoY., Tada M., Haseyama T., Ogawa I. and Matsuki S
Phys. Rev. A **72**, 033414(2005)

30 Zhan M.S., Liu J., Cao J.W. and Connerade J_P
J. Phys. B: At. Mol. Opt. Phys. **34**, 1175 (2001)

Chapter 2

Experimental Instrumentation and Techniques

2.1 Introduction

There are various methods to prepare Rydberg atoms either from the atomic bound state by optical excitation or electron impact or from the positive continuum state by electron–ion recombination like in the interstellar medium. For alkaline-earth atoms, optical excitation which has a high degree of energy and polarization selectivity is the most versatile method to prepare Rydberg atoms. Starting from an atomic ground state the atom is excited to a Rydberg state with well-defined principal quantum numbers n, ℓ and magnetic quantum number m decided by the parity and spectroscopic selection rules using one or more photons within the spectral coverage of efficient tunable laser sources, mostly in the visible or ultraviolet region. Higher angular momentum states can be excited by angular momentum mixing induced by external perturbations such as collisions and electric fields. Metastable atoms also can be used as the starting point for laser excitation.

In this study Rydberg atoms of strontium and barium with high principal quantum numbers were generated by resonant two-photon excitation in an atomic jet using a narrow bandwidth tunable dye laser pumped by a xenon chloride excimer laser system at the Laser Laboratory in the Physics Department of Kuwait University, Kuwait. Photos 1-5 show the lasers and other instrumentation used in the study reported in this thesis.

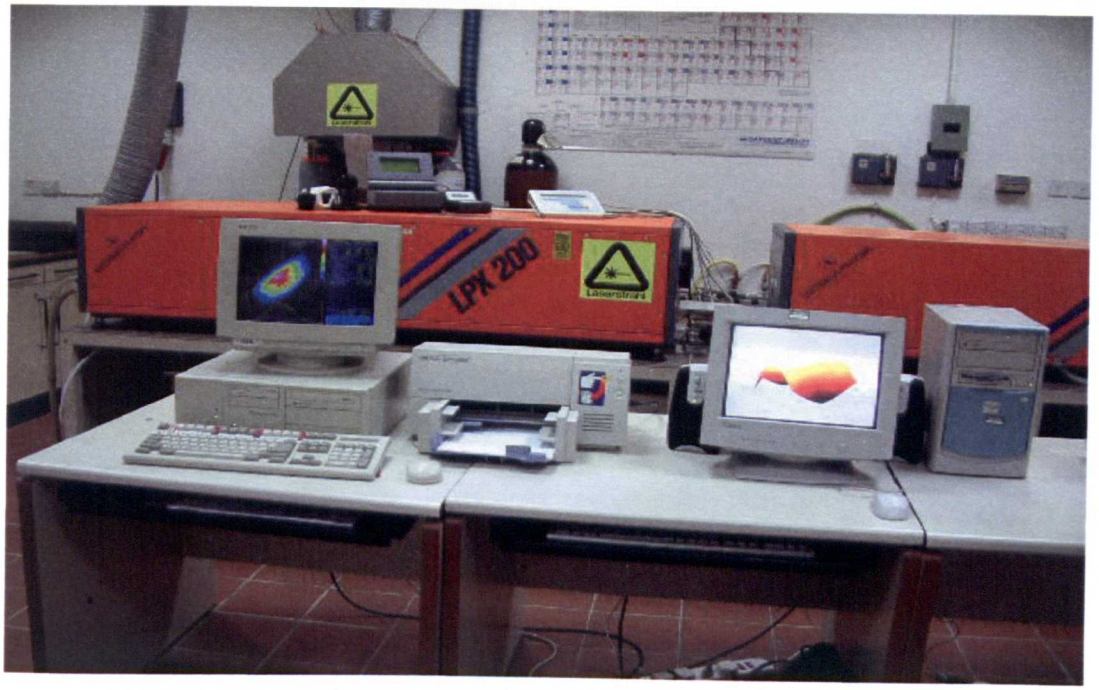

Photo 2.1 Experimental setup with LPX 210i excimer laser and LPD 3002 dye laser with a personal computer used for data acquisition

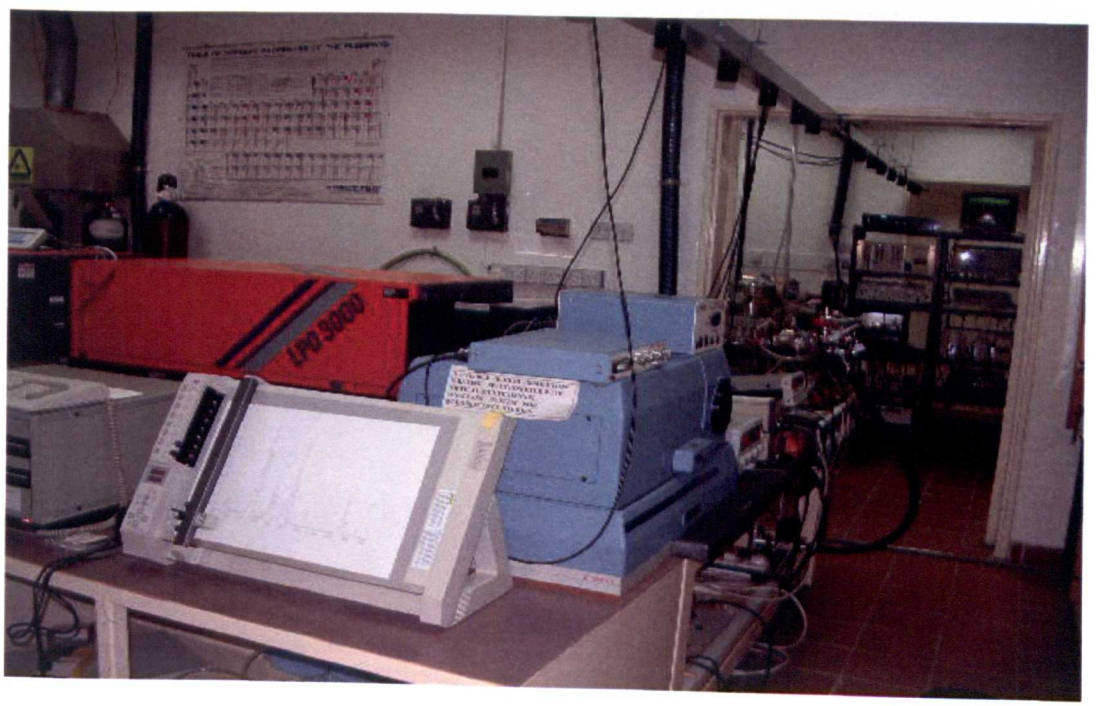

Photo 2.2 LPD 3002 dye laser with optical detection setup using OMAIII & Monochromator

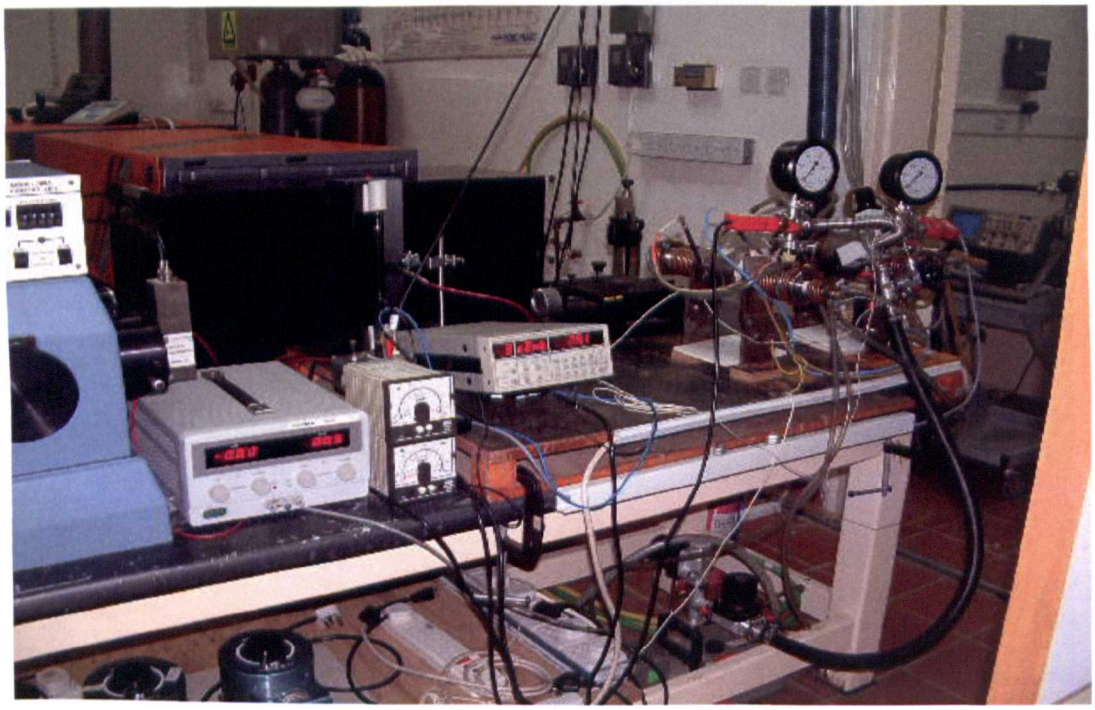

Photo 2.3 Multi-photon excitation site with heat-pipes and detection setup

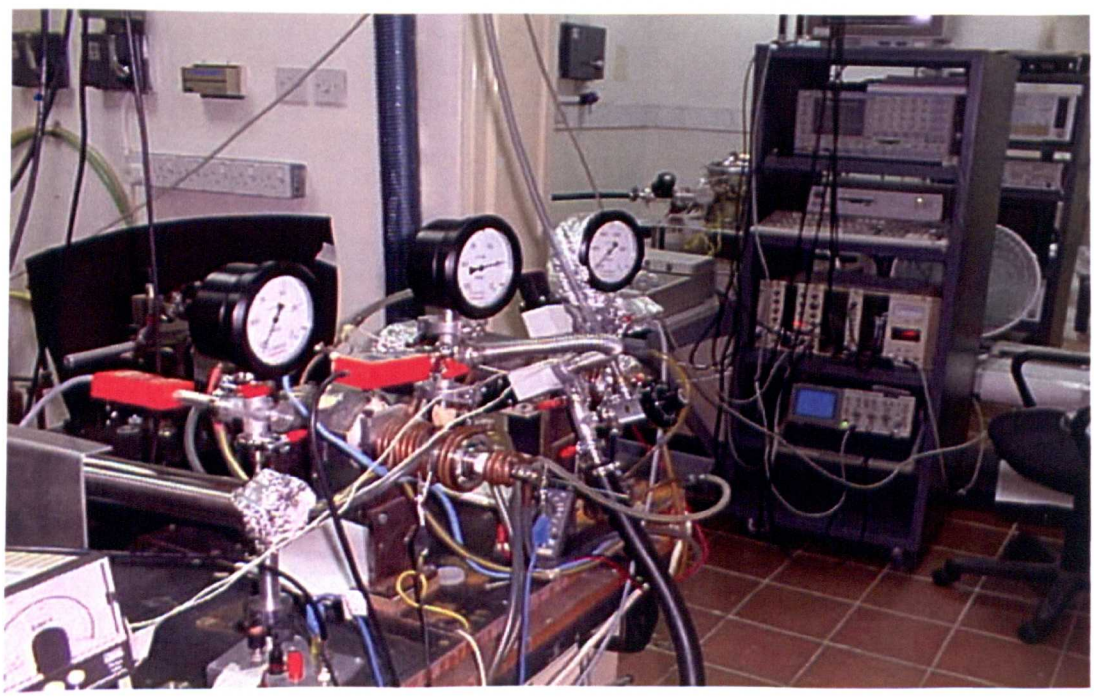

Photo 2.4 Heat-pipe assembly with ionization detection setup for different atomic samples

Photo 2.5 Optical detection using interchangeable OMA III / photomultiplier setup with fiber-optic link for fluorescence emission measurements

INSTRUMENTATION USED IN EXPERIMENTS REPORTED IN THE THESIS RESERCH

1. LAMBDA PHYSIK LPX 210i , Xe Cl. Excimer Laser
2. LAMBDA PHYSIK LPD 3002 CES Dye Laser
3. EG&G –PARC OMA III Optical Multi-channel Analyzer system
4. Mc PHERSON high resolution Scanning Monochromator
5. Mc PHERSON Photometer System with photomultiplier
6. GOULD INSTRUMENTS Digital Storage Oscilloscope
7. SRS Boxcar Averager and Gated Integrator
8. Coherent Laser Power Meter
9. Fast Photodiodes (Melles Griot)
10. Precision Laser Beam Splitters and Polarization Optics (Melles Griot)
11. Edwards vacuum stations with vacuum gauges and pressure gauges
12. Personal Computers and Plotters/ Printer
13. 16-channel Thermo-Couple Temperature Controller / Indicators
14. Regulated Power Supplies
15. Wavelength calibration Hollow Cathode Lamps
16. Digital Delay and Pulse Generator- Stanford Research Systems

A schematic of the setup for two-photon spectroscopy is shown in Fig. 2.1

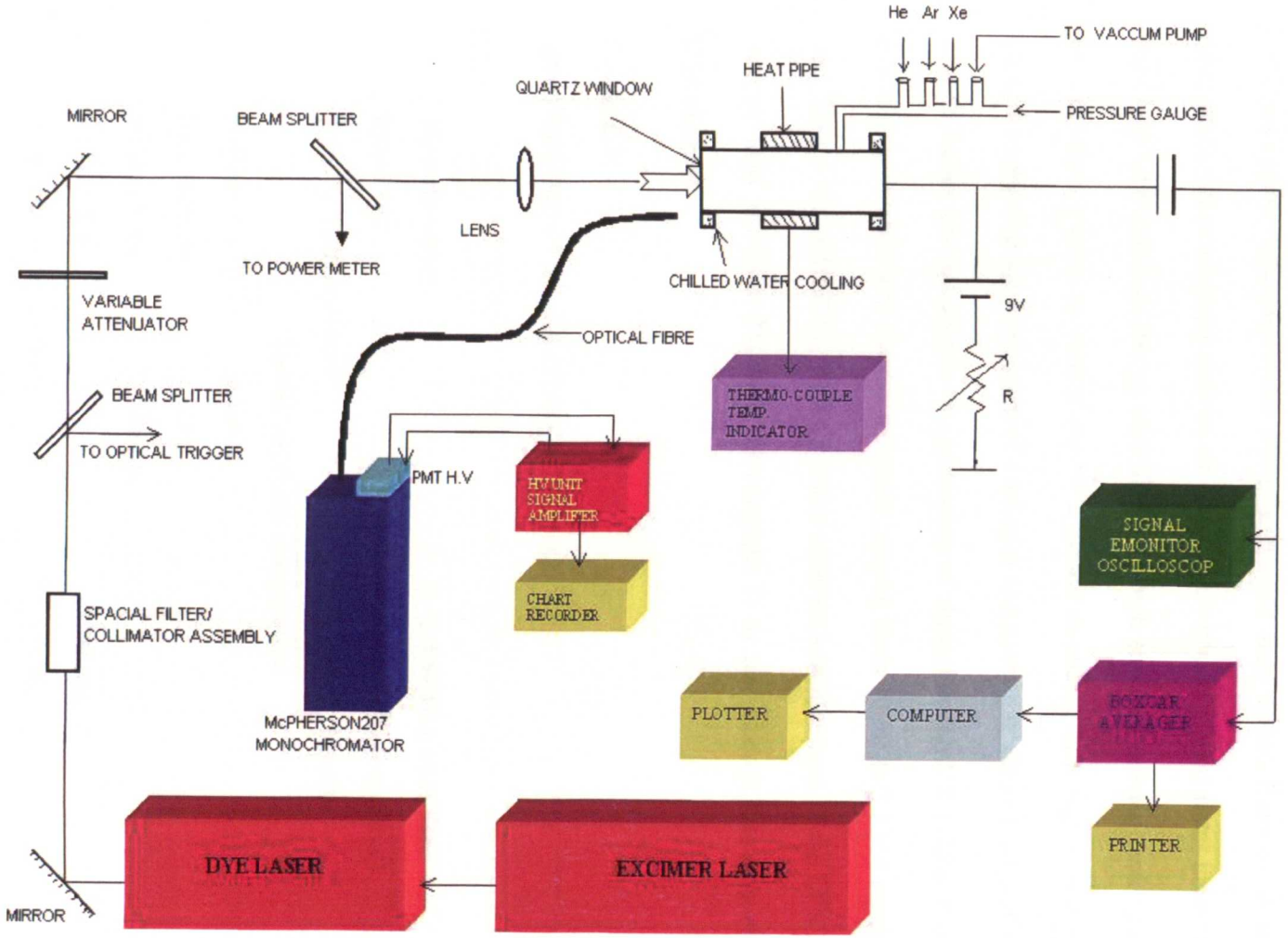

Fig.2.1. Schematic of the experimental setup for two-photon spectroscopy

2.2 The Laser System

2.2.1 Excimer Laser

The excimer lasers (the most important of which are the rare-gas-halides-ArF, KrF, XeCl and XeF), that produce intense ultraviolet light on distinct lines in the 193 nm -351 nm region take their name from the excited state dimers from which lasing takes place. Since excimers have no or only weakly bound ground states these lasers have high gain and high energy capabilities. In high energy industrial laser systems the excitation process is carried out by a pulsed discharge in a high pressure gas mixture containing small amounts of a halogen and a rare gas, diluted in helium and or neon buffer gas resulting in the generation of short duration UV pulses of a few tens of nanoseconds with energy per pulse ranging from 10 mJ to 2 J and repetition rates from 1 Hz to 1000 Hz. Table 2.1 lists relevant specifications of the LPX 210i excimer laser used for this study (Photograph.1) as per product literature of the Manufacturer.

Table 2.1

Specifications of the Xe Cl excimer laser

Manufacturer		**LAMBDA PHYSIK**
Model No.		**LPX 210** i (Industrial)
Type of laser (medium)		**Xenon Chloride**
Lasing medium composition		
Halogen (HCl)-	80 mbar	
Rare (Xenon) -	60 mbar	
Buffer (Neon) -	2760 mbar	
Wavelength		**308** nm
Pulse Energy (maximum)		450 mJ
Repetition Rate (maximum)		100 Hz
Pulse Duration (nominal)		17 ns

The output energy per pulse with the above composition of the excimer lasing medium for different voltages applied to the laser head is shown in Fig. 2.2.

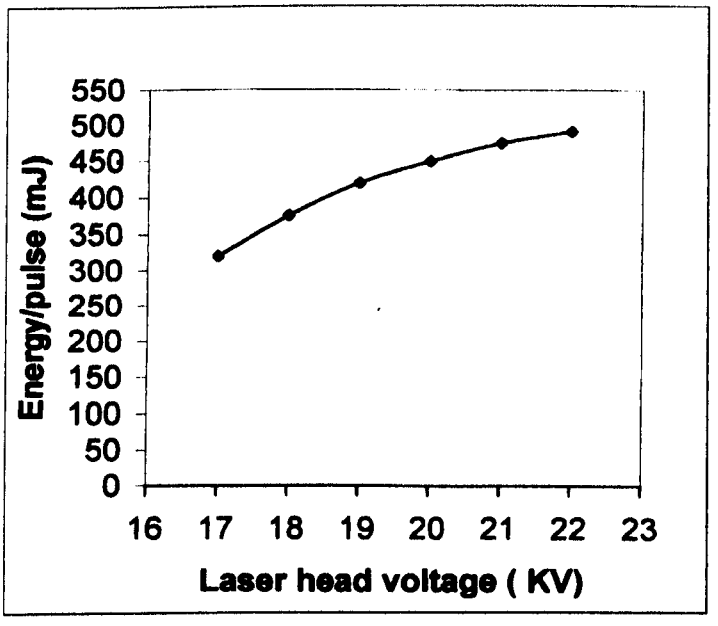

Fig.2.2. LPX 210i Excimer Laser energy output

2.2.2 Dye Laser

Since their discovery in 1966, powerful tunable dye lasers have become the workhorses of modern spectroscopy and these lasers also stimulated the development of sensitive detection techniques in multi-photon spectroscopy. With the breakthrough in excimer laser technology, the early dye lasers in which the pumping sources were flash lamps, ruby laser, Nd:glass lasers or nitrogen lasers were replaced with the recent generation excimer pumped high power dye lasers which offer several advantages such as broad fundamental tuning range (320 nm-970 nm), high repetition rate (250 Hz or more), high pulse energy (up to 100 mJ) and the remarkable ease with which the laser can be operated. Since the 308 nm line emitted by a XeCl excimer laser can efficiently pump all important dyes emitting in

the 330 nm - 970 nm region, schemes involving expensive and complex wavelength tuning by frequency doubling and frequency tripling can be dispensed with.

In general, a pulsed dye laser system consists of an oscillator for wavelength selection and an amplifier system consisting of one or more stages for beam power enhancement. Since the oscillator determines the quality of the beam it is the most important and sensitive part of any dye laser. The oscillator essentially has a grating for wavelength tuning and a beam expanding prism optics and a flowing dye cell which is the lasing medium and an output coupler.

The LAMBDA PHYSIK FL3002 dye laser (Photograph 2) used for the two-photon spectroscopy reported herein is a high performance (superior beam quality and high efficiency) dye laser with two-stage amplification of the oscillator output beam and is pumped using the Xe-Cl excimer laser described previously. Conventional dye lasers suffer from amplified spontaneous emission (ASE) centered on the maximum of the tuning range originating from the oscillator. In the LAMBDA PHYSIK LPD3002 dye laser, ASE is suppressed substantially using a special output coupling scheme and a patented ("LAMBDAPURE") filtering process. It has a Littrow-scheme oscillator with a single grating for the entire spectral coverage (320 nm - 970 nm). The wavelength calibration and selection is achieved by a hand–held minicontroller via a local area network (LAN) link.

The LPD3002 CES is the narrow bandwidth version of the LPD3002 dye laser and incorporates an intracavity etalon to reduce the bandwidth to 0.04 cm^{-1} from 0.18 cm^{-1}. Angle tuning of the grating is done by a stepper motor unit and the synchronous tilting of the grating and the etalon is done with the aid of the stepper

motor control microprocessor. Etalon pressure tuning up to 10 Å range using N_2 gas and frequency extension to the UV region (217 nm –348 nm) by frequency doubling can also be achieved in LPD FL3002 whose specifications are given in Table 2.2.

Table 2.2

Specifications of LAMBDA PHYSIK FL3002 Dye Laser

Oscillator	Littrow-type with 600 grooves / mm grating ASE suppression and prism beam expander
Wavelength Tuning Range:	
With XeCl pump	**332 nm- 970 nm** extendable to: 217 nm - 348 nm by Frequency doubling
Bandwidth	**0.018** cm^{-1}, reduced to 0.04 cm^{-1}(with etalon)
Dye laser efficiency Xe-Cl- Pumping	14% for Rhodamine 6G dye @ 581nm
Pulse Duration	≈ **14** ns
Beam Divergence	≈ 0.5 mrad

The bound Rydberg, autoionizing Rydberg and other excited states in neutral strontium and barium atoms are accessed by two-photon excitations using the high performance laser dyes supplied by Lambda Physik GmbH listed in Table 2.3.

Table 2.3

Wavelength tuning range of laser dyes used for two-photon spectroscopy of SrI and Ba I

Lambdachrome Laser Dye	**Solvent**	**Concentration (10^{-3} Mole)**	**Useful Tuning Range (nm)**
Rhodamine 6G	Methanol	1.5	570—596
Coumarine 102	Methanol	5.0	485—555
Coumarine 120	Methanol	7.0	422—467

The typical performance characteristics of Lambdachrome LC4400 laser dye used in this study is shown in Fig. 2.3.

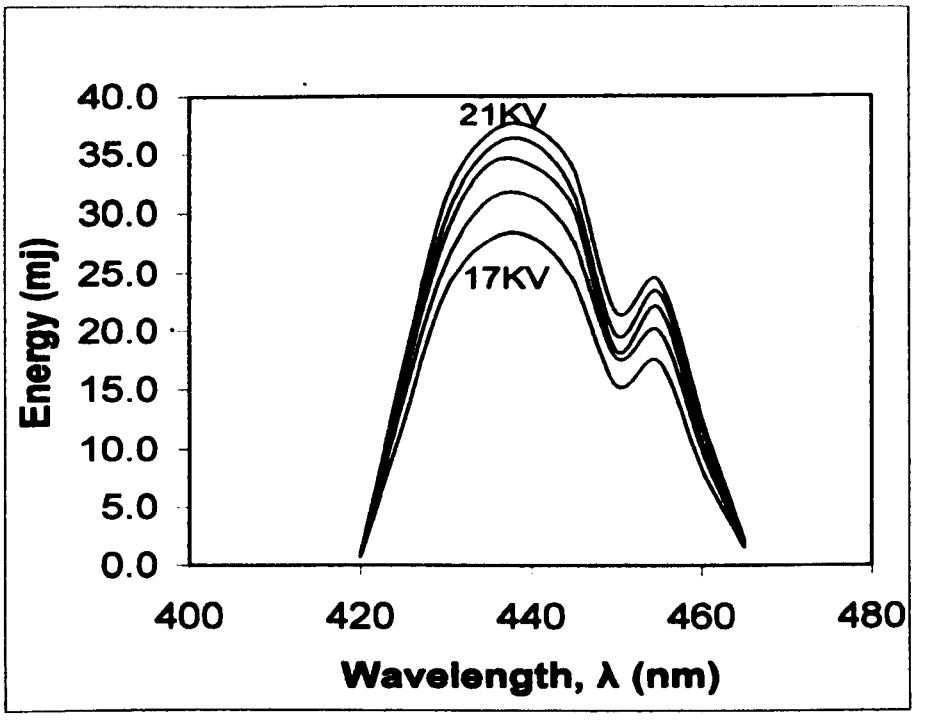

Fig. 2.3 Dye laser output curves (for different excimer laser input voltages) for Coumarine 120 (LC4400) dye used in two-photon spectroscopy of Sr I

Using neutral density filters and non-polarizing beam splitters the dye laser beam was attenuated to deliver 1 μJ -15 μJ per pulse. Wavelength calibration was carried out using hollow cathode lamp (HCL) calibration sources. Photograph 2.6 shows a barium hollow cathode lamp output detected using Coherent Beamview Analyzer.

The dye laser beam bandwidth is determined from fringe measurements with a monitor etalon and telescope using the arrangement shown in Fig. 2.4. Photo 2.7 shows the fringes obtained for laser dyes using the monitor etalon with a free spectral range (**FSR**) of 0.67 cm^{-1}. The schematic of the bandwidth calculation is indicated in figure 2.5.

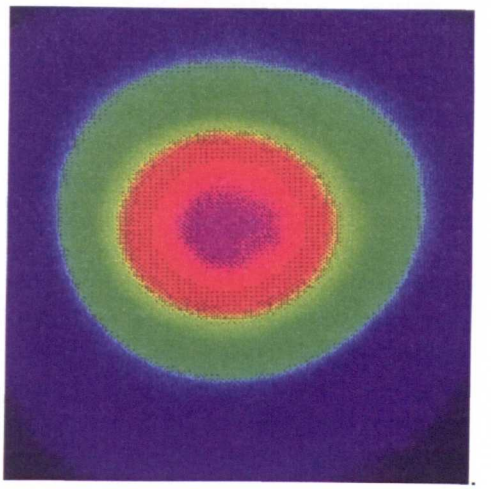

Photo 2.6 Barium Hollow cathode lamp glow recorded using Coherent beam-view analyzer

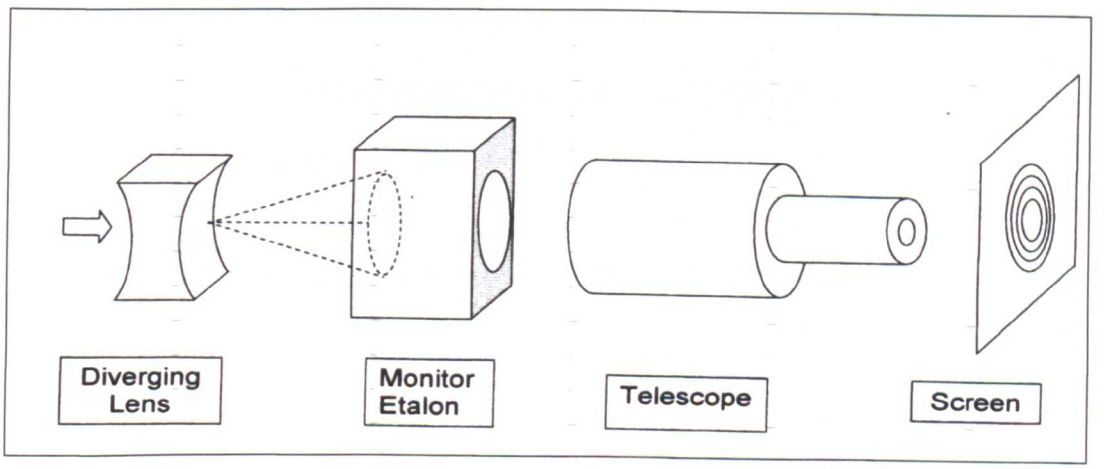

Fig. 2.4 Schematic of the experimental setup for dye laser beam bandwidth measurement.

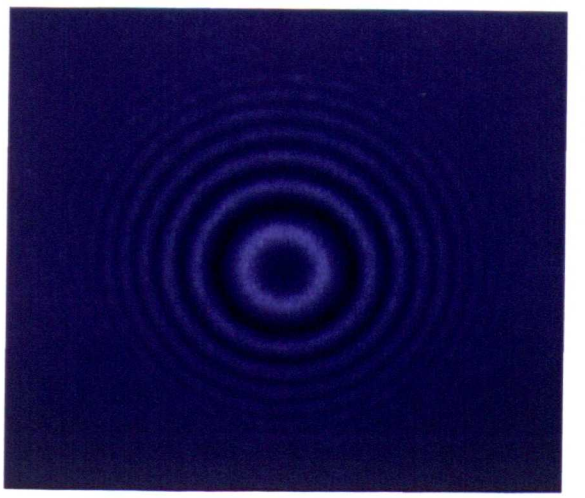

Photo 2.7 Blue Fringes

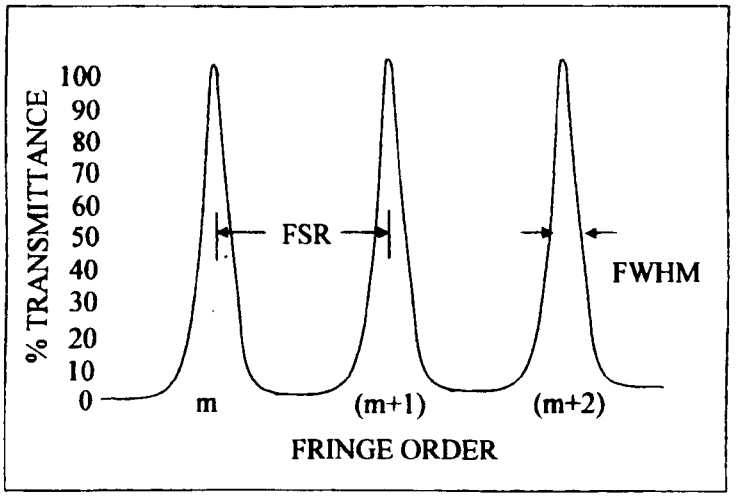

Fig.2.5. Schematic of bandwidth calculation from fringes

Bandwidth β is calculated using the formula:

β = FSR x (Width of fringe /Distance between fringes)

FSR – free spectral range

Finesse = FSR/ FWHM

Measured average value of the bandwidth of FL3002 is 0.17 cm^{-1}.

2.3 Heat-pipe and disposable cartridge for high density atomic jet for orthogonal excitation by laser

For measurements in atomic spectroscopy involving absorption of a laser beam by the atomic species, a homogeneous temperature and number density distribution with sufficient vapour pressure remaining steady over several hours is required. Due to its low cost and ease of operation, for the past several years, spectroscopic studies in alkali and alkaline-earth metals have been often carried out in heat-pipe setups (Vidal and Cooper 1969) in which the atom number density can be varied by varying the temperature of the hot zone of the heat-pipe.

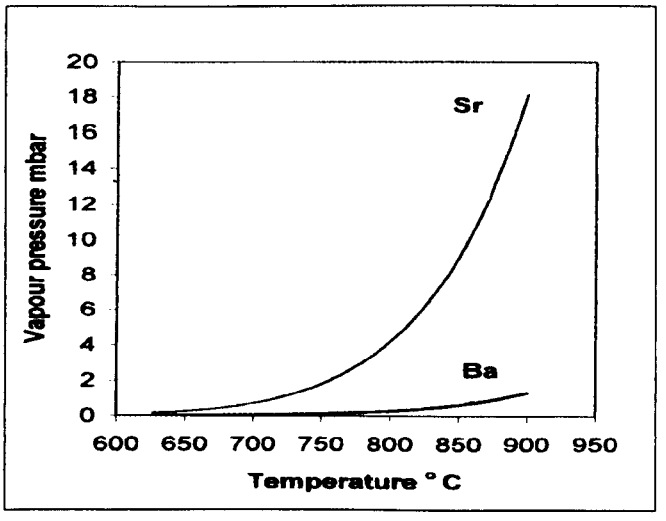

Fig. 2.6. Vapour pressure curves for strontium and barium

Figure 2.6 shows the vapour pressure curves for strontium and barium plotted using the data from CRC Handbook (Alcock *et al* 1984). These data give vapour pressure values to an accuracy of ± 5% below the melting point. These data are useful to fix the operating temperature of the heat-pipe.

Vapour pressure p is calculated using the relation:

$$\log p(atm) = A + BT^{-1} + C \log T \qquad (2.1)$$

T is the temperature in K

Element	A	B	C	Melting Point ^{0}C
Strontium	9.226	-8572	-1.1926	769
Barium	12.405	-9690	-2.2890	729

The conventional heat-pipes suffer from several problems which drastically affect their performance. By using an inert-gas buffer like helium or argon the degradation of the optical window transmittance resulting from condensation of the metal vapour can be avoided to some extent. But this can last only for a limited time and,

gradually, the windows get coated with the metal vapour, thereby decreasing the window transmittance abruptly. Also, there can be fluctuations in atom density in the laser-atom interaction region due to large thermal gradients by convection effects. Heat should be supplied to the element in such a way that large thermal gradients are avoided. To avoid erratic evaporation and splashing of the material by rapid expansion of the gas trapped inside the material it should be enclosed in a constant temperature capsule. Therefore, long duration stable operation of a conventional heat-pipe with a homogeneous temperature and density distribution, that is essential for reliable measurements, is extremely difficult. Furthermore, there may be large scale amplitude fluctuations in the ionization signals due to vibration of the probes used for electron or ion collection. The method usually used to remove electrode vibration is clamping it with a ceramic support in addition to the support at the rear end window of the heat-pipe. However, this second support introduces additional inconvenience and problems due to electrical short circuiting resulting from conducting tracks on the ceramic support. This limits the detection sensitivity, especially for measurements for highly excited states. As an alternative, an atomic beam set up offers several advantages over heat-pipes. However, this is highly expensive and poses considerable experimental difficulties for laboratories which are operating with low budget and manpower constraints.

In consideration of the several problems with the conventional heat-pipes, a simple, inexpensive and highly efficient atomic beam setup has been constructed inside a heat-pipe setup combining the advantages of both heat-pipes and atomic beam geometry. A variety of spectroscopic measurements were carried out with

remarkable simplicity using the modified heat-pipe setup incorporating highly efficient ionization detection with a completely indigenous and inexpensive design.

2.3.1 Heat-pipe Design

Out of the three designs made, linear and crossed heat-pipes with vertical and horizontal atomic jet geometry, a linear heat-pipe with a vertical atomic jet was used for the two-photon spectroscopy discussed in this thesis. A crossed heat-pipe has four arms welded at right angles to each other and four optical end-windows for laser entry and detection setup. Fluorescence can be viewed transverse to the incident beam in a crossed heat-pipe.

A linear heat-pipe used in this study is shown in Photo 2.8. It consists of a 31 cm long stainless steel pipe with 38 mm internal diameter and 62 mm outside diameter machined out of oxygen-free high quality stainless steel rod for suitable demountable end-window couplings, both straight and Brewster quartz optic windows with vacuum seal. A large wall thickness (12 mm) helps convenient mounting, without welded joints, for removable end-couplings with high temperature O-ring vacuum seal for 50 mm quartz window for laser beam entry and for electrical feed-through. Also it provides high heat capacity for stable operation. A single 8 mm diameter port for vacuum and buffer gas inlet is provided with a stainless steel vacuum connection (Edwards NW22) at the water cooled end of the heat-pipe.

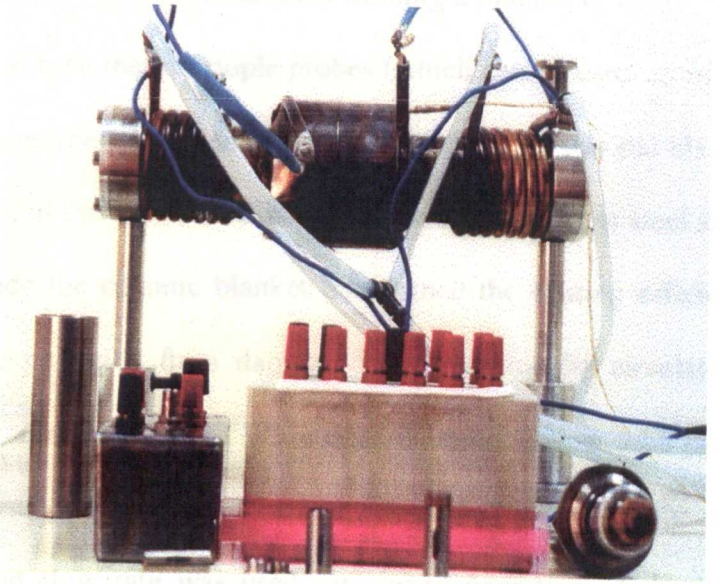

Photo 2.8.Linear heat-pipe with tubular heating rod and sample cartridges. Detector biasing circuit and electrical feed-through can also be seen in the photo

The central 10 cm long region is the hot zone of the heat-pipe which could be maintained at a desired temperature (750 ^{0}C - 950 ^{0}C required for strontium and barium) by resistive heating using non-inductive winding of 80% Nickel + 20% Chromium resistance heating wire (Omega NI80-040-200) which can be used up to 1150 ^{0}C with single-hole ceramic beads (Omega) forming an insulating sleeve up to 1600 ^{0}C and connected to a homemade DC power supply. Typically 41 turns were wound with 1540 ceramic beads on the heat-pipe and the measured resistance of the wire was 9.2 Ω. Alternatively, a 10.9 mm flexible heater (Omega tubular heater) with incoloy sheath which can withstand temperature up to 900 ^{0}C wound tightly on the heat-pipe and fastened with stainless steel clamps also was used in experiments which required only lower temperatures. The electrical insulation between the stainless steel heat-pipe wall and the heating wire or rod is kept above 17 MΩ to avoid any possible interference in the signal detection. The entire hot zone was plastered uniformly with a layer of high temperature embedding and insulating air-

set ceramic powder (Omega Bond-400) forming a blanket of about 5 mm thickness. Three Omega K type thermocouple probes (which can be used up to 1250 ^{0}C) were embedded (one at the center and two on each end) in the thermal blanket to monitor the temperature of the hot zone. Finally a 1mm thick stainless steel sheet jacket was provided outside the ceramic blanket to enhance the heating efficiency. The end-windows were protected from damage due to heating by circulating cold water through seven complete turns of ¼" internal diameter copper tube fixed to the heat-pipe wall at each end by silver brazing. A chilled water supply with adjustable temperature and flow rate was used for steady operation of the heat-pipe. The typical flow rate for water was 18 litres per minute at 10 ^{0}C.

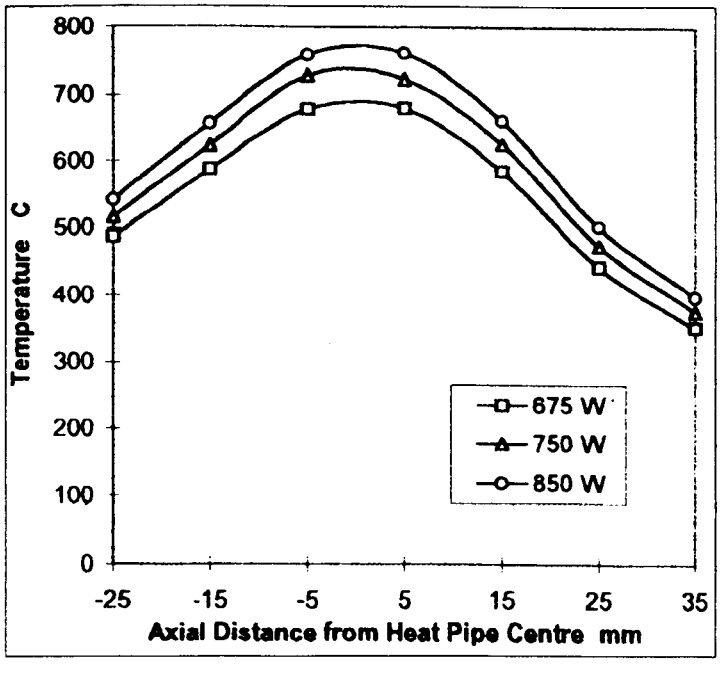

Fig. 2.7 (a) Axial temperature profile of the heat-pipe

A two dimensional temperature probe assembly consisting of 7 horizontal and 4 vertical thermocouples was used to determine the axial and radial temperature distribution inside the heat-pipe. These thermocouples are fixed to an 8 cm long, 10 mm diameter stainless steel rod with a 20 mm long, 5 mm X 2 mm rectangular arm

fixed at 90° at the center of the rod which can be inserted in to the hot zone of the heat-pipe. The electrical connection can be provided through drilled holes in the vacuum end-windows or through vacuum feed-throughs. Figures 2.7(a-b) show both axial and radial temperature profiles for typical operating conditions of a linear heat-pipe used in the present study. Figure 2.8 shows the linearity of resistive heating of the heat-pipe for applied voltage.

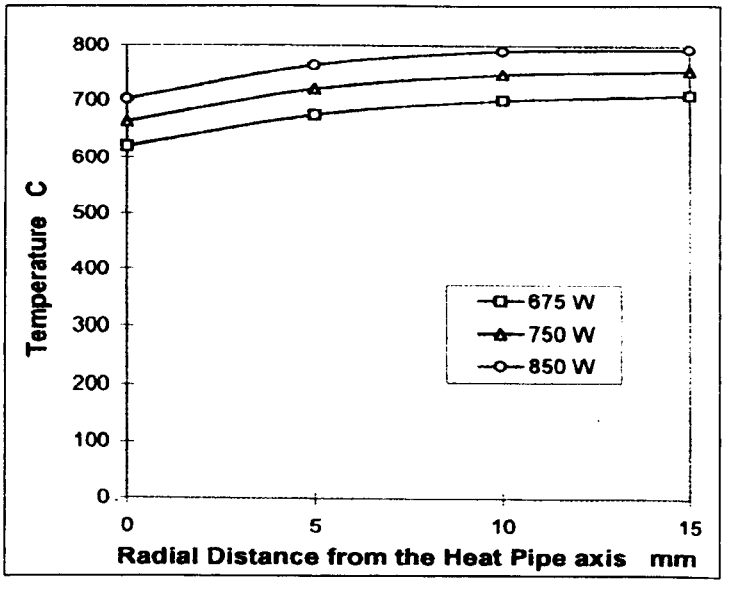

Fig. 2.7(b) Radial temperature profile of the heat-pipe

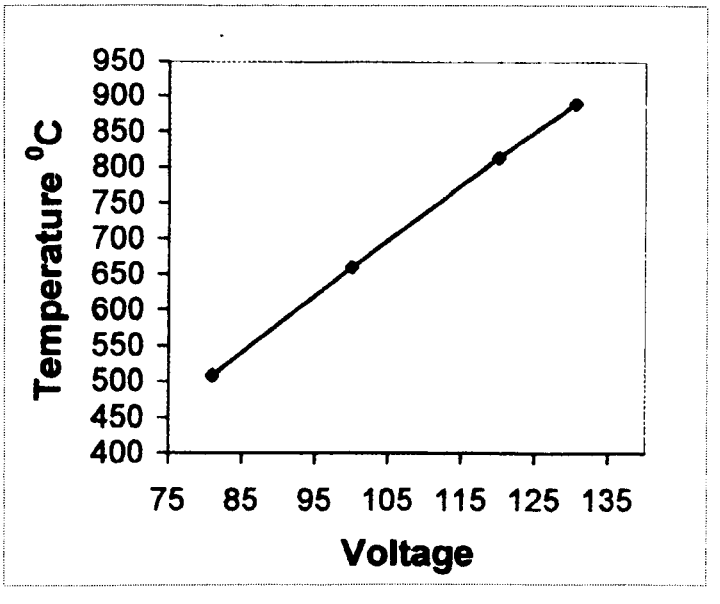

Fig. 2.8.Temperature- voltage relation for a linear heat-pipe made from Ni-Cr resistance wire

2.3.2 Disposable Atomic Jet Cartridge

In order to circumvent the major problems associated with a conventional heat-pipe oven such as window fogging by metal vapour deposition, erratic vaporization of the sample which produces atom density fluctuations, deposition of the sample on the electrical probe which spoils the detection sensitivity, an inexpensive and efficient atomic jet target facility (Philip 2007) with a sensitive ionization detection was constructed which provides a clean environment for preparing Rydberg states of the alkaline-earth atoms (especially strontium and barium) using two-photon excitation. This simple scheme in which the sample material is encapsulated in a cartridge type oven located inside the hot zone of a heat-pipe and is made to effuse in to a jet after evaporation combines the advantages of both heat-pipes (Beigang 1982) and atomic beams (Dai 1995), namely high atom density and efficient detection characteristics of thermionic diodes and the directionality of the atomic beam geometry. This new setup with several unprecedented advantages over conventional heat-pipe setup has been demonstrated to be very useful in a variety of experiments in multi-photon spectroscopy (Philip 2008). Such a device may be useful to construct a prototype of a laser from strontium and barium metal vapours by enclosing the discharge medium in an optical resonator in a crossed heat-pipe. The total construction cost of a linear heat-pipe set up with one disposable atomic jet cartridge and the ionization detection does not exceed US$ 350, excluding the cost of quartz windows, vacuum manifold and heater DC power supply.

Fig. 2.9 shows the schematic of a disposable sample cartridge used for the two-photon spectroscopy of strontium and barium. The cartridge is machined from oxygen free superior quality stainless steel rod with 9 mm internal boring. Two end-

caps are provided for efficient pre-cleaning of the cartridge. A machined slot (1 mm X 10 mm) on the top flattened surface as indicated in Fig. 2.9 which can be narrowed down to a 0.2 mm x 10 mm slot using adjustable knife edges serves as the opening for the atomic jet. This simulates a row of several atomic beams merging together to form a rectangular atomic jet directed vertically upwards offering a convenient geometry for orthogonal excitation by a horizontal laser beam, thereby substantially decreasing the Doppler broadening. The pure sample metal is filled inside the cartridge by opening one end-cap and, after sealing, is quickly transferred in to the center of the heat-pipe by guiding with a 2 mm thick, 6 cm long stainless steel cylindrical jacket (38 mm diameter) which slides smoothly inside the heat-pipe. A small quantity (approximately 0.6 gm) of the sample metal (Sr or Ba) was found sufficient for a series of experiments spread over several days and each lasting for several hours, thereby ensuring highly efficient utilization of the sample.

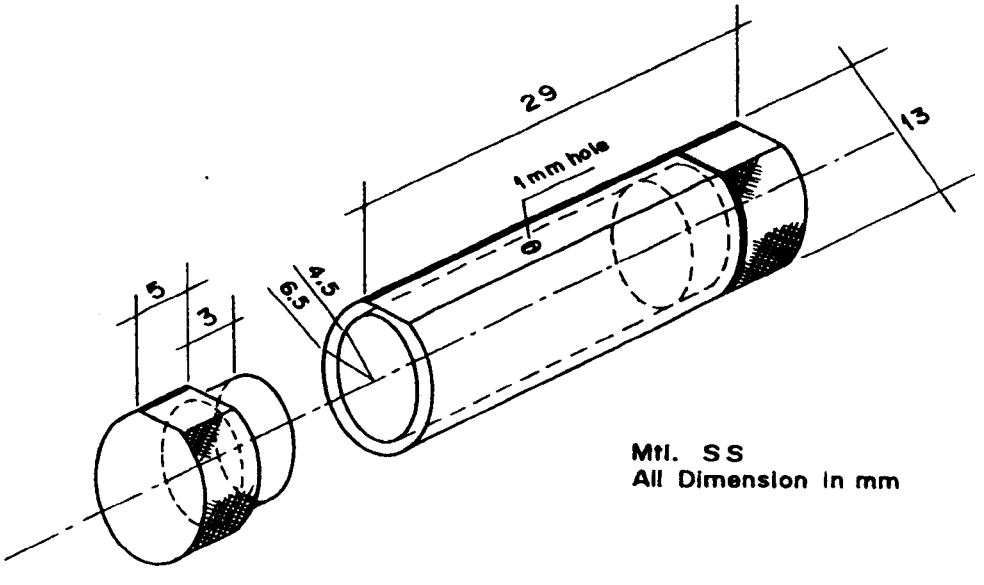

Fig.2.9 Schematic of a cartridge oven

The cartridge atomic jet target has been operated efficiently for several experiments without window degradation until the sample is completely exhausted. Also, this

arrangement has the added advantage that a single heat-pipe can be used for different sample metals by simply replacing the cartridge and its holder jacket. This scheme dispenses with the serious difficulties in cleaning the conventional heat-pipe after each experiment besides substantially reducing the cost of experiment by eliminating the need for constructing several heat-pipes for different tasks. Further, the experimental results reported in this thesis establish the potential applications of the inexpensive setup for two-photon spectroscopy with several new observations besides extending many previous data for strontium and barium. A crossed heat-pipe design is suitable for an optical detection setup for transverse fluorescence emission measurement as shown in the schematic in Fig. 2.10. This scheme can be used for interferometry (Mach–Zender interferometer) to determine neutral atom number density in the atomic jet. Also, by scanning across the width of the atomic jet for laser absorption the atomic jet profile can be determined.

A crossed heat-pipe is particularly suitable for two-photon Doppler-free spectroscopy with two counter propagating beams. A setup with two independent heat-pipes, each with a cartridge atomic jet is ideal for experiments dedicated to the measurement of line broadening and line shift. In the scheme in Fig.2.10 an auxiliary nitrogen pumped dye laser is shown which can be triggered with a controlled delay by the excimer laser pumped dye laser for experiments involving step-wise multi-photon excitation.

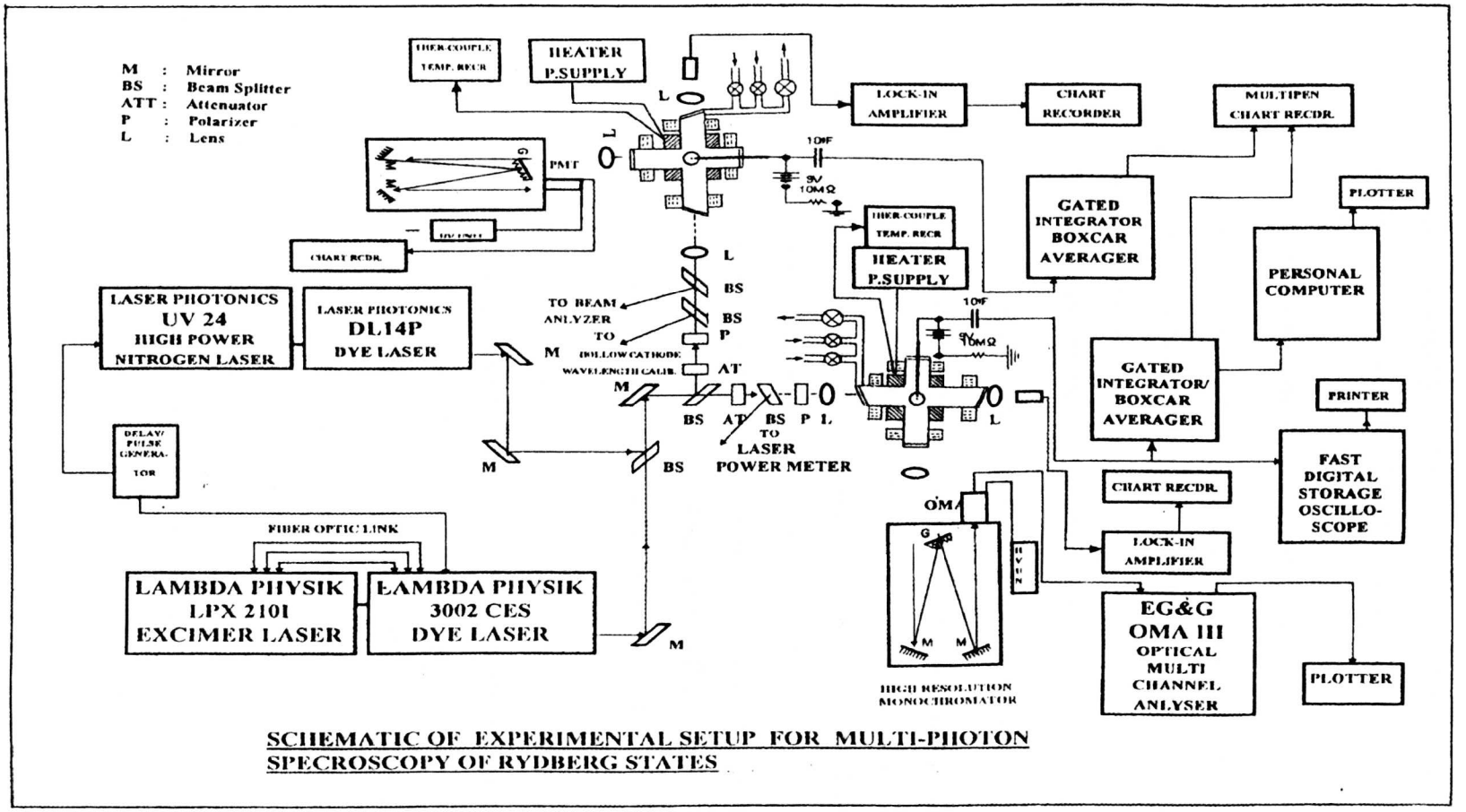

Fig. 2.10. Schematic of experimental setup for stepwise multi-photon excitation with complimentary ionization and optical detection (*Applied Phys. B* **90**, 40, 2008)

Important advantages of the cartridge atomic jet target over the conventional heat-pipe for multi-photon absorption are summarized below.

i. A gas dynamically stabilized sheet of atomic vapour with high number density and uniform distribution in the laser-atom interaction region;

ii. Atom diffusion is substantially decreased;

iii. Elimination of window fogging and heat-pipe contamination by vapour deposition thereby enhancing the useful operating time of a single fill for several days;

iv. Focal spot alignment becomes very easy;

v. Elimination of direct laser-induced gas breakdown;

vi. Improvement in temperature and density gradients which eliminates fluctuations in signal detection;

vii. Requirement of the laser power is substantially decreased because of efficient multi-photon absorption in a high density jet;

viii. Convenient geometry for transverse excitation to minimize Doppler broadening and also to study polarization effects;

ix. Remarkable control on experiments involving electric field and collisions;

x. Disposable cartridge eliminates need to clean the heat-pipe.
Single heat-pipe can be used for different atomic species by simply interchanging the sample cartridge and the holder without contamination. This saves considerable amount of time and cost;

xi. Efficient utilization of metal sample thereby reducing substantially the consumption of costly material.
In effect, the operating cost of the experiment is reduced to a remarkably low value, (below 50 %) as compared to a conventional heat-pipe operation with its inherent constraints.

2.4 Detection of Rydberg atoms

2.4.1 Ionization Detection-combination of collisions with electric field in a space-charge-diode

Classical absorption spectroscopy involves the measurement of relatively small attenuation of large signals and is limited to single-photon transitions. Absorption spectroscopy with photographic detection was also used with limited sensitivity (Rubbmark *et al* 1977). For multi-photon absorption, the most common methods are ionization detection and fluorescence detection. Since Rydberg atoms are weakly bound they can be easily ionized by collisions and or electric field and, by far, the ionization detection which is independent of the excitation channel is the most sensitive method for detection of highly excited atoms. Fluorescence detection is complimentary to the ionization detection and is sensitive to the excited state.

The opto-galvanic effect (OGE) first observed by Penning (Penning 1928), has been demonstrated as a very sensitive diagnostic tool after the advent of tunable dye lasers and can be used as an alternative to absorption or fluorescence techniques with a wide range of applications (Barbieri and Beverini 1990). OGE refers to a change in the electrical conductivity of a self-sustained gaseous discharge when illuminated by radiation resonant with an atomic or molecular transition of the gaseous species. Highly efficient detection of OGE signal, which is not affected by the background radiation or by scattering, results from the signal due to electron-ion pairs following resonant multi-photon absorption process. This technique also has been extensively used in heat-pipes (Camus *et al* 1982).

A widely used space-charge amplification technique (Popescu *et al* 1973), particularly for detection of Rydberg states, takes advantage of the fact that Rydberg atoms have long lifetimes and can be almost 100% ionized by collisions. This technique has been used extensively in laser spectroscopy for the past several decades for the detection of multi-photon ionization in alkali and alkaline-earth metal vapours with marginal variation in different designs (Popescu *et al* 1974, Esherick *et al* 1976, Ewart and Purdie 1976, Camus and Morillon 1977, Beigang and Timmermann 1982, Niemax 1985, Zhang and Lu 1987, Kalyar *et al* 2007). Also, this technique was used in synchrotron experiments. The space-charge–limited diode ionization technique is the simplest and least expensive detection with an inherent gain of about 10^4-10^5 (Marr and Wherrett 1972) and hence the need for further amplification is eliminated. High signal-to-noise ratio, especially for the highly excited sate, is easily achieved in this extremely sensitive technique which is due to positive ions trapped in the potential well by the negative space charge. The ions neutralize the space charge and lower the potential barrier enabling large number of electrons to be collected by the positive electrode.

The highly efficient and simple ionization detection set up (Schematic in Fig.2.1) which is linear over a wide range and was used in several measurements reported in this thesis consists of, essentially, a thoriated tungsten wire electrode, 3 mm diameter and 17 cm long, fitted through the central hole in a 50 mm diameter quartz optical window which vacuum seals the rear end of the 31 cm long stainless steel linear heat-pipe. The vibration of the tungsten wire electrode is isolated by suspending a stainless steel cylindrical mass (approximately 60 gm) below the electrode, 30 mm away from its tip. Alternatively, a high vacuum electrical

feedthrough can be used with the tungsten electrode welded to the central copper electrode of the feedthrough (Photo 2.8). When the central, 10 cm long, hot zone of the heat-pipe is heated the tip of the tungsten electrode is also indirectly heated and provides the necessary seed electrons by thermionic emission. The probe is connected to a variable (0 - 45 V) DC power supply assembled with alkaline batteries. When biased positively with respect to the wall of the heat-pipe this electrode serves as the electron collecting probe. With zero external biasing, this probe collects the ion current due to the negative potential from space charge effect by thermionic emission. A 100 KΩ variable resistor is used to limit the current. The signals with fast rise time through a 20 pF capacitor are fed to the input stage of a boxcar averager and gated integrator after rejecting undesirable components. Electrical measurements for Volt- Current (*V-I*) characteristics are made using a digital microammeter and voltmeter assembly. Such a device works in a similar way to a space-charge-limited thermionic diode in which ionization signals corresponding to excited states can be controlled by the electric field and the pressure inside the heat-pipe.

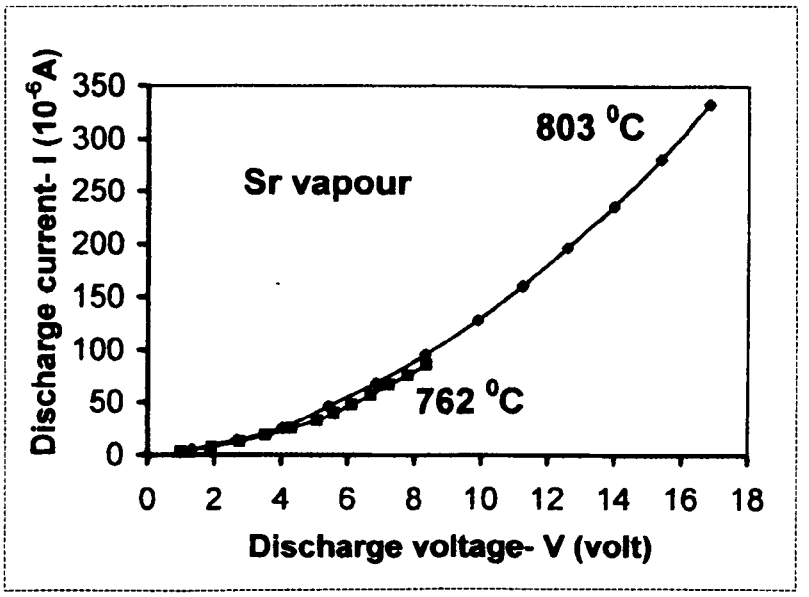

Fig.2.11. Current- Voltage (*I-V*) characteristics in Sr vapour

Fig 2.11 shows the electrical characteristics of the detector in strontium vapour at two temperatures. In Fig. 2.12., the probe current I is plotted against (voltage, $V)^{3/2}$ and in Fig. 2.13., the current is plotted against (pressure, $p)^{½}$. The linearity in the two curves shows that the space charge current in the diode varies as $V^{3/2}$ and $p^{-½}$.

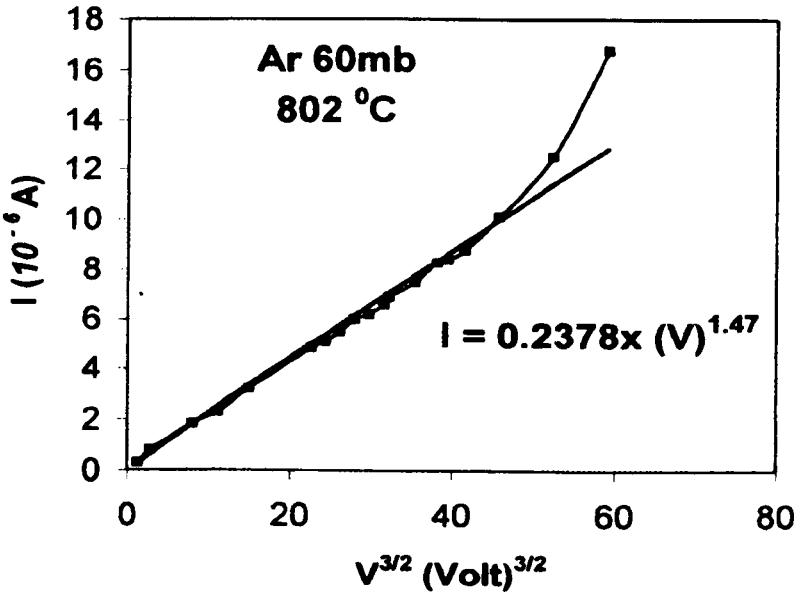

Fig.2.12 Space-charge-limited operation of the thermionic diode with current proportional to (voltage)$^{3/2}$

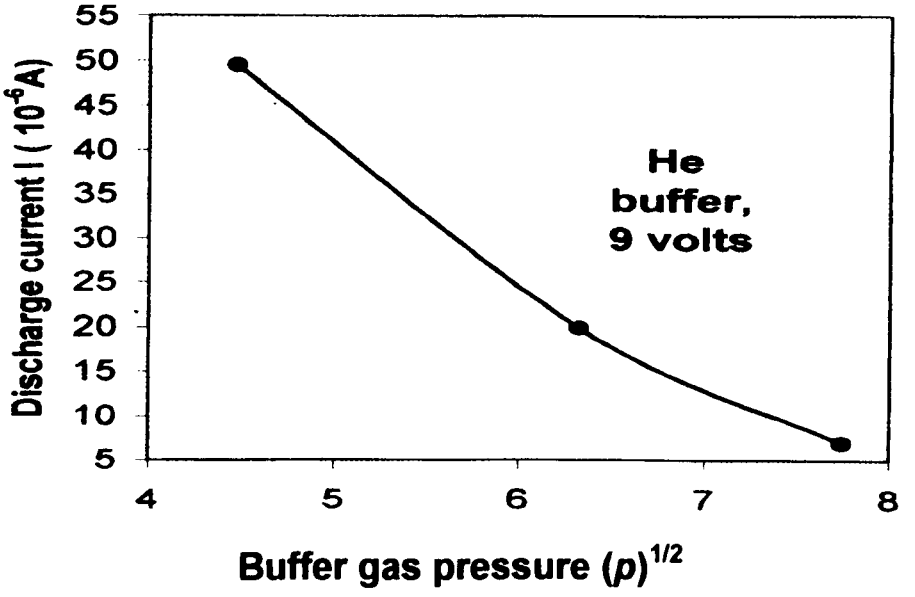

Fig. 2.13, Current varies as buffer gas (pressure mbar)$^{-1/2}$

The effect of buffer gas composition and pressure on the electric discharge is revealed in the *V-I* characteristics shown in Fig. 2.14. It was observed that the spatial distribution of the electric field as well as the ratio of the electric field to pressure (*E/p*) play important roles in the Stark mixing and excitation of forbidden transitions. The oscillator strength of the forbidden transitions resulting from field-induced ℓ-mixing could be controlled by varying the pressure and polarizability of the buffer gas used (Philip and Makdisi 2006).

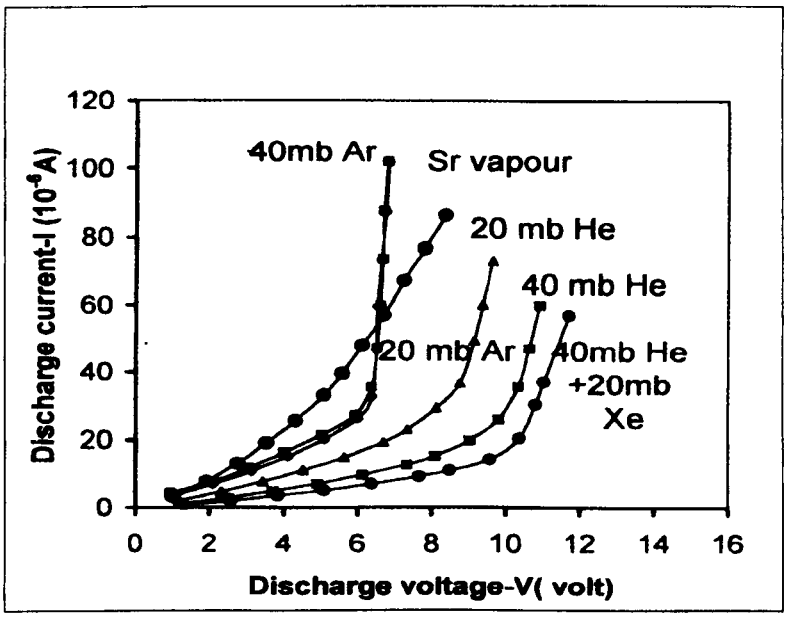

Fig.2.14. Effect of buffer gas pressure and composition on the *V-I* characteristics of the electric discharge

The ionization signals resulting from resonant two-photon absorption to the bound Rydberg states were monitored by a fast digital oscilloscope (Gould DSO 4094) and fed to the input of a boxcar averager and gated integrator (Stanford Research Systems SR250). Undesirable signals due to direct multi-photon ionization and saturation effects were eliminated by attenuating the dye laser beam using a variable neutral density beam splitter. Most of the experiments were carried out with dye

laser energy in the range 1 μJ - 15 μJ per pulse and repetition rate 7 Hz or 13 Hz to avoid interference due to 50 Hz line frequency. The linearity of the signal detection was ensured by adjusting the gain of the signal processing electronics network. The boxcar averager was triggered by the signal from the dye laser beam monitoring photodiode optical trigger. The boxcar averager was usually set to average out 10-20 samples per trigger and the gate width was kept at 2-3 ns. The averaged out signal was fed to a personal computer as well as to a strip chart recorder for direct analog output. Data acquisition software supplied by the Manufacturer (Stanford Research Systems- SR272) was used to acquire and process the spectral data.

A typical ionization signal following two-photon excitation of a Rydberg state is shown in photo 2.9. The ionization signal width (FWHM) $\approx$ 110 μs gives approximately the typical time for trapping of ions and lowering of the potential barrier which enables electrons to be collected by the axial positive electrode. The ionization signal width is highly sensitive on the design of the detection system. For optimum performance the ionization signal width should be minimized and should have a fast rise-time. The effect of buffer gas pressure on the ionization signal width is shown in photo 2.10.

The highly efficient ionization detection technique was also used to study electric field and collision induced perturbations in Rydberg series (Philip and Makdisi 2006) and for controlled excitations to forbidden transitions (Philip and Connerade 2007). The simple design of ionization detection in the space-charge-controlled diode was found to be versatile in signal detection to study highly excited states under a variety of test conditions such as collisions, static and pulsed electric fields and to study Stark mixing and the temporal evolution of excited states reported here.

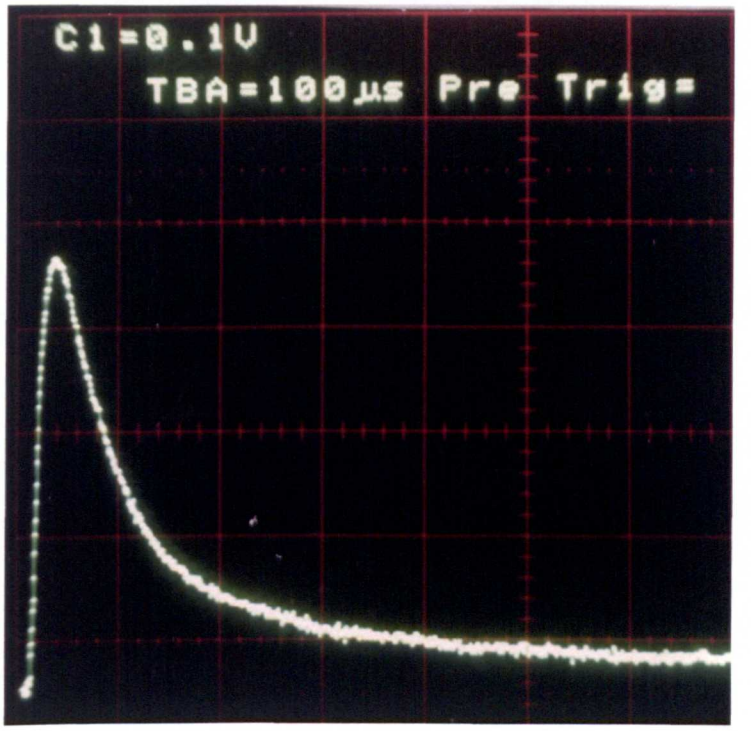

Photo 2.9 Ionization signal following two-photon absorption

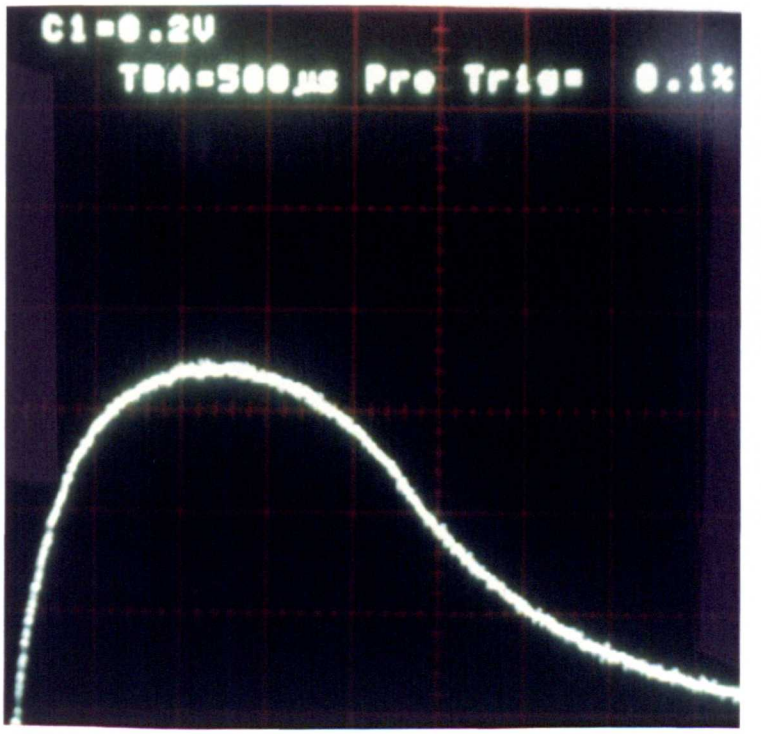

Photo 2.10 Effect of buffer gas pressure on the ionization signal

2.4.2 Fluorescence emission detection setup

Optical detection was used as complimentary to electrical detection. Unlike the electrical detection, the fluorescence detection is sensitive to the states involved. The emission signal is guided through an optical fibre and coupled to the 0.67 metre scanning monochromator (McPherson 207) fitted with interchangeable gratings and OMA (optical multi-channel analyzer) or photomultiplier detection system. The optical detection provides a convenient alternative for the detection of fluorescence emission from Rydberg states as well as from states populated by electron impact excitations in the field region inside the thermionic detector. Optical detection is particularly important in measurements involving collisional broadening effects due to foreign gas.

2.5 Detection of the Time Decay of Rydberg atoms - Gated Pulse Technique (GPT)

A novel experimental technique involving time-resolved pulsed field thermionic diode detection (Philip and Connerade 2008) has been employed in the heat-pipe setup to examine the time decay of high-lying Rydberg states of atoms yielding their effective lifetimes. The gated pulsed-field technique (GPT for short), with an accuracy limited by the rise-time of the pulsed field (~100ns), uses low field strengths (2.2 - 4 volt-cm^{-1}) for ionization detection and reproduces important features of the two-photon spectra including the singlet-triplet mixing of the 5s*n*d $^{1,3}D_2$ series and all perturbations. The novelty of GPT lies in the finding that this technique is attractive for states with very long lifetimes in presence of collisions, with the unique possibility of simultaneous determination of lifetime data for all

members of a sequence, which is not possible by other methods such as fluorescence detection. The results obtained also indicate that the decay of the Rydberg atoms can be controlled by adjusting the collision parameters with a possibility of exciting states which survive with excessively long lifetimes. The design details of the gated pulse detection technique (GPT) are discussed with the measurements and results in Chapter 3 of the Thesis.

References -Chapter 2 (alphabetical order)

1 Alcock C.B., Itkin V.P. and Horrigan M.K.
"*Canadian Metallurgical Quarterly*" **23**, 309, (1984)

2 Barbieri Beniamino and Beverini Nicolo
Review of Modern Physics **62**, 603, (1990)

3 Beigang R., Lucke K., Timmermann A., West P.J. and Frolich D
Opt. Commun **42**, 19(1982)

4 Beigang R. and Timmermann A
Phys. Rev. A **25**, 1496 (1982)

5 Camus P. and Morillon C
J.Phys. B: At. Mol. Opt. Phys. **10**, L133 (1977)

6 Camus P., Dieulin M. and El Himdy A
Phys. Rev. A **26**, 379(1982

7 Dai C.J
Phys. Rev. A **52**, 4416(1995)

8 Esherick P., Armstrong J. A., Dreyfus R.W.and Wynne J.J
Phys. Rev. Lett. **36**, 1296 (1976)

9 Ewart P. and Purdie A.F
J. Phys. B: At. Mol. Opt. Phys. **9**, L437 (1976)

10 Kalyar M.A., Rafiq M. and Baig M.A
J. Phys. B: At. Mol. Opt. Phys. **40**, 4317 (2007)

11 Marr G.V. and Wherrett S.R
J. Phys. B: At. Mol. Opt. Phys. **5**, 1735(1972)

12 Niemax K
Appl. Phys.B. **38**, 147(1985)

13 Penning F.M
Physica **8,** 137(1928)

14 Philip G
Rev. Sc. Instr. **78,** 113101 (2007)

15 Philip G. and Makdisi Y
Opt. Commun. **266**, 253 (2006)

16 Philip G. and Connerade J._ P
Opt. Commun. **279**, 141 (2007)

17 Philip G
Appl. Phys. B **90**, 407 (2008)

18 Popescu D., Collins C.B., Johnson B.W. and Popescu I
Phys. Rev. A **9**, 1182 (1974)

19 Popescu D., Pascu M.L., Collins C.B., Johnson B.W. and Popescu I
Phys. Rev **8**, 1666 (1973)

20 Rubbmark J.R., Borgstrom S.A. and Bockasten K
J. Phys. B: At. Mol. Opt. Phys. **10**, 421 (1977)

21 Vidal C.R. and Cooper J
J. Applied Phys **40**, 3370(1969)

22 Zhang J.Y. and Lu K.T
J. Phys. B: At. Mol. Opt. Phys **20**, 5065 (1987)

Chapter 3

Spectroscopy of Rydberg Atoms

3.1 Introduction

The spectroscopy of Rydberg atoms allows the systematic study of the atomic structure and properties over a wide range of n (principal quantum number) and ℓ (angular momentum quantum number) values and the evolution of these properties when the electron energy approaches the ionization limit. The departure from the simple hydrogen like atom with interaction between two point charges allows one to get a deeper understanding of the properties of the atomic core and its interaction with the outer electron, analogous to the difference between the actual orbit of a planet and its Keplerian orbit which gives information about the mass distribution inside the planet. In one-electron atoms like the alkali metals, the potential differs from a pure Coulomb potential near the atomic core and also away from the core because of the polarization of the atomic core. In two-electron atoms which are intermediaries between the one-electron system and the many-electron system simple spectra can be obtained with excitation of one electron and complex spectra due to the simultaneous excitation of both the electrons. When the Rydberg electron is far outside the atomic core region the system can be treated with the classical closed-orbit theory. But in the neighbourhood of a perturbing state such as a doubly-excited (for example the 5d7d $^1D_2$ state in barium) state the Rydberg electron can be scattered temporarily in to a doubly excited state when passing through the core region and the classical closed orbit can be modified. Two-electron system which played an important role in the development of atomic physics and the revival of the

old quantum theory continues to remain an active topic of research because it is highly complex for theoretical formulation although simple to obtain accurate experimental and numerical data for testing theoretical approximations. Similar to the statement by Martin Gutzwiller (1998) which reads as:

"Moon-earth-sun, the oldest, best known but least understood three-body problem" probably applies to the two-electron atoms with three point charges because of the nonseparability of the equations of motion and the existence of chaos in the dynamics of the three-body system (Tanner *et al* 2000).

3.1.1 Bound Rydberg series

The spectra of alkaline-earth Rydberg atoms have several important features due to the presence of the short-range part of the interaction between the highly excited electron and the parent ion core as well as polarization interaction and other corrections to the pure Coulomb potential. The alkaline-earth atoms with two electrons outside closed shell exhibit several peculiar properties in the spectra– the presence of bound and autoionizing Rydberg series converging to different ionization thresholds and electron-electron correlation effects. Unlike for hydrogen, the potential for the alkaline-earth atom is modified by a non-Coulombic term because of the spatial extent of the core which includes the nucleus and the inner electrons in filled shells. Thus two-electron system which forms a three-body Coulomb system provides the best basis for a many-electron system.

The bound state spectra of the two-electron atoms could be calculated accurately with formulations such as Hartree-Fock self-consistent field method (Bethe and Jackiw 1968). However, the doubly excited states could not be explained by single-

particle Hartree-Fock method. Ever since the famous experiment by Madden and Codling (1963) showed that doubly excited states of two-electron atoms represent the paradigm for electron-electron correlations in atomic systems, these states have been under intensive theoretical and experimental investigations. Compared to helium, alkaline-earth atoms have the experimental advantage of a low two-electron excitation energy which can be easily achieved by multi-photon laser excitation.

3.1.2 Quantum defect

For an electron with orbital angular momentum quantum number ℓ, moving in a pure Coulomb field, the potential at the electron position r can be written as:

$$V_{Coulomb}(r) = -\frac{Ze^2}{r} + \frac{l(l+1)\hbar^2}{2\mu r^2} \qquad (3.1)$$

Here Z is the atomic number and μ is the reduced mass and h is Planck's constant. If we neglect the fine structure, hyperfine structure effects and the quantum electrodynamics (QED) corrections, the radial Schrodinger equation gives the energy levels E_n of hydrogen and hydrogenic atoms (species) by the formula:

$$E_n = I - \frac{R_M Z^2}{n^2}; n = l+1, l+2, \ldots \qquad (3.2)$$

Where n is the principal quantum number, I is the series limit or the ionization threshold and R_M is the mass corrected Rydberg constant for the atom (species). Z = 1 for neutral atom and Z = 2 for singly-charged ion etc. These energy levels obtained by solving the radial Schrodinger equation are $(2\ell+1)$-fold degenerate in the angular momentum ℓ and n^2-fold degenerate in magnetic sublevels. The potential for a many-electron atom departs from a pure Coulomb potential at short distance due to the finite extent of the core and we can write an effective potential:

$$V_{effective}(r) = V_{Coulomb}(r) + V_{shortrange}(r) \qquad (3.3)$$

and $r \to \infty, V_{shortrange}(r) = 0$

Consequently, the valence electron of a neutral many-electron atom follows a modified Rydberg relation for the energy levels given by,

$$E_{n,l} = I - \frac{R_M}{(n^*)^2}; n^* = n - \mu_l \qquad (3.4)$$

n^* is the effective principal quantum number and μ_l is the quantum defect for a given series of angular momentum ℓ. Conventionally the energy of the bound electron is negative and that of a free electron (continuum) is positive. The mass corrected Rydberg constant for the atom R_M is given in terms of the Rydberg constant for the infinite mass R_∞:

$$R_M = \frac{R_\infty}{(1 + m_e/M)} \qquad (3.5)$$

$$R_\infty = \frac{m_e e^4}{8\varepsilon_0^2 h^2} \qquad (3.6)$$

M is the mass of the atom, m_e is the mass of electron, e is the electronic charge, h is Planck's constant and ε_0 is the permittivity of the free space. The Rydberg constant, with a value R_∞ = 109737.31569 cm $^{-1}$, is the most accurately known constant in physics (Connerade 1998).

Rydberg formula given by equation 3.4 indicates the $(n^*)^{-3}$ dependence of the energy interval $(E_{n+1} - E_n)$ for the successive members of a Rydberg series as shown in figure 3.1(a). A log-log plot of the effective principal quantum number versus the energy interval $(E_{n+1} - E_n)$ for the successive members gives a straight line with a slope approximately equal to -3 as indicated in figure 3.1(b).

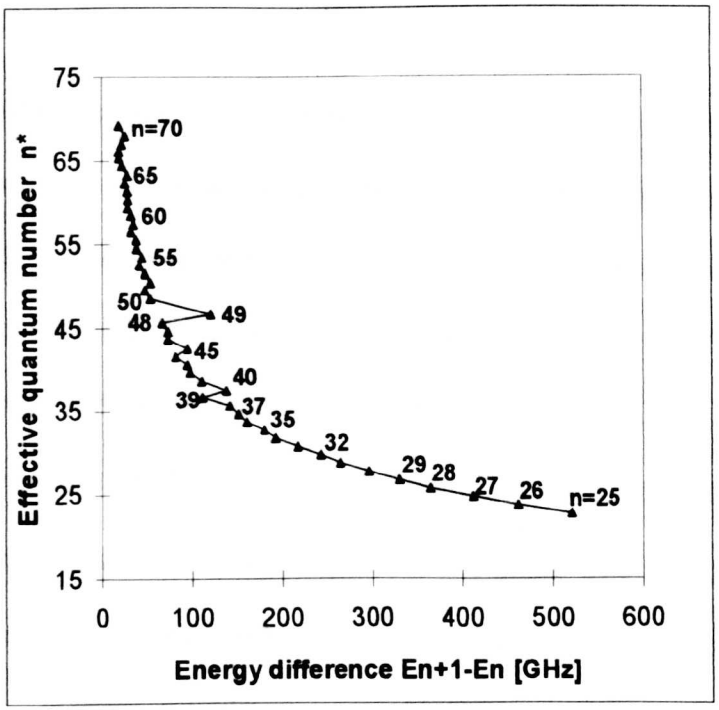

Fig.3.1 (a) Effective quantum number versus energy difference E_{n+1}- E_n between successive terms for Sr I 5s*n*d $^1D_2$ Rydberg series showing the n^{*-3} dependence (*J. Phys.B: At. Mol. Opt. Phys.* **34**, 521, 2001)

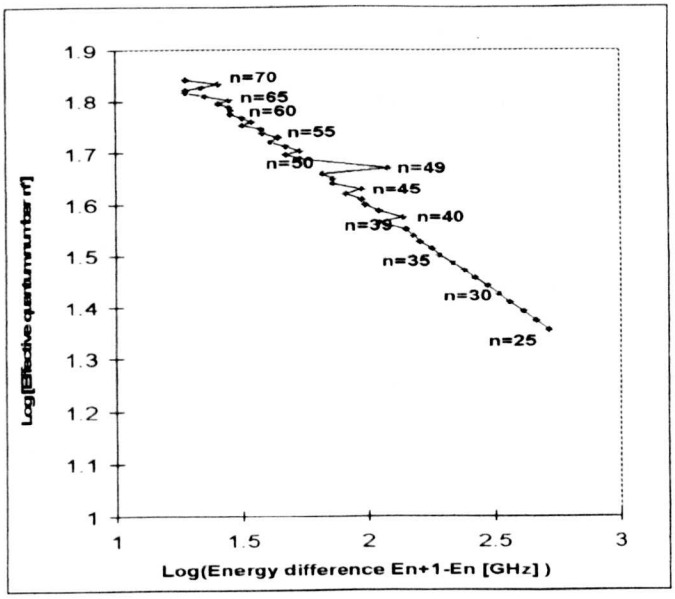

Fig.3.1 (b) Log-log plot of Effective quantum number versus energy difference E_{n+1}- E_n between successive terms for Sr I 5s*n*d $^1D_2$ Rydberg series showing the n^{*-3} dependence
(*J. Phys. B: At. Mol. Opt. Phys.* **34**, 521,(2001)

Alkali atoms have a compact core with one valence electron and the space within the atom can be divided into two distinct regions, an inner many-body core region where all the electrons except the valence electron are present together and interact strongly and an outer region where the valence electron is present. The expression (3.4) for $E_{n,\ell}$ differs from the energy level structure of the Hydrogen atom by the presence of the quantum defect μ_ℓ which decides the non-Coulomb part of the electron-core interaction for alkali-metal Rydberg atom. The quantum defect μ_ℓ appears as a parameter to account for the many-body effects of the core to deduce the effective one-electron wavefunction outside the core region and is a slowly varying function of n. However, μ_ℓ has a strong dependence on the orbital quantum number 'ℓ' with μ_ℓ falling off rapidly as 'ℓ' increases due to a decrease in probability of the Rydberg electron coming near to the parent ion core and due to the decrease in the polarization part of electron-core interaction. Quantum defects are large for states that penetrate the core and small for states with core penetration prevented by centrifugal barrier. (The repulsive centrifugal term in the effective potential $V_{effective}(r) = -\frac{Ze^2}{r} + \frac{l(l+1)\hbar^2}{2\mu r^2}$ present in the radial Schrodinger equation for all atoms, is responsible for excluding radial wavefunction from the centre for $l > 0$). If l_c is the highest angular momentum of the core electron, the quantum defect μ_l is large for $l < l_c$ and small for $l > l_c$.

Quantum defect is a measure of the difference between energy levels of many-electron atoms and energy levels of hydrogenic systems. One-electron (like alkali) atom wavefunction behaves like that of hydrogen with a small phase shift at large radial distance. This is due to the finite extent of the core which is non-hydrogenic.

For small 'l' the valence electron's classical orbit can penetrate the core and thus the valence electron can be, temporarily, at smaller distance than one or more core electrons and hence can feel larger effective nuclear charge and Coulomb potential. This introduces a phase shift for the valence electron wavefunctions compared to the hydrogen wavefunctions and also the energy levels get shifted.

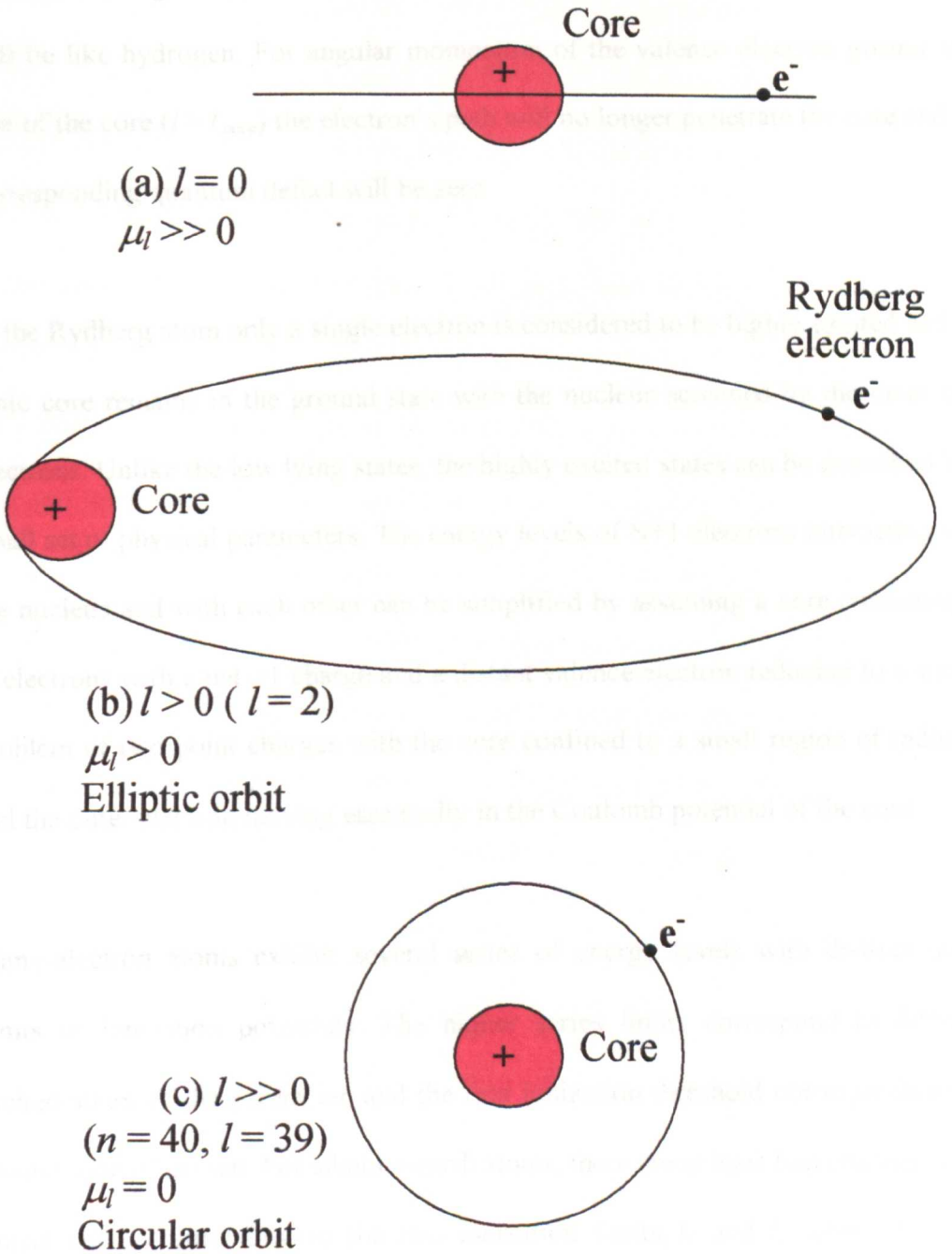

Fig.3.2 (a-c) Classical path of electron for different values of ℓ and dependence of quantum defect μ_ℓ on ℓ

Dependence of the quantum defect on angular momentum quantum number 'l' is indicated in figures 3.2(a-c). Quantum defect can be seen maximum for $l = 0$ and decreasing as l increases. A classical particle with $l = 0$ will pass through the nucleus. As l increases, the shape of the orbit changes from ellipse to circular. An electron moving in a circular orbit will be away from the core most of the time and will be like hydrogen. For angular momentum of the valence electron greater than that of the core ($l > l_{core}$) the electron's path will no longer penetrate the core and the corresponding quantum defect will be zero.

In the Rydberg atom only a single electron is considered to be highly excited and the ionic core remains in the ground state with the nucleus screened by the inner core electrons. Unlike the low lying states, the highly excited states can be described by a small set of physical parameters. The energy levels of N+1 electrons interacting with the nucleus and with each other can be simplified by assuming a core consisting of N electrons with a net +1 charge and a distant valence electron reducing to a simple problem of two point charges with the core confined to a small region of radius r_c and the outer electron moving essentially in the Coulomb potential of the core.

Many-electron atoms exhibit several series of energy levels with distinct series limits or ionization potentials. The higher series limits correspond to different excited states of the parent ion and the first ionization threshold corresponds to the ground state of the ion. For alkaline-earth atoms, there are at least two channels to be considered corresponding to the two ionization limits I_1 and I_2, where I_1 is the ionization threshold corresponding to the ground state of the ion with ms core and s Rydberg electron and I_2 is the ionization threshold corresponding to the first excited

state of the ion with *m*p core and p Rydberg electron. Thus $I_1 = I_{s1/2}$ and I_2 is the average of $I_{p1/2}$ and $I_{p3/2}$. (m = 5 for Sr and m = 6 for Ba).

3.1.3 The Quantum Defect Theory

Quantum defect theory (QDT) is a theoretically based parameterization to obtain the wavefunctions and their dependence on the principal quantum number n by which several measurable quantities can be calculated. The single-channel QDT applies to unperturbed Rydberg series with constant quantum defect μ and involves excitation process in which one electron is excited independently of the others. Here a Rydberg series defined by the quantum numbers and parity with its associated continuum is termed as a "channel". The wavefunction obtained from QDT differs from that of H in the sense that the zeros in the wavefunction Ψ occur at values which depend both on n and μ unlike in H which depend solely on n. At highly excited states (at very high n), as the series limit is approached, the bound state wavefunction tends to be an oscillatory function of the continuum defined by a phase and the wavefunction changes smoothly into the free electron's wavefunction just above the threshold. The deviation of the potential experienced by the Rydberg electron from a pure Coulomb potential below the continuum threshold is described by the quantum defect μ and above the continuum threshold is defined by a phase shift δ. As the continuum threshold is approached, (as $n \rightarrow \infty$, $E_n \rightarrow I$), the connection between the quantum defect and the phase shift at $E_n = I$ is given by 'Seatons' theorem' which defines the continuity across the threshold:

$$\delta = \pi\mu \qquad (3.7)$$

A change of phase shift of π (one half wave) above the threshold corresponds to a change of unity in the effective principal quantum number and hence in the quantum

defect below the threshold. The close connection between the quasi continuum of the bound states just below threshold and pure continuum above the threshold is a specific property of the long-ranged Coulomb potential ($1/r$ dependence) with wavefunctions exhibiting finite oscillations below and infinite oscillations above the threshold due to the modification of the Coulomb potential by addition of a short range part. The two physically different situations, yet mathematically identical, just below and just above the continuum threshold can be written in an equation of one-channel QDT (Friedrich 1990):

$$\tan[\pi(\nu+\mu)]=0 \qquad (3.8)$$

In equation 3.8, the function μ describes the physical effects due to the added short range part of the potential: below the continuum threshold μ is the quantum defect and above the threshold μ is the phase shift δ divided by π. Below the threshold ν is the effective principal quantum number and above the threshold ν denotes the phase shift divided by $-\pi$:

For $E \leq I$,

$$\nu(E)=\left(\frac{R_M}{I-E}\right)^2 \qquad (3.9)$$

For $E \geq I$,

$$\nu(E)=-\frac{\delta(E)}{\pi} \qquad (3.10)$$

Below the threshold, $\nu(E) + \mu(E)$ must be an integer for the bound state.

The 'One-channel quantum defect theory' is applicable to an atomic system such as helium which has large first excitation energy for the ion and consequently all spectral series converge to the common limit with the ion left in the ground state. However, for series which are interacting and hence are perturbed, the quantum

defects are no longer constant. Such series are described by the 'multichannel quantum defect theory' (MQDT).

3.1.4 The Multichannel Quantum Defect Theory (MQDT)

In quantum defect theory the treatment of configuration interaction between two or more mutually perturbing series is, conventionally, by utilizing plots of the quantum defect ($\mu = n - n^*$) against the term values ($T_n = I - E_n$). However, these plots will show irregularities wherever a perturbing level of another series intrudes in to the spectrum. This will lead to ambiguity in assignment of the levels and periodicity of the perturbing series which converges to a different limit other than that of the perturbed series. Such limitations are overcome by the Multi-channel quantum defect theory (MQDT), first developed by Seaton(1966) and later extended by Lu and Fano(1970). MQDT is one of the most successful methods for the interpretation of the spectra of the perturbed Rydberg and autoionizing series of systems with closed shell configuration and with two valence electrons like the alkaline-earth atoms Ca through Ba. MQDT predicts the energies of the levels in terms of a small number of adjustable parameters (such as the quantum defect and the matrix describing the channel coupling) for interacting Rydberg series and is based on the fact that the Rydberg electron sees a Coulomb potential during most of its orbit and, therefore, it is possible to use well-known analytical wavefunctions which are linear combination of regular and irregular Coulomb functions for that part of the electron orbit. The radial wavefunction of the electron in the inner region $r < r_c$ is described by energy independent wavefunction and the structure of the wavefunction is changed only in the outer region where solutions of Schrodinger equations are valid.

The different regions corresponding to the position of electron, $r \leq r_c$, $r > r_c$ and $r >> r_c$ are illustrated in figure 3.3.

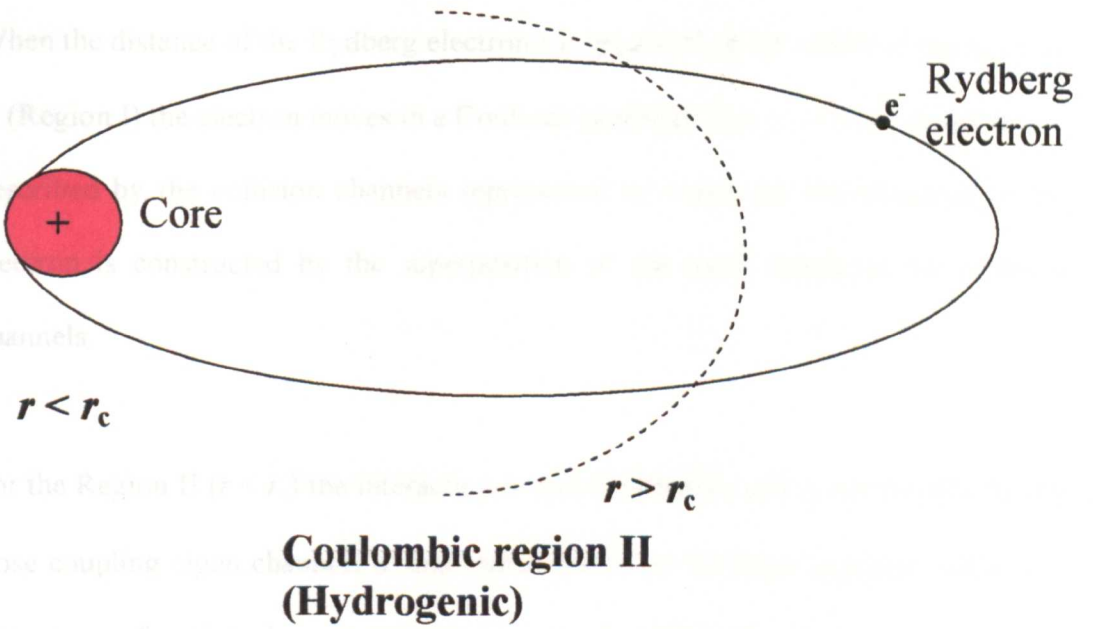

Fig. 3.3 Different regions of relevance to MQDT

Detailed MQDT formulation has been discussed in several references in the literature (Seaton 1966, Seaton 1983, Aymar *et al* 1996, Friedrich and Trost 1996) and only basic principles are discussed here. For a discrete Rydberg series specified by the quantum number J and parity the number of interacting channels M and the number of series limits $N \leq M$ can be obtained from experimental data. In MQDT two types of channels (Fano 1975) are defined: (i) the "Collision Channel" which describes a set of states that consists of a Rydberg electron with arbitrary energy and a core in a definite energy level with specifications for their angular momenta and coupling and (ii) " Close-coupling or α- channels" which are derived from the

collision channels by a unitary transformation matrix $U_{i\alpha}$. The region of interaction between the Rydberg electron and the ion core is divided in to two parts:

Region I $r \geq r_c$, where r_c is the radius of the core

and, Region II $r < r_c$

When the distance of the Rydberg electron r is greater than the radius of the ion core r_c (Region I) the electron moves in a Coulomb potential. For $r >> r_c$ the interaction is described by the collision channels represented by i and the wavefunction of the electron is constructed by the superposition of the wave functions for collision channels.

For the Region II ($r < r_c$) the interaction is non-Coulombic and is represented by the close coupling eigen channels α_i and characterized by the eigen quantum defect μ_α. The wave function is constructed by an incoming Coulomb wave with a superposition of a reflected wave with a phase shift. An orthogonal transformation matrix $U_{i\alpha}$ connects the collision channels i with the eigen channels α. The two wavefunctions are continuous on the core boundary ($r = r_c$). For the bound Rydberg states the boundary condition at $r \rightarrow \infty$ leads to an equation of the form:

$$\sum_{\alpha=1}^{M} A_\alpha U_{i\alpha} \sin \pi(\nu_i + \mu_\alpha) = 0 \qquad (3.11)$$

(for all i and the summation is over the number of channels M)

μ_α is the eigen quantum defect for the eigen channel α and ν_i is the effective principal quantum number corresponding to each series limit I_i. ν_i's are non-integers (except for hydrogen) and the nonintegral part decides the mutual interaction between the series. For this reason in MQDT the effective quantum numbers are considered as modulo1 and the quantum defect μ is given in terms of the fractional part of $-\nu$ (Armstrong *et al* 1977).

The number N of series limits is the number of different core configurations. Thus, for example, in the case of Sr I, $J = 0$ even-parity states there are two series limits corresponding to the core configurations in 5s and 5p. For the $J = 2$, states there are 3 series limits with core configurations in 5s, 5p or 4d by neglecting the triplet splittings 5p ^3P_J and 4d ^3D_J of the ion. Each observed energy level E_n has N effective quantum numbers ν_i such that:

$$E_n = I_i - \frac{R_y}{\nu_i^2}, i = 1.....N \tag{3.12}$$

I_i is the i^{th} ionization limit, R_y is the Rydberg constant for the atom and n is the principal quantum number.

There are N-1 independent equations:

$$I_i - \frac{R_y}{\nu_i^2} = I_j - \frac{R_y}{\nu_i^2}, i \neq j \tag{3.13}$$

The wave function of an excited state can be expressed in terms of the wave function of the eigen (close coupling) channels as follows:

$$\Psi = \sum_\alpha A_\alpha \Psi_\alpha \tag{3.14}$$

The wave functions for the bound states should satisfy the asymptotic boundary condition given in (3.11), $\sum_\alpha^M A_\alpha U_{i\alpha} \sin \pi(\nu_i + \mu_\alpha) = 0$.

The non-trivial solution of the equation (3.11) requires that:

$$Det\left[U_{i\alpha} \sin \pi(\nu_i + \mu_\alpha)\right] = 0 \tag{3.15}$$

The theoretical ν_i's of the bound states are obtained from simultaneous solutions of equations (3.13) and (3.15) and the theoretical fit to the spectrum consists of adjusting the MQDT parameters μ_α and $U_{i\alpha}$ so that the calculated energy values agree with experimental values. In the graphical method (Lu-Fano plots) 1-ν_i

(modulo 1) versus ν_i (modulo 1) curves are constructed and the MQDT parameters are determined by fitting the theoretical energy values with the experimental values.

MQDT calculations for strontium have been compared with laser spectroscopic measurements by several authors (Esherick 1977, Rubbmark and Borgstrom 1982, Beigang and Schmidt 1983, Xu *et al* 1986). In the MQDT formulation for the autoionizing Rydberg series, the collision channels are described in *j-j* coupling to account for the spin-orbit effects and the eigen channels are treated as *L-S* coupled. The even-parity $J = 2$ spectrum of barium shows significant departure from *L-S* coupling and this spectrum has several bound perturbers. Aymar and Robaux (1979) used a 9-channel MQDT formulation to accurately fit the energy values of the even-parity levels lying below the first ionization threshold.

3.1.5 The Lu-Fano Graph

The spectra of many-electron atoms are, in most cases, perturbed and will have several series, some of which converge to the ground state while others converge to the excited states of the ion forming a "multi-channel" system. Lu-Fano graphical method (Lu and Fano 1970) provides a convenient method of analysis to find out all level positions in the perturbed series by the application of Seaton's multi-channel quantum defect theory (MQDT).

Consider the simple case of two interacting Rydberg series, one converging to the lower limit I_1 and the other to the higher limit I_2 with the bound sates of the former perturbed by the lower bound states of the latter. If the coupling between the two series (inter-channel coupling) is taken as an adjustable parameter and if one considers the best fit to the two series with two constant quantum defects μ_1 and μ_2

corresponding to the limits I_1 and I_2, a Lu-Fano graph may be constructed with the fractional part of μ's on both axes.. For constant quantum defects μ_1 and μ_2, the points will lie on two intersecting straight lines as given in figure 3.4 (a) (Connerade 1998).

However, if the two series are interacting, the quantum defects will no longer remain constant and the graph will be modified from a true crossing into an "*avoided crossing*" as shown in the figure 3.4(b). For series members close to the avoided crossing the distance to the two branches becomes equal and the identification of a series member becomes ambiguous (mixing of the two series). The magnitude of the avoided crossing in the diagram is a measure of the many-body effects or the breakdown of the independent electron approximation. For two series there will be one avoided crossing.

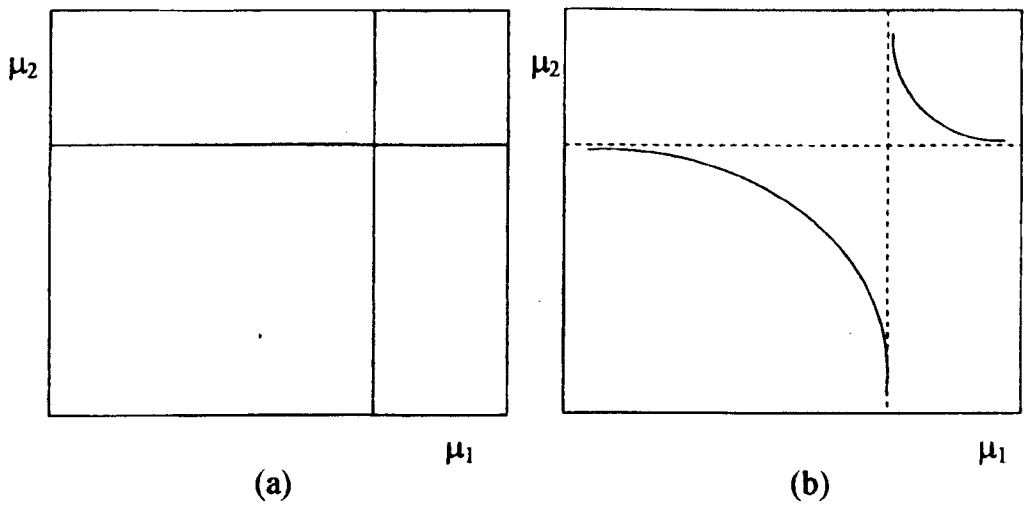

Fig. 3.4 (a-b) Lu-Fano plots for constant quantum defects
In (b) avoided crossing for two interacting series

It is conventional to plot μ_1 against the fractional part of ν_2 (modulo 1) representing a continuous variation of μ_1 as a function of the energy variable ν_2. This type of graphs are convenient to analyze interaction between series involving two limits in

which case the graph can be represented in a plane. In the case of series involving several series limits, the interaction becomes much complex and the graph becomes an N-dimensional cube, where N is the number of series limits (Connerade 1998).

For two series involving series limits I_1 and I_2, we have

$$I_1 - \frac{R}{\nu_1^2} = I_2 - \frac{R}{\nu_2^2} \tag{3.16}$$

Where the variables ν_1 and ν_2 which vary as smooth functions of energy are used for the effective principal quantum number n^*. The bound states of the Rydberg series are obtained from the solution of an equation of the form,

$$\tan\left[\pi(\nu_1 + \mu_1)\right] = F_1(\nu_2) \tag{3.17}$$

where, $F_1(\nu_2)$ stands for the perturbation due to the second series which is significant wherever there is a bound state of the series 2 and is negligible otherwise. Similarly, for the second series, we can write:

$$\tan\left[\pi(\nu_2 + \mu_2)\right] = F_2(\nu_1) \tag{3.18}$$

The solution of the above equation can be written as,

$$\tan\left[\pi(\nu_1 + \mu_1)\right]\tan\left[\pi(\nu_2 + \mu_2)\right] = R_{12}^2 \tag{3.19}$$

where, R_{12} is the interchannel coupling strength. This is the equation for a two-channel QDT. The experimental points lie on the intersection between this curve and the function defined by the equation (3.16). Equation (3.19) can be written in the determinant form:

$$\begin{vmatrix} \tan\left[\pi(\nu_1 + \mu_1)\right] & R_{12} \\ R_{12} & \tan\left[\pi(\nu_2 + \mu_2)\right] \end{vmatrix} = 0 \tag{3.20}$$

If $R_{12}^2 = 0$, we have two non-interacting series, each with a constant quantum defect. There are three limiting cases of mixing between series.

$R_{12} >> 1$ (strong mixing),

$R_{12} << 1$ (weak mixing),

and $R_{12} = 1$ (equal mixing).

Equation (3.20) can be generalized to many channel interactions as:

$$\left|\tan\left[\pi(\nu_i + \mu_i)\right]\delta_{ij} + (1-\delta_{ij})R_{ij}\right| = 0 \qquad (3.21)$$

The Lu-Fano graphs used very successfully to represent bound Rydberg series and to extrapolate their properties in to the first autoionizing range can also be extended to represent series consisting of entirely autoionizing resonances with no bound states converging on a pair of limits and experimentally the graphical technique has been well established (Connerade 1998).

3.1.6 Selection Rules

In the electric dipole approximation which is satisfied at long wavelength region, (not valid in the x-ray range) the strength of the transition between two states $|i\rangle$ and $|j\rangle$ depends on the value of dipole the matrix element $\langle i|\boldsymbol{r}|j\rangle$. If this is zero, the transition is dipole forbidden. Electric dipole transitions are those involving matrix elements with linear dependence on $\boldsymbol{r}$, the separation between the positive and negative charges of the atom. Multi-pole transitions (magnetic dipole, electric quadrupole, etc.) involve higher order terms such as r^2, etc. and these give much weaker transition probabilities compared to the electric dipole transitions (Connerade 1998)

For single-photon transitions involving excitations with weak intensity radiation the electric dipole transitions are the strongest. The selection rules for such transitions can be regarded as the conservation of angular momentum which implies that, by

absorption of a photon having an angular momentum ±1 atomic units, the angular momentum of the atom must also change by ±1. For negligible spin-orbit interaction, the spin of the atom does not change in an electric dipole transition. Therefore, transitions are possible between terms of the same multiplicity and inter-combination transitions are forbidden.

In the absence of external fields, the parity selection rule that it should change by unity (even→ odd and vice versa) is a strong rule. Similarly, the difference in total angular momentum quantum number between initial and final states, $\Delta J = \pm 1$ and $J = 0 \rightarrow J = 0$ is forbidden is also a strong rule. The additional rules valid in the L-S coupling, $\Delta L = \pm 1$ and $\Delta S = 0$ are called weak selection rules. Although the parity, defined as $(-1)^L$ where $L = \Sigma_i l_i$ is a good quantum number, the individual values of l_i are not unique. This allows the excitation of more than one electron (observed double excitations) in photoexcitation (Connerade 1998).

Selection rules for one-photon transitions

The parity which is defined as $(-1)^{\Sigma i \ell i}$ must change as :

odd → even; even → odd

and the total angular momentum change ΔJ is given by

$\Delta J = 0, \pm 1$; $J = 0 \rightarrow J = 0$ is forbidden

Additional rules which are valid only for L-S coupling are,

$\Delta L = \pm 1$ and $\Delta S = 0$.

Excitations by intense radiation involves the absorption of two or more photons and the selection rules for multi-photon excitations are different from the dipole

selection rules mentioned above, since each photon carries an angular momentum ±1. The two-photon selection rules are summarized as follows (Connerade 1998):

Selection rules for two-photon transitions		
$\Delta J \leq 2$	$; J_1 + J_2 =$ integer	
and, for equal frequency photons,		
$\Delta J : 0 \rightarrow 1$		Forbidden for all polarizations
If $\lvert\Delta J\rvert = 1$	$\Delta M: 0 \rightarrow 0$	Forbidden for all polarizations

That is, for two-photon transition, $\Delta J = 0, \pm 2$. Further condition is imposed by the polarization of the exciting laser beam. $\Delta J = 0$ transitions are allowed only if the laser is linearly polarized. The selection rules for two-step excitations involving an intermediate state are somewhat different from the above rules for two-photon excitations.

Above selection rules break down in the presence of external fields and the polarizations of the exciting laser beam becomes important. Selection rules for orbital angular momentum are broken in strong electric fields and in the presence of a magnetic field the different polarization of the exciting light beam induces different transitions between different magnetic sublevels. Moreover, there can be experimentally controlled access to certain excited states which are otherwise forbidden by the normal selection rules (Philip and Connerade 2007).

3.2 Rydberg series of the alkaline-earth atoms

3.2.1 Single electron excitations

The heavy alkaline-earth atoms (Sr and Ba discussed in this thesis) have played an important role in the understanding of atomic structure and for the development of theory for the spectra of many-electron atoms. These atoms have two s electrons outside filled shells and the ground state is $ms^2\ ^1S_0$ (m = 5 for strontium and m = 6 for barium). The nuclear charge is screened by the electrons of the filled shells and therefore, the effective charge of the atomic core is +2. Since the valence electrons are far away from the nucleus the ionization energy is considerably low as compared to the ionization energy of He which is 24.5eV. Just like in He the single-electron excitation gives rise to two sets of spectral series- singlet series due to S = 0 (antiparallel spins) and triplet series due to S = 1 (parallel spins) except for ℓ = 0 case. However, in alkaline-earth atoms, the normal selection rule ΔS = 0 is not strictly obeyed and therefore inter-combination transitions (singlet-triplet transitions) are also observed in the spectra of these atoms due to strong spin-orbit coupling.

The spectra of Rydberg states of alkaline-earth atoms have several peculiarities, most interesting of which is the presence of several doubly-excited valence states below and above the first ionization limit which are the members of series converging to the (m-1)d or mp ionization limits. Also, there is the presence of perturbations among series with different ionization limits. The first three excited states forming the ^3P_J manifold in strontium and barium are metastable and the excitations to $^3P_1$ from the ground states $^1S_0$ are spin-forbidden and to $^3P_{0,2}$ are dipole-forbidden. These metastable manifolds are important for physics of cold atoms (Katori *et al* 1999).

In conventional absorption spectroscopy (Garton and Codling 1968) only electric dipole-allowed transitions were possible. Ever since powerful tunable lasers became available, extensive studies of the spectra of highly excited states of alkaline-earth atoms using step-wise (Rubbmark *et al* 1977, Rubbmark and Borgstrom 1978) or multi-photon (Esherick 1977, Aymar *et al* 1978, Armstrong *et al* 1979) schemes were initiated. Two-photon spectroscopy is the most widely used technique since it allows the transitions between states of the same parity unlike in single-photon absorption. Physical properties of the two alkaline-earth atoms used for the study discussed in this thesis are summarized in Table 3.1.

Table 3.1

Physical properties of Sr I and Ba I

Element	***Z***	***A***	**Confign**	**Melting Point ^{0}C**	**Density gm/cm^3**	**Ionization Potential eV**	**Rydberg constant R_y (cm^{-1})**
Strontium Sr I	38	87.62	Kr[5s^2]	769	2.54	5.6949 * (I = **45932.10cm^{-1}**)	**109736.6**
Barium Ba I	56	137.33	Xe[6s^2]	729	3.59	5.2117** (I = **42034.85cm^{-1}**)	**109736.88**

* Rubbmark J.R, Borgstrom *Physica Scripta* **18**, 196(1978)
** Post B.H, Vassen W, Hogervorst W , Aymar M , Robaux O
J. Phys. B. At. Mol. Opt. Phys. **18**, 187(1985)

3.3. Important experimental studies in Sr I by others

The early spectral data for strontium were presented by Saunders (1922), Russel and Saunders (1925) and the compilation in Volume II of Atomic Energy levels by Moore (1952). Strontium atom (Sr I, Z = 38) with the ground state configuration [Kr] 5s^2 ^{1}S$_0$ has an unfilled 4d shell. Besides the regular series, spectral terms due to transitions involving the excitation of both electrons (doubly-excited configurations)

as mentioned by Russel and Saunders (1925) are also observed in the spectra of strontium atom. The ground state 5s and the first excited state 4d of Sr II ion are very close in energy and therefore these states have considerable configuration interaction, as observed by the perturbation in the 5s*n*p $^1P_1$ principal series by the 4d*n*p $^1P_1$ doubly excited configuration. Garton and Codling (1968) applied classical ultraviolet absorption spectroscopy for the excitations from the ground state $5s^2\ ^1S_0$ leading to the extension of Sr I, 5s5p $^1P_1$ principal series to $n = 33$. They observed inter-combination transitions $5s^2\ ^1S_0 \rightarrow$ 5s5p $^3P_1$ appearing as satellites to the long wavelength (red wing) side of the principal series for the range $22 < n < 33$. They also obtained an improved value for the first ionization threshold for strontium as 45932.0 ± 0.2 cm^{-1}.The doubly excited configuration 4d5p $^1P_1$ (41172.12 cm^{-1}) was found to be the lowest member of the series 4d*n*p $^1P_1$ whose all other members lie above the first ionization threshold and, therefore, are autoionizing and broadened by interaction with the 5s*ε*p $^1P_1^0$ continuum upon which they are coupled. Garton and Codling further observed 94 lines most of which are double-electron 4d*n*ℓ (ℓ = p, f) transitions converging on the 4d ($^2D_{3/2,\ 5/2}$) states of Sr II ion at 60487.9 cm^{-1} ($4d_{3/2}$) and 60768.2 cm^{-1} ($4d_{5/2}$). The two-electron excitation spectra of strontium are much more complex than those of the barium spectrum.

3.3.1 Important compilations for Sr I in Moore's table

(a) Even –parity Rydberg states

5s*n*s $^1S_0$ from $n = 5$ to 11(44097.1 cm^{-1})

5s*n*s $^3S_1$ from $n = 5$ to 12 (44457.3 cm^{-1})

5s*n*d $^1D_2$ from $n = 4$ to 9 (43780.6 cm^{-1})

5s*n*d ^3D_J from $n = 4$ to 16 (45372.6 cm^{-1})

(b) Odd –parity Rydberg states

$5snp\ ^1P_1^0$ from n = 5 to 14(44903.5 cm^{-1})

$5snp\ ^3P_{0,1,2}^0$ from n = 5 to 7(39411.703, 39426.471, 39457.409 cm^{-1})

$5snf\ ^1F_3^0$ from n = 4 to 13 (45277.9cm^{-1})

$5snf\ ^3F_{2,3,4}^0$ from n = 4 to 13 (45274.1cm^{-1})

(c) Doubly-excited intruder states

$5p^2\ ^3P_{0,1,2}$ (35193.47, 35400.138, 35674.668 cm^{-1})

$5p^2\ ^1D_2$ (36960.881 cm^{-1})

$5p^2\ ^1S_0$ (37160.278 cm^{-1})

$4d^2\ ^3P_{0,1,2}$ (44525.88, 44595.97, 44729.67 cm^{-1})

(d) First ionization threshold (series limit) 45925.6 cm^{-1}

3.3.2 Laser spectroscopy studies in Sr I by others

Early study of the even-parity Rydberg series of strontium using tunable dye laser was reported by Ewart and Puride (1976). Their spectra covering the 590 nm - 430 nm wavelength region indicated two-photon and three-photon excitations. This study could extend the previous listing by Moore (1952) for the $5sns\ ^1S_0$ series from n = 11 to n = 19 and for the $5snd\ ^1D_2$ series from n = 9 to n = 35. A strong resonance at 431.1 nm, previously unobserved, was also reported by Ewart and Purdie (1976) which they had assigned as $4d^2\ ^1D_2$ autoionizing resonance.

Esherick (1977) studied the two-photon spectrum of J = 0, 2 strontium from the $^1S_0$ ground state by multi-photon ionization spectroscopy and then analysed using multi-channel quantum defect theory (MQDT). Esherick (1977) extended the previous

experimental data for 5s*n*s from $n = 10$ to $n = 21$ giving additional 10 states with the lowest state observed at 43512.00 cm^{-1}. Also, he could resolve the 5s*n*d $^1D_2$ series up to $n = 60$ which is approximately 30 cm^{-1} below the ionization limit and the 5s*n*d $^3D_2$ series were extended up to $n = 37$. Esherick used results of Garton and Codling (1968) to get a MQDT fit of 5s*n*p $^1P_1$ series and used these improved energy levels as reference for the two-photon measurements of the even-parity spectra. MQDT calculations by Esherick presented energy level data for 5s*n*s $^1S_0$ series up to $n = 40$ and for 5s*n*d $^1D_2$ sequence up to $n = 70$. The MQDT included perturbations of the 5s*n*d $^1D_2$ and 5s*n*d $^3D_2$ series by 4d6s$^1D_2$ and 4d6s$^3D_2$ configurations. Esherick clearly observed the avoided crossing between the $^1D_2$ and $^3D_2$ series near $n = 16$. Also he reported about an auotoionizing resonance nearly 450 cm^{-1} above the first threshold.

Rubbmark and Borgstrom (1978) extended the energy level data for strontium 5s*n*ℓ $^1S_0$, $^1P_0$, $^1D_2$, $^1F_3$ and $^3F_{2,3,4}$ Rydberg series by step-wise two-photon spectroscopy and gave an improved ionization limit. Using nitrogen pumped dye lasers and a heat-pipe setup and a 2m Ebert spectrograph with photographic recording of the absorption spectrum they could reconfirm most of the levels compiled by Moore (1971).

Starting from laser populated 5s5p$^1P_1$ level, Rubbmark and Borgstrom (1978) excited 5s*n*s $^1S_0$ for *n* from 7 up to 36 and 5s5p$^1P_1 \rightarrow$ 5s*n*d $^1D_2$ transitions for *n* up to 52 without observing 5s23s $^1S_0$ because of mixing with 5s22d $^1D_2$. They also observed collisional excitation of 5s*n*d $^1D_2$ and 5s4d $^3D_{1,2,3}$ levels which they further used as intermediate levels to excite 5s*n*f $^1F_3$ up to $n = 29$ and starting with 5s4d $^3D_{1,2,3}$ levels the 5s*n*f $^3F_{2,3,4}$ levels up to $n = 28$. Rubbmark and Borgstrom (1978)

values of 5s*n*p $^1P_1$ energy levels relied strongly on the assignment of the lower level 5s4d $^1D_2$. They reported an ionization energy for strontium as 45932.09 ± 0.15 cm^{-1} and had used a modified Langer's (1930) formula (Shenstone and Russel (1932).

$$n - n^* = a + bT_n + cT_n^2 + \sum_i \frac{\alpha_i}{(T_n - T_i)} \qquad (3.22)$$

where $n^* = \frac{\sqrt{R_{Sr}}}{T_n}$

and $$T_n = I - E_n \qquad (3.23)$$

T_n's are the term values for different n; T_i's are the term values of the perturbing energy levels. a, b, c and α_i's are the constants describing the series and n^* is the effective quantum number. R_{Sr} is the Rydberg constant for strontium.

Beigang *et al* (1982a) excited the 5s*n*s $^3S_1$ and 5s*n*d $^1D_2$ and 5s*n*d $^3D_{1,2,3}$ Rydberg series of strontium via one-photon transitions from a DC discharge populated 5s5p $^3P_{0,1,2}$ metastable states using pulsed dye laser and thermionic diode detection in a heat-pipe setup. Energy level data are given for the 5s*n*s $^3S_1$ series up to principal quantum number n = 45 and for the 5s*n*d ^3D_J series up to n = 32 (J = 1), n = 40 (J = 2) and n = 45 (J = 3). They had observed nearly constant quantum defect for the $^3S_1$ series whereas the quantum defect was dependent on n for the ^3D_J series and the quantum defect calculated using the extended Rydberg-Ritz formula was found breaking down because of strong triplet-singlet mixing and crossing over of the 5s*n*d $^{1,3}D_2$ series at n = 16. Moreover, the fine structure splitting of the ^3D_J states are also found to show irregular behaviour and a violation of the Lande interval rule ($^3D_3$-$^3D_1$ spacing) due to the mixing between 5s*n*d$^1D_2$ and 5s*n*d $^3D_2$ series. The crossing over of the $^1D_2$ and $^3D_2$ series is also found to lead to a degeneracy between $^1D_2$ and $^3D_2$ series at n = 19. Beigang *et al* (1982a) determined the level energies of 5s*n*s $^1S_0$

and 5s*n*d $^1D_2$ Rydberg series of Sr I between principal quantum numbers $10 < n < 80$ by Doppler-free spectroscopy.

For theoretical description of the perturbed Rydberg series using MQDT (multi-channel quantum defect theory), reliable information on both even-parity and odd-parity states are required. Two-photon excitation from the ground state $ms^2\ ^1S_0$ produces even-parity Rydberg series whereas odd-parity spectra can be obtained by single-photon excitation. Baig and Connerade (1984) made a high resolution study of the single-photon absorption ($5s^2\ ^1S_0 \rightarrow 5snp\ ^1P_1$) spectrum of Sr I using synchrotron radiation and extended the 5s*n*p $^1P_1$ principal series up to $n = 84$ which was the then highest value of n accessed in laboratory experiments. Also they presented a new value for the ionization potential as 45932.10 ± 0.03 cm^{-1} which was an improvement on the previous values given by Garton and Codling (1968), $45932.0 \pm .0.2$ cm^{-1}; Eshercik (1977), 45932.19 ± 0.03 cm^{-1}; Rubbmark and Brgstrom (1978), 45932.09 ± 0.15 cm^{-1}. Baig and Connerade (1984) also found excellent agreement for their new experimental energy level data with two-channel quantum defect theory (MQDT) analysis.

The $(m\text{-}1)d^2$ configuration in alkaline earth atoms ($m = 5$ for Sr; $m = 6$ for Ba, as before) are the important perturbations to the even-parity spectra. The mp^2 configuration also intrudes in to the even-parity series. For strontium, the $J = 1$ Rydberg series are not significantly perturbed by interlopers and the perturbation of the interloper 4d5p is confined to a very narrow range ($6 < n < 7$). However, the $J = 2$ even-parity Rydberg series in strontium are heavily perturbed by eight perturbers, namely $4d^2\ ^3P_2$, $^1D_2$, $^3F_2$; $5p^2\ ^3P_2$, $^1D_2$, $^3F_2$ and 4d6s $^1D_2$, $^3D_2$. The three perturbers originating from the $4d^2$ may be ignored (Esherick 1977). But in the presence of

collisions, and due to the presence of an autoionizing resonance with a $(4d^2+5p^2)$ configuration just above the ionization threshold this may not be true (Nawaz *et al* 1992). Also, the perturbed $J = 2$, even-parity $5snd\ ^{1,3}D_2$ Rydberg series swap over around $n = 16$ because of the break down of *L-S* coupling. Nawaz *et al* (1992) extended the $5s5p\ ^1P_1$ principal series of strontium up to $n = 91$ using laser spectroscopy and observed several anomalies including the collision-induced excitation of even-parity series.

Below the 5s ionization limit, the $J = 0^e$ spectrum consists of the Rydberg series $5sns$ and the doubly excited states $5p^2\ ^3P_0$ and $4d^2\ ^3P_0$. The superscript (^{e}) indicates even-parity. The earlier assignment of the $5p^2\ ^1S_0$ as a bound state has been corrected by Aymar and Telmini (1991) as an autoionizing resonance. The $J = 2^e$ spectrum consists of the $5snd\ ^{1,3}D_2$ Rydberg series and the doubly-excited states pertaining to the $4d^2$, $5p^2$ and 4d6s configurations. The location and assignment of the d^2 and p^2 configurations in strontium and barium have been under controversy (Kompitsas *et al* 1991).

Dai (1995) measured the energy levels of the Sr $5snd\ ^{1,3}D_2$ Rydberg series using an isolated core excitation scheme (Dai *et al* 1990). Three lasers were used to populate the $5p_{1/2}nd$ aoutoionizing levels from the ground state $5s^2\ S_0$ via the sequence $5s^2\ S_0 \rightarrow 5s5p\ ^1P_1 \rightarrow 5snd\ ^{1,3}D_2 \rightarrow 5p_{1/2}nd$. Experimental energy level values for the $5snd\ ^1D_2$ series were extended up to $n = 70$ and compared with those calculated by Esherick (1977) using MQDT. Also, the previous experimental energy level data by Esherick (1977) for the $5snd\ ^3D_2$ sequence were reestablished up to $n = 37$. Multi-channel quantum defect theory calculations by Dai found satisfactory agreement with his experimental data. A somewhat similar autoionization scheme employing

three dye lasers was used by Dai and Zhao (1995) to measure the energy levels of Sr 5s*n*s $^1S_0$ Rydberg series. Two lasers were used to prepare the Sr 5s*n*s $^1S_0$ states from the ground state and a third laser was used to drive the core transition 5s $\rightarrow$ $5p_{1/2}$ to reach the final $5p_{1/2}$ *n*s autoionization states. The auoionization process was used to produce ions which were detected to determine the levels of Sr 5s*n*s $^1S_0$ states. The above method of detection of Rydberg states using the autoionization process via isolated core excitation requires only low laser energy to ionize 5s*n*s states through the 5s*n*s $\rightarrow 5p_{1/2}$ transition. Dai and Zhao (1995) reported that for $n \approx 20$, the 5s*n*s $^1S_0$ series are merging with 5s(*n*-1)d $^1D_2$ series and are unresolved. By polarizing the first two lasers in the same direction, the $J = 2$, 5s*n*d $^1D_2$ series could be excited.

A three photon resonant excitation scheme was employed by Baig *et al* (1998) to excite the Sr I, 5s*n*p $^1P_1$ and 5s*n*f $^1F_3$ Rydberg series from the ground state in the wavelength range 650 – 660 nm using an atomic beam and thermionic detector. They compared the three-photon excitation energy accurate to $\pm$ 0.5 cm^{-1} for the 5s*n*p $^1P_1$ series for the range $25 < n < 43$ and for the 5s*n*f $^1F_3$ series for the range $22 < n < 26$ with measurement by others using different techniques. For strontium the perturbation for the 5s*n*d $^{1,3}D_2$ Rydberg series are due to $4d^2$ $^3P_2$ at 44729.56 (Esherick 1977), 4d6s $^3D_2$ and 4d6s$^1D_2$ which are degenerate with 6s17s $^1S_0$. The energy values reported for these levels have some discrepancy.

Level	**Energy** cm^{-1} Ewart and Purdie (1976)	**Energy** cm^{-1} Baig *et al* (1998)
$4d^2$ $^3P_2$	44729.4	
4d6s $^1D_2$	45350.1	45255
4d6s $^3D_2$	45276.5	45426

Two-photon spectra of the high members of the J = 2, even-parity $5snd^{1,3}$ D_2 Rydberg series of strontium using laser and an atomic beam in a heat-pipe setup with thermionic diode detection were obtained by Makdisi *et al* (2001). Strong-spin-orbit interaction and the breakdown of parity and selection rules combined with 'ℓ' mixing were observed. Highly localized doubly-excited $4d^2\ ^3P_J$, $5p^2\ ^1D_2$ which intrude in to the even-parity spectrum are found to survive collisions and field effects. Makdisi *et al* (2001) presented new experimental energy values for Sr I $5snd\ ^{1,3}D_2$ Rydberg series : $25 < n < 73$ for singlet and $25 < n < 47$ for triplet members thereby extending the previous energy level data of Dai (1995). Further, they have reported the emergence of the members of the odd-parity Rydberg series, $5snp\ ^1P_1$, $5snp\ ^3P_2$ and $5snf\ ^1F_3$ which are two-photon forbidden transitions from the ground state. Recently Haq *et al* (2006) reported new measurement of photoionization cross-section of strontium using two-step excitation from the ground state $5s^2\ ^1S_0$ with $5s5p\ ^1P_1$ and $5s6s\ ^1S_0$ as intermediate steps. Using three-photon ionization for the first time they also determined the photoionization cross-section for the $5s6s\ ^1S_0$.

The earliest report on photo-absorption cross-section was from Goppert-Meyer (1931) for two-photon absorption. Parkinson *et al* (1976) used the 'Hook method' to determine the f-values of the principal series of strontium and barium. Aymar (1987) calculated the photoionization cross-section below the $5p_{3/2}$ threshold using R-matrix method. Mende and Kock (1996) used the 'saturation technique' to measure the photoionization cross-section of strontium and reported the oscillator strengths for the $5snp\ ^1P_1$ Rydberg series via transitions $5s^2\ ^1S_0 \rightarrow 5snp\ ^1P_1$.

For the $(4d^2 + 5p^2)\ ^1D_2$ autoionization resonance various groups have reported the resonance energy E_R and width Γ as reproduced in Table 3.2.

Table 3.2

Experimental resonance energy (E_R) and width Γ of the $(4d^2+5p^2)^1D_2$ autoionizing resonance in strontium:

Energy E_R (cm^{-1})	Width Γ (cm^{-1})	Reference
46380.0	60	Esherick (1977)
46376.8	56.2	Mende *et al* (1995)
46380.1	59.6	Dai *et al* (1996)
46380.0	56	Baig *et al* (1998)
46379.0	45	Haq *et al* (2006)
46379.7	71.2 (40mbar Ar buffer)	Philip (2008)*

Philip (2008)* *to be published*

3.3.3 Energy Level diagram for Sr I

An Energy level diagram showing the important transitions observed in the two-photon spectroscopy of strontium is shown in figure 3. 5.

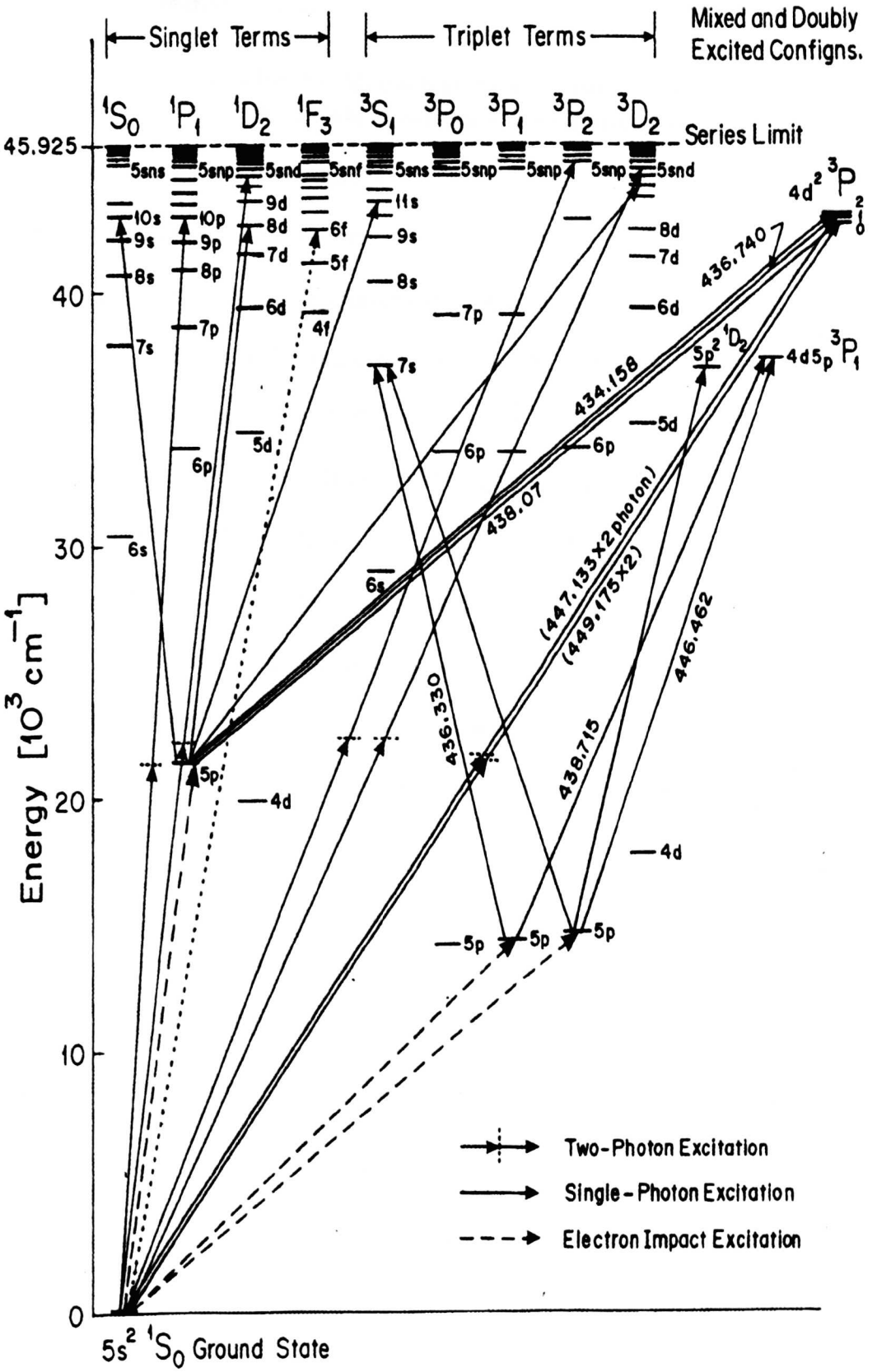

Fig.3.5 Schematic of the Energy Level diagram for Sr I showing observed excitations (*J. Phys. B. At. Mol. Opt. Phys.* **34**, 1(2001)

3.4 Important Results in Sr I Spectroscopy from thesis

3.4.1 The $J = 2$, even-parity spectra of Sr I $5snd\ ^{1,3}D_2$ Rydberg series (initial study)

Initial study using direct two-photon transverse excitation of an atomic beam inside a heat-pipe setup by the excimer laser pumped dye laser with the ionization detection and other related instrumentation described in Chapter 2 provided the experimental energy level values for the $J = 2$ even-parity spectrum of high members of the Sr I $5snd\ ^{1,3}D_2$ Rydberg series. This study could extend the previous energy level data for Sr I in NIST (Tables) and the important observations were published (J. Phys. B. At. Mol. Opt. Phys. 34, 1,2001). The revised data are available in NIST. New energy level values for Sr I $5snd\ ^{1,3}D_2$ are in good agreement with previously published data: $n = 25 - 73$ for $5snd\ ^1D_2$ and $n = 25 - 47$ for the triplet ($5snd\ ^3D_2$) members. These energy level values are reproduced in Table 3.3. Important extracts from two-photon spectra recorded in this study are also reproduced here.

Figure 3.6 shows the two-photon spectrum to Sr I $5snd\ ^{1,3}D_2$ Rydberg states corresponding to the laser tuning range 440- 445 nm. Strong mixing and exchange of character for the triplet-singlet members can be observed around $n = 16$ in Fig.3.6.

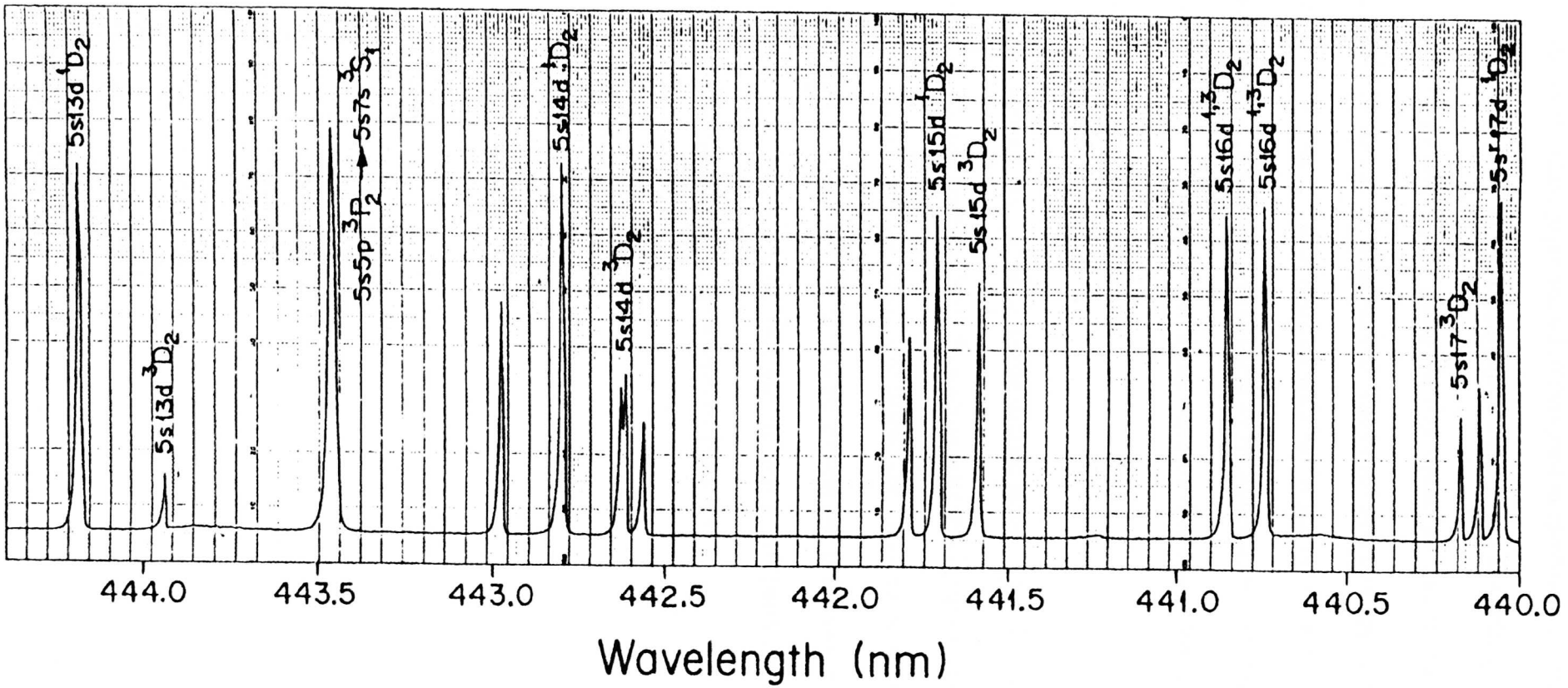

Fig. 3.6 Two-photon spectrum of Sr I showing low *n* members of 5s*n*d ^{1,3}D2 Rydberg series which swap over at *n* = 16 (*J. Phys. B. At. Mol. Opt. Phys.* **34**, 1, 2001)

Figure 3.7 shows the chart paper record of two-photon spectrum of neutral strontium taken with combination of He 40 (mbar) and Ar (60 mbar) as buffer gas mixture and a laser beam energy of 12 μJ / pulse. In this figure all transitions in the $J = 2$ spectrum listed in Table 3. 3 are observed. The broad structure appearing between $n = 27$ and 28 in figure 3.7 which evolved with buffer gas collision was investigated extensively in subsequent experiments using an improved atomic jet facility and it is conjectured that this corresponds to a highly compact doubly-excited state with a $4d^2$ character.

Besides the two-photon excitation from the ground state, Esherick (1977) observed one-photon resonances from the 5s5p $^1P_1$ intermediate level populated by collisional process. These one-photon sequential excitations are found to be strongly affected by the buffer gas pressure and the discharge current but unaffected by laser beam polarization effects. By using low buffer gas pressure (< 10 Torr) these collisionally induced sequential transitions are eliminated by Esherick.

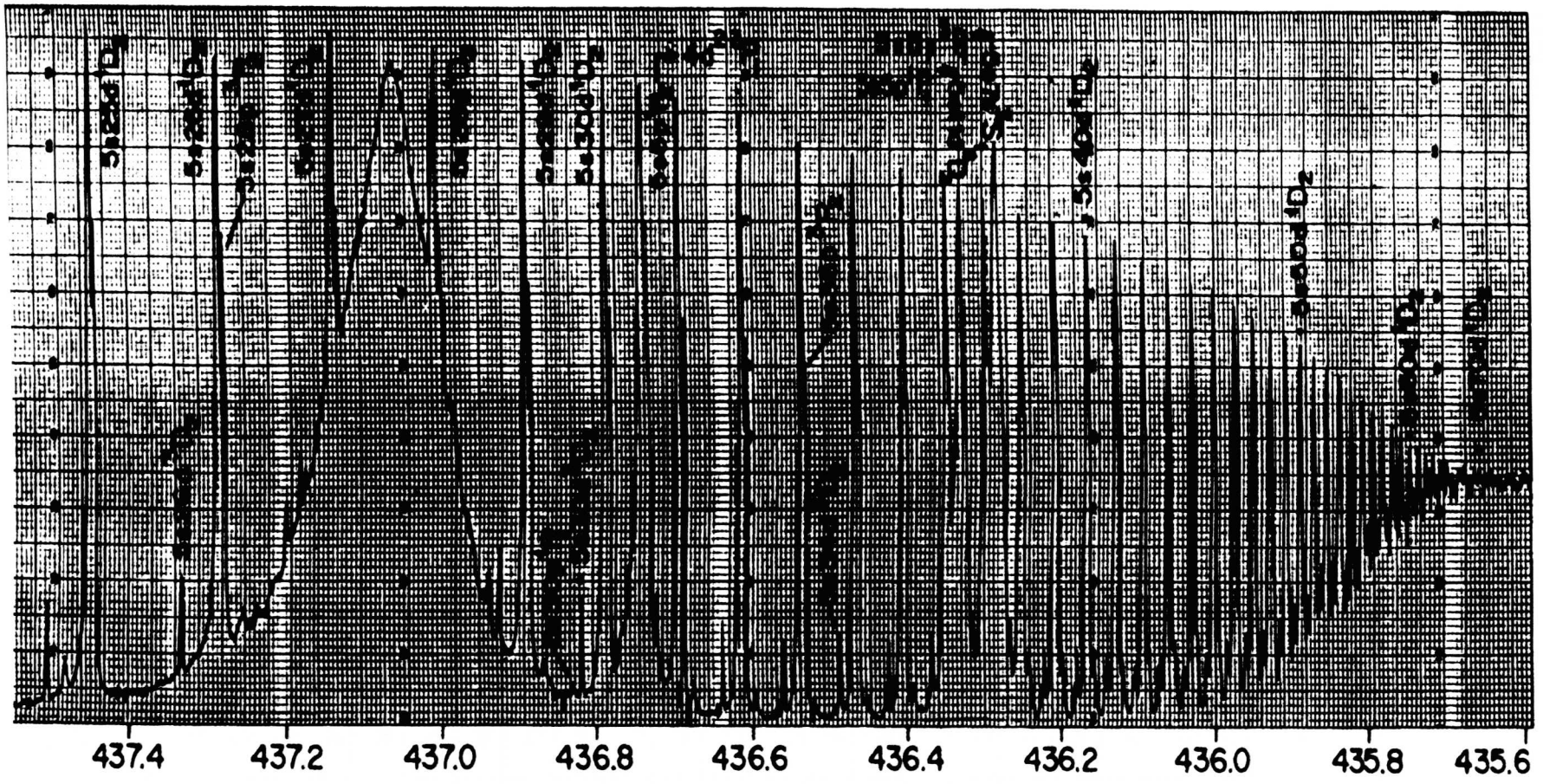

Fig. 3.7 Two-photon spectrum of Sr I 5s*n*d $^{1,3}D_2$ Rydberg series for $25 < n < 73$ (*J. Phys. B. At. Mol. Opt. Phys.* **34**, 1, 2001)

Table 3. 3

Energy Levels of Strontium 5snd $^{1,3}D_2$ Rydberg Series
(*J. Phys. B. At. Mol. Opt. Phys.* 34, 521, 2001)

Principal Quantum Number *n*	Level Label	Laser Wavelength λ_{vac} (nm)	Energy Level Our Expt. cm^{-1}	Energy Level Esherick* Expt. cm^{-1}	Energy Level Dai** Expt.cm^{-1}
25	$5s25d^3D_2$	437.509	45713.34	45713.51	45713.48
	$5s25d^1D_2$	437.452	45719.30	45719.25	45719.16
26	$5s26d^3D_2$	437.337	45731.32	45731.80	45731.76
	$5s26d^1D_2$	437.286	45736.65	45736.80	45736.83
27	$5s27d^3D_2$	437.182	45747.53	45747.81	45747.71
	$5s27d^1D_2$	437.139	45752.03	45752.22	45752.24
28	$5s28d^3D_2$	437.056	45760.33	-	-
	$5s28d^1D_2$	437.008	45765.75	45765.79	45765.77
29	$5s29d^3D_2$	436.928	45774.13	45774.58	45774.56
	$5s29d^1D_2$	436.892	45777.90	45777.97	45778.02
30	$5s30d^3D_2$	436.820	45785.44	45785.87	45785.81
	$5s30d^1D_2$	436.787	45788.90	45788.90	45788.92
31	$5s31d^3D_2$	436.724	45795.51	45795.91	45795.94
	$5s31d^1D_2$	436.693	45798.76	45798.65	45798.69
32	$5s32d^3D_2$	436.636	45804.74	45805.02	45804.97
	$5s32d^1D_2$	436.609	45807.57	45807.46	45807.43
33	$5s33d^3D_2$	436.558	45812.92	45813.15	45813.16
	$5s33d^1D_2$	436.532	45815.65	45815.60	45815.53
34	$5s34d^3D_2$	436.486	45820.49	45820.69	45820.71
	$5s34d^1D_2$	436.463	45822.89	45822.71	45822.51
35	$5s35d^3D_2$	436.421	45827.30	45827.55	45827.53
	$5s35d^1D_2$	436.402	45829.30	45829.32	45829.34
36	$5s36d^3D_2$	436.363	45833.40	45833.54	45833.56
	$5s36d^1D_2$	436.345	45835.29	45835.30	45835.36

Table 3.3. (Contd.)

Energy Levels of Strontium 5snd $^{1,3}D_2$ Rydberg Series
(*J. Phys. B. At. Mol. Opt. Phys.* 34, 521, 2001)

Principal Quantum Number *n*	Level Label	Laser Wavelength λ_{vac} (nm)	Energy Level Our Expt. cm^{-1}	Energy Level Esherick* Expt. cm^{-1}	Energy Level Dai** Expt.cm^{-1}
37	$5s37d^3D_2$	436.311	45838.90	45839.32	45839.34
	$5s37d^1D_2$	436.294	45840.64	45840.85	45840.43
38	$5s38d^3D_2$	436.263	45843.90	-	-
	$5s38d^1D_2$	436.246	45845.69	45845.85	45845.73
39	$5s39d^3D_2$	436.216	45848.84	-	-
	$5s39d^1D_2$	436.201	45850.42	45850.53	45850.54
40	$5s40d^3D_2$	436.174	45853.26	-	-
	$5s40d^1D_2$	436.161	45854.12	45854.77	45854.81
41	$5s41d^3D_2$	436.135	45857.36	-	-
	$5s41d^1D_2$	436.122	45858.72	45858.72	45858.76
42	$5s42d^3D_2$	436.100	45861.04	-	-
	$5s42d^1D_2$	436.087	45862.40	45862.44	45862.41
43	$5s43d^3D_2$	436.066	45864.61	-	-
	$5s43d^1D_2$	436.056	45865.66	45865.76	45865.81
44	$5s44d^3D_2$	436.037	45867.66	-	-
	$5s44d^1D_2$	436.026	45868.82	45869.01	45868.99
45	$5s45d^3D_2$	436.007	45870.82	-	-
	$5s45d^1D_2$	436.000	45871.55	45871.84	45871.94
46	$5s46d^3D_2$	435.980	45873.66	-	-
	$5s46d^1D_2$	435.970	45874.71	45874.57	45874.61
47	$5s47d^3D_2$	435.956	45876.18	-	-
	$5s47d^1D_2$	435.947	45877.13	45877.12	45877.16
48	$5s48d^1D_2$	435.924	45879.55	45879.50	45879.56
49	$5s49d^1D_2$	435.903	45881.76	45881.76	45881.82

Table 3.3 (Contd.)

Energy Levels of Strontium 5snd $^{1,3}D_2$ Rydberg Series
(*J. Phys. B. At. Mol. Opt. Phys.* 34, 521, 2001)

Principal Quantum Number *n*	Level Label	Laser Wavelength λ_{vac} (nm)	Energy Level Our Expt. cm^{-1}	Energy Level Esherick* Expt.cm^{-1}	Energy Level Dai** Expt.cm^{-1}
50	$5s50d^1D_2$	435.884	45883.76	45883.83	45883.86
51	$5s51d^1D_2$	435.866	45885.66	45885.75	45883.80
52	$5s52d^1D_2$	435.848	45887.55	45887.61	45885.61
53	$5s53d^1D_2$	435.833	45889.13	45889.38	45889.38
54	$5s54d^1D_2$	435.816	45890.92	45891.03	45891.03
55	$5s55d^1D_2$	435.801	45892.50	45892.59	45892.59
56	$5s56d^1D_2$	435.788	45893.87	45894.04	45894.04
57	$5s57d^1D_2$	435.774	45895.34	45894.39	45895.39
58	$5s58d^1D_2$	435.762	45896.61	45896.74	45896.74
59	$5s59d^1D_2$	435.750	45897.87	45898.01	45898.01
60	$5s60d^1D_2$	435.740	45898.93	45899.20	45899.20
61	$5s61d^1D_2$	435.729	45900.08	-	45900.27

Table 3.3 (Contd.)

Energy Levels of Strontium 5snd $^{1,3}D_2$ Rydberg Series
(*J. Phys. B. At. Mol. Opt. Phys.* 34, 521, 2001)

Principal Quantum Number *n*	Level Label	Laser Wavelength λ_{vac} (nm)	Energy Level Our Expt. cm^{-1}	Energy Level Esherick* Expt.cm^{-1}	Energy Level Dai** Expt.cm^{-1}
62	$5s62d\,^1D_2$	435.719	45901.14	-	45901.33
63	$5s63d\,^1D_2$	435.710	45902.09	-	45902.34
64	$5s64d\,^1D_2$	435.701	45903.04	-	45903.30
65	$5s65d\,^1D_2$	435.692	45903.98	-	45904.22
66	$5s66d\,^1D_2$	435.684	45904.83	-	45905.09
67	$5s67d\,^1D_2$	435.675	45905.77	-	45905.92
68	$5s68d\,^1D_2$	435.668	45906.52	-	45906.72
69	$5s69d\,^1D_2$	435.662	45907.15	-	45907.48
70	$5s70d\,^1D_2$	435.656	45907.78	-	45908.19
71	$5s71d\,^1D_2$	435.649	45908.51	-	--
72	$5s72d\,^1D_2$	435.641	45909.36	-	-
73	$5s73d\,^1D_2$	435.635	45909.99	-	-

*Esherick P., *Phys. Rev.* A **15**, 1920 (1977)
Dai C.J., *Phys. Rev.* A **52, 4416 (1995)

3.4.2 Fluorescence emission spectra of Sr I

Fluorescence emission measurements offered the evidence for electron impact excitation of the metastable states $5snp\ ^3P_J$ and the resonance state $5s6p\ ^1P_1$ which could serve as the intermediate states for sequential excitations. Figure 3.8 shows the 400 nm -500 nm portion of the observed fluorescence emission captured with the scanning monochromator-OMA / photomultiplier spectral recoding system.

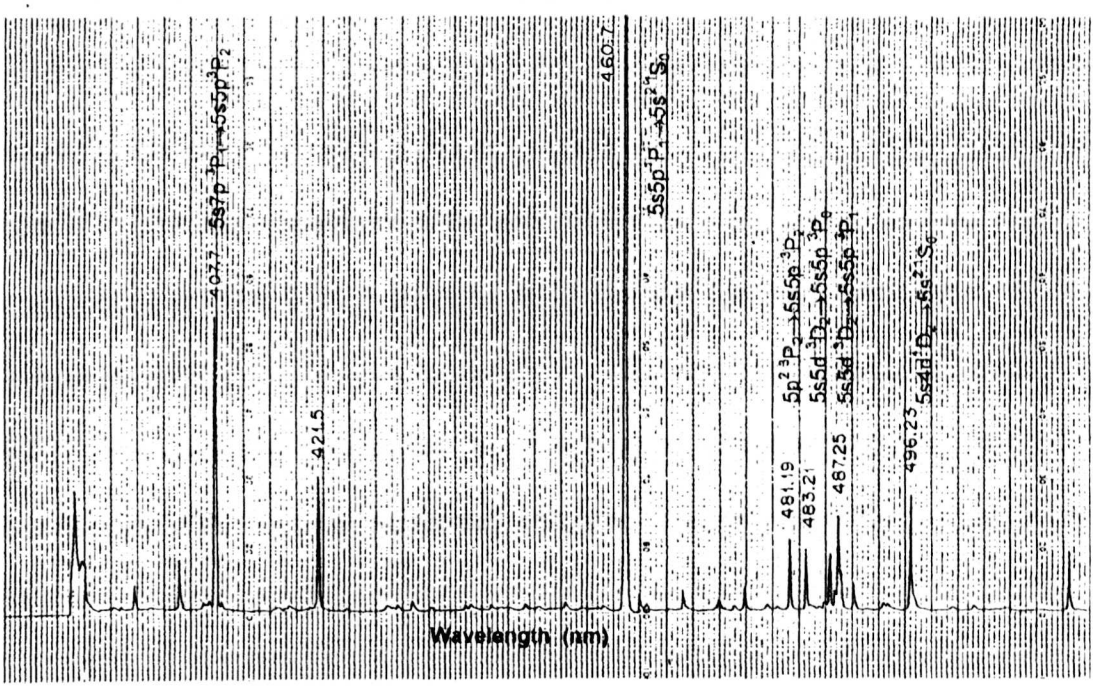

Fig. 3.8 Part of the fluorescence emission spectrum of Sr I in the heat-pipe setup recorded using Monochromator- Photomultiplier recoding system (*J. Phys. B. At. Mol. Opt. Phys.* **34**, 1, 2001)

3.4.3 Extended study of the Rydberg series of Sr I

Substantial extension and improvement on the previously published spectroscopic data in strontium was achieved by a novel experimental scheme employing an atomic jet in a heat-pipe setup (Philip 2007, Philip 2008) with efficient thermionic diode detection and improved laser beam profile with controlled intensity. A nearly collimated rectangular atomic jet (0.2 mm x 10 mm) exiting vertically upward from

a disposable effusive cartridge filled with 99.99% pure strontium (Goodfellowmetals LS136222 after purification) placed inside the central hot zone of a heat-pipe (described in Chapter 2) was intercepted orthogonally by the narrow bandwidth (0.18 cm^{-1}) tunable dye laser (LPD 3002 CES pumped by LPX 210i as discussed in Chapter 2). A single dye: coumarine 120 ((Lambdachrome LC4400) with a broad tuning range (425 nm - 460 nm) with approximately 17% efficiency was used for all the bound and autoionizing transitions observed in strontium as reported in this thesis. An efficient thermionic diode type ionization detection was used with variable bias using both DC and pulsed fields. The laser beam was linearly polarized parallel to the electric field (π-geometry to excite, both $J = 0$ and $J = 2$ series starting from $J = 0$). Laser beam intensity was controlled using non-polarizing beam-attenuators (typically 2 - 2.5 μJ/pulse at 13 Hz was the laser energy used in the experiments with good linearity for the signal detection). Ionization signals resulting from photoabsorption were fed to the boxcar averager/integrator (SR250). Wavelength calibration was performed using the previously published energy level data.

3.4.3.1 The $J=2$ even-parity $5snd$ $^{1,3}D_2$ Rydberg series of Sr I

The initial study by two-photon spectroscopy using an atomic beam in a heat-pipe setup had generated the energy level data listed in Table 3.3 for the bound even-parity $5snd$ $^{1,3}D_2$ Rydberg series accessed by direct excitation from the ground state $5s^2\ ^1S_0$. In the new study, carried out using the atomic jet and associated instrumentation discussed above, extended the energy level data for the bound $J = 2$ even-parity Rydberg series to both low and high members. Two-photon spectra recorded using the new facility covering the wavelength range 460 nm - 425 nm are

shown in figures 3.10 (a-b), Fig. 3.11 and 3.12 These spectra show the various channels of excitations such as two-photon allowed transitions to the even-parity, J = 0 and J = 2, 5s*n*d $^{1,3}D_2$ Rydberg states, two-photon forbidden excitations to the odd-parity 5s*n*p $^1P_1^0$, 5s*n*p $^3P_2^0$ and 5s*n*f $^1F_3^0$ and to the doubly-excited $5p^2$, $4d^2$,4d5p and 4d*n*s configurations. Furthermore, the spectra include a broad autoionizing resonance with a peak that corresponds to 431.22 nm wavelength for two-photon excitation from the ground state, approximately 450 cm^{-1} above the first ionization threshold.

A strong autoionizing resonance was reported by Rubbmark and Borgstrom (1978) in absorption from 5s5p $^1P_1$ at 46380 cm^{-1}. Esherick (1977) also reported the strong autoionizing resonance 450 cm^{-1} above the first ionization limit with peak at 46380cm^{-1} with a FWHM of 60 cm^{-1}. Esherick gave $4d^2$ $^1D_2$ as a possible assignment for this autoionizing resonance by polarization test. However, Esherick had some doubt on the J assignment to this broad resonance because of the inconsistency with MQDT analysis.

The multi-photon absorption spectra of strontium are found to have single-photon resonances to the 5s*n*s $^1S_0$ and 5s*n*d $^{1,3}D_2$ states besides those to the doubly excited $4d^2$ ^3P_J configuration which result from sequential excitation from the resonance level 5s5p $^1P_1$ and metastable 5s 5p ^3P_J states which are populated by electron impact excitation and molecular dissociation of Sr_2 dimers in presence of buffer gas collisions. Important one–photon transitions from 5s5p $^1P_1$ observed by Esherick to the doubly excited states are:

5s5p $^1P_1 \rightarrow$ 4d ^{2} $^3P_0$ @ 22827.4 cm^{-1}

5s5p $^1P_1 \rightarrow$ 4d ^{2} $^3P_1$ @ 22896.8 cm^{-1}

$5s5p\ ^1P_1 \rightarrow 4d^{2}\ ^3P_2$ @ 23031.0 cm^{-1}. This state was also observed by two-photon excitation from the ground state @ 44525.83 cm^{-1}.

In the study reported herein two-photon excitations to the doubly-excited states from the ground state of Sr I were observed as under:

(i) $5s^2\ ^1S_0 \rightarrow \mathbf{4d^2\ ^3P_0}$ λ_{vac} = 449.175 nm

(ii) $5s^2\ ^1S_0 \rightarrow 4d^2\ ^3P_1$ Not observed

(iii) $5s^2\ ^1S_0 \rightarrow \mathbf{4d^2\ ^3P_2}$ λ_{vac} = 446.983 nm

However, the above doubly-excited states were also populated by single-photon resonances at the following wavelengths (vacuum).

(i) $5s5p\ ^1P_1 \rightarrow \mathbf{4d^2\ ^3P_0}$ λ_{vac} = 438.07 nm

(ii) $5s5p\ ^1P_1 \rightarrow \mathbf{4d^2\ ^3P_1}$ λ_{vac} = 436.74 nm

(iii) $5s5p\ ^1P_1 \rightarrow \mathbf{4d^2\ ^3P_2}$ λ_{vac} = 434.195 nm

It has been observed that the single-photon transitions that originate from the sequential excitation following the molecular dissociation of Sr_2 dimers grow rapidly with increase in the buffer gas pressure. The intensity distribution is an essential property of the spectrum and even in the absence of perturbers there can be significant departure from the normal course of intensity distribution within a Rydberg series (n^{*-3} dependence) due to centrifugal barrier effects (Connerade 1998). Furthermore, not only the intensity distribution among the members of a series but the line profile (intensity distribution within a single line) also is important and this provides information about the environment in which the atoms are placed- the external fields and collisions. For single-photon transitions involving excitations with weak intensity radiation the electric dipole transitions are the strongest. Figure 3.9 shows the ratio of the intensities of the photoabsorption signals corresponding to single-photon excitation to those of two-photon excitation for a Rydberg state (5s11s

$^1S_0$) and a doubly-excited ($4d^2\ ^3P_0$) state. These states are populated by single-photon excitation: $5s5p\ ^1P_1 \rightarrow 5s11s\ ^1S_0$ and $5s5p\ ^1P_1 \rightarrow 4d^2\ ^3P_0$ and by two-photon excitation: $5s^2\ ^1S_0 \rightarrow 5s11s\ ^1S_0$ and $5s^2\ ^1S_0 \rightarrow 4d^2\ ^3P_0$. The spectrum was taken using argon buffer gas at 10.6 μJ / pulse laser energy.

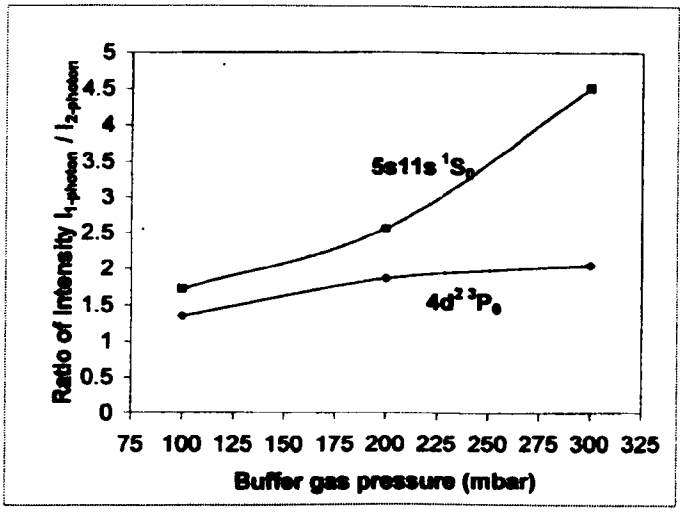

Fig.3.9 Intensity ratio for single-photon to two-photon transitions in Sr I for 100 mbar Ar buffer

Figure 3.10 (a) is a two-photon spectrum of Sr I taken with 100mbar argon in the heat-pipe setup with the atomic jet operated at 802 ± 2^0 C with +9 V bias applied to the thermionic detector. For the tuning range (460 nm – 432 nm) of the LPD 3002CES dye laser with coumarine 120 dye at 10.6 μJ energy / pulse at 13 Hz used in this experiment, all transitions are well established. Two competing excitation processes are observed: (i) direct two-photon excitation from the ground state $5s^2\ ^1S_0$ and (ii) single-photon excitations from the $5s5p\ ^1P_1$. The lowest transition identified in this spectrum is $5s^2\ ^1S_0 \rightarrow 5s10s\ ^1S_0$ which occurs at the laser wavelength 456.470 nm in air. At this pressure of argon buffer, all sequential excitations from $5s5p\ ^1P_1$ level are found to be strong and broad. In figure 3.10(b) the short wavelength (436nm - 432nm) region of the two-photon spectrum shown in figure 3.10(a) is reproduced for enhanced clarity for the single-photon transitions.

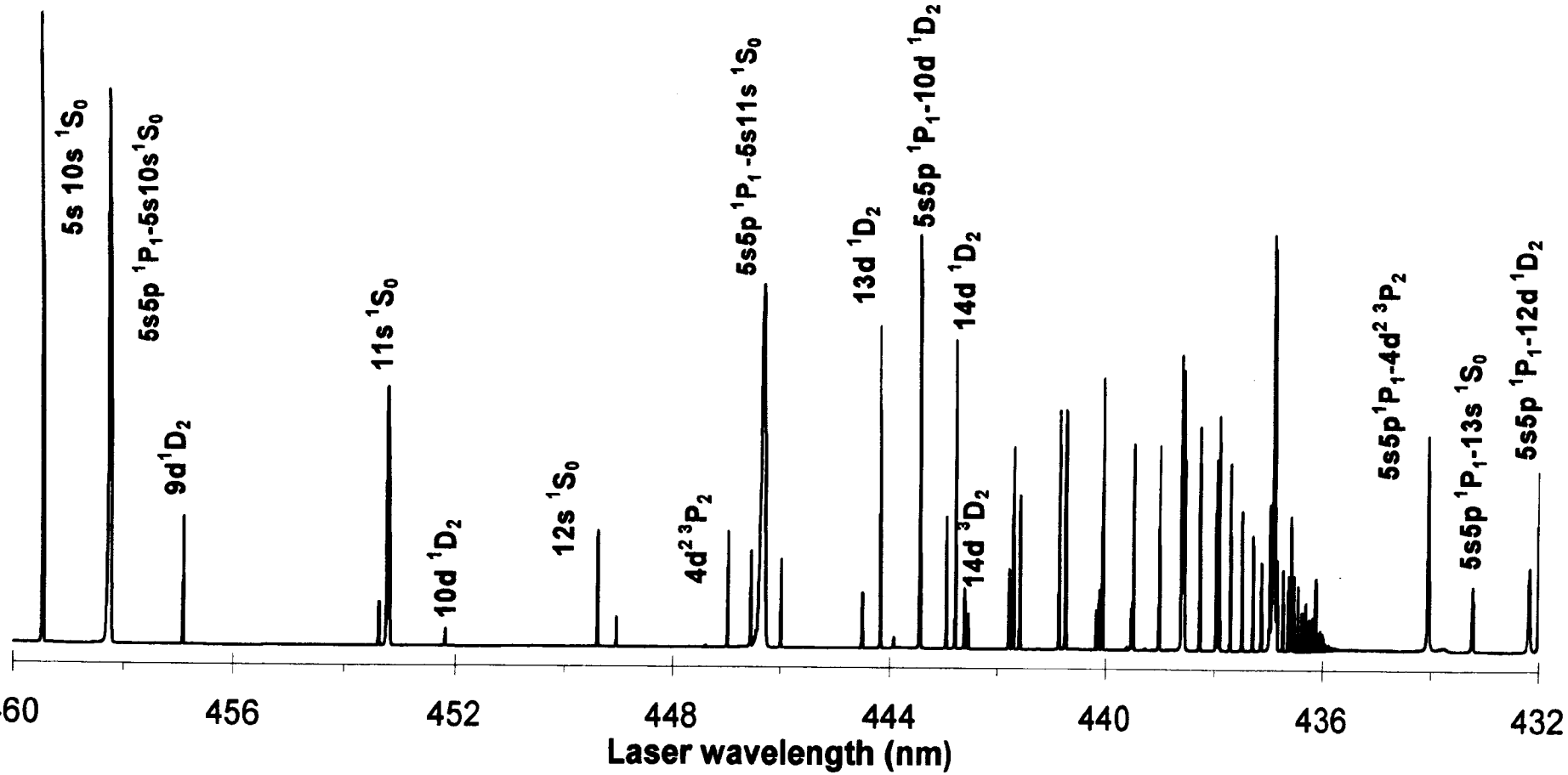

Fig. 3.10(a) Two-photon spectrum of Sr I with 100 mbar Ar buffer showing two modes of excitations: excitations from the 5s5p $^1P_1$ states are shown with two-photon excitations from the ground state 5s^2 $^1S_0$

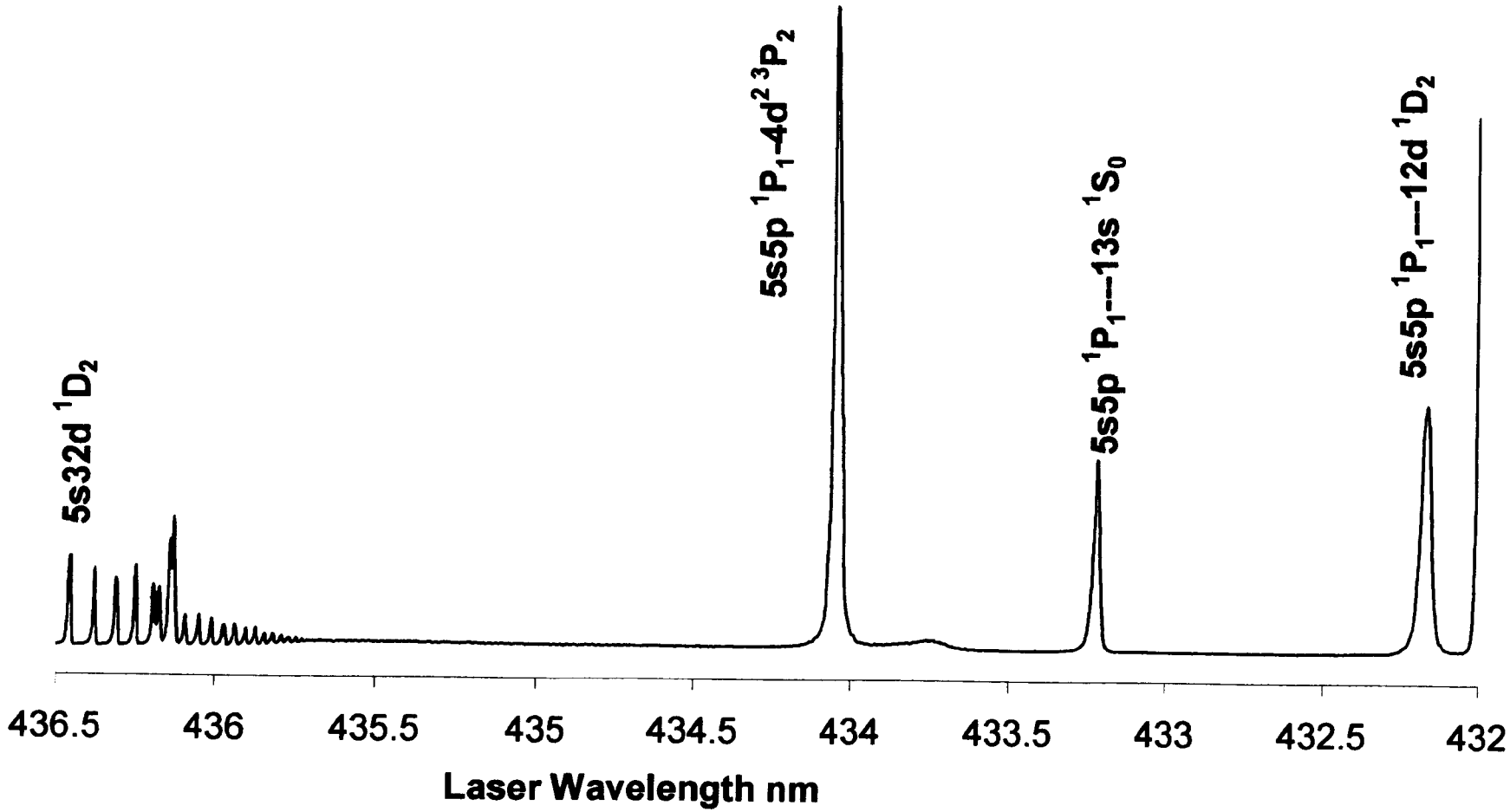

Fig. 3.10 (b) Two-photon spectrum of Sr I with 100 mbar Ar buffer showing some prominent single-photon transitions from 5s5p $^1P_1$ state

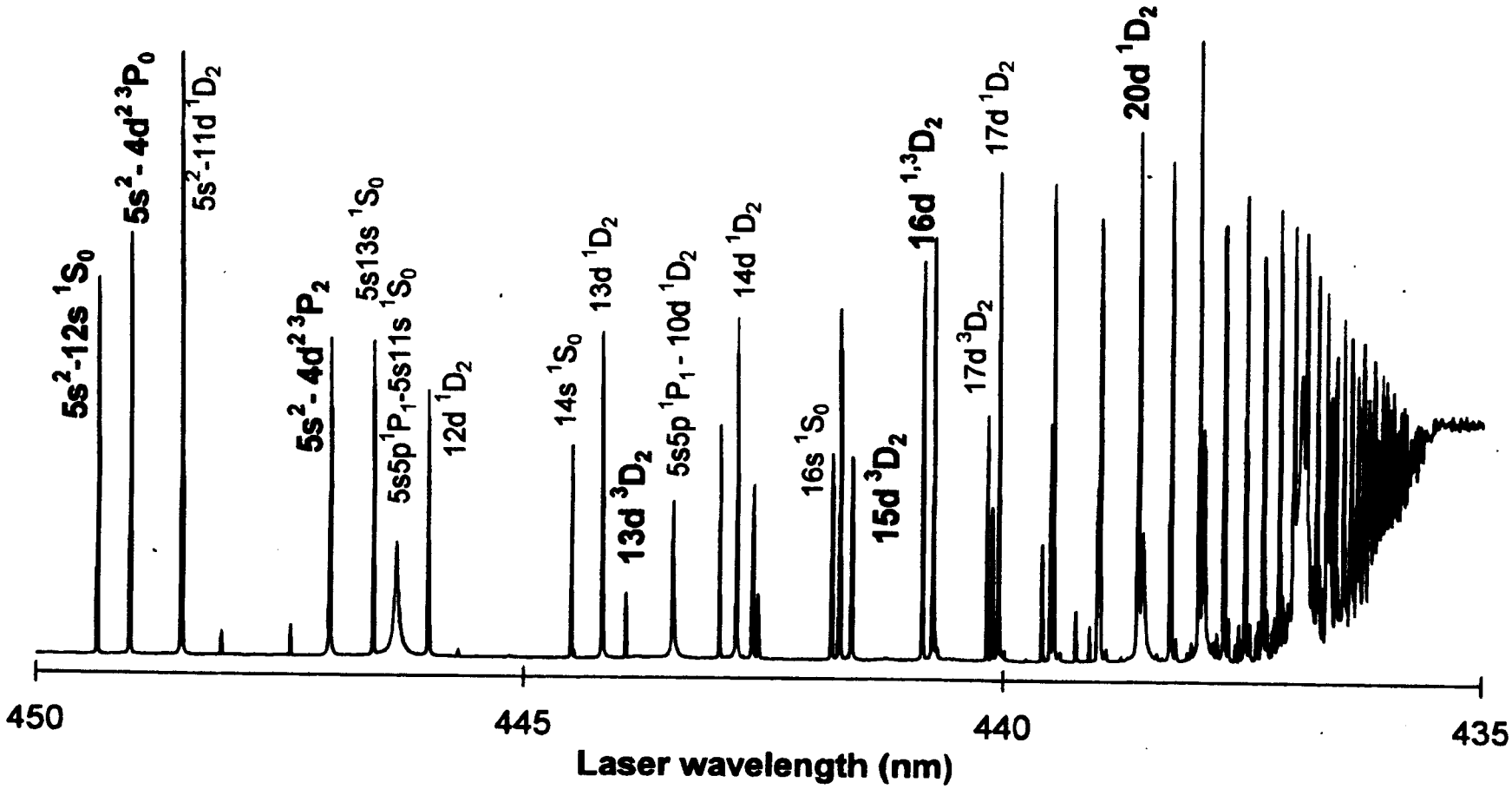

Fig. 3.11 Two-photon spectrum showing the even-parity $J = 0$, and $J = 2$, 5s*n*d $^{1,3}D_2$ Rydberg series of Sr I (20 mbar Ar buffer and 2μJ dye laser energy/pulse)

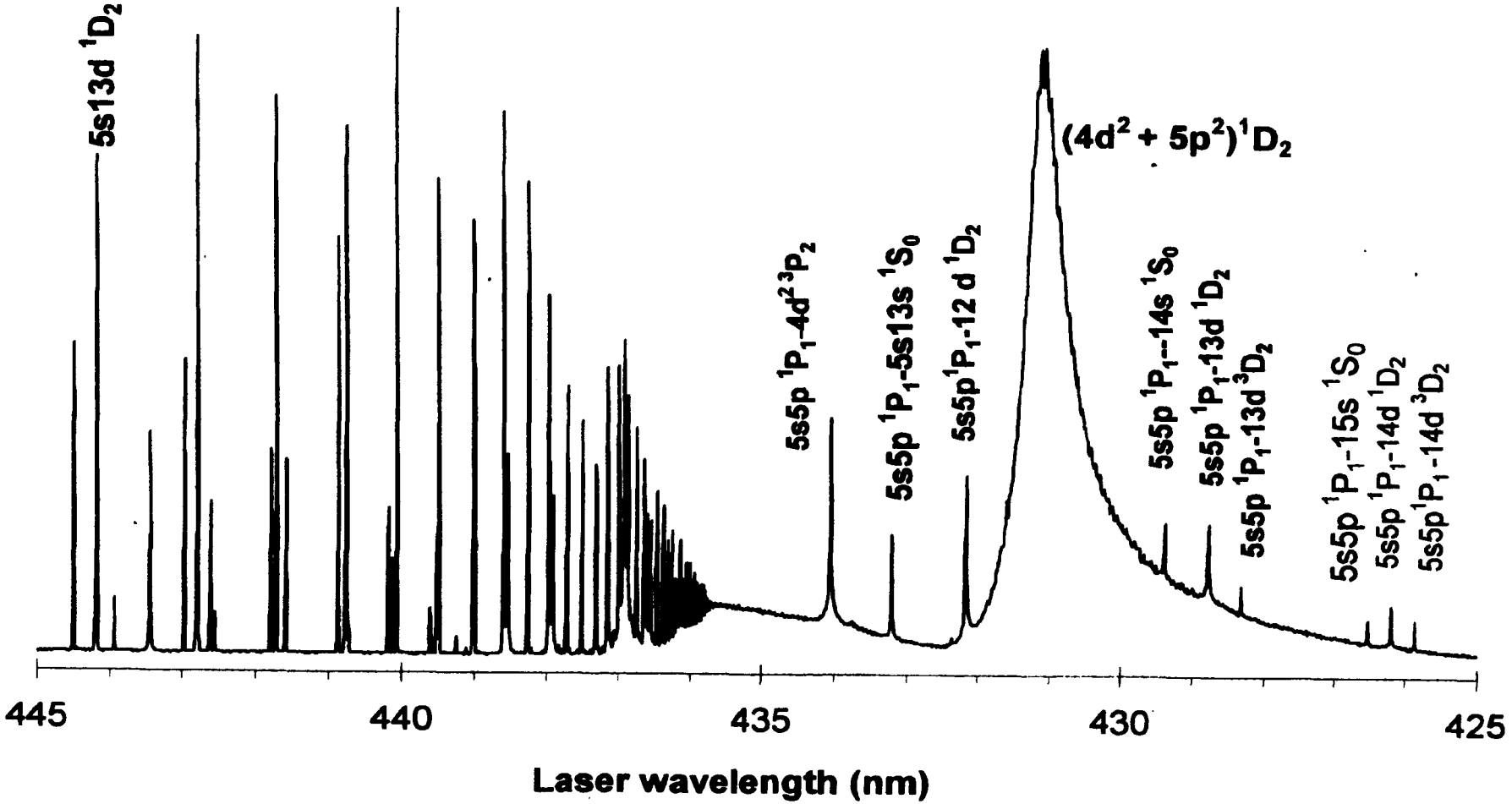

Fig. 3.12 Two-photon spectrum of the $J = 0$, and $J = 2$, 5s*n*d $^{1,3}D_2$ Rydberg series of Sr I and the autoionizing resonance. (40 mbar He buffer and 2μJ dye laser energy/pulse)

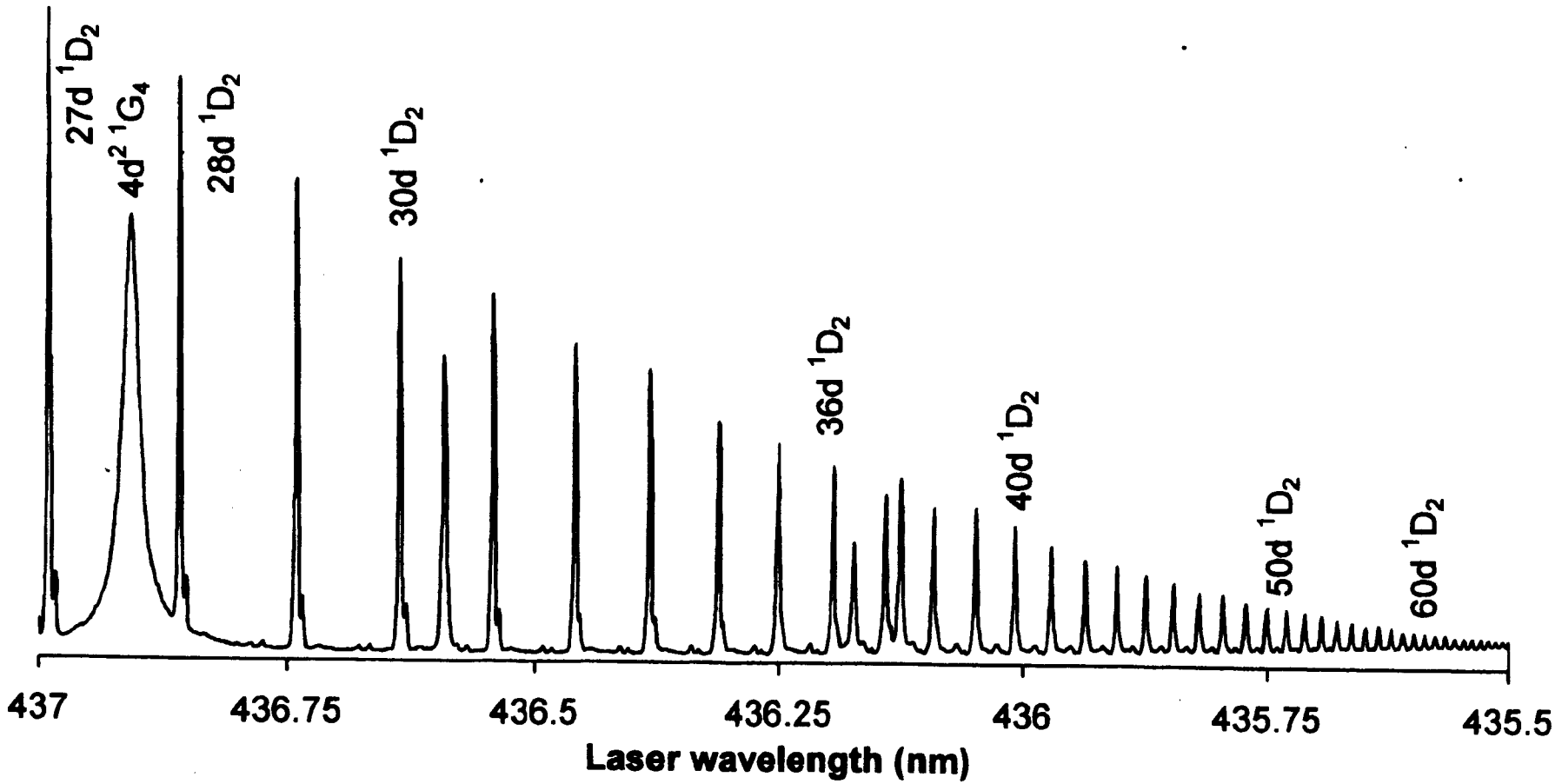

Fig. 3.13 Two-photon spectrum of Sr I in the wavelength range 437 nm → 435.5nm (40mbar He buffer) showing high ($27 < n < 70$) members of the $5snd\,^1D_2$ Rydberg series (*Opt. Commun.* **266,** 253, 2006)

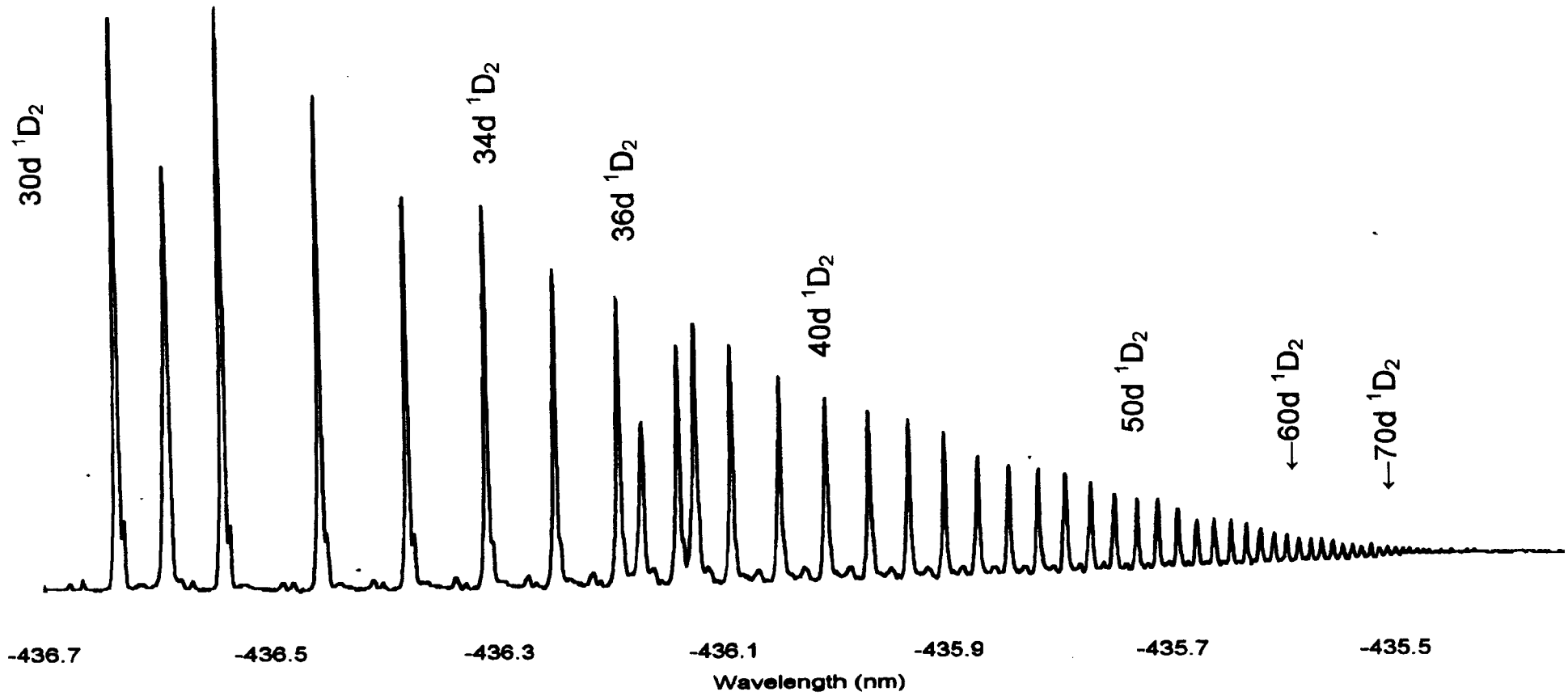

Fig.3.14 Two-photon spectrum of Sr I in the wavelength range 436.7nm → 435.4nm (20 mbar Ar buffer). High members of the $5snd^1D_2$ Rydberg series can be followed for $n \geq 75$. Forbidden transitions are also observed as weak satellites between successive Rydberg members

3.4.3.2Extension of the $J = 2$ even-parity $5snd\ ^1D_2$ Rydberg series of Sr I

Previous data for the $J = 2$, $5snd\ ^1D_2$ Rydberg series have been extended to present the new energy level data for neutral strontium. The two-photon spectra extending to high-lying members of the $5snd\ ^1D_2$ Rydberg series are shown in figures 3.13 and 3.14. Table 3.4 gives the energy level data for very high members of the $5snd\ ^1D_2$ Rydberg series covering the range $74 < n < 82$. This is believed to be the first time extension in the literature to such high principal quantum numbers for these Rydberg members using two-photon spectroscopy in similar experiments.

Table 3. 4

THESIS extension of Energy Levels of Strontium $5snd\ ^1D_2$ Rydberg series. Comparison with data in the literature

Principal Quantum Number n	Level Label	Laser Wavelength λ_{vac} (nm)	Energy Level Thesis cm^{-1}	Energy Level * Esherick Expt.cm^{-1}	Energy Level Dai** Expt.cm^{-1}
74	5s74d $^1D_2$	435.634	**45910.132**	-	45910.81
75	5s75d $^1D_2$	435.629	**45910.660**	-	45911.39
76	5s76d $^1D_2$	435.623	**45911.291**	-	-
77	5s77d $^1D_2$	435.619	**45911.696**	-	-
78	5s78d $^1D_2$	435.614	**45912.187**	-	-
79	5s79d $^1D_2$	435.610	**45912.612**	-	45913.50
80	5s80d $^1D_2$	435.606	**45912.020**	-	45913.98
81	5s81d $^1D_2$	435.602	**45913.469**	-	-
82	5s82d $^1D_2$	435.598	**45913.877**	-	-

* Esherick P., *Physical Review* **A. 15**, 1920 (1977)

** Dai C.J. , *Physical Review* **A 52,** (6). 4416 (1995)

Table 3.5

THESIS extension of Energy Levels of low n members of Strontium $5snd\ ^{1,3}D_2$ Rydberg series -Comparison with data in the literature

Principal Quantum Number n	Level Label	Laser Wavelength λ_{vac} (nm)	Energy Level Thesis cm^{-1}	Energy Level Esherick* Expt. cm^{-1}	Energy Level Dai** Expt.cm^{-1}
9	5s9d $^1D_2$	457.050	**43758.8**	43755.88	43755.98
	5s9d $^3D_2$	-	--	43804.89	43804.69
10	5s10d $^1D_2$	-		44241.70	44241.86
	5s10d $^3D_2$			44287.05	44286.91
11	5s11d $^1D_2$	-		44578.58	44578.6
	5s11d $^3D_2$			44620.08	44619.84
12	5s12d $^1D_2$	446.137	**44829.28**	44829.40	44829.47
	s12d $^3D_2$			44860.28	44859.31
13	5s13d $^1D_2$	444.330	**45011.59**	45011.77	45011.81
	5s13d $^3D_2$	444.085	**45036.42**	45036.85	45036.52
14	5s14d $^1D_2$	442.940	**45152.84**	45153.10	45153.03
	5s14d $^3D_2$	442.760	**45171.20**	45171.54	45171.43
15	5s15d $^1D_2$	441.855	**45263.72**	45263.62	45263.62
	5s15d $^3D_2$	441.730	**45276.53**	45276.62	45276.45
16	5s16d $^{1,3}D_2$	441.010	**45350.44**	45350.35	45350.57
	5s16d $^{1'3}D_2$	440.900	**45361.80**	45362.03	45362.17
17	5s17d $^3D_2$	440.325	**45421.00**	45420.78	45421.04
	5s17d $^1D_2$	440.205	**45433.38**	45433.14	45433.26
18	5s18d $^3D_2$	439.755	**45479.87**	45479.88	45479.92
	5s18d $^1D_2$	439.635	**45492.28**	45492.48	45492.74
19	5s19d $^3D_2$	439.118	**45530.29**	45530.17	45530.53
	5s19d $^1D_2$	439.155	**45542.01**	45542.12	45542.54$

$ Calculated value

* Esherick P., *Physical Review* **A. 15**, 1920 (1977)

** Dai C.J. , *Physical Review* **A 52,** (6). 4416 (1995)

Table 3.5 (contd..)

THESIS extension of Energy Levels of low n members of Sr I 5s*n*d $^{1,3}D_2$ Rydberg series -Comparison with data in the literature

Principal Quantum Number *n*	Level Label	Laser Wavelength λ_{vac} (nm)	Energy Level Thesis cm^{-1}	Energy Level Esherick* Expt. cm^{-1}	Energy Level Dai** Expt.cm^{-1}
20	**5s20d $^3D_2$**		---	----	45573.51$
	5s20d $^1D_2$	438.75	**45584.05**	45584.17	45584.23
21	**5s21d $^3D_2$**	----	---	----	45610.12$
	5s21d $^1D_2$	438.41	**45619.40**	45619.60	45619.63
22	**5s22d $^3D_2$**	----	---	45641.68	45641.69
	5s22d $^1D_2$	438.115	**45650.11**	45650.26	45650.27
23	**5s23d $^3D_2$**	----	---	45669.14	45669.09
	5s23d $^1D_2$	437.865	**45676.18**	45676.51	45676.49
24	**5s24d $^3D_2$**	----	---	45692.81	45692.84
	5s24d $^1D_2$	437.645	**45699.14**	45699.25	45699.31

$ Calculated value
* Esherick P., *Physical Review* **A. 15**, 1920 (1977)
** Dai C.J. , *Physical Review* **A 52,** (6). 4416 (1995)

Previously published energy level values for the members of the 5s*n*d $^{1,3}D_2$ Rydberg series are also extended to lower principal quantum numbers covering the lower range $9 < n < 24$ and are presented in Table 3.5. The energy level values have excellent agreement with data in the literature by other authors who used different experimental schemes.

Unlike in the sequential excitation (5s5p $^1P_1 \rightarrow$ 5s*n*d $^{1,3}D_2$) spectra (Baig *et al* 1999) in which the $^1D_2$ members were much weaker than the corresponding $^3D_2$ members and only $^3D_2$ members were observed beyond $n > 19$, the two-photon spectra ($5s^2\ ^1S_0 \rightarrow$ 5s*n*d $^{1,3}D_2$ transitions) reported in this study show all $^1D_2$ members stronger than

the corresponding $^3D_2$ members (except for the region of strong singlet-triplet mixing). Another important observation is that in the sequential excitation spectra, the transition probabilities for 5s*n*p $^1P_1 \rightarrow$ 5s*n*d $^{1,3}D_2$ are higher compared to that for the 5s5p $^1P_1 \rightarrow$ 5s*n*s $^1S_0$ transitions because in the former case ΔS, ΔL and ΔJ change in the positive direction (+1) while for the latter the change is in the negative direction (-1). This explains why the 5s*n*s $^1S_0$ series were not observed in the sequential excitation by Baig *et al* (1999).

3.4.3.3 The $J = 0$ even-parity 5s*n*s $^1S_0$ Rydberg series of Sr I

In figure 3.11 the two-photon spectrum covering the range 450 nm – 435 nm is presented indicating typical transitions observed. Since a linearly polarized (π-excitation) laser beam was used in all the experiments reported in this thesis, strong two-photon absorption resonances are also observed for the transitions to the $J = 0$, even-parity states. The lowest $J = 0$, 5s*n*s $^1S_0$ transition observed was identified as 5s10s $^1S_0$ as in figure 3.10(a) at the two-photon wavelength 459.619 nm in air. The next member of this series is observed as a strong transition as in figure 3.10 (a) at the two-photon wavelength 453.365 nm in air. In Fig. 3.11 the lowest member of the 5s*n*s $^1S_0$ series is identified as 5s12s $^1S_0$ at an energy level 44492.69 cm^{-1} which is followed by the transition 5s^2 $^1S_0 \rightarrow$ 4d^2 $^3P_0$ at 44526.18 cm^{-1}. This series can be followed till $n = 19$ and beyond $n = 20$ suddenly disappears. At $n = 21$ these series merge with the 5s*n*d $^1D_2$ Rydberg members. However, the higher members of this series reappear, identifiable at $n \geq 26$ and up to $n \sim 46$ by suitably controlling the excitation conditions like the static electric field, collisions, laser beam intensity etc. (Philip and Connerade 2007).

In the spectrum shown in figure 3.15 (a) covering the 6nm wavelength range (438 nm – 444 nm range) with the exciting dye laser beam attenuated to deliver 2.1μJ energy/pulse at the heat-pipe maintained at 830 ± 2 ^{0}C with 20 mbar argon gas (99.99% pure) buffer and with +9 volts biasing of the detector, 5s (n+1) $^1S_0$ Rydberg members appear on the lower energy side of the 5snd $^1D_2$ series up to n ~ 19 and suddenly disappear around n ~ 20. Further, the 5s(n+1)s $^1S_0$ series swaps over with 5snd $^1D_2$ series at n ~ 23 and thereafter appears on the higher energy side of 5snd $^1D_2$ series. Due to singlet-triplet mixing of the 5snd $^{1,3}D_2$ series at $n \approx 16$ and due to the degeneracy with 4d6s $^1D_2$, the level 5s17s $^1S_0$ is absent in figure 3.15(a).

In Table 3.6 energy level data for the Sr I-5sns $^1S_0$ Rydberg series are presented for the range 12 < n < 46 and compared with those from earlier studies by Esherick (1977) and Rubbmark and Borgstrom (1978). Esherick (1977) observed the 5sns $^1S_0$ series members up to n = 21 by two-photon excitation from the ground state whereas Rubbmark and Borgstrom (1978) could excite this series up to n = 36 by single-photon absorption from the 5s5p $^1P_1$ level. Mende and Kock (1997) observed forbidden transitions to the even-parity 5snd $^1D_2$ and 5sns $^1S_0$ states due collisional formation of Sr_2 dimers in the measurement of the oscillator strength of Sr I principal series. Figure 3.15(b) shows a two-photon spectrum taken with all conditions identical to the spectrum shown in figure 3.15(a) except that the detector bias was set to zero to isolate any possible electric field-induced 'ℓ' mixing and forbidden transitions. Since the relative intensity of the 5sns $^1S_0$ series is not affected by removing the external electric field it can be inferred that this series is not electric field-induced. An important observation is that the interloper which is the 5s5p $^1P_1$ → 5s12s $^1S_0$ appearing past the transition 5s20d $^1D_2$ in figure 3. 15(a) is absent in figure. 3. 15(b).

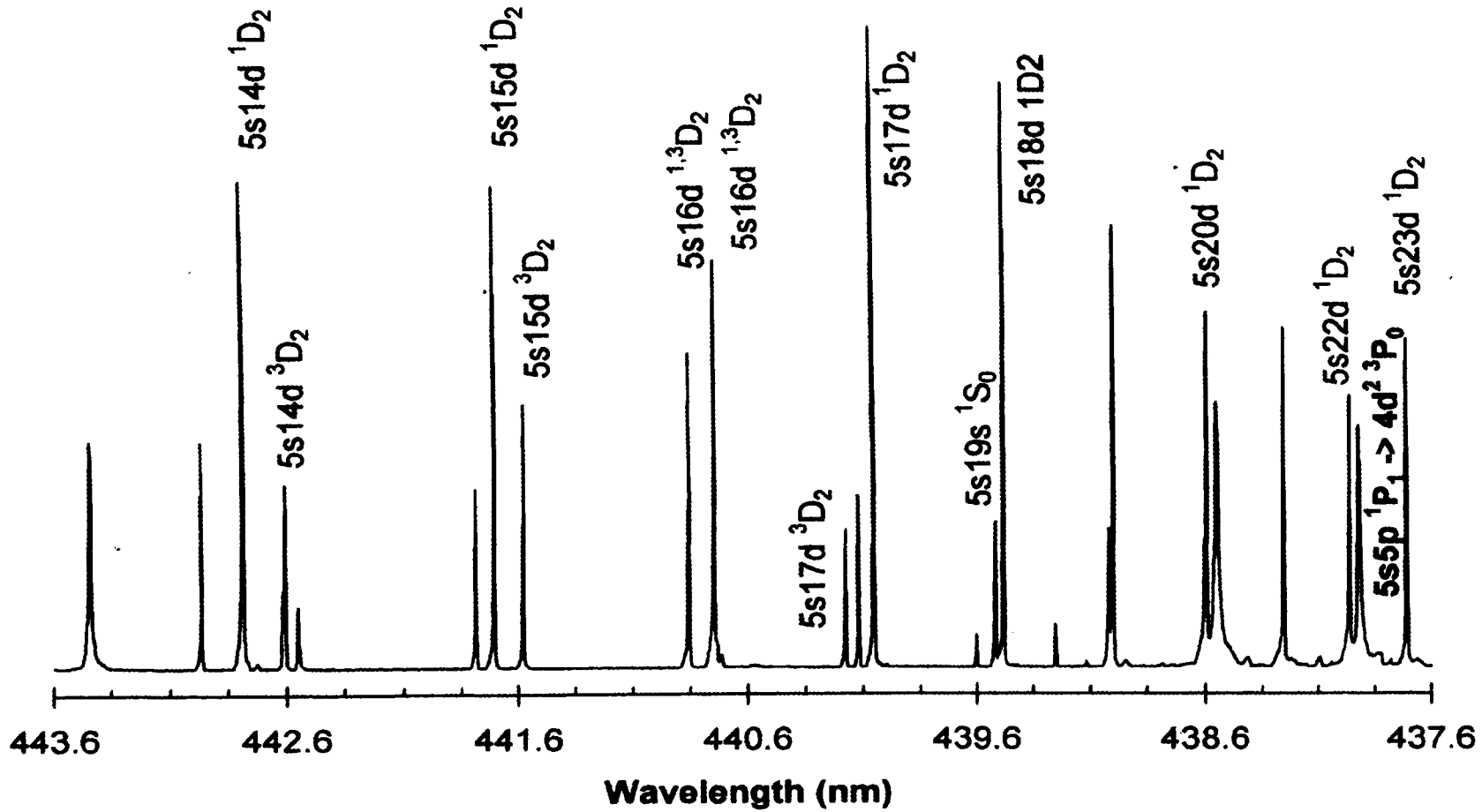

Fig.3.15(a). Two-photon spectrum of Sr I showing low members of the J = 0, 5sns $^1S_0$ and the J = 2, 5snd $^{1,3}D_2$ Rydberg series

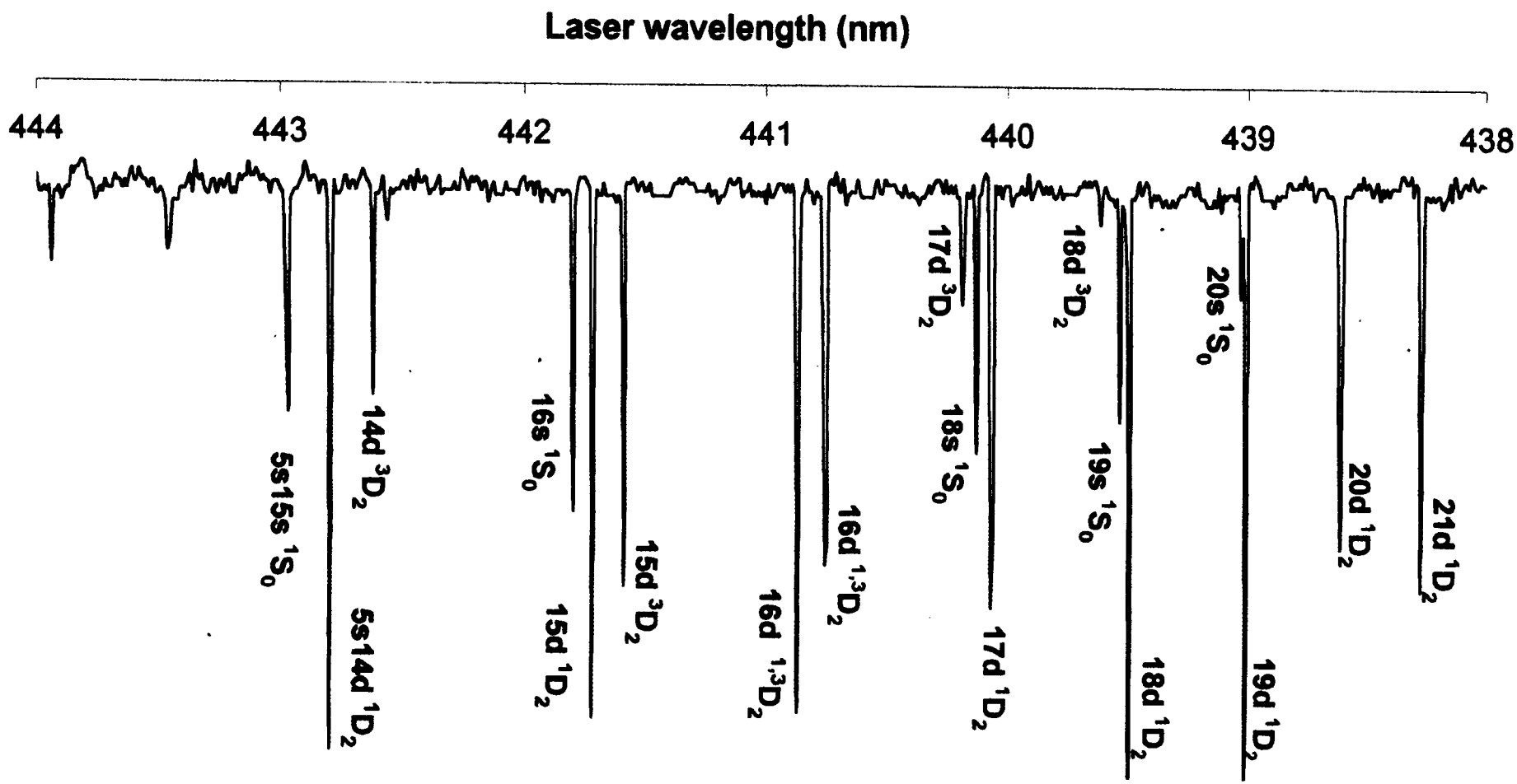

Fig. 3.15 (b) Two-photon spectrum of Sr I in the wavelength range 443.6 nm → 476.8 nm recorded with detector bias set to zero. Singlet–triplet swap over around n = 16 can be seen clearly. (*Opt. Commun.* **279,** 141, 2007)

A two-photon spectrum of Sr I for the laser wavelength range 438 nm - 435.5nm taken with 20 mbar argon buffer and 4.8 volt thermionic diode detector bias is shown in figure 3.15(c). In this spectrum most of the weak satellites are quenched and the excitations are predominantly to the $J = 2$, 5s*n*d $^1D_2$ states. However, the sequential excitations from the intermediate level 5s5p $^1P_1$ are also relatively strong to the doubly excited $4d^2\ ^3P_0$ and $4d^2\ ^1G_4$ states.

In figure 3.15(d) two-photon spectrum taken for the same wavelength range, but with the detector bias set to zero is shown. It can be seen that the two-photon allowed transitions to the 5s*n*d $^1D_2$ Rydberg states are all preserved with intensity following the n^{*-3} law (approximately) as in figure 3.15 (c). Also it can be seen that the single-photon excitations are all quenched in the spectrum taken with zero detector bias. However, the features of the spectrum shown in figure 3.15 (c) are all preserved in the spectrum shown in figure 3.15(d). The small drift in the baseline below the series limit is the experimental artifact.

The effects of exciting laser intensity and buffer gas pressure and composition on the two-photon spectra can be observed in the spectra shown in figures 3.16 (a) and 3.16 (b) taken at enhanced laser beam intensity (laser energy set at 12 μJ/ pulse). In figure 3.16 (a) measurements using helium gas (99.99%pure) at 40 mbar pressure and keeping other experimental conditions same as in figure 3.13 (a) 5s*n*s $^1S_0$ series members are observed up to $n \sim 46$, and the energy level values are given in Table 3.6.

Figure 3.16(b) shows a part of the spectrum taken after adding 60 mbar argon to the 40 mbar helium buffer, with conditions otherwise the same as in figure 3.16(a).

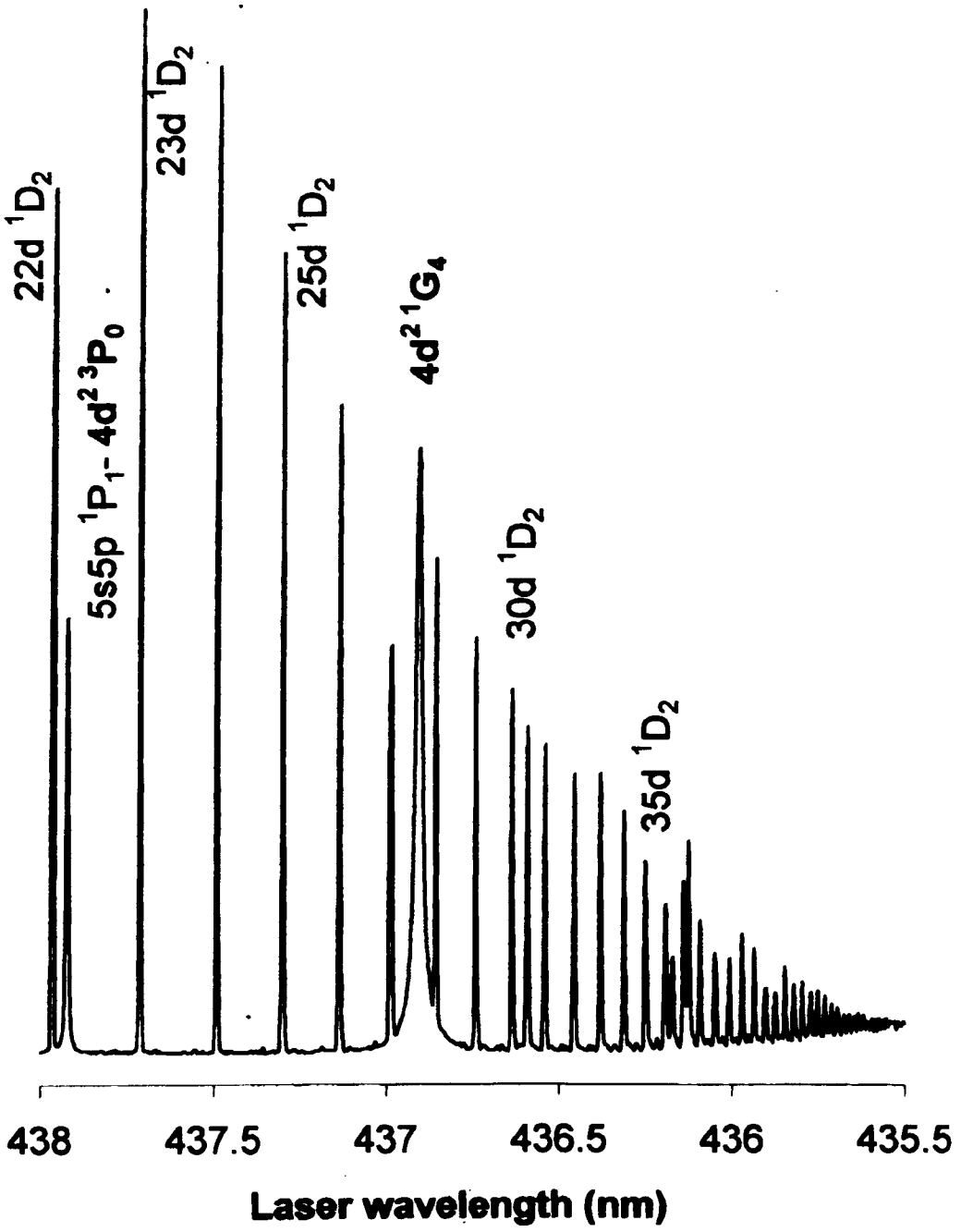

Fig. 3.15 (c) Two-photon spectrum of Sr I showing highly excited states for the laser two-photon wavelength range indicated. Strong single-photon resonances to the doubly excited states can be seen in the spectrum taken with 20 mbar Ar buffer and +4.8 volt bias for the thermionic detector.

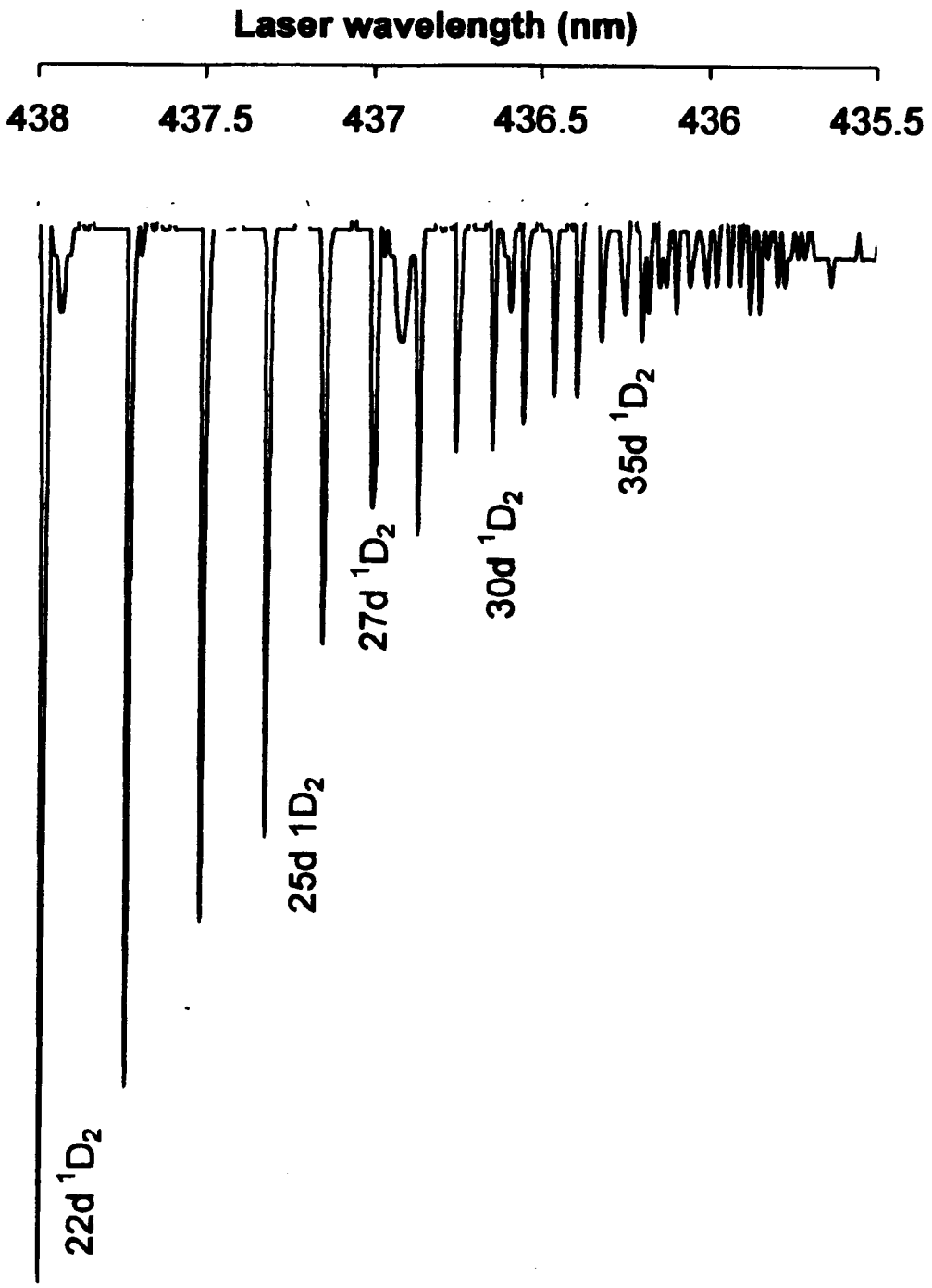

Fig. 3.15 (d) Two-photon spectrum of Sr I showing highly excited states for the laser two-photon wavelength range indicated. Single-photon resonances to the doubly excited states are all quenched in the spectrum taken with 20 mbar Ar buffer and zero volt bias for the thermionic detector. The baseline shift near the series limit is an experimental artifact.

Table 3.6
Energy level values for the $J = 0$ even-parity members of the Sr I Rydberg series $5s^2\,{}^1S_0 \rightarrow 5sns\,{}^1S_0$ (*Opt. Commun.* **279**, 141, 2007)

Principal Quantum Number *n*	Level designation	Two-photon Wavelength (λ_{vac}) nm Present Expt.	Energy level E_n cm^{-1} Thesis Expt.	Esherick[$] Expt. & MQDT*calc.	Rubbmark& Borgstrom[+] Expt.
12	$5s12s\,{}^1S_0$	449.512	**44492.69**	44492.83	44492.81
13	$5s13s\,{}^1S_0$	446.693	**44773.48**	44773.36	44773.66
14	$5s14s\,{}^1S_0$	444.651	**44979.09**	44979.25	44979.42
15	$5s15s\,{}^1S_0$	443.115	**45135.01**	45134.88	45134.89
16	$5s16s\,{}^1S_0$	441.940	**45255.02**	45255.31	45255.24
17	$5s17s\,{}^1S_0$	441.010	**45350.45**	45350.35	45350.21
18	$5s18s\,{}^1S_0$	440.270	**45426.67**	45426.52	45426.54
19	$5s19s\,{}^1S_0$	439.670	**45488.66**	45488.74	45488.77
20	$5s20s\,{}^1S_0$	---------	----------	45540.10*	45540.17
21	$5s21s\,{}^1S_0$	---------	----------	45583.18*	45583.15
22	$5s22s\,{}^1S_0$	---------	----------	45619.43*	45619.44
23	$5s23s\,{}^1S_0$	---------	----------	45650.33*	----------
24	$5s24s\,{}^1S_0$	---------	----------	45676.86*	45676.87
25	$5s25s\,{}^1S_0$	---------	----------	45699.82*	45699.82
26	$5s26s\,{}^1S_0$	437.446	**45719.92**	45719.82*	45719.83
27	$5s27s\,{}^1S_0$	437.281	**45737.18**	45737.34*	45737.35
28	$5s28s\,{}^1S_0$	437.133	**45752.67**	45752.78*	45752.80
29	$5s29s\,{}^1S_0$	437.001	**45766.49**	45766.45*	45766.48
30	$5s30s\,{}^1S_0$	436.887	**45778.43**	45778.62*	45778.65
31	$5s31s\,{}^1S_0$	436.782	**45789.43**	45789.49*	45789.49
32	$5s32s\,{}^1S_0$	436.690	**45799.08**	45799.25*	45799.22
33	$5s33s\,{}^1S_0$	436.604	**45808.10**	45808.05*	45808.01
34	$5s34s\,{}^1S_0$	436.528	**45816.08**	45815.99*	45816.00
35	$5s35s\,{}^1S_0$	436.460	**45823.21**	45823.20*	45823.13
36	$5s36s\,{}^1S_0$	436.399	**45829.62**	45829.76*	45829.81
37	$5s37s\,{}^1S_0$	436.344	**45835.40**	45835.74*	
38	$5s38s\,{}^1S_0$	436.289	**45841.17**	45841.22*	
39	$5s39s\,{}^1S_0$	436.245	**45845.80**	45846.24*	
40	$5s40s\,{}^1S_0$	436.203	**45850.21**	45850.85*	
41	$5s41s\,{}^1S_0$	436.161	**45854.63**		
42	$5s42s\,{}^1S_0$	436.122	**45858.73**		
43	$5s43s\,{}^1S_0$	436.089	**45862.20**		
44	$5s44s\,{}^1S_0$	436.056	**45865.67**		
45	$5s45s\,{}^1S_0$	436.027	**45868.72**		
46	$5s46s\,{}^1S_0$	435.998	**45871.77**		

[$]Esherick P, *Phys. Rev.* A **15**, 1920 (1977)
[+]Rubbmark J.R. and Borgstrom S.A, *Phys. Scr.***18**, 196 (1978)

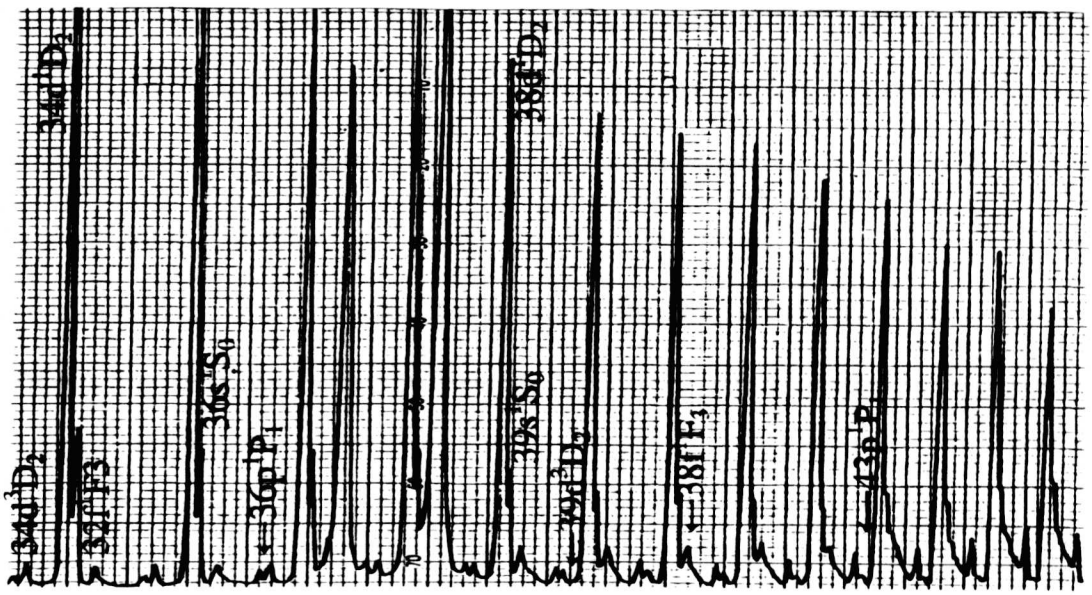

Fig. 3.16 (a) Two-photon spectrum of Sr I with 40 mbar He showing 5s*n*s $^1S_0$ and the forbidden $^1P_1$ and $^1F_3$ series. Detection by +9 volt DC

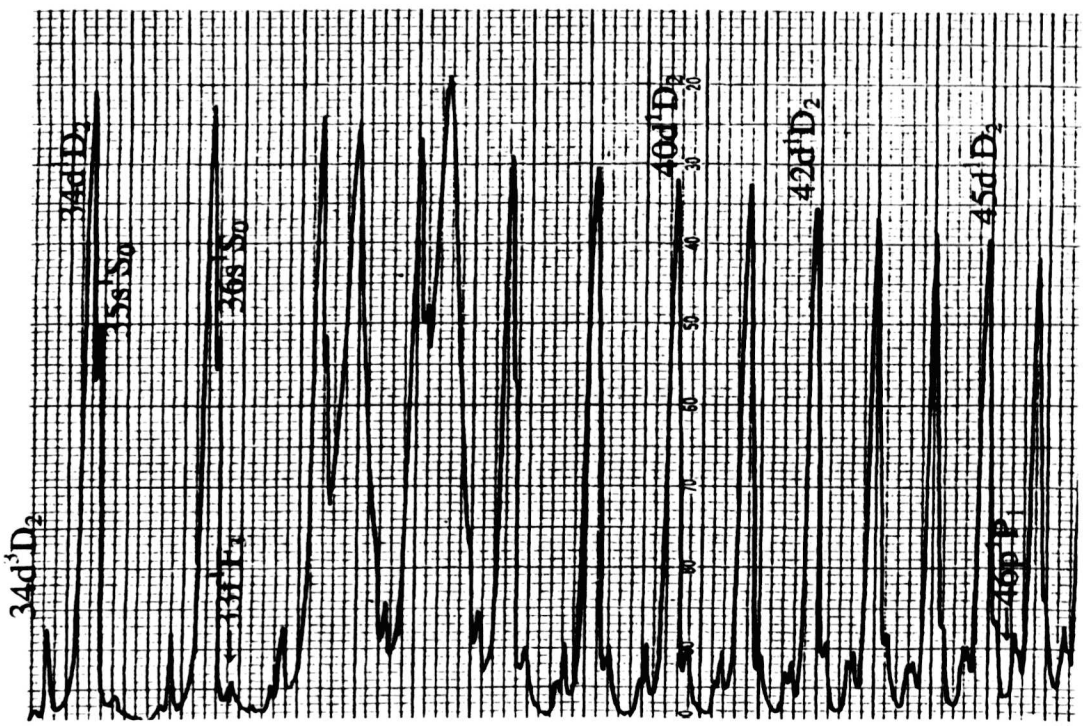

Fig.3.16 (b) Two-photon spectrum of Sr I @ (40 mbar He + 60 mbar Ar) showing 5s(*n*+1)s $^1S_0$ members on the blue wing of 5s*n*d $^1D_2$ members. Forbidden 5s*n*p $^1P_1$ and 5s*n*f $^1F_3$ series are also seen. Detection by +9 volt DC (*Opt. Commun.* **279,** 141, 2007)

The enhancement of the intensity of the $5s^2\ ^1S_0 \rightarrow 5sns\ ^1S_0$ transitions by increasing the argon buffer gas partial pressure suggests an increase in the probability of the formation of Sr_2 and Sr*-Ar dimers at moderately high composition and / or changes in their ionization properties in the exciting region. However, due to the Ramsauer effect in argon, $5s(n+1)s\ ^1S_0$ Rydberg members are red-shifted and merge with the $5snd\ ^1D_2$ series. This is why they cannot be resolved beyond $n = 36$ in figure 3.16(b) whereas the same series can be seen up to $n = 46$ with 40 mbar helium (figure 3.16(a)).

Ramsauer-Townsend effect discovered in 1921 represents the existence of a sharp minimum in the cross section for low-energy electron scattering by heavy noble gas atoms, argon krypton and xenon (around 0.7 eV for argon). The collision cross section decreases with increasing electron energy (the scattering length is negative) leading to a minimum value in the cross section (Brode 1933) .Such a minimum is a manifestation of the polarization of the atomic core by the scattered electron (Johnson and Guet 1994). Since the scattering length is negative the energy shifts due to collision (pressure shift) by Ar, Kr and Xe are negative (redshift) whereas collisions by He and Ne give rise to positive shifts (blue shifts) because the scattering lengths are positive for them. These effects can be easily observed in collisions involving Rydberg states where the inelastic scattering of the slow Rydberg electron by the perturber atom and the long range polarization interaction between the Rydberg atom ionic core and the perturber dominate at intermediate and high values of the principal quantum number n.

In figure 3.17 the relative strength of two-photon transition signals for the stated two buffer gas compositions are shown. Although enhancement is observed in moderate

argon pressures, at high pressures, (> 100mbar), the 5s*n*s $^1S_0$ series could not be observed beyond 19s $^1S_0$. This arises because the electric field to pressure (E/p) ratio is drastically altered: the indications are that the buffer gas pressure alone is not responsible for the excitation. The number density of strontium atoms relative to argon and the polarizability of the buffer gas are also important in the enhancement of these transitions to $J = 0$ states.

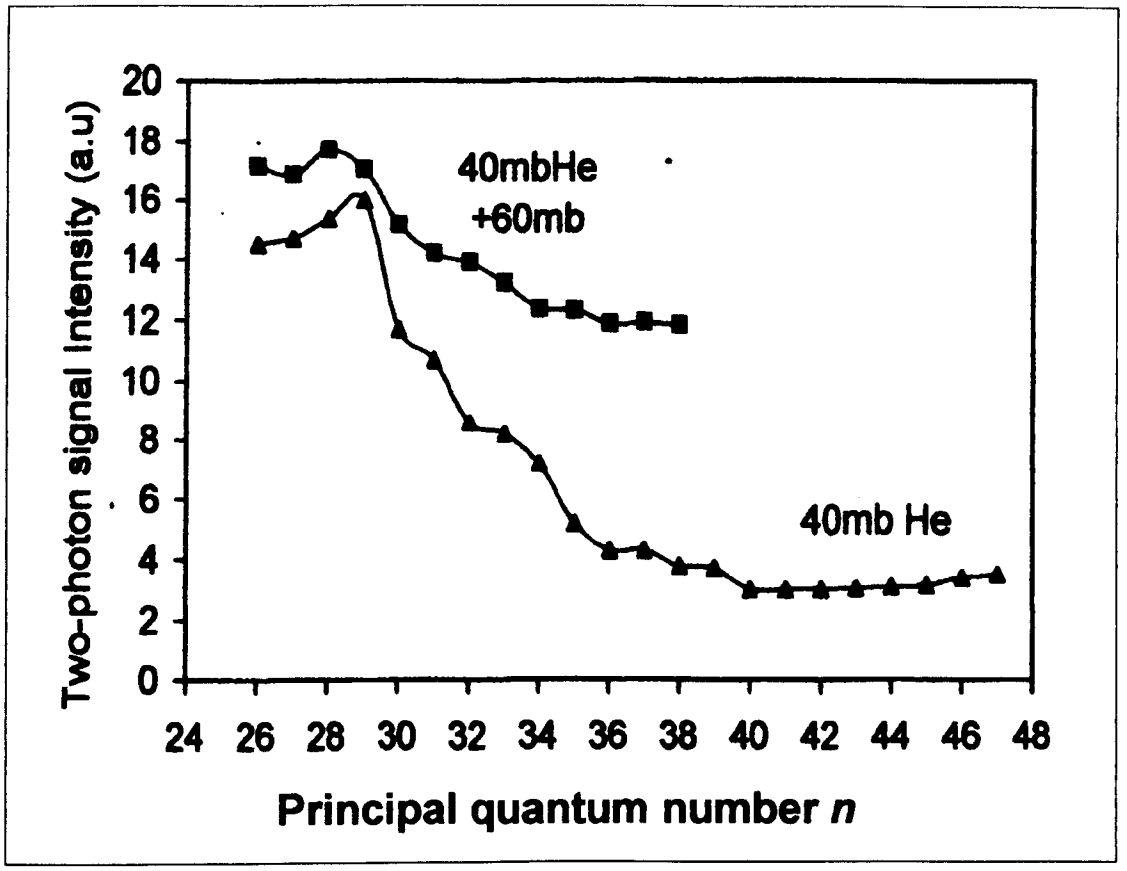

Fig. 3.17 Relative signal strength for the two-photon transitions to 5s*n*s $^1S_0$ Rydberg states at two compositions of the buffer gas

3.4.3.4 The controlled excitation of two-photon Forbidden $5s^2\ ^1S_0 \rightarrow 5snp\ ^1P_1$ and $5s^2\ ^1S_0 \rightarrow 5snf\ ^1F_3$ transitions by using collisions and electric fields

In figure 3.15 (a) weak transitions appearing towards high n beyond 5s18d $^1D_2$ are identified as the lower members of the $5s^2\ ^1S_0 \rightarrow 5snp\ ^1P_1$ and $5s^2\ ^1S_0 \rightarrow 5snf\ ^1F_3$ odd-parity transitions which are two-photon forbidden by parity and selection rules. These states are completely absent from the spectra taken without external electric field (Fig.3.15 (b)) and are found to gain oscillator strength at high principal quantum numbers in the presence of external electric fields, as in figures 3. 16(a) and 3.16 (b). Since parity and J are the important quantum numbers, the perturbations for the $J = 1$, odd-parity $5snp\ ^1P_1^0$ series are due to the doubly excited configurations 4d5p $^1P_1^0$; $^3P_1^0$; $^3D_1^0$ and mixing with the $5snp\ ^3P_1^0$ series members. At high n, mixing between the odd-parity $5snp\ ^1P_1$ members and the adjacent even-parity $5snd\ ^3D_2$ members are observed. For $n > 46$, $5snp\ ^1P_1$ members could not be resolved from $5snd\ ^3D_2$ members.

The term values for the two-photon forbidden $5s^2\ ^1S_0 \rightarrow 5snp\ ^1P_1$ transitions given in Table 3.7 are found to be consistent with accurate measurements using synchrotron radiation (Baig and Connerade 1984) and with the more recent laser based measurements (Baig *et al* 1999). This establishes that the excitation processes used in the present study to obtain the tabulated data, while they affect transition strengths, do not result in observable shifts in this energy range at the resolution used.

Table 3.7

Energy level values for the two-photon forbidden Sr I $5s^2\ ^1S_0 \rightarrow 5snp\ ^1P_1$ Rydberg series (*Opt. Commun.* **279**, 141, 2007)

Principal Quantum Number *n*	Level designation	Two-photon Wavelength (λ_{vac}) nm	Energy level E_n cm^{-1} Present Expt.	Baig & Connerade *
32	$5s32p\ ^1P_1^0$	436.642	45804.11	45804.102
33	$5s33p\ ^1P_1^0$	436.563	45812.40	45812.422
34	$5s34p\ ^1P_1^0$	436.491	45819.95	45819.941
35	$5s35p\ ^1P_1^0$	436.426	45826.78	45826.781
36	$5s36p\ ^1P_1^0$	436.368	45832.87	45832.988
37	$5s37p\ ^1P_1^0$	436.316	45838.34	45838.731
38	$5s38p\ ^1P_1^0$	436.266	45843.59	45843.922
39	$5s39p\ ^1P_1^0$	436.221	45848.32	45848.762
40	$5s40p\ ^1P_1^0$	436.178	45852.84	45853.160
41	$5s41p\ ^1P_1^0$	436.139	45856.94	45857.219
42	$5s42p\ ^1P_1^0$	436.102	45860.83	45861.120
43	$5s43p\ ^1P_1^0$	436.070	45864.09	45864.461
44	$5s44p\ ^1P_1^0$	436.038	45867.56	45867.711
45	$5s45p\ ^1P_1^0$	436.010	45870.51	45870.691
46	$5s46p\ ^1P_1^0$	435.983	45873.35	45873.539

* Baig M.A, Connerade J._P *J. Phys. B: At. Mol. Opt. Phys* **17**, L271(1984)

It is interesting to note in figures 3.16 (a) and 3.16 (b) that, for high Rydberg members, the weak transitions appearing between two adjacent members, $5snd\ ^1D_2$ and $5s(n+1)d\ ^1D_2$, have the following sequence:

$5snd\ ^1D_2$; $5s(n+1)s\ ^1S_0$; $5s(n-2)f\ ^1F_3$; $5s(n+1)p\ ^1P_1$; $5s(n+1)d\ ^3D_2$; $5s(n+1)d\ ^1D_2$.

The intensities of the two-photon forbidden odd-parity weak transitions $5s^2\ ^1S_0 \rightarrow 5snp\ ^1P_1$ and $5s^2\ ^1S_0 \rightarrow 5snf\ ^1F_3$ are also modified by electric field spatial distribution.

Table 3.8 presents the term values for the observed forbidden transitions $5s^2\ ^1S_0 \rightarrow 5snf\ ^1F_3$. For the $5snf\ ^1F_3$ Rydberg series, only a few measurements were reported previously and no data are available for high *n*. Rubbmark and Borgstrom (1978) list term values for this series from $n = 4$ up to $n = 29$ which is an extension of the previous tabulation up to $n = 13$ by Moore (1971). Recent data on this series are reported by Baig *et al* (1998) within the limited range, $22 < n < 26$. Strong perturbation by the $4d5p\ ^1F_3$ level causes cancellation of the lower members of the $5snf\ ^1F_3$ series (Vaeck *et al* 1988).

Table 3.8

Energy level values for the two-photon forbidden Sr I $5s^2\ ^1S_0 \rightarrow 5snf\ ^1F_3$ Rydberg series (*Opt. Commun.* **279**,141, 2007)

Principal Quantum Number *n*	Level designation	Two-photon Wavelength (λ_{vac}) nm	Energy level E_n cm^{-1} Present Expt.	Rubbmark & Borgstrom*
29	$5s29f\ ^1F_3^0$	436.670	45801.18	45801.03
30	$5s30f\ ^1F_3^0$	436.590	45809.57	
31	$5s31f\ ^1F_3^0$	436.514	45817.55	
32	$5s32f\ ^1F_3^0$	436.450	45824.26	
33	$5s33f\ ^1F_3^0$	436.388	45830.77	
--	———	———	———	
--	———	———	———	
36	$5s36f\ ^1F_3^0$	436.234	45846.95	
37	$5s37f\ ^1F_3^0$	436.190	45851.58	
38	$5s38f\ ^1F_3^0$	436.150	45855.78	
39	$5s39f\ ^1F_3^0$	436.112	45859.78	
40	$5s40f\ ^1F_3^0$	436.080	45863.14	
41	$5s41f\ ^1F_3^0$	436.045	45866.82	
42	$5s42f\ ^1F_3^0$	436.015	45869.98	
43	$5s43f\ ^1F_3^0$	435.990	45872.61	
44	$5s44f\ ^1F_3^0$	435.964	45875.35	

*Rubbmark J.R and Borgstrom S. A *Phys. Scr.* **18**, 196 (1978)

In figure 3.18 the growth of the forbidden transitions is plotted as a function of increasing principal quantum number 'n' which is in marked contrast with the allowed two-photon transitions ($^3D_2$), for which the intensity decreases, as expected, approximately as $(n^*)^{-3}$ with increasing n.

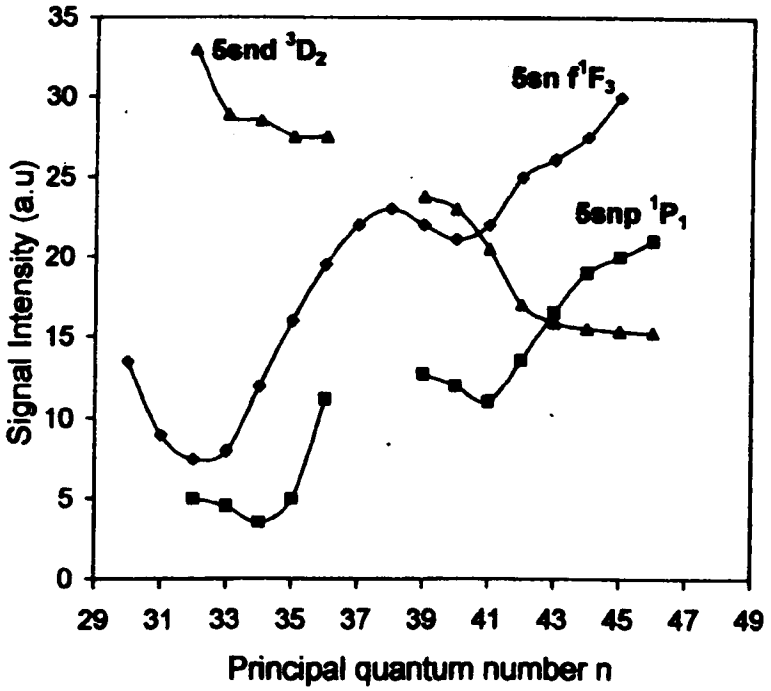

Fig. 3.18 Signal intensity variation with n for allowed $^3D_2$ (decay) and forbidden $^1P_1$ and $^1F_3$ (growth) transitions in Sr I.

The intensity of the forbidden transitions depends strongly on the principal quantum number and, for $n > 60$, the forbidden line intensities become comparable to the allowed transitions even for the low field strength ($\approx$ 14 volts/cm as estimated from the applied probe bias of +9 volt DC) used in this experiment. By using a mixture of He (40 mbar) and Ar (60 mbar) as the buffer gas, the Stark shift for the states is minimized because of the opposite collisional shifts for He and Ar. The frequency shift is estimated by spectral calibration using frequency marker transitions determined initially by running the heat-pipe setup with 10 mbar He which

compensates the Stark shift at probe bias of +2.3 volt DC. Fluctuations in intensity are observed in the neighbourhood of intruders. Although the buffer gas collisions induce the formation of Sr_2 and Sr*-Ar excimers and the resulting quasi-molecular transitions exhibit the break down of the ΔJ selection rule and parity, the present study shows that two-photon forbidden transitions to odd-parity states are quenched at high ($\geq$ 100mbar) buffer gas pressure.

The $J = 2$ even-parity 5s*n*d $^{1,3}D_2$ Rydberg series of Sr I are very complex due to several doubly excited intruders originating from the $4d^2$, $5p^2$ and 4d*n*s configurations , identified as **$4d^2$** $^3P_2$, $^1D_2$, $^3F_2$; **$5p^2$** $^3P_2$, $^1D_2$, $^3F_2$ and **4d*n*s** $^1D_2$,$^3D_2$. The $4d^2$ $^3P_2$ has been observed at 44729.42 cm^{-1} by two-photon excitation from the ground state $5s^2$ $^1S_0$ and at 23031.13 cm^{-1} via sequential excitation from 5s5p $^1P_1$. Also the strong autoionizing resonance, identified as ($4d^2$+$5p^2$) $^1D_2$, in figure 3.12 perturbs the 5s*n*d $^{1,3}D_2$ series. Due to the strong perturbations, especially by $5p^2$ $^1S_0$, the 5s*n*s $^1S_0$ series show abnormal intensity behaviour at low *n*. Strong singlet-triplet mixing and the breakdown of *L-S* coupling are apparent for the 5s*n*d $^{1,3}D_2$ series around $n = 16$ as in figure 3.15(a).The remarkable broad resonance in figure 3.13 with an asymmetric profile (labeled as $4d^2$ $^1G_4$ in Philip and Makdisi 2006) between 5s27d $^1D_2$ and 5s28d $^1D_2$ is also an important perturbation for the $J = 2$, Sr I 5s*n*d ^{1,3} D_2 Rydberg series. This intruder is believed to be highly localized by its observed survival in presence of heavy buffer gas collisions.

In figure 3.19 experimental quantum defects ($\mu_l = n - n^*$) for the members of the various Rydberg series (both two-photon allowed and forbidden transitions) are plotted. In Figure 3.20 the same quantum defects are plotted against energy (E_n- I). Quantum defects are found to be approximately constant for highly excited states.

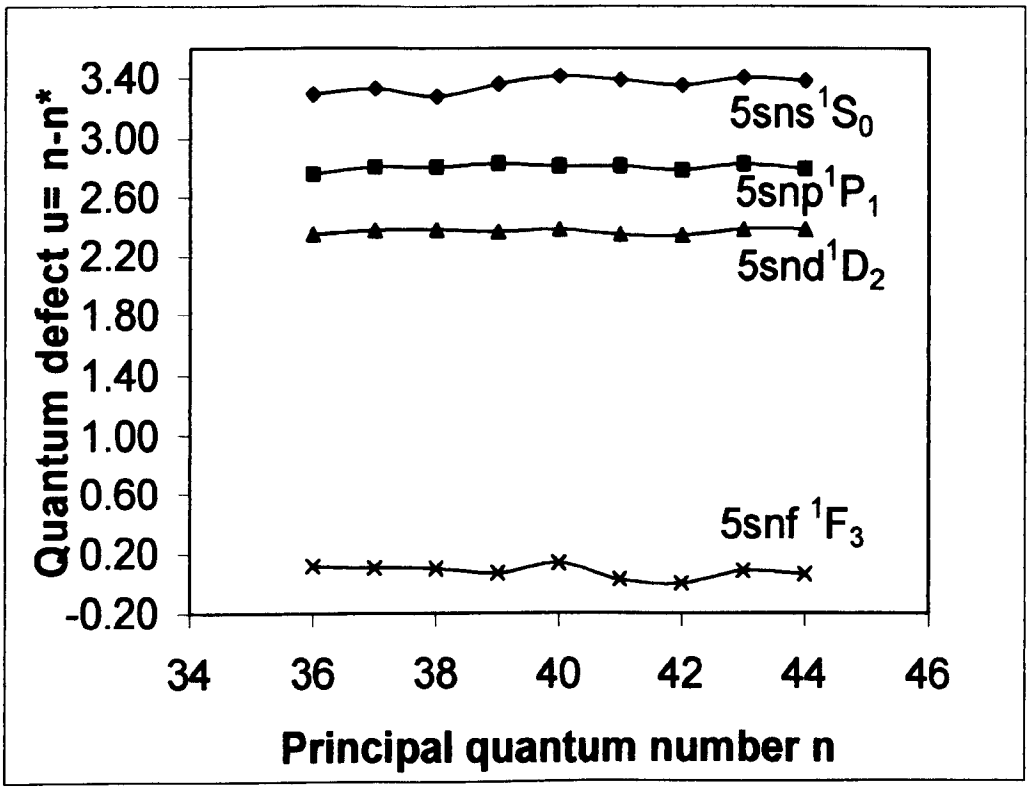

Fig. 3.19 Quantum defect plots for Sr I.
Fluctuations are seen around perturbing transitions

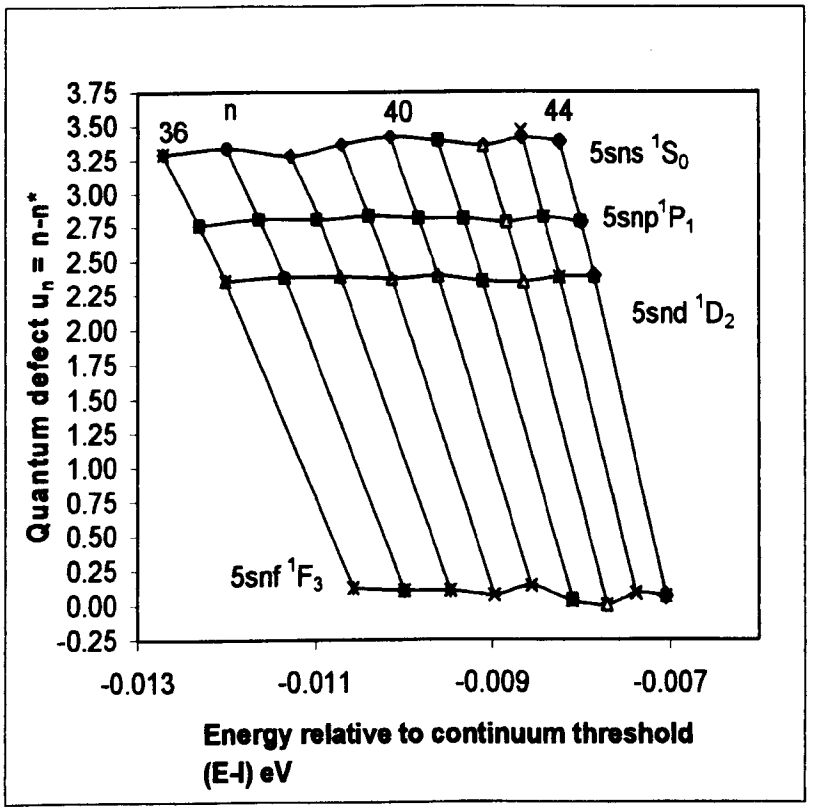

Fig. 3.20 Experimental quantum defects plotted
against energy relative to the continuum threshold

3.5 Single electron excitations in barium

Ba I has the ground state configuration $6s^2$ and the two excited configurations $6sn\ell$ and $5dn\ell$. Due to overlap between these, there are configuration mixing and therefore the level designations for many cases are ambiguous. For example, the level at 35344 cm^{-1} was originally labeled as $6p^2\ ^1D_2$. But Aymar and Robaux (1979) suggested $6s7d\ ^1D_2$ for this level. Recently Karlsson and Litzen (1999) revised the Ba I energy levels and wavelengths. They gave the label $6p^2\ ^3P_2$ for the level at 35344 cm^{-1}. The spectra of barium had played a very important role in the development of atomic theory and atomic structure calculations of heavy atoms because of the availability of large amount of experimental laser spectroscopic data for perturbed Rydberg series, hyperfine structure, oscillator strengths, lifetime etc. Also, barium is important in the collapse of the 4f wave function (Connerade and Mansfield 1975, Connerade 1978).

Ultraviolet extension of the absorption spectra of barium using a King furnace and photographic recording by Garton and Codling (1960) was of great historical importance in the study of spectra of alkaline-earth atoms. They reported about the presence of an autoionizing resonance (tentatively labeled as $5d8p\ ^1P_1^0$) just above the lowest ionization limit which has a striking effect on the $6s\varepsilon(p)$ photoionization cross section and on the high members of the $6snp\ ^1P_1$ Rydberg series which they extended to $n = 37$. They also observed the presence of several multiplets due to the simultaneous excitation of two valence electrons as recognized for the first time by Russel and Saunders (1925). These lines which involve doubly excited states are due to the fact that the ground state of barium has empty 5d-subshell, and filled 6s-subshell with 2 valence electrons. Several members of the series from double

excitations, most of which lie above the first ionization threshold and hence autoionizing, were also listed by Garton and Codling(1960). These are the following:

1. Members of the series converging on the Ba^+ 5d $^2D_{5/2}$ limit at 47708 cm^{-1}
   $6s^2\ ^1S_0 \rightarrow 5dmp\ ^1P_1^0$, for m = 8-26 and $6s^2\ ^1S_0 \rightarrow 5dmf\ ^1P_1^0$, for m = 4-8

2. Members of the series converging on the Ba^+ 5d $^2D_{3/2}$ limit at 46907 cm^{-1}
   $6s^2\ ^1S_0 \rightarrow 5dmp\ ^3P_1^0$, for m = 8-16, $6s^2\ ^1S_0 \rightarrow 5dmp\ ^3D_1^0$, for m = 8-11
   and $6s^2\ ^1S_0 \rightarrow 5dmf\ ^3P_1^0$, for m = 4-12

3.5.1 Important compilations for Ba I in Moore's table

(a) Even –parity Rydberg states

$6sns\ ^1S_0$ from n = 6 to 9 (38267.59 cm^{-1})
$6sns\ ^3S_1$ from n = 6 to 11 (39624.69 cm^{-1})
$6snd\ ^1D_2$ from n = 5 to 9 (39334.94 cm^{-1})
$6snd\ ^3D_2$ from n = 5 to 11 (40380.32 cm^{-1})

(b) Odd –parity Rydberg states

$6snp\ ^1P_1^0$ from n = 6 to 12(40421.23 cm^{-1})
$6snp\ ^3P_{0,1,2}^0$ from n = 6 to 7(30743.533, 30815.562, 30987.277 cm^{-1})
$6snf\ ^1F_3^0$ from n = 4 to 9 (40614.15 cm^{-1})
$6snf\ ^3F_{2,3,4}^0$ from n = 4 to 15 (41530.05cm^{-1})

(c) Doubly-excited intruder states

$5d^2\ ^1D_2$ (23062.06cm^{-1})
$5d^2\ ^3P_{0,1,2}$ (23209.11, 23480.01, 23918.94 cm^{-1})
$6p^2\ ^1S_0$ (34370.78cm^{-1})
$6p^2\ ^3P_{0,1,2}$ (34493.898, 34823.420, 35616.947 cm^{-1})
$6p^2\ ^1D_2$ (35344.423cm^{-1})

(d) First ionization threshold (series limit) 42032.4 cm^{-1}

By Rydberg extrapolation Garton and Codling (1960) revised the first ionization threshold listed by Moore and presented a new value: I_i = 42033.0 cm^{-1}.

3.5.2 Energy Level diagram for Ba I

A simplified energy level diagram for neutral barium is shown in figure 3.21 (for the range 3400cm^{-1} - the first ionization threshold). Several doubly excited states are also indicated

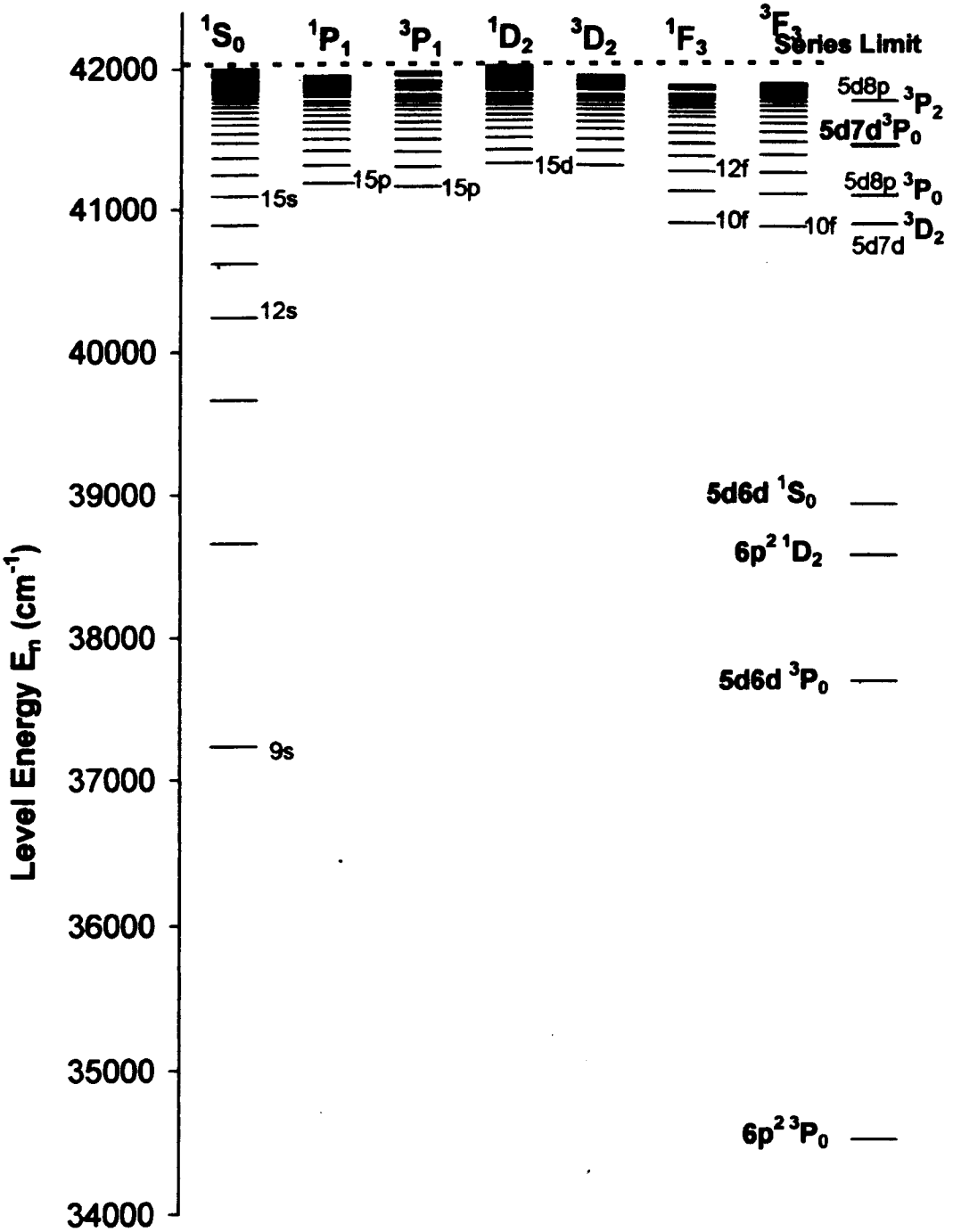

Fig.3. 21, Energy Level diagram of Ba I for the energy range 34000 cm^{-1} - first threshold.

3.6 Important previous multi-photon absorption studies for Ba I by others

Selective multi-photon absorption spectra was recorded using a spectrograph and a heat-pipe setup for barium by Bradley *et al* (1973) immediately after the advent of high power tunable pulsed dye lasers. They extended the 6s6p $^1P_1 \rightarrow$ 6s*n*d $^1D_2$ Rydberg series from n = 9 - 41. Also, they observed the 6s6p $^1P_1 \rightarrow$ 6s(n+1)s $^1S_0$ series. Bradley *et al* (1973) observed a perturbation at 420.39 nm which intrudes on the 6s*n*d $^1D_2$ Rydberg series around $26 < n < 27$ and it was assigned to the level 5d7d $^1D_2$. Only two members of the series were observed by Bradley *et al* (1973) for the transitions 6s6p $^1P_1 \rightarrow$ 6s(n+1)s $^1S_0$ because the higher members were found unresolved from 6s*n*d $^1D_2$ members. Another perturbation for the 6s*n*d $^1D_2$ sequence at $10 < n < 11$ was also reported by Bradley *et al* (1973) which was assigned the label 5d8s $^1D_2$. They also presented a listing of an autoionization series 6s6p $^1P_1 \rightarrow$ 5d*n*s $^1D_2$ for the range n = 8-11 from microdensitometer traces of the photographic plates.

Using pulsed tunable dye laser and photographic recording Rubbmark *et al* (1977) obtained the Ba I absorption spectrum and extended the previous energy level data of Bradley *et al* (1973). By quantum defect analysis and using Langer's formula, series members of the 6s*n*s $^1S_0$ were extended from n = 9 to n = 31, of 6s*n*d $^1D_2$ from n = 41 to n = 52 and of 6s*n*d $^3D_2$ from n = 11 to n = 28. Rubbmark *et al* (1977) used a revised value for the series limit as I = 42034.85 cm^{-1}.Using argon as buffer gas, Rubbmark *et al* (1977) observed a redshift of 0.3 cm^{-1} /100torr for most lines having quantum numbers $n \geq 12$.

The first improvement and extension of the observations in high-lying even-parity Rydberg states in barium made by Rubbmark *et al* (1977) was due to Camus and Morillon (1977) who employed two-photon spectroscopy and space charge amplification method in a heat-pipe set up. They extended the series 6s*n*s $^1S_0$ and 6s*n*d $^1D_2$ from $n = 31$ to $n = 46$ and from $n = 52$ to $n = 77$ respectively. Camus and Morillon (1977) also observed new autoionized levels belonging to 5d*n*s and 5d*n*d configurations besides the previously reported (Bradley *et al* 1973) perturbation of the 6s*n*d $^{1,3}D_2$ series due to the 5d7d $^1D_2$ level.

An extension and improvement on the data by Camus and Morillon (1977) and the previous data by Bradley *et al* (1973) and by Rubbmark *et al* (1977) for the even-parity $J = 0$ and $J = 2$ levels of Ba I was presented by Aymar *et al* (1978) using two-photon absorption spectroscopy and space-charge detection who observed members of the Rydberg series 6s*n*s $^1S_0$ ($16 \leq n \leq 61$), 6s*n*d $^1D_2$ ($15 \leq n \leq 81$) and 6s*n*d $^3D_2$($15 \leq n \leq 30$). New energy level values of these series members were also presented by Aymar *et al* (1978) besides assigning two levels at 38924 cm^{-1} and 41441 cm^{-1} to 5d6d $^1S_0$ and 5d 7d $^3P_0$ respectively which perturb the 6s*n*s $^1S_0$ series. Experimental energy levels of 6s*n*s $^1S_0$ levels were accurately fitted by a four-channel multichannel quantum-defect theory (MQDT) calculation for the first time by the same group and obtained a value of the first ionization limit $I_{6s} = 42035.04$ cm^{-1}. Aymar and Robaux (1979) used a nine-channel MQDT calculations for the parameterization of the $J = 2$ energy levels and analyzed the configuration interaction as well as the perturbation of the 6s*n*d $^{1,3}D_2$ Rydberg series by the 5d*n*s, 5d*n*d and $6p^2$ configurations. Moreover, they revised the previous assignment of certain low-lying levels, especially the $6p^2$ $^1D_2$ level located at 38556 cm^{-1}.

As a sensitive tool to test the MQDT predicted wavefunctions, Neukammer and Rinneberg (1982) experimentally measured the positions of the hyperfine components of the 6s14d configuration ($^1D_2$ and $^3D_{0,1,2}$ levels) of barium and probed the admixture coefficients of the 5d7d (5d7d $^3P_0$ and 5d7d $^3F_2$) perturbing configuration. They observed certain deviations from the predictions made by the multichannel quantum-defect theory (Aymar and Robaux 1979) and suggested that term values alone cannot reliably derive the wavefunctions but other data like the hyperfine structure also have to be incorporated in the MQDT analysis.

Camus *et al* (1982) used two-step pulsed laser excitation and optogalvanic detection for the J =1,3,4 and 5 even levels below the 6s ionization limit in barium. They have reported the observation for the first time for the 6s*n*s $^3S_1$ ($13 \leq n \leq 47$) and 6s*n*d $^3D_1$ ($12 \leq n \leq 38$) series.

In barium, due to considerable experimental difficulties in populating the odd-parity states, much attention had been given to the even-parity Rydberg series (Bradley *et al* 1973, Rubbmark *et al* 1977, Aymar *et al* 1978, Aymar and Robaux 1979, Camus *et al* 1982, Aymar *et al* 1983, Aymar and Camus 1983). With regards to the odd-parity Rydberg series, energy level values were available for the 6s*n*p $^1P_1$ series (up to n = 75), 6s*n*p $^3P_1$ series (n = 6 - 43), the 6s*n*p $^3P_2$ series (n = 6, 7; 11 - 54) and for some perturber states belonging to the 5d*n*p and 5d*n*f configurations besides MQDT calculations (Armstrong *et al* 1979) for some of the 6s*n*p (J = 1, 2) and 6s*n*f $^3F_3$ levels.

Accurate values of the level energies of the 6s*n*f $^1F_3$, $^3F_2$ and $^3F_3$ series (n = 13 - 55) had been reported by Post *et al* (1984). Post *et al* (1985) presented experimental

values for the energy of the odd-parity J = 0,1,2,3,4 levels of barium using laser-atomic-beam spectroscopy. Rydberg series 6s*n*p $^3P_0$ (n = 14 - 48), 6s*n*p $^3P_1$ (n = 15-48), 6s*n*p $^3P_2$ (n = 16 - 48), 6s*n*p $^1P_1$ (n = 15 - 48), 6s*n*f $^3F_2$ (n = 9 - 45), 6s*n*f $^3F_3$ (n = 10 - 45), 6s*n*f $^3F_4$ (n = 11 - 45), 6s*n*f $^1F_3$ (n = 10 - 45) besides some of the perturbing 5d8p levels had been observed by Post *et al* (1985). Some of these results were reported for the first time in the literature. They also presented the MQDT analysis of the J = 0,2,3,4 levels. An improved value of the first ionization limit (I_{6s} = 42034.90±0.01 cm^{-1}) was also presented by Post *et al* (1985). Post *et al* (1986) investigated the hyperfine structure of the transitions to odd-parity 6s*n*p and 6s*n*f configurations.

Rinneberg *et al* (1985) were the first to produce Rydberg atoms with the highest principal quantum number in laboratory conditions. They detected barium Rydberg atoms with principal quantum number up to n = 290 corresponding to a diameter of about 0.01 μm. Starting from the ground state 6s^2 $^1S_0$ populated the 6s*nt* states by resonant two-step excitation via the 6s6p $^1P_1$ intermediate level using two tunable narrow bandwidth (1MHz) CW lasers. Highly excited states are easily perturbed by small external electric and magnetic fields. Rinneberg *et al* (1985) observed '*l*' mixing at fields as low as F ≈ 1 volt/cm and H ≈ 850 Gauss. Using high spectral resolution (Δν = 5 MHz) they could record Stark and diamagnetic manifolds at high principal quantum numbers. Because of the large oscillator strength of the 6s6p $^1P_1$ → 6s*n*d $^1D_2$ transitions barium is particularly suitable for reaching very high principal quantum numbers (6s*n*d $^1D_2$ Rydberg series ranging from n = 100 up to n = 520) as recorded by Nuekammer *et al* (1987) in zero electric field. Probably this is the highest value of the principal quantum number achieved in the laboratory

whereas in outer space Rydberg states with much higher values of n have been detected by radio astronomy. At $n = 500$, the atomic diameter ($2\langle r\rangle = 3n^2a_0$) will be approximately 40 μm. At very high principal quantum number the photoabsorption cross section decreases rapidly with large deviation from the n^{-3} scaling law possibly due to the Stark mixing of the 6snd $^1D_2$ states with neighbouring Rydberg states which results in line broadening and hence redistribution of oscillator strengths (Neukammer *et al* 1987). Highly excited Rydberg atoms can be used to detect the presence of small electric fields and to map their spatial distribution from electric field-induced mixing of states of opposite parity as observed in strontium by Philip and Makdisi (2006).

An extensive measurement of energies of high-n Rydberg states of barium using high-resolution laser spectroscopy was reported by Neukammer *et al* (1988). Starting from the $6s^2\ ^1S_0$ ground state, they accessed the 6sns $^1S_0$ and 6snd $^{1,3}D_2$ Rydberg states via the 6s6p $^1P_1$ intermediate level. A DC discharge was used to populate the metastable state 5d6s $^1D_2$ and Stark mixing was used to excite the odd-parity 6snf $^1F_3$ and 6snh $^1H_5$ states. Neukammer *et al* (1988) were able to measure the energies of 6sns $^1S_0$ ($30 \le n \le 214$), 6snp $^1P_1$($60 \le n \le 214$) and 6snd $^1D_2$ ($30 \le n \le 285$) Rydberg states of barium with an accuracy of ± 60 MHz using two counter propagating, linearly polarized CW dye lasers, stabilized to a bandwidth of nearly 1 MHz, orthogonally intersecting an atomic beam. In addition, they reported the energies of Ba I 6snf $^1F_3$, 6sng $^1G_4$, 6sng $^3G_4$ and 6snh $^1H_5$ states at principal quantum numbers between $n = 47$ and $n = 78$. The singlet-triplet splitting between 6snd $^1D_2$ and 6snd $^3D_2$ states was also reported for the principal quantum numbers ranging between $n = 30$ and $n = 190$.

An improvement on the accuracy of the barium 6s*n*d $^1D_2$ Rydberg series consistent with MQDT calculations by Aymar and Robaux (1979) was presented recently by Shuman *et al* (2007) who reported the two-photon microwave transitions for Ba $6s(n+3)d\,^1D_2 \rightarrow 6sng\ ^1G_4$ for the principal quantum number range $31 \leq n \leq 44$.

In barium the perturbation of the 6s*n*d $^{1,3}D_2$ Rydberg series due to the 5d7d $^1D_2$ valence state around $n \approx 26$ produces a "hole" (dip) in the intensity distribution in the absorption spectrum (Sandner *et al* 1986) because these states are linear combination of the Rydberg and 5d7d $^1D_2$ valence states. There is a discrepancy in labeling and intensity fluctuations between the spectra observed by Allegrini *et al* (1988) and that reported in this thesis. For barium the 6s*n*d $^{1,3}D_2$ Rydberg series, the region $24 < n < 27$, which is heavily perturbed by the even-parity 5d7d $^1D_2$ doubly excited state, has been studied for several years (for example Gallagher *et al* 1981(a), Bhatti *et al* 1981, Matthias *et al* 1983, Leuwen *et al* 1983, Mullins *et al* 1985, Schumaker *et al* 1997, Bates *et al* 2001). Furthermore, due to the 5d7d $^1D_2$ doubly excited state at 6s26d $^1D_2$ < 5d7d $^1D_2$ < 6s27d $^1D_2$ with energy $\approx$ 41841.60 cm^{-1} (Aymar *et al* 1978) deviation from the $f \propto n^{-3}$ scaling law has been observed in the perturbed region for the 6s*n*d $^{1,3}D_2$ Rydberg series.

In the spectrum in this thesis, the valence state 5d7d is very strong because of prompt detection of a short lived valence state using a DC electric field in a thermionic diode. The spectral features reflect the thermionic detection process which represents the ionization. In a collision-free spectrum this state has lower strength and it becomes increasingly prominent as the buffer gas pressure is increased.

Energy level data for the bound (for example Rubbmark *et al* 1977, Aymar *et al* 1978, Armstrong *et al* 1979, Aymar and Robaux 1979, Camus *et al* 1982) and the autoionizing (for example Camus *et al* 1983, Bartschat *et al* 1991, Hieronymus *et al* 1992, Griesman *et al* 1992, Gallagher 1994, Lagadec *et al* 1996) Rydberg series of barium have been well documented. However, very few measurements are reported for the photoionization cross-section and oscillator strengths which are also important atomic properties. Parkinson *et al* (1976) used the 'hook method' to determine the f-values for the principal series of Sr I and Ba I. Connerade *et al* (1992) gave accurate values of the absolute oscillator strengths of barium principal series for the range $16 < n < 42$ using magneto-optical rotation (MOR) method. Mende and Kock (1996) used thermionic diode detection to measure the oscillator strengths of the high-lying states of barium 6s*n*d $^1D_2$ Rydberg series. Most recently Kalyar *et al* (2007a, b, c) reported new measurements for the oscillator strengths for the 6s6p $^{1,3}P_1 \rightarrow$ 6s*n*d $^{1,3}D_2$ Rydberg transitions using thermionic diode ion detection. They have obtained the *f*-values from photoionization cross-section measurements for the first ionization threshold from 6s6p^{1,3} P_J states using the 'saturation' method. Saturation method has also been used for the determination of oscillator strengths by others (Burkhardt *et al* 1988, Mende *et al* 1995, Saleem *et al* 2006, Amin *et al* 2006, Haq *et al* 2007).

Intensity fluctuation in barium, as reported by Garton and Codling (1960), in which intensity of the 6s^2 $^1S_0 \rightarrow$ 6s6p $^1P_1$ transition decreases suddenly at $n \approx 22$ and reappears in increasing strength as the series limit is approached is because the ground state of Ba II $^2S_{1/2}$ ion and the doubly-excited Ba I 5d8p $^1P_1$ have energy degeneracy.

3.7 Important Results in Ba I Spectroscopy from Thesis

3.7.1 The J=0, 2, even-parity spectra of Ba I 6sns $^1S_0$ and $^{1,3}D_2$ Rydberg series

The J = 2 bound spectrum consists of the two Rydberg series 6snd $^{1,3}D_2$ converging on the 6s $^2S_{1/2}$ series limit. The members of the series converging on the 5d or 6p limits are the configurations 5dnd, 5dns and $6p^2$ for which the lower members below the first ionization limit at 6s $^2S_{1/2}$ ($6p^2$, 5d6d, 5d7d and 5d8p) are also indicated in figure 3.21. The $5d^2$ (n = 5 in the 5dnd configuration) levels lie below the range in the energy level diagram given in figure 3.21. The 5d7d configuration in barium is a strong perturber for the J = 2, even-parity Rydberg series and this perturbation has been investigated in several studies (for example Bradley *et al* 1973, Rubbmark *et al* 1977, Aymar and Robaux 1979). Also, $6p^2$ $^1D_2$ labeled at 38556.18cm^{-1}(Aymar and Robaux 1979) is a strong perturbation for the 6snd $^1D_2$ Rydberg series.

Figures 3.22 - 3.26 show the two-photon spectra taken with transverse excitation of the atomic jet with barium using disposable cartridge in the heat-pipe and themionic diode detection. A single dye coumarine LC4800 provided the required tuning range to excite the bound and autoionizing transitions covered in the spectral region 466 nm - 495 nm. Typical operating temperature of the heat-pipe was 780 ^{0}C with 15 mbar He buffer. The spectral recording was identical to the two-photon spectroscopy of strontium and therefore the description is not repeated here. All measurements were taken with the dye laser pulse energy of 2.5 μJ / pulse at a repetition rate of 13 Hz. Wavelength calibration was carried out using the energy level data by Aymar *et al* (1978) using two-photon absorption spectroscopy and space-charge detection.

Figure 3.22 shows the $J = 0$, and the $J = 2$, 6s*n*s $^1S_0$ and 6s*n*d $^{1,3}D_2$ states. Members of the Rydberg series observed are: 6s*n*s $^1S_0$ from $n = 13$ and the 6s*n*d $^{1,3}D_2$ series from $n = 11$. A strong interloper, 5d7d $^1D_2$ at two-photon laser wavelength in air at 477.858 nm next to 6s26d $^1D_2$ perturbs the 6s*n*d $^1D_2$ Rydberg series while a weak intruder, 5d7d $^3P_2$ at two-photon wavelength at 477.556 nm perturbs the 6s*n*d $^3D_2$ Rydberg series.

Figure 3.23 is a two-photon spectrum of Ba I for the wavelength region 480 nm-477 nm. This spectrum is taken with 40 mbar helium buffer, with all other operating conditions kept same as in figure 3.22. It can be observed that the intensity of the perturber appearing next to 6s26d $^1D_2$ at 41841.33 cm^{-1} (level 5d7d $^1D_2$) is highly sensitive on the pressure of the buffer gas.

Figure 3.24 shows the two-photon spectrum of the high members of the $J = 0,2$ even- Rydberg series for laser two-photon wavelength range 478 nm – 475 nm. 6s*n*d $^1D_2$ series members can be followed for the range $26 < n < 60$ in this well-resolved spectrum. The perturber labeled as 5d7d $^1D_2$ is also seen in this spectrum.

Figure 3.25 is a spectrum of Ba I for the two-photon wavelength 477 nm – 467 nm. In this spectrum the autoionizing level labeled as 5d5f $^1P_1$ can be clearly observed. The width and asymmetry of the profile which can be fitted on the Fano formula depends on the environment in which the atoms are placed.

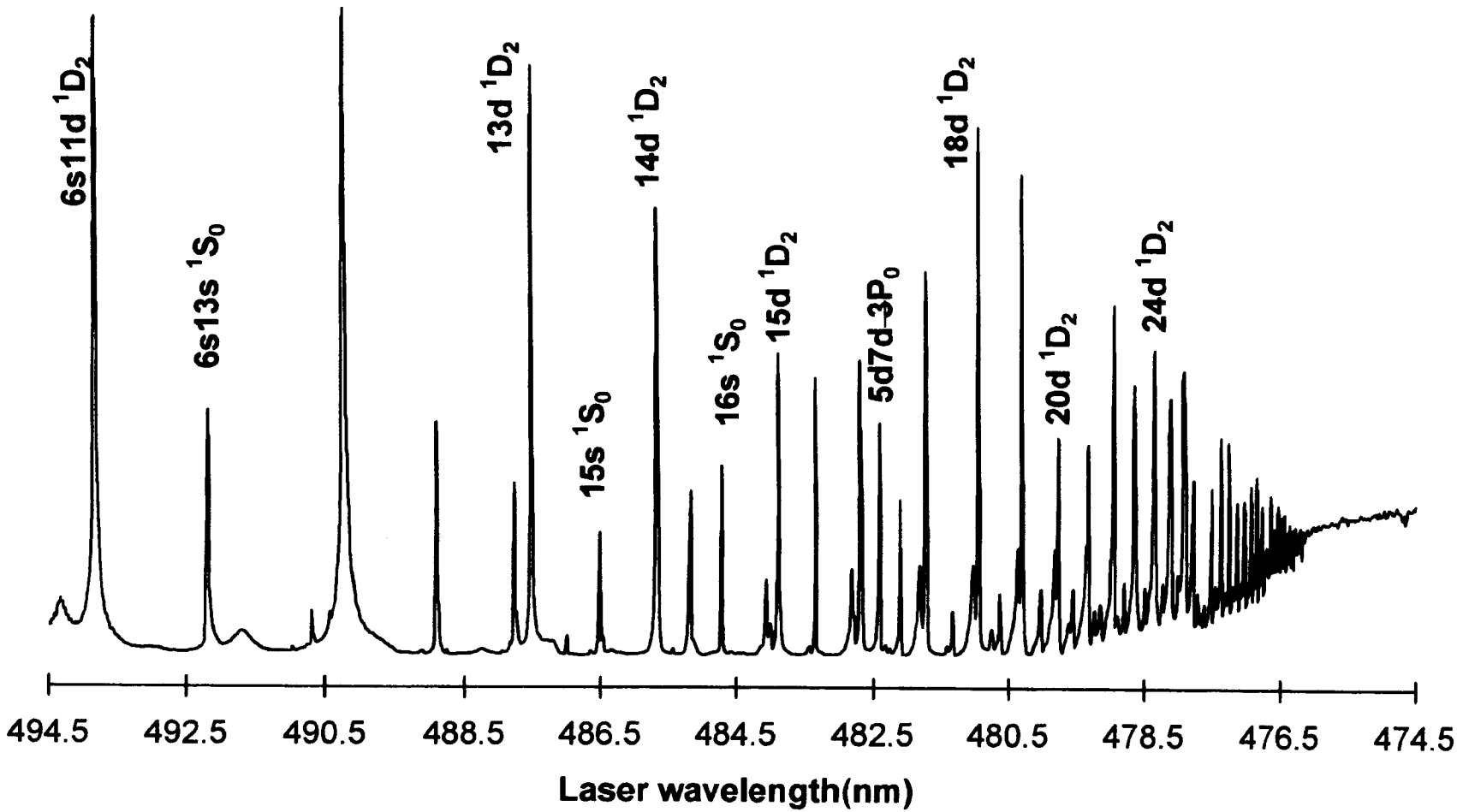

Fig. 3.22 Two-photon spectrum of Ba I showing the $J = 0, 2$ even-parity 6s*n*s $^1S_0$ and 6s*n*d $^{1,3}D_2$ Rydberg members

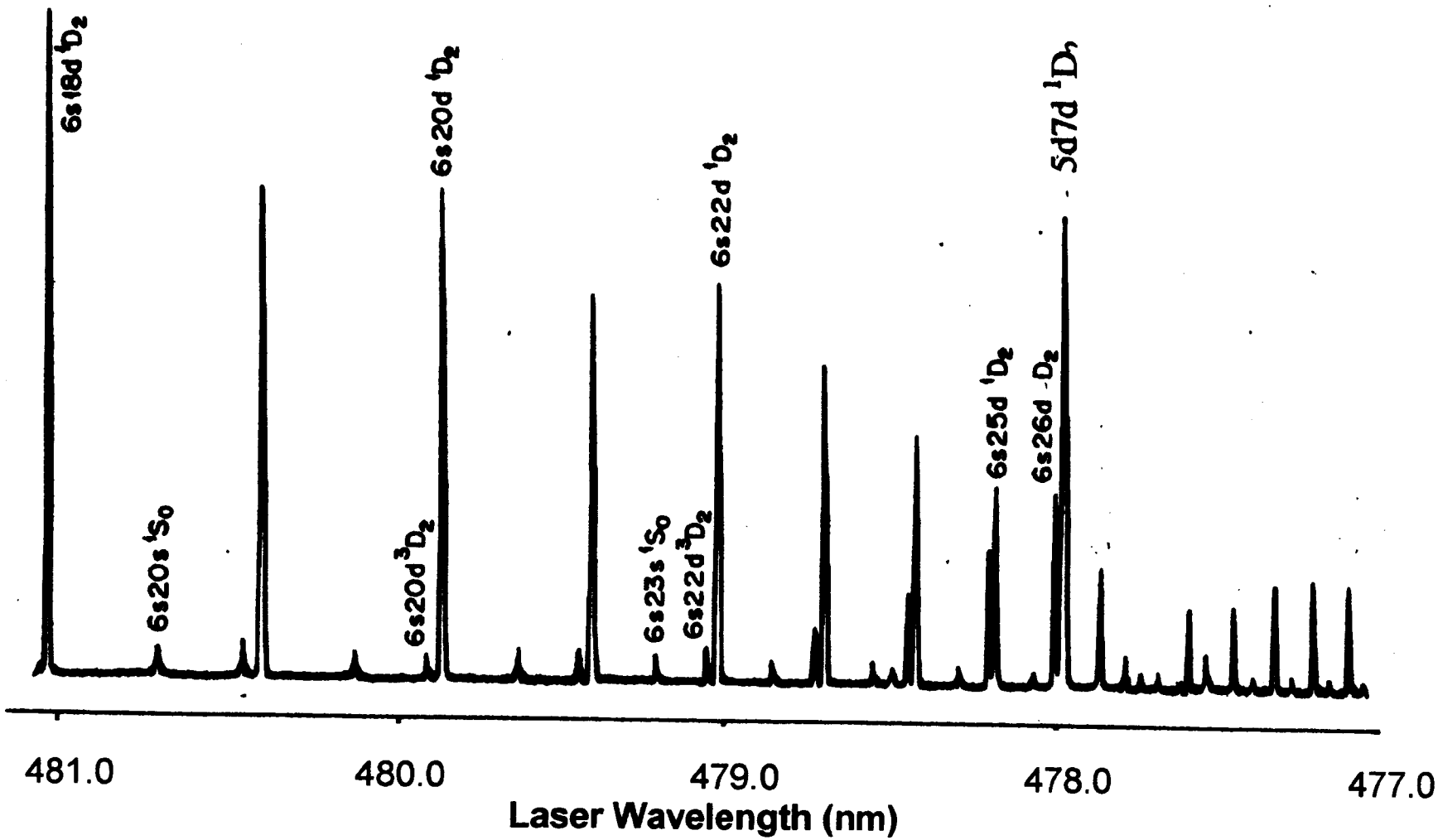

Fig. 3.23 Two-photon spectrum of Ba I showing the $J = 0, 2$ Rydberg series. Effect of collision on 5d7d $^1D_2$ is seen (He buffer)

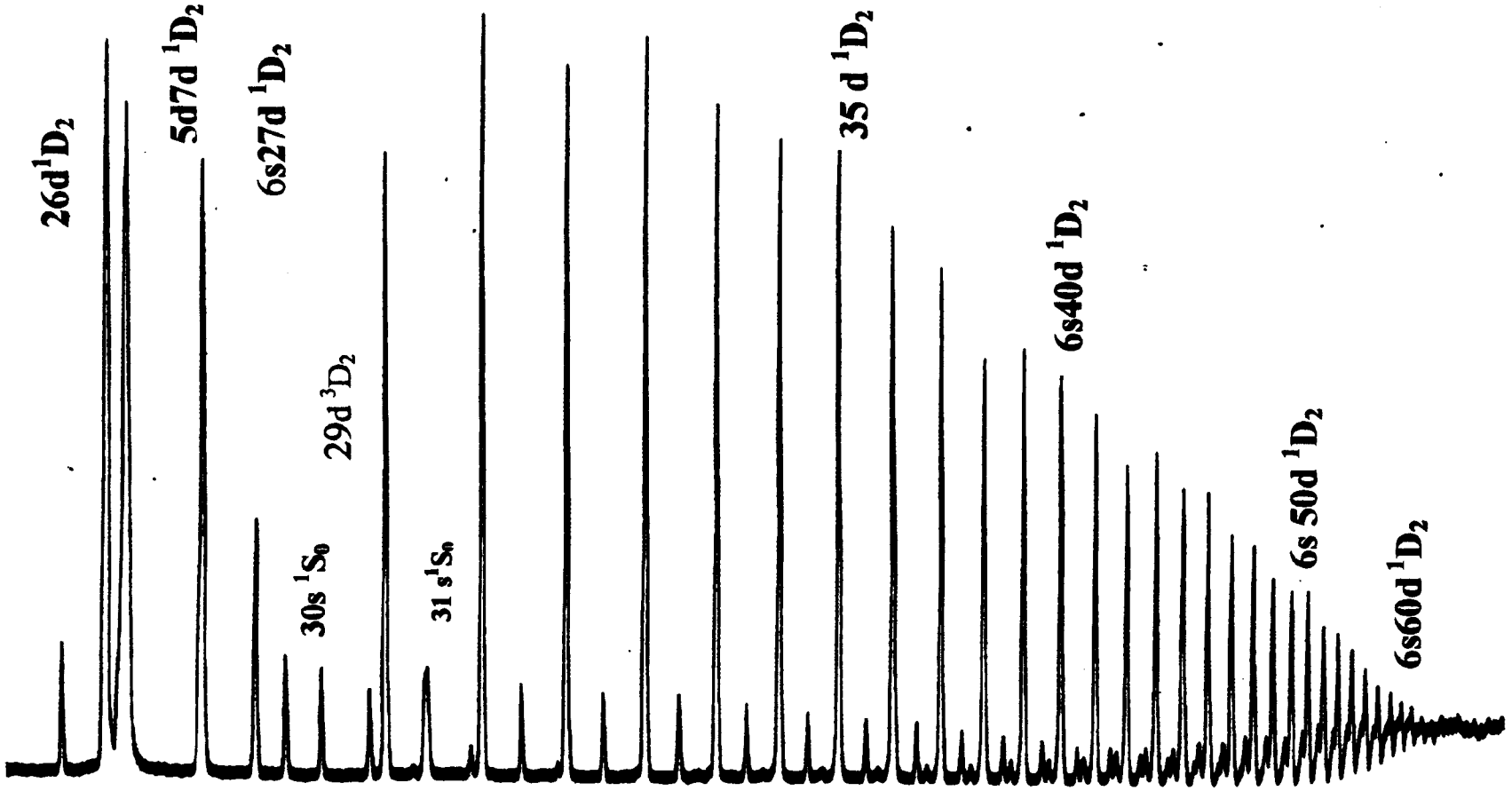

Fig. 3.24 A well-resolved two-photon spectrum of Ba I showing the $J = 0,2$ even-parity Rydberg members Also seen are the emergence of forbidden transitions due to 'ℓ' mixing at high n similar to an observation in Sr I.

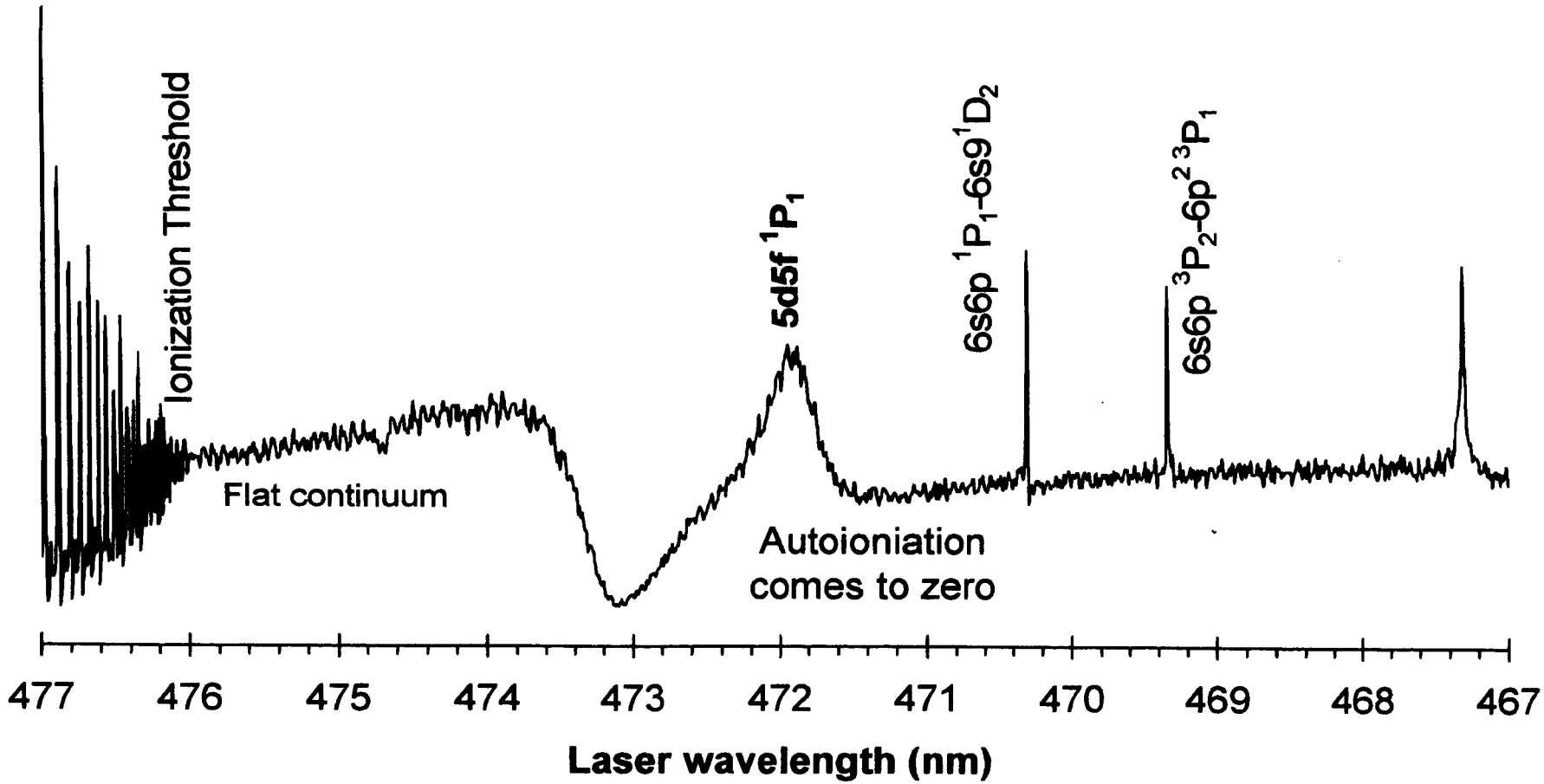

Fig. 3.25 Two-photon spectrum of Ba I showing the ionization threshold and the autoionizing level labeled as 5d5f $^1P_1$. Single-photon resonances also are observed which are due to sequential excitation from the intermediate 6s6p $^1P_1$ and 6s6p ^3P_J levels.

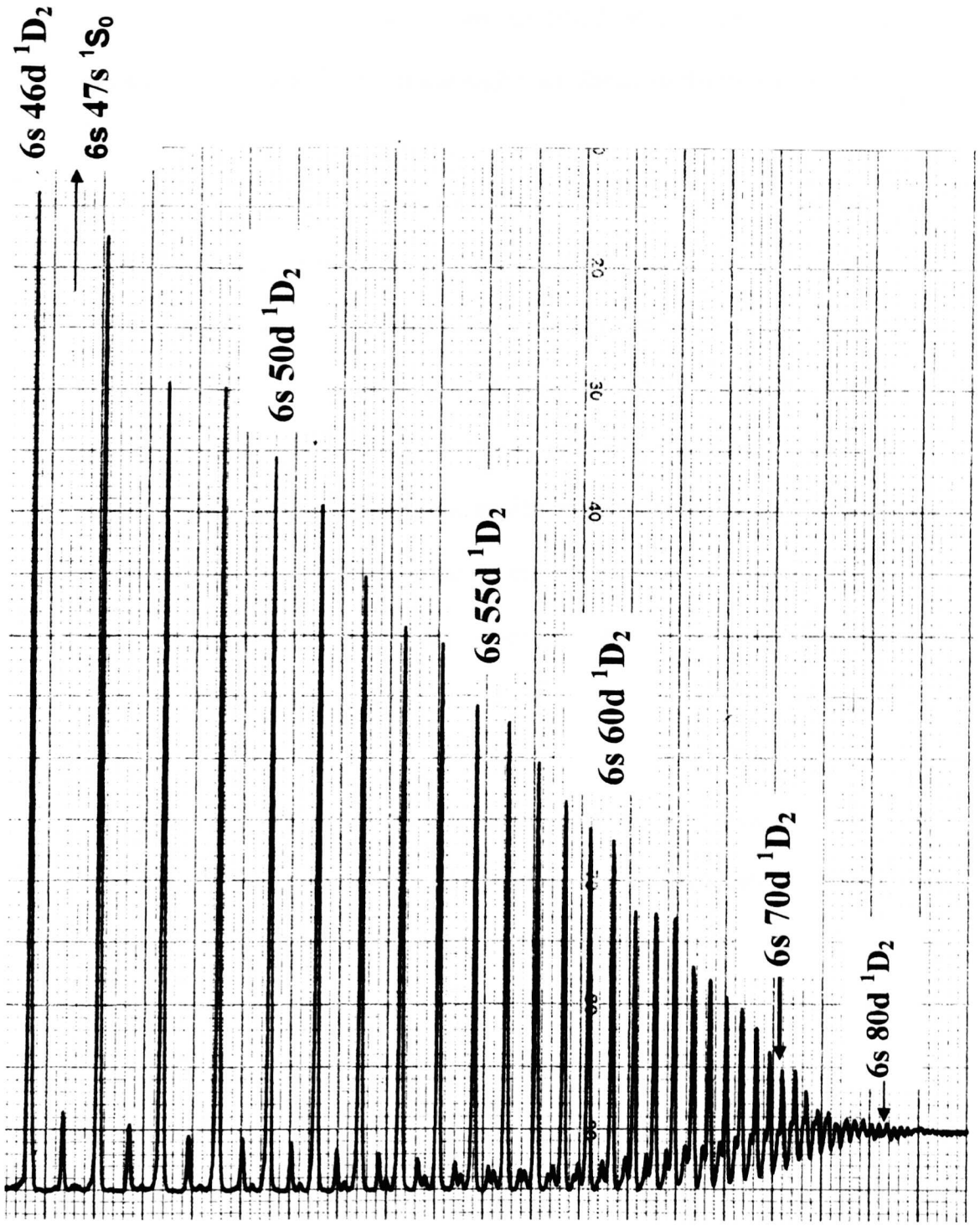

Fig. 3.26 A two-photon spectrum of Ba I showing the high members of the J = 0,2: 6sns $^1S_0$ ($47 < n < 68$) and 6snd $^1D_2$ ($46 < n < 88$) Rydberg series. Also seen is the emergence of forbidden transitions due to ℓ-mixing at high n similar to an observation in Sr I.

Figure 3.26 is a two-photon spectrum of Ba I showing the high members of the $J = 0$ and 2 even-parity Rydberg series. In this spectrum energy level values of $6sns\ ^1S_0$ ($47 < n < 68$) and $6snd\ ^1D_2$ ($46 < n < 88$) are identified. Also seen is the emergence of forbidden transitions due to '*l*' mixing at high *n* similar to an observation in Sr I.

Extensive new and improved experimental data for the $J = 0$ and $J = 2$ even-parity levels of barium obtained from the two-photon spectroscopy are presented in this thesis. The energy level values of these even-parity levels are given in Tables 3.9-3.11. Members of the $6sns\ ^1S_0$ Rydberg series are observed from $n = 13$ to $n = 68$ and these data are given in Tables 3.9 - 3.10. This is, probably, the highest member of the $J = 0$ series reported in the literature for similar experimental schemes. The energy level values for $6sns\ ^1S_0$ Rydberg sequence are compared with experimental values reported by Aymar *et al* (1978) for the range $16 < n < 61$ and are found to have excellent agreement with their values.

The members of the $6snd\ ^3D_2$ Rydberg series are observed for the range $11 < n < 46$ which is also a substantial extension of the previous experimental data by Aymar *et al* (1978) who reported experimental term values for the range $15 < n < 30$ for the triplet series. The energy level values are given in Table 3.11 with the singlet members. Furthermore, the experimental energy level data are obtained for the $6snd\ ^1D_2$ Rydberg series and are given in Table 3.11 for the range $11 < n < 88$, thereby reporting a new original data for the range $82 < n < 88$ for these members. Comparison with experimental data reported by Aymar *et al* (1978) gives excellent agreement for the range $15 < n < 81$. The $J = 0$ and $J = 2$ even-parity Rydberg series are perturbed by the 5d7d and 6s7d configurations which are also observed.

Table 3.9

Observed two-photon excitations to the bound $J = 0$, even-parity $6s^2\ ^1S_0 \rightarrow 6sns\ ^1S_0$ Rydberg series

Principal quantum number *n*	Level label	Energy level Thesis Experiment cm^{-1}	Energy level Aymar *et al* (1978) Expt.* cm^{-1}
13	$6s13s\ ^1S_o$	40617.86	40618.194
14	$6s14s\ ^1S_o$	40891.21	40891.560
15	$6s15s\ ^1S_o$	41092.36	41092.994
16	$6s16s\ ^1S_o$	41245.75	41245.163
17	$6s17s\ ^1S_o$	41362.45	41362.350
Intruder	**$5d7d\ ^3P_o$**	**41440.88**	41441.221
18	$6s18s\ ^1S_o$	41467.59	41467.798
19	$6s19s\ ^1S_o$	41534.88	41535.233
20	$6s20s\ ^1S_o$	41595.55	41595.895
21	$6s21s\ ^1S_o$	41645.87	41646.379
22	$6s22\ s\ ^1S_o$	41688.26	41688.729
23	$6s23s\ ^1S_o$	41723.88	41724.546
24	$6s24s\ ^1S_o$	41754.65	41755.001
25	$6s25s\ ^1S_o$	41781.64	41781.278
26	$6s26s\ ^1S_o$	41803.69	41804.003

Principal quantum number *n*	Level label	Energy level Thesis Experiment cm^{-1}	Energy level Aymar *et al* (1978)Expt.* cm^{-1}
27	$6s27s\,^1S_o$	41823.27	41823.818
28 Intruder	**$6s28s\,^1S_o$/ $5d7d\,^1D_2$**	**41841.33**	41841.197
29	$6s29s\,^1So$	41856.08	41856.491
30 Intruder	**$6s30s\,^1S_o$/ $5d7d\,^3P_2$**	**41869.58**	41870.092
31	$6s31s\,^1S_o$	41881.82	41882.156
32	$6s32s\,^1S_o$	41892.58	41893.021
33	$6s33s\,^1S_o$	41902.41	41902.733
34	$6s34s\,^1S_o$	41911.40	41911.463
35	$6s35s\,^1So$	41919.17	41919.306
36	$6s36s\,^1S_o$	41926.38	41926.434
37	$6s37s\,^1S_o$	41932.66	41933.055
38	$6s38s\,^1S_o$	41938.59	41938.896
39	$6s39s\,^1S_o$	41943.77	41944.307
40	$6s40s\,^1S_o$	41949.11	41949.361
41	$6s41s\,^1S_o$	41953.73	41953.943
42	$6s42s\,^1S_o$	41957.90	41958.162
43	$6s43s\,^1S_o$	41961.84	41962.068

Principal quantum number *n*	Level label	Energy level Thesis Experiment cm^{-1}	Energy level Aymar *et al* (1978)Expt.* cm^{-1}
44	$6s44s\,^1S_0$	41965.35	41962.068
45	$6s45s\,^1S_0$	41968.68	41969.011
46	$6s46s\,^1S_0$	41971.73	41972.205
47	$6s47s\,^1S_0$	41974.98	41975.0980
48	$6s48s\,^1S_0$	41978.02	41977.786
49	$6s49s\,^1S_0$	41980.49	41980.362
50	$6s50s\,^1So$	41982.96	41982.681
51	$6s51s\,^1S_0$	41984.93	41984.960
52	$6s52s\,^1S_0$	41987.16	41986.968
53	$6s53s\,^1S_0$	41988.99	41988.982
54	$6s54s\,^1S_0$	41991.32	41990.769
55	$6s55s\,^1S_0$	41992.47	41992.43600
56	$6s56s\,^1S_0$	41994.35	41994.149
57	$6s57s\,^1S_0$	41995.80	41995.683
58	$6s58s\,^1S_0$	41996.72	41997.214
59	$6s59s\,^1S_0$	41998.65	41998.480
60	$6s60s\,^1S_0$	41999.94	41999.735
61	$6s61s\,^1S_0$	42001.11	42001.026

*Aymar M, Camus P, Dieulin M and Morillon C
Phys. Rev. A **18**, 2173 (1978)

Table3.10

THESIS *Extension of two-photon excitations to the bound J = 0, even-parity BaI $6s^2\ ^1S_0 \rightarrow 6sns\ ^1S_0$ Rydberg series

Principal quantum number n	Level label	Energy level Thesis Experiment cm^{-1}	Energy level OtherExpt.$ cm^{-1}
62	* $6s62s\ ^1S_0$	42002.26	-
63	* $6s63s\ ^1S_0$	42003.39	-
64	* $6s64s\ ^1S_0$	42004.45	-
65	* $6s65s\ ^1S_0$	42005.51	42005.206*
66	* $6s66s\ ^1S_0$	42006.44	-
67	* $6s67s\ ^1S_0$	42007.32	-
68	* $6s68s\ ^1S_0$	42008.17	-

$ Neukammer J, Jonsson G, Koenig A, Vietzke K, Hieronnymus H and Rinneberg H, *Phys. Rev.* A **38**, 2804 (1988)

The energy level values of the perturbing transitions observed are also given in Tables 3.9 - 3.11.These are:

($5d7d\ ^3P_0$ @ 41440.88 cm^{-1}, $5d7d\ ^1D_2$ @ 41841.33 cm^{-1} $6s7d\ ^3P_2$ @ 41868.6 cm^{-1})

Figure 3.27 shows the fluorescence emission of Ba I in the atomic jet setup clearly indicating the sequential excitation from $6s6p\ ^1P_1$ and $6s6p\ ^3P_J$ levels similar to the observations in strontium. In Fig.3.28 the experimental energy difference E_{n+1} - E_n is plotted against the effective principal quantum number for the J = 0, 2 Rydberg seriesof BaI. The $(n^*)^{-3}$ relation is evident in these curves. Figure 3.29 gives the quantum defect curves for the high members of the J = 0, 2 Rydberg series of Ba I.

Table 3.11

Two-photon excitations to the Ba I $6s^2\ ^1S_0 \rightarrow 6snd\ ^1D_2$ Rydberg series

Principal quantum number *n*	Level label	Energy level Thesis Expt. cm^{-1}	Energy level Aymar *et al* Expt.* cm^{-1}
11	$6s11d\ ^3D_2$	40449.80	-
11	$6s11d\ ^1D_2$	40483.62	-
12	$6s12d\ ^3D_2$	40743.16	-
12	$6s12d\ ^1D_2$	40781.37	-
13	$6s13d\ ^3D_2$	40987.81	-
13	$6s13d\ ^1D_2$	41007.98	-
14	$6s14d\ ^3D_2$	---	-
14	$6s14d\ ^1D_2$	41162.21	-
15	$6s15d\ ^3D_2$	41300.98	41300.39
15	$6s15d\ ^1D_2$	41315.66	41315.55
16	$6s16d\ ^3D_2$	41406.85	41407.25
16	$6s16d\ ^1D_2$	41417.16	41417.64
17	$6s17d\ ^3D_2$	41491.68	41492.21
17	$6s17d\ ^1D_2$	41499.80	41500.07
18	$6s18d\ ^3D_2$	41560.44	41561.11
19	$6s19d\ ^3D_2$	41617.49	41617.7
19	$6s19d\ ^1D_2$	41622.56	41622.47

Principal quantum number *n*	Level label	Energy level Thesis Expt. cm^{-1}	Energy level Aymar *et al* Expt.* cm^{-1}
20	$6s20d^3D_2$	41663.98	41664.77
20	$6s20d^1D_2$	41668.35	41668.53
21	$6s21d^3D_2$	41703.90	41704.21
21	$6s21d^1D_2$	41707.18	41707.3
22	$6s22d^3D_2$	41736.77	41737.69
22	$6s22d^1D_2$	41739.60	41740.18
23	$6s23d^3D_2$	41765.88	41766.26
23	$6s23d^1D_2$	41767.80	41768.35
24	$6s24d^3D_2$	41791.42	41790.84
24	$6s24d^1D_2$	41792.88	41792.62
25	$6s25d^3D_2$	41811.28	41811.94
25	$6s25d^1D_2$	41813.32	41813.57
26	$6s26d^3D_2$	41829.74	41829.49
26	$6s26d^1D_2$	41831.30	41831.91
Intruder	**$5d7d\ ^1D_2$**	**41841.33**	41841.66
27	$6s27d^3D_2$	41847.36	41848.27
27	$6s27d^1D_2$	41852.75	41852.06
28	$6s28d^3D_2$	41862.10	41862.68
28	$6s28d^1D_2$	41865.12	41864.69

Principal quantum number *n*	Level label	Energy level Thesis Expt. cm^{-1}	Energy level Aymar *et al* Expt.* cm^{-1}
Intruder	**$6s7d^3P_2$**	**41868.60**	41868.21
29	$6s29d^3D_2$	41875.32	41875.49
29	$6s29d^1D_2$	41877.64	41877.01
30	$6s30d^3D_2$	41866.68	41886.86
30	$6s30d^1D_2$	41888.16	41888.11
31	$6s31d^3D_2$	41896.87	
31	$6s31d^1D_2$	41898.11	41898.21
32	$6s32d^1D_2$	41907.38	41907.37
33	$6s33d^3D_2$	41913.46	
33	$6s33d^1D_2$	41915.76	41915.57
34	$6s34d^3D_2$	41921.19	
34	$6s34d^1D_2$	41923.06	41923.1
35	$6s35d^3D_2$	41927.92	
35	$6s35d^1D_2$	41929.85	41929.83
36	$6s36d^3D_2$	41934.10	
36	$6s36d^1D_2$	41936.03	41936.12
37	$6s37d^3D_2$	41939.90	
37	$6s37d^1D_2$	41941.74	41941.8
38	$6s38d^3D_2$	41944.84	
38	$6s38d^1D_2$	41946.93	41946.99
39	$6s39d^3D_2$	41949.79	
39	$6s39d^1D_2$	41951.93	41951.79
40	$6s40d^3D_2$	41954.51	
40	$6s40d^1D_2$	41956.16	41956.18
41	$6s41d^3D_2$	41958.85	
41	$6s41d^3D_2$	41960.27	41960.17
42	$6s42d^3D_2$	41962.42	
42	$6s42d^1D_2$	41963.74	41964.0
43	$6s43d^3D_2$	41966.18	
43	$6s43d^1D_2$	41967.70	41967.45
44	$6s44d^3D_2$	41969.22	
44	$6s44d^1D_2$	41970.74	41970.75

Principal quantum number *n*	Level label	Energy level Thesis Expt. cm^{-1}	Energy level Aymar *et al* Expt.* cm^{-1}
45	$6s45d^3D_2$	41972.56	
45	$6s45d^1D_2$	41973.49	41973.7
46	$6s46d^3D_2$	41975.26	
46	$6s46d^1D_2$	41976.30	41976.44
47	$6s47\ d^1D_2$	41979.06	41979.01
48	$6s48d^1D_2$	41981.47	41981.53
49	$6s49d^1D_2$	41983.80	41983.85
50	$6s50d^1D_2$	41986.02	41985.98
51	$6s51d^1D_2$	41988.05	41988
52	$6s52d^1D_2$	41989.84	41989.89
53	$6s53d^1D_2$	41991.87	41991.6
54	$6s54d^1D_2$	41992.91	41993.3
55	$6s55d^1D_2$	41994.85	41994.95
56	$6s56d^1D_2$	41996.34	41996.42
57	$6s57d^1D_2$	41997.39	41997.79
58	$6s58d^1D_2$	41998.74	41999.17
59	$6s59d^1D_2$	41999.98	42000.38
60	$6s60d^1D_2$	42001.28	42001.63
61	$6s61d^1D_2$	42002.70	42002.73
62	$6s62d^1D_2$	42003.73	42003.83
63	$6s63d^1D_2$	42004.81	42004.84

Principal quantum number *n*	Level label	Energy level Thesis Expt. cm^{-1}	Energy level Aymar *et al* Expt.* cm^{-1}
64	$6s64d\,^1D_2$	42005.78	42005.81
65	$6s65d\,^1D_2$	42006.71	42006.72
66	$6s66d\,^1D_2$	42007.61	42007.63
67	$6s67d\,^1D_2$	42008.43	42008.48
68	$6s68d\,^1D_2$	42009.26	42009.29
69	$6s69d\,^1D_2$	42010.01	42010.02
70	$6s70d\,^1D_2$	42010.60	42010.68
71	$6s71d\,^1D_2$	42011.42	42011.47
72	$6s72d\,^1D_2$	42012.06	42012.16
73	$6s73d\,^1D_2$	42012.61	42012.73
74	$6s74d\,^1D_2$	42013.25	42013.32
75	$6s75d\,^1D_2$	42013.86	42013.86
76	$6s76d\,^1D_2$	42014.39	42014.61
77	$6s77d\,^1D_2$	42014.97	42015.13
78	$6s78d\,^1D_2$	42015.42	42015.7
79	$6s79d\,^1D_2$	42015.93	42016.21
80	$6s80d\,^1D_2$	42016.36	42016.67
81	$6s81d\,^1D_2$	42016.85	42017.12

* Aymar M., Camus P., Dieulin M. and Morillon C
Phys. Rev. A **18**, 2173 (1978)

Table 3.12

**THESIS Extension of the two-photon excitations to the Ba I $6s^2\ ^1S_0 \rightarrow 6snd\ ^1D_2$ Rydberg series

Principal quantum number *n*	Level label	Energy level Thesis Expt. cm^{-1}
82	** **6s82d $^1D_2$**	**42017.26**
83	** **6s83d $^1D_2$**	**42017.77**
84	** **6s84d $^1D_2$**	**42018.16**
85	** **6s85d $^1D_2$**	**42018.65**
86	** **6s86d $^1D_2$**	**42018.93**
87	** **6s87d $^1D_2$**	**42019.40**
88	** **6s88d $^1D_2$**	**42019.78**

As in strontium, the fluorescence emission of Ba I in the atomic jet setup presented in figure 3.27 clearly indicates the sequential excitation from 6s6p $^1P_1$ and 6s6p ^3P_J levels.

The $(n^*)^{-3}$ dependence of the energy interval $E_{n+1} - E_n$ for the successive members of the $J = 0$ and $J = 2$ Rydberg series of Ba I is observed in figure 3.28. In figure 3.29 quantum defects are plotted for these members.

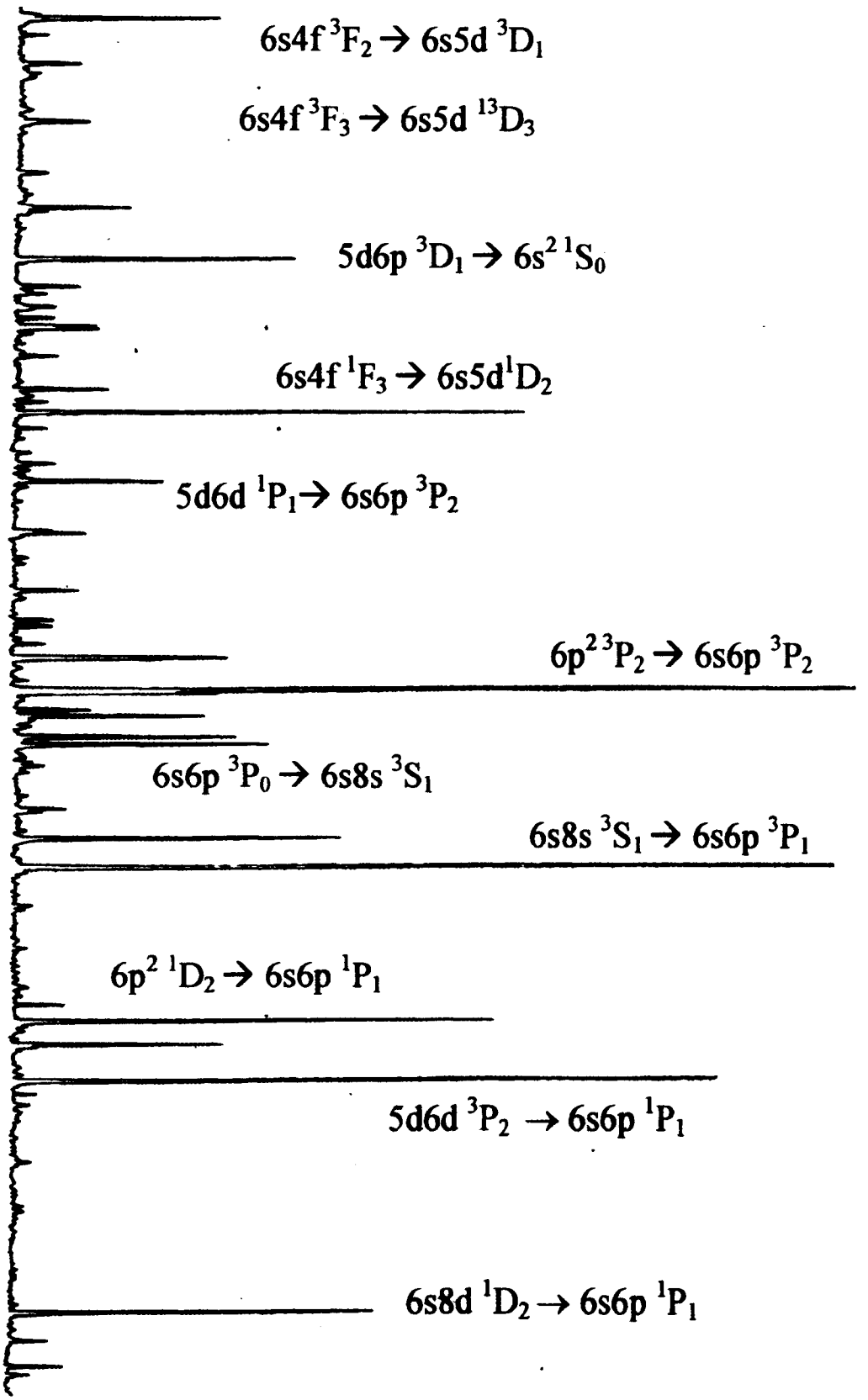

Fig. 3.27 Observed fluorescence emission of Ba I in the atomic jet setup clearly indicating the sequential excitation from 6s6p $^1P_1$ and 6s6p ^3P_J levels.

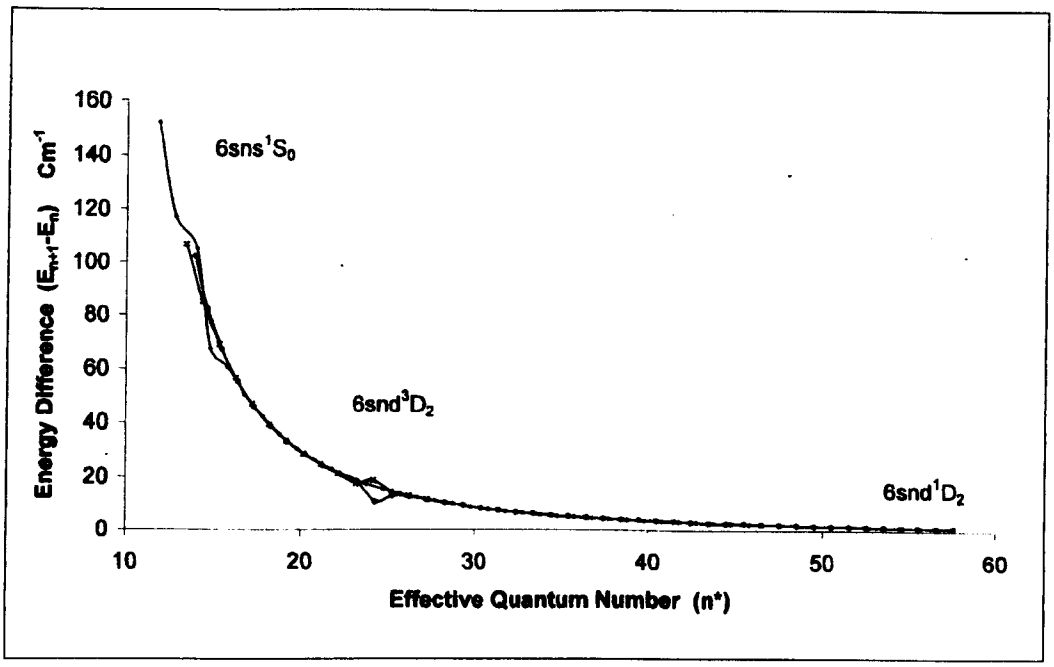

Fig.3.28. Experimental energy difference E_{n+1} - E_n plotted against the effective principal quantum number for the J = 0, 2 Rydberg series of BaI. The $(n^*)^{-3}$ relation is evident in these curves.

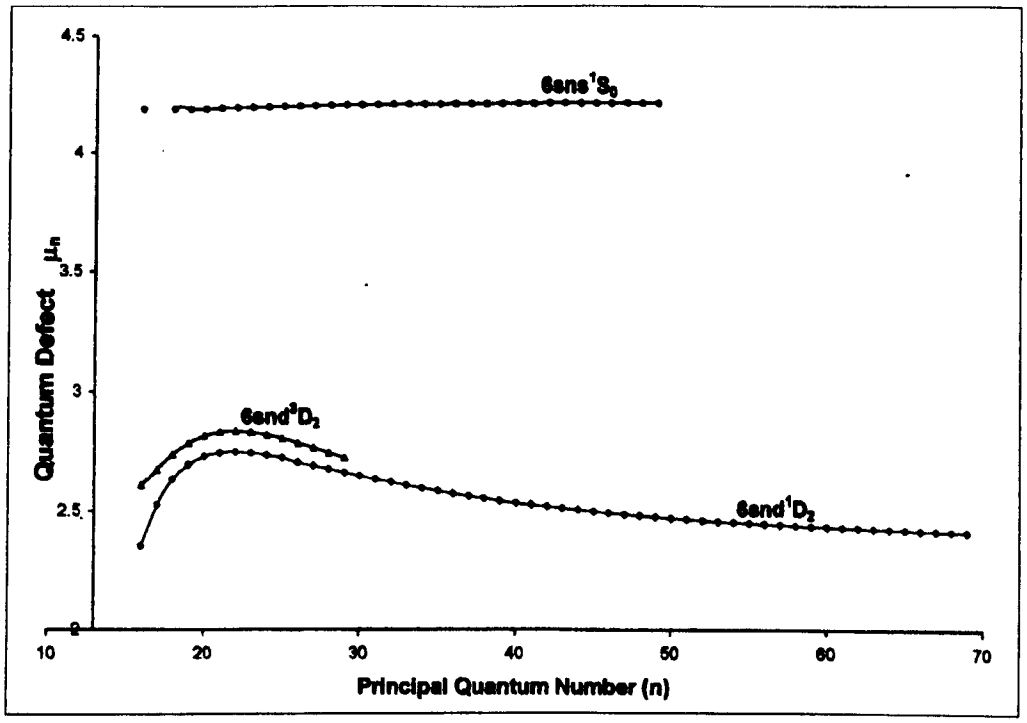

Fig.3.29 Quantum defect curves for the high-lying members of the J = 0,2 Rydberg series of Ba I.

3.8 Double electron excitations and autoionization in alkaline-earth atoms

3.8.1 Double electron excitations in alkaline-earth atoms

Double Rydberg states involve the excitation of both valence electrons according to the scheme $s^2 \rightarrow n_1\ell_1 n_2\ell_2$ in alkaline-earth atoms. By fixing either $n_1\ell_1$ or $n_2\ell_2$ to denote an excited state of the parent ion and allowing the running electron all possible bound excited states until it becomes free one obtains a doubly excited-Rydberg series converging to widely spaced series limits which are the various excited states of the parent ion. The doubly excited states can be thought of two independent single-electron systems with Rydberg series terminating at two different ionization limits. Doubly excited states (originally discovered by Bohr and Wenzel in 1923) lie so close in energy that they are sometimes confused with the single-excitations. Autoionizing Rydberg states with one valence electron in an orbit of high angular momentum around an excited ion core are very important in the dielectronic recombination process (Jacobs *et al* 1976) because of the large multiplicity of such states. The autoionizing states are also important, as pointed out by Gallagher *et al* (1980) for laser action without population inversion using autoionizing decay and for the construction of lasers extending to vacuum ultraviolet region. As a result of autoionization the parent ion may be in an excited state which decays by fluorescence specific to the autoionization process. First demonstration of laser action in atomic ion pumped by selective autoionization was reported by Boker *et al* (1982) who observed lasing action in the visible using step-wise two-photon excitation of the autoionizing states via $6sn\text{p}\ ^1\text{P}_1$ intermediate states in neutral barium.

Double excitation which refers to the simultaneous excitation of two electrons by a single photon is forbidden in the independent electron model and by normal dipole selection rules. Such an excitation can be thought of occurring due to a breakdown in the characterization (configuration mixing) of either the initial state or the final state (Connerade 1998). Atomic states in which two electrons with the same value of the principal quantum number n have highly correlated motion and hence the structure, coupling and wavefunctions of these states are quite different from those of the conventional atomic states. Symmetric doubly-excited states with $n_1 = n_2$ and $\ell_1 = \ell_2$ were considered first by Wannier (1953) and such states approaching the double-ionization threshold are called "Wannier states". These states have several interesting properties, most importantly; they remain highly correlated as the series limit is approached and are highly stable because of symmetry. Figure 3.30 shows the schematic of an alkaline-earth Rydberg state and figure 3.31 shows a schematic of the Wannier states.

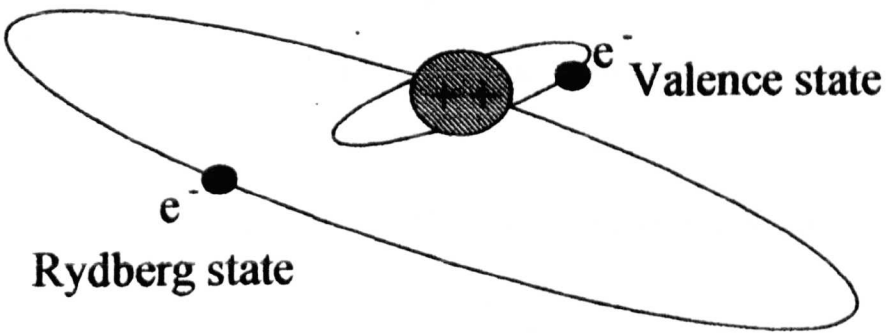

Fig. 3.30 Schematic of a Rydberg state in an alkaline-earth atom

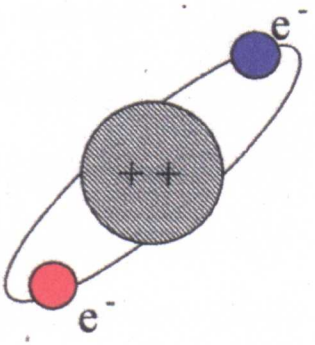

Double-excited Wannier states

Fig, 3.31 Schematic of a Wannier state in an alkaline-earth atom

Madden and Codling (1965) were the earliest to obtain the He high resolution doubly-excited spectrum. Since their pioneering single-photon absorption experiment using synchrotron radiation the doubly-excited helium atom became the paradigm for investigating the correlated motion of two electrons. While He requires nearly 75 eV for both electrons to be simultaneously excited, the alkaline-earth atoms require only one-fifth (15 eV) for two-electron excitation.

In recent years the three-body Coulomb problem of two excited electrons moving in the field of an ion have been investigated with both valence electrons in core penetrating orbits (Camus *et al* 1989, Jones and Gallagher 1990) and with one electron in non-core-penetrating orbits (Eichmann *et al* 1990, Camus *et al* 1993). A true three-body Coulomb system with both valence electrons in non-core-penetrating orbits was experimentally realized by Eichmann *et al* (1990).

The alkaline-earth atoms differ from a pure three-body Coulomb problem handled in theory because of the spatial extent of the 2^{+}core which modifies the Coulomb potential and removes the 'ℓ' degeneracy for the valence electron states that penetrate the core. For high-ℓ states there is no significant penetration of the core due

to the centrifugal barrier effect and therefore, to observe three-body Coulomb states in alkaline-earth atoms, both valence electrons have to be excited to high-ℓ states. Direct double excitation from the ground state of alkaline-earth atoms are possible using synchrotron radiation and multi-photon excitation using several lasers. In laser excitation the advantage is that different angular momentum selection can be made by proper choice of polarization and excitation path in a controlled manner.

Extension of the double excitations can be used to prepare the atoms in which both the outer electrons can be in spatially extended orbitals (the planetary atoms) which could behave like giant two-electron atoms and the correlation properties of such planetary atoms will be very interesting to study. Theoretical interest in double excitation started with the study of planetary electrons with one of the electrons excited to a substantially large orbit compared to the other orbit. Percival (1977) coined the term "*planetary atoms*" for high-lying doubly excited atoms due to their similarity with the gravitational three-body system. In planetary atoms the interaction between electrons is of the same order of magnitude as each electron's interaction with the nucleus. Figure 3.32 shows the schematic of a planetary atom.

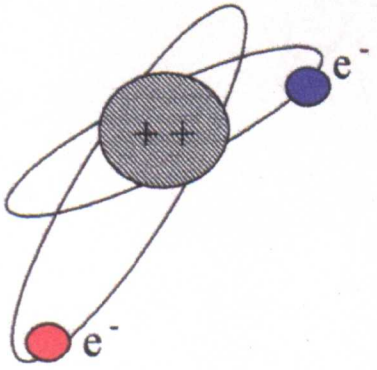

Double-excited planetary states

Fig. 3.32 Schematic of a planetary alkaline-earth atom

3.8.1.1 Double electron excitations in strontium

The spectrum of Sr between the $5s_{1/2}$ threshold and the 5p series limit is dominated by several doubly excited states. Only a few members of the doubly excited states in Sr are located below the $5s_{1/2}$ threshold. These are the $5p^2\ ^3P_{0,1,2}$ and $4d^2\ ^3P_{0,1,2}$. The doubly excited states in strontium observed in the present study by direct two-photon excitation are compared with Rubbmark and Borgstrom (1978) below.

Rubbmark and Borgstrom (1978)	Thesis Expt.
$5p^2\ ^3P_0$ 35193.40 cm^{-1}	
$5p^2\ ^3P_1$ 35400.114 cm^{-1}	
$5p^2\ ^3P_2$ 35674.642 **(Moore's Table)**	
$4d^2\ ^3P_0$ 44 44525.82 cm^{-1}	**44526.07** cm^{-1}
$4d^2\ ^3P_1$ 44595.93 cm^{-1} **(Moore's Table)**	
$4d^2\ ^3P_2$ 44729.61 cm^{-1}	**44729.42** cm^{-1}

Besides the direct two-photon excitations to the doubly-excited $4d^2\ ^3P_J$ configuration listed above, single-photon resonances to the $4d^2\ ^3P_J$ configuration in the one-photon wavelength range 434 nm – 438 nm were also observed due to sequential excitation from the intermediate level $5s5p\ ^1P_1$. These are (Philip and Makdisi 2006) compared with previous observations by Esherick (1977) and Baig *et al* (1999). (λ_{vacuum} are given)

Transition	**Thesis Expt.**	Esherick (1977)	Baig *et al* (1999)
$5s5p\ ^1P_1 \rightarrow$ **$4d^2\ ^3P_2$** @ **434.195** nm		434.20 nm	434.19 nm
$5s5p\ ^1P_1 \rightarrow$ **$4d^2\ ^3P_1$** @ **436.730** nm.		436.74 nm	436.74 nm
$5s5p\ ^1P_1 \rightarrow$ **$4d^2\ ^3P_0$** @ **438.072** nm.		438.07 nm	438.07 nm

Another doubly excited state in strontium, the broad intruder, tentatively labeled as $4d^2\ ^1G_4$, at $27 < n < 28$ in Sr I, $5snd\ ^1D_2$ Rydberg series has two 4d electrons which are highly localized and hence survives the buffer gas collisions while the Rydberg

states are fast quenched (Philip and Connerade 2007). This doubly-excited state is also due to single-photon excitation at the vacuum wavelength indicated.

$5s5p\ ^1P_1 \rightarrow$ **$4d^2\ ^1G_4$ @ 437.065 nm (Thesis)** ; 437.05 nm (Baig *et al* 1999)

3.8.2 Autoionization in alkaline-earth atoms

Above the series limit is a continuum with possible discrete energy states characterized by the same quantum numbers *L, S, J* and parity as the bound states below the series limit. An electron excited to a discrete state in the continuum above the first ionization threshold is in a condition of autoionization (White 1931, Shenstone 1931). Alkaline-earth atoms are experimentally the most convenient two-electron systems to study the bound and autoionizing states. If the two outer electrons of the alkaline-earth atom are excited, the energy levels, in most cases, lie above the ionization limit for single-electron and therefore will be autoionizing.

In highly excited atoms some of the bound states may have the same energy as the continuum states with the same parity and angular momentum making the eigen function of the bound state to have some characters of the continuum. In such case there exists a finite probability for such a state to make a radiationless transition from the bound state to the continuum resulting in ionization (ion and free electron). This process is called "autoionization". Since the autoionization decay can occur via several channels, the absorption line will be a broad resonance with an asymmetric profile (Fano 1961).

Autoionization is one of the most fundamental electron-electron correlation effects observed in many-electron atoms in highly-excited configurations above the first ionization threshold via one of the two possible mechanisms: double excitation and

inner-shell excitation. It involves the coupling between the discrete state of one channel and the continuum of another which is excluded in the independent particle model. Experimental observation of several of double excitations giving strong autoionizing resonances in alkaline-earth atoms gives tangible evidence for the breakdown of the independent particle approximation for many-electron atoms which allows only single-electron excitations (Connerade 1998).

Autoionization was discovered by Buetler (1934) and the theory of autoionization was established by Fano (1961) and hence the name "Buetler-Fano resonance". The first measurement of the autoionizing spectrum of strontium in the range between the first ionization threshold at 45932.19 cm^{-1} and at the $4d_{3/2}$ series limit at 60488.09 cm^{-1} in strontium was reported by Garton and Codling (1968) which was followed by Garton *et al* (1968) , Hudson *et al* (1969).

The profile of the autoionization resonance is given by Fano's formula (Fano 1961):

$$\sigma(\varepsilon) = \frac{|D|^2 (q+\varepsilon)^2}{1+\varepsilon^2} \qquad (3.22)$$

Where q is the profile index of the resonance, a dimensionless quantity to describe the asymmetry of the line and ε is given by:

$$\varepsilon = \frac{(\nu - \nu_0)}{\Gamma} \qquad (3.23)$$

$(\nu - \nu_0)$ is the detuning and Γ is the halfwidth, D is the dipole operator.

If q = 0, we get an inverted profile and a symmetrical anti-resonance (also known as window resonance). On the other extreme case, when $q \rightarrow \infty$ we have a pure, symmetric resonance with a Lorentzian shape.

The physical significance of the asymmetric profile for autoionization is well discussed by Connerade (1998). Consider there are two different paths for an autoionization, for example one is the direct transition from an initial state to the autoionization state and the other involves the transition from the initial state to the autoionization state via an intermediate compound state. If the two paths are coupled, then there can be interference between the two paths resulting in to constructive interference on one side and destructive interference on the other thereby producing the asymmetry for the autoionization resonance. Figure 3.33 shows the family of curves generated using the Fano lineshape formula for different values of the shape index q ($1 < q < 7$).

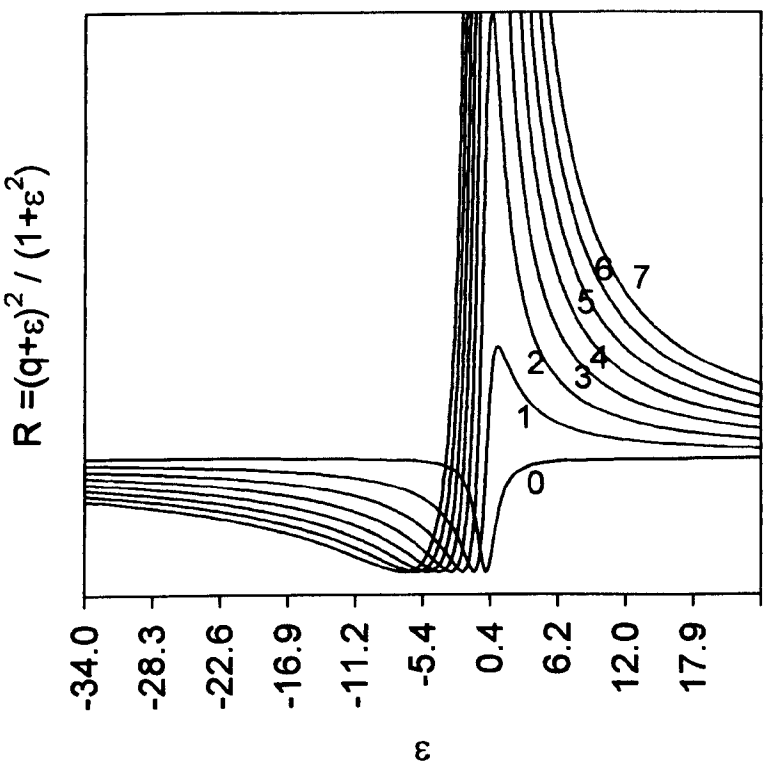

Fig. 3.33 Fano line shape function plotted for different values of the shape index q

The simple Fano formula given in equation (3.22) applies well to a single, isolated resonance with a nearly flat continuum and is coupled to a single continuum

(Connerade (1998). Also, the autoionization width decreases as $(n^*)^{-3}$ as indicated in figure 3.34 and has a decay time much shorter than radiative lifetimes.

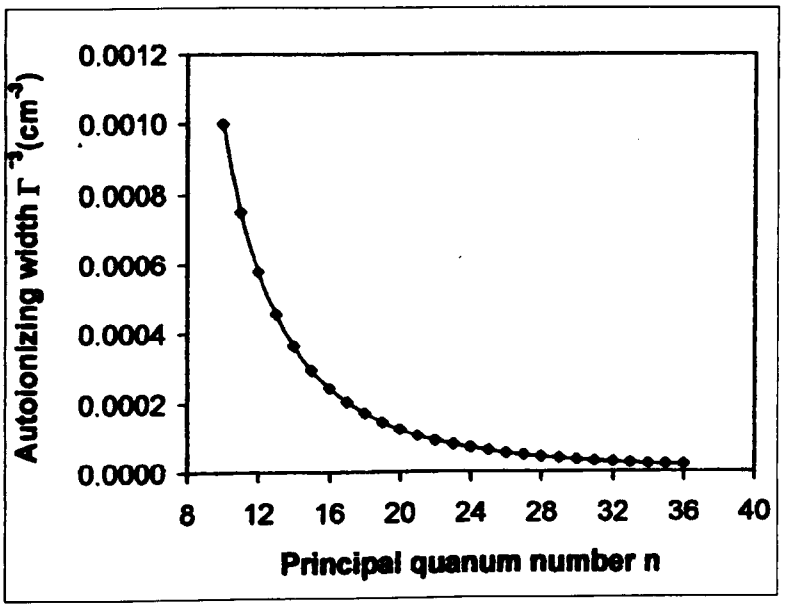

Fig. 3.34 Typical graph showing the $(n)^{-3}$ scaling law for Sr $5p_{1/2}ns_{1/2}$ autoionizing width (Expt. values for Γ from *Xu et al* 1986)

Originally the autoionizing levels in alkaline-earth atoms were accessed by classical single-photon absorption in the vacuum ultraviolet region from the ground state ms^2 $^1S_0$ and, therefore, only $J = 1$ states were populated, resulting in the well-known Beutler-Fano resonances. The first important measurement in strontium in the spectral range between the first ionization threshold and the 4d ($^2D_{3/2, 5/2}$) series limit was by Garton and Codling (1968) using classical absorption spectroscopy and photographic recording. They presented the $J = 1^0$ odd-parity spectrum and the doubly excited states converging to the 4d $^2D_{3/2}$(60488.09 cm^{-1}) and 4d $^2D_{5/2}$ (60768.43 cm^{-1}) limits besides the Rydberg series converging to the first threshold (45932.19 cm^{-1}). Garton *et al* (1968) presented an analysis of the autoionizing resonances using Fano's (1961) formula for line shape for the $5s^2$ $^1S_0 \rightarrow 4dnp,nf$ resonances. This was followed by Hudson (1969) who presented the absorption cross section in the autoionizing region.

Extensive experimental studies of autoionizing Rydberg series of alkaline-earth atoms have been reported ever since the first study by Garton and Codling (1969). Ewart and Purdie (1976) used laser two-photon spectroscopy to study the even-parity Rydberg and autoionizing levels in strontium and reported term values for $5snS$ $^1S_0$ and $5snd$ $^1D_2$ series besides configuration mixing in $^1D_2$ series and identification of an autoionizing term just above the $5s_{1/2}$ threshold which they had identified as $4d^2\ ^1D_2$. From J value assignment using circularly polarized light and from quantum defect estimates the strong broad resonance in the two-photon spectrum at 431.1 nm wavelength was identified as $4d^2\ ^1D_2$. Connerade *et al* (1980) employed synchrotron radiation and photography to study the $J = 1$ Rydberg series converging to the 4d ($^2D_{3/2,5/2}$) and 5p ($^2P_{1/2,3/2}$) ionic levels. By the availability of efficient tunable lasers multi-photon techniques allowed selective excitation of well-defined autoionizing states with a variety of J levels to be accessible from the ground state.

For example, multi-step multi-photon excitation by using 3 lasers is a convenient scheme to study the autoionizing spectrum of the alkaline-earth such as Sr I. Starting from the ground state two lasers are used for excitation $5s^2 \rightarrow 5s5p \rightarrow 5snd$ and then a third laser to the final $5p_{1/2}$ and $5p_{3/2}$ autoionizing states. The transitions can take place with a probability for Rydberg orbital nd with an s electron in the core or a different Rydberg orbital n'd with one p electron in the core such that $n \neq n'$. Due to the interference of the two transitions the well-known Beutler-Fano asymmetric profile (Fano1961) will be observed.

Double excitations in strontium have attracted several experimental and theoretical investigations. Some of the earlier experimental studies reported include Armstrong

et al (1977), Aymar and Robaux (1979), Cooke and Bhatti (1982), Feldman and Welge (1982), Feldmann *et al* (1982), Kim and Lambropoulos(1982), Gounand *et al* (1983), Chin and Lambropoulos (1984), Xu *et al* 1986, Zhu *et al* 1987, Lambropoulos *et al* (1988) Camus *et al* (1989), Lange *et al* (1989), Jones *et al* (1990), Kompitsas *et al* (1990). Theoretical description of the doubly excited states in alkaline-earth atoms was given by combining multichannel quantum defect theory with R-matrix methods (Green 1985, Aymar 1987, Aymar *et al* 1987, Aymar and Lecomte 1989, Kompitsas *et al* 1990). In strontium between the $5s_{1/2}$ threshold and the $4d_{3/2}$ limit are the **$5p^2$** and **5p6p** doubly excited configurations. These are labeled as:

$5p^2\ ^1D_2$, $5p^2\ ^1S_0$; 5p6p ^3P_J, 5p6p $^1P_1$, 5p6p $^1D_2$, 5p6p $^3S_1$ and 5p6p ^3D_J.

Kompitsas *et al* (1991) used two-step excitation via the intermediate 4d5p $^1P_1$ level for the excitation of even-parity, $J = 0,1,2$ autoionizing spectra of strontium below the $4d_{3/2}$ limit. They observed the 4d*n*d series to be strongly influenced by $5p^2\ ^1S_0$ and 5p6p $^3P_0$ levels. They identified a broad resonance at 54451 cm^{-1} which was interpreted as $5p^2\ ^1S_0$ level. Initially $5p^2\ ^1S_0$ was labeled for the level at 37160.28cm^{-1} in Moore's table and later theoretical calculations (Aymar *et al* 1987) corrected this level as one with a $4d^2$ character and predicted the $5p^2\ ^1S_0$ level to lie above the first ionization threshold. Griesmann *et al* (1994) found excellent agreement with the R-matrix calculations by Green and Aymar (1991) for the autoionizing series in strontium. Farooqi *et al* (1992) also studied the photoionization of strontium around the $5p_{1/2}$ series limit.

Conventional uv spectroscopy (Connerade *et al* 1980) is not very convenient for autoionizing states because of the discrete-discrete and discrete-continuum

interactions. An important method widely used for preparation of the autoionizing state is the inner core excitation (ICE) technique first employed by Cooke *et al* (1978) by which several states which cannot be accessed from the ground state due to selection rule restrictions can be accessed. ICE technique (Cooke and Gallagher 1978) offers a selective excitation of well-defined and clean autoionizing spectra with minimum interference from the continuum state. The angular momentum of the autoionizing state is set by the number of photons absorbed and the polarization of the laser beams. ICE involves multi-step excitation with single-electron transitions in each step and the spectral profile obtained will be symmetric with nearly Lorentzian resonances (without Rydberg electron shakeup and Beutler-Fano resonance profile) corresponding to core excitation. The autoionization width will be proportional to the autoionization rate. For example the excitation of the autoionizing states $5pn\ell$ in strontium and $6pn\ell$ in barium are produced in a two-step laser excitation process starting from the respective bound states $5sn\ell$ and $6sn\ell$ states. In the first step one of the valence electrons is excited to a Rydberg state ($n\ell$). In the second step, the remaining core electron in the 5s state in strontium or 6s state in barium is excited to the $5p_{1/2}$ or $6p_{1/2}$ state respectively with the Rydberg electron ($n\ell$) remaining as a spectator (as illustrated in figure 3.35). The spectrum reveals the fine details of the autoionizing states and the interaction between the 5p (or 6p) and $n\ell$ electrons in strontium (or barium) and the auotionization rate of the $5p_{1/2}n\ell$ (or $6p_{1/2}n\ell$) state scales as $(n^*)^{-3}$, where n^* is the effective principal quantum number.

The ICE scheme is highly efficient and the transition from $5sn\ell$ to $5p_{1/2}n\ell$ with the outer Rydberg electron as spectator is like the resonance transition of the Sr^+ ion. Further, by applying a DC electric field, the many states with different 'ℓ' can be

switched on and adiabatically switched off to get the zero-field state (Stark switching technique (Freeman and Kleppner 1976).

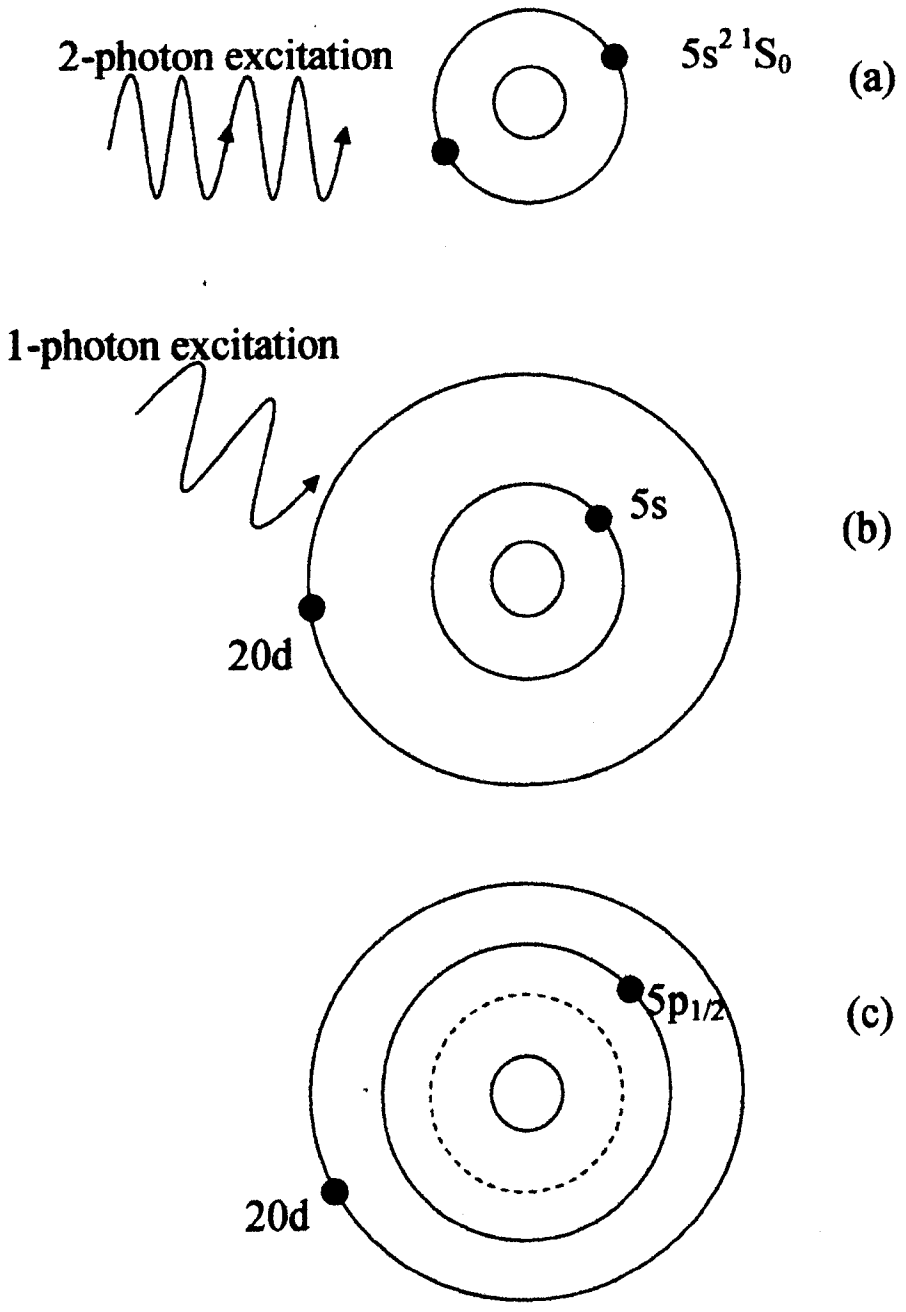

Fig. 3.35 $5p_{1/2}20d$ excitation in Sr I using ICE technique

Dai *et al* (1995) and Dai (1995) used the ICE technique in conjunction with ion detection to measure the even-parity $5s\ell$ levels of Sr I. It was shown that this new technique is highly efficient for the detection of Rydberg atoms by driving them to

autoionizing states and detecting the ions from autoionization decay. A similar method was also used by Lu *et al* (1999) for the study of the even-parity $J = 0$ spectrum of barium. Xu *et al* (1986) made a detailed experimental study of the $J = 1$, $5p_{1/2}ns_{1/2}$ and $5p_{3/2}ns_{1/2}$ autoionizing series of Sr I using ICE technique and compared the results with theoretical calculations using MQDT. Their scheme consisted of transverse excitation of an atomic beam sequentially in time using three linearly polarized lasers as follows:

1st Laser $5s^2\ ^1S_0 \rightarrow 5s5p\ ^1P_1$ (Resonance line);

2nd Laser $5s5p\ ^1P_1 \rightarrow 5snp\ ^1S_0$ (Rydberg state with outer electron far away from the Sr^+ ($5s_{1/2}$ core);

3rd laser is used to excite the autoionizing transition $5s \rightarrow 5p_J$ of the Sr^+ core

The ICE technique has also been employed recently by Jones *et al* (2000) for the measurement of 6p*n*'k' autoionizing states from 6s*n*k Stark states in barium. Cooke *et al* (1978) and Xu *et al* (1987) reported experimental quantum defects for 5p*n*d autoionizing states of strontium higher than those of Sr I 5s*n*d $^1D_2$ Rydberg series where as Dai and Lu (1996) obtained quantum defect values for the autoionizing states smaller than those of the bound 5s*n*d $^1D_2$ states consistent with the theoretical prediction by Aymar and Lecomte (1989). Waigorski *et al* (1997) used a modified ICE technique for overcoming the difficulties with the laser line bandwidth in measuring the autoionizing resonance width. Recently the even-parity $J = 0,1,2$, 5p*n*p autoionizing spectra of strontium was investigated experimentally using two-step ICE technique by Cohen *et al* (2001).

A possible scheme for strontium $5p_{3/2}ns$ autoionization using two-photon excitation and ICE technique using two lasers is shown in figure 3.36. Alternatively, the

autoionization path through ICE can be achieved by first populating the atoms in the 5s5p $^1P_1$ state using electron impact excitation as achieved in the heat-pipe setup employed in this thesis study. This is followed by excitation to the 5s*n*s Rydberg state by single-photon excitation using the first laser and finally to the $5p_{3/2}$ *n*s autoionizing state by the second laser.

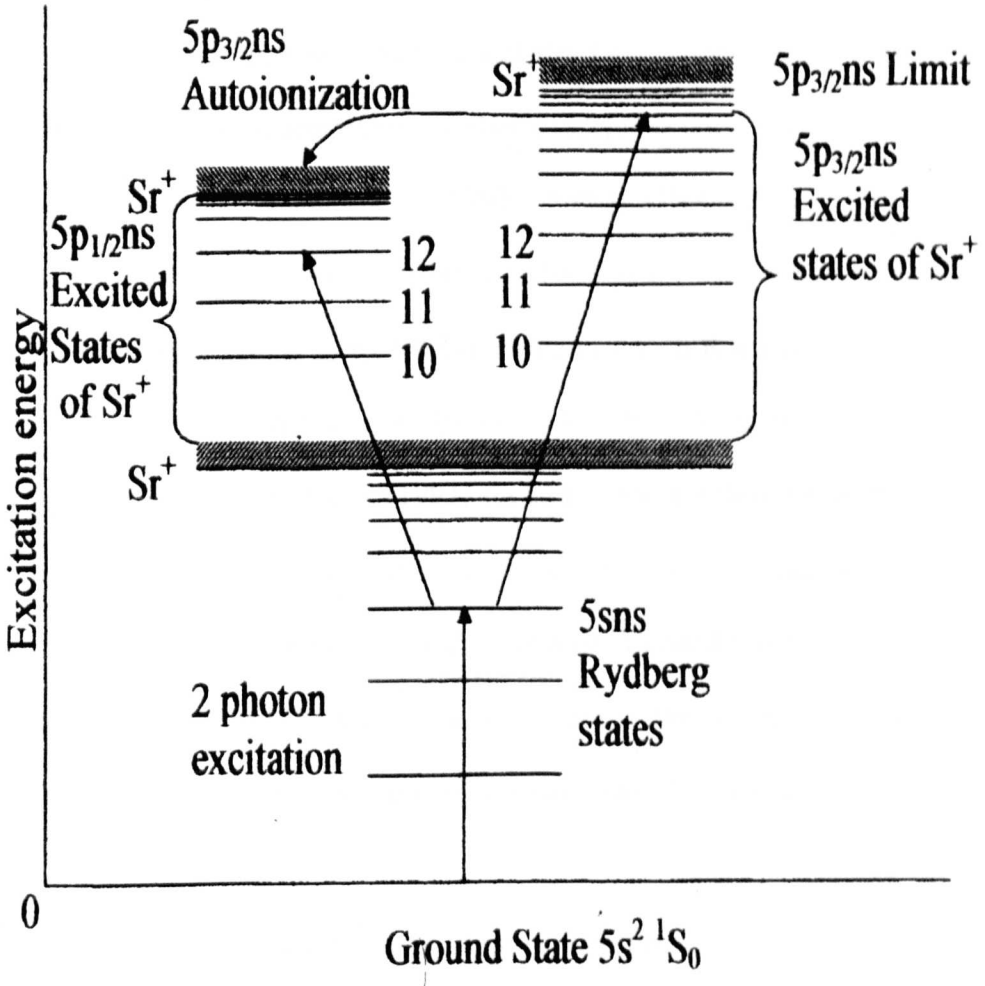

Fig. 3.36 Schematic of $5p_{3/2}$*n*s autoionization in strontium using ICE technique combined with two-photon excitation

3.8.3 Barium doubly-excited autoionizing series

For the past several decades extensive investigations have been reported for the autoionizing series of barium. Garton and Codling (1957) studied the absorption spectrum of barium using a vacuum spectrograph and identified several doubly excited states. Garton and Tomkins (1969) photographed six 5d*nt* autoionizing lines converging to the 5d $^2D_{3/2}$ and 5d $^2D_{5/2}$ limits. Several important observations reported in recent years include investigations by Gounand *et al* (1991) using multi-step laser excitation, single-photon excitation of the $J = 1^0$, 5d*nt* autoionizing series by Abutaleb *et al* (1991), measurement of photoabsorption cross section of the5d*nt* autoionizing series by Griesmann *et al* (1992). Aymar (1990), Green and Aymar (1991), Aymar *et al* (1996) presented theoretical calculations for the photoabsorption cross sections using MQDT combined with R-matrix method. The even-parity 6p*n*p [$6p_{1/2,3/2}$, *n*p]$_{J=0,1,2}$ series of barium have been well-investigated (Carre *et al* 1990). Wilke and Kock (1993) measured the absolute photoabsorption cross-section from the barium 6s6p $^1P_1$ state for the wavelength range 417 nm-370 nm using tunable laser and thermionic diode detection. Recently Maeda *et al* (2000) measured the photoionization cross-section of barium in the wavelength range 209 nm - 221 nm covering the autoionizing region between 6s $^2S_{1/2}$ and 5d $^2D_{5/2}$.

The level at 38663 cm^{-1} in barium was initially identified as 6p^2 $^1S_0$ in Moore's Table (1958). MQDT calculations by Aymar *et al* (1978) reassigned this level as 6s10s $^1S_0$ which is mixed with the 5d6d $^1S_0$ level at 38924 cm^{-1} and predicted that 6p^2 $^1S_0$ should lie above the first ionization threshold at 42035 cm^{-1}. Detailed experiments by Camus *et al* (1982) using two-step laser excitation and optogalvanic detection for the even-parity autoionizing spectrum of barium identified the 6p^2 $^1S_0$

at 44800 cm^{-1} as the lowest member of the 6p*n*p $^1S_0$ Rydberg series converging on the 6p $^2P_{3/2}$ threshold (Aymar *et al* 1982) and confirmed the prediction by Aymar *et al* (1978). Bente and Hogervorst (1989) used laser spectroscopy and MQDT analysis to obtain energies and linewidths of the 5d*n*f autoionizing Rydberg series of barium converging to the $5d_{3/2,5/2}$ ionization limits. Lange *et al* (1991) used MQDT combined with R-matrix calculations to compare their experimental results for the *J* = 1, 6p*n*s autoionizing Rydberg series of barium.

Experimental studies of 6p*n*s (Kachru *et al* 1985), 6p*n*p (Story *et al* 1989, de Graaff *et al* 1990), 6p*n*d (Bhatti *et al* 1981, Gounand *et al* 1983), 6p*n*f (Abutaleb *et al* 1991), 6p*n*g (Jaffe *et al* 1985), 6p*n*h (Bente and Hogervorst 1990) and very high angular momentum 6p*n*ℓ (ℓ = *n*-1) circular states for up to *n* = 13 (Jones and Gallagher (1988) have been also reported in the literature for barium . For high angular momentum states the centrifugal barrier pushes the Rydberg electron farther from the core electron thereby reducing their interaction.

Similar to the auotionization scheme mentioned previously for strontium, a possible two-photon, two laser excitation path for obtaining the spectra corresponding to barium $5d_{5/2}$*n*p and $6p_{3/2}$ autoionization is shown in figure 3.37. In this scheme the 6s*n*p $^1P_1$ state can be populated by single-photon and the final ICE excitation can be, possibly achieved by suitable two-photon excitation. For the autoionizing states also, the quantum defect μ can be calculated using the usual Rydberg formula: $E_n = I - R_M / (n-\mu)^2$, where I is the ionization limit. Thus for example, for strontium the ionization limits (as available in literature) are, Sr^+ $I_{p1/2}$ = 69647.38 cm^{-1} and Sr^+ $I_{p3/2}$ = 70448.84 cm^{-1}.Similarly for barium, the ionization limits are: Ba^+ $I_{p1/2}$ = 62296.470 cm^{-1} and Ba^+ $I_{p3/2}$ = 63987.314 cm^{-1}.

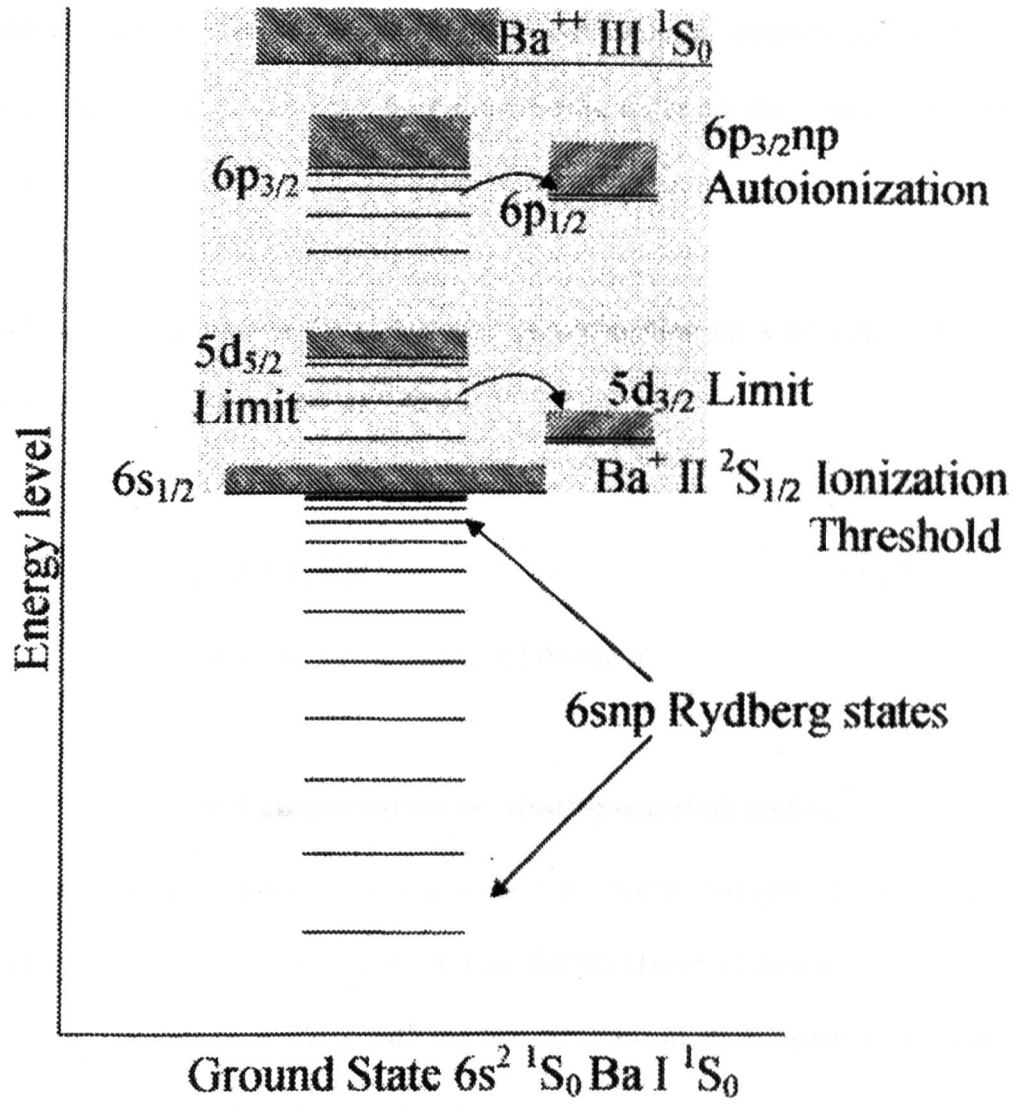

Fig. 3.37 Schematic of $5d_{5/2}$, $6p_{3/2}ns$ autoionization in barium

3.8.4 Dielectronic recombination

Dielectronic recombination (DR) is the time-reversed autoionization process (Bugess 1964) of a positive ion and a free electron for the formation of a doubly excited state followed by the emission of a photon. For example, a dielectronic recombination process in strontium can be written as:

$Sr^{+}(5s) + e^{-} \rightarrow Sr\,(5pn\ell) \rightarrow Sr\,(5sn\ell) + h\nu$.

After the radiationless capture, the electron in Sr 5p$n\ell$ may either decay back to Sr^+ ε5s continuum or in to Sr^+ε4d continuum or remain in the $n\ell$ orbital allowing the core to relax via $Sr^+(5p) \rightarrow Sr^+(5s)$ with the captured electron remaining as the spectator. Similarly, in barium 6p$n\ell$ autoionizing states are important for dielecronic recombination.

Both autoionization and the dielectronic recombination rates (γ) follow the scaling laws for the respective rates as follows:

$$\Gamma_s(nl) = \gamma_s(l)n^{-3} \qquad (3.24)$$

$$\Gamma_d(nl) = \gamma_d(l)n^{-3}, \qquad (3.25)$$

Where, Γ is the respective autoionizing or DR width.

3.8.5 Importance of doubly-excited states

Atomic Coulomb systems consisting of two highly excited electrons and one positive ion core can be considered as two distinct classes of states:

(i) Wannier states with the two electrons move at nearly equal distances from the ion ($r_1 = r_2$) and,

(ii) Planetary states in which the two orbital radii are different ($r_1 \neq r_2$).

The planetary states are the states with asymmetric double excitations with one electron in highly excited state while the other electron remains in a relatively low state. With asymmetric double excitations the planetary atoms behave like giant two-electron atoms with highly correlated motion which makes them very interesting (Roussel *et al* 1990, Eichmann *et al* 1992, Seng *et al* 1995). The three-body Coulomb systems have so far been experimentally limited to low-lying states. Theoretical modeling using the K-matrix formulation based on multi-channel

scattering of the outer electron from an ionic core, besides the inner electron excitation, has also been reported (Kim and Green 1987, Aymar 1987, Aymar and Lecomte 1989). Multi-photon laser excitation of alkaline-earth atoms (strontium and barium) can be used to excite both outer electrons to very high angular momentum states, ($\ell \geq 3$ for strontium and $\ell \geq 4$ for barium) with minimum core penetration to observe the correlated motion of the two electrons and the three-body Coulomb states.

The first reported effort to find the evidence of the planetary states was due to Gallagher *et al* (1981) who studied the excitation spectra of the 7s*n*d states in barium and concluded that the highly excited Rydberg *n*d electron partially shields the inner 7s electron from the nucleus. Evidence of electronic correlation in high-lying doubly excited states have been observed in barium by Camus *et al* (1989), Eichmann *et al* (1990) and Jones and Gallagher (1990). The correlation effects can be observed as a polarization and Stark-like splitting of the inner electronic states by the electric field of the outer electron which is assumed to be frozen. Eichmann *et al* (1990), using six-laser excitation, reported the observation of planetary atomic states (nℓ *N*d) in barium with both valence electrons excited to states with large principal quantum number ($n \geq 30$, $N \geq 60$ and $\ell \geq 4$) which are equivalent to a true three-body Coulomb system. They observed strong positional correlation effects which were explained in terms of the repulsion between the "frozen" outer electron and the highly polarizable inner electron. Also, using multi-photon laser excitation complimented by electric field, Eichmann *et al* (1990) produced high angular momentum states in strontium with negligible Sr^{++} core penetration and penetration between the outer electron wave functions, thereby experimentally realizing true excitation of the so-called *"planetary states"* in strontium.

van Leeuwen *et al* (1996) observed electron correlation effects in a special class of a three-body Coulomb system in barium with double Rydberg states of the type $Ng\ ng$ [N = 5-9, $n >> N$, where N (n) is the principal quantum number of the inner (outer) valence electron]. Unlike in planetary atoms for which the orbital angular momentum of the outer electron is much larger than that of the inner electron, van Leeuwen *et al* (1996) excited both valence electrons in non-core-penetrating orbits with the same angular momentum so that the electrons move in orbits having approximately the same classical turning points. The multi-step pulsed laser experiment using the isolated-core-excitation scheme involved the systematic variation of the principal quantum number of one of the valence electrons while keeping the other constant. Recently Cohen *et al* (2005) reported extensive investigation of asymmetric double Rydberg (ADR) states of barium using two-photon 6s $\rightarrow$ 8s ICE technique from the initial bound 6snt (t = 5) Rydberg states.

3.9 Autoionizing resonances observed in strontium and barium by two-photon excitation

The autoionizing resonance will have a shape given by the simple Fano formula (Eqn. 3.22) when the autoionizing state is just above the first ionization threshold and is coupled to only one continuum- the "first autoionization range" as observed in strontium shown in figure.3.38 (a). In figure 3.38 (b) the same two-photon spectrum taken with a different composition of the buffer gas is shown. It can be seen that the continuum just above the first ionization threshold and the relative intensity of the single-photon resonances are increased by a change of the buffer gas composition.

In Fig. 3.39 the autoionizing resonance (labeled as 5d8p $^1P_1$) observed in the two-photon spectrum of barium is shown. The doubly-excited state labeled as 5d5f $^1P_1$ is also observed in this spectrum. (Fig. 3.25 is repeated here because of its relevance).

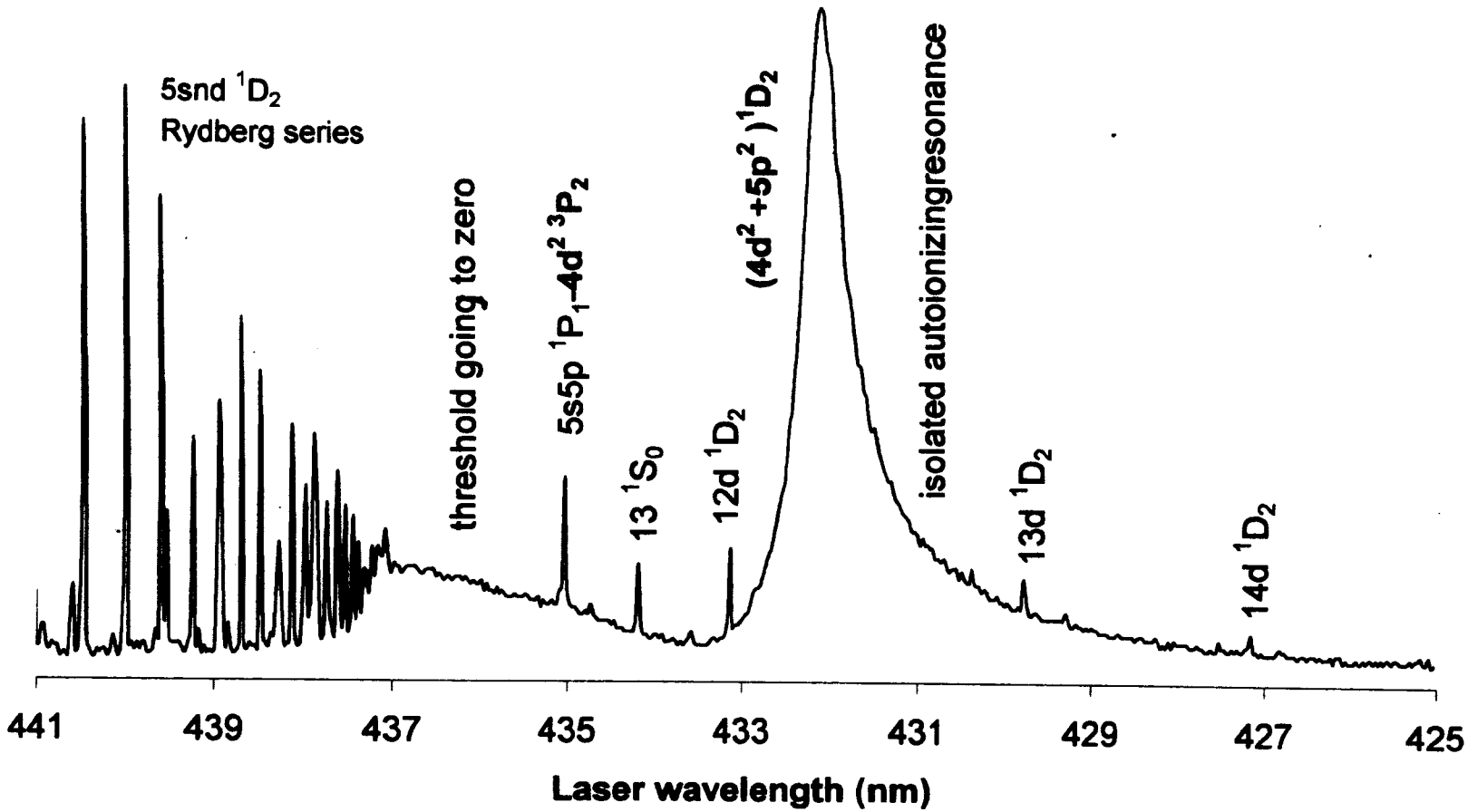

Fig. 3.38 (a) Two-photon spectrum of Sr I showing the $(4d^2 + 5p^2)\ ^1D_2$ autoionizing resonance just above the first ionization threshold. (40 mbar He buffer and 2μJ dye laser energy/pulse, +7Volt detector bias). The continuum above the first threshold approaches zero outside the autoionizing resonance

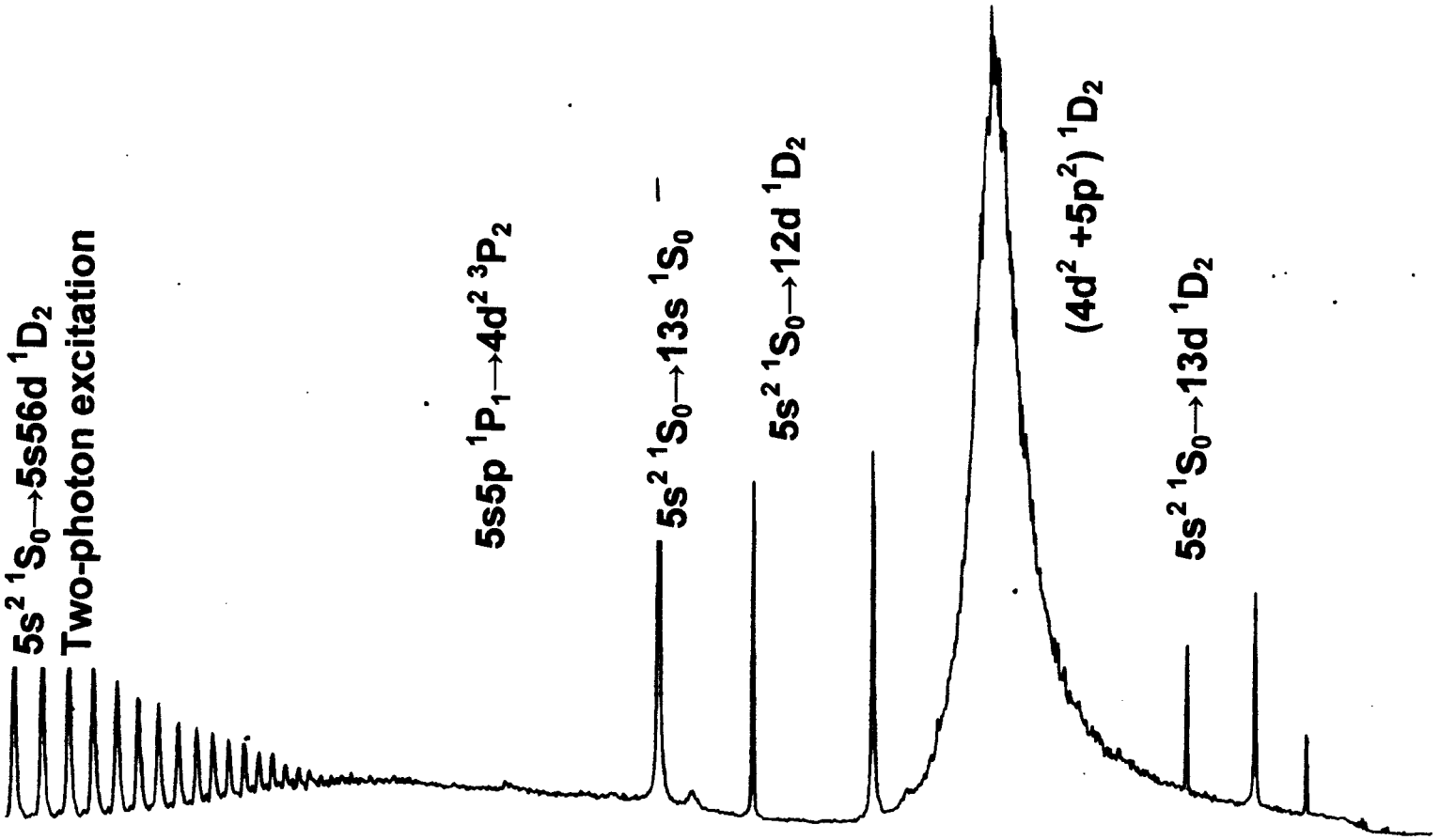

Fig.3.38 (b) .Two-photon spectrum of Sr I showing the $(4d^2 + 5p^2)\ ^1D_2$ autoionizing resonance just above the first ionization threshold (10 mbar Ar buffer and 2 μJ dye laser energy/pulse, +7 volt detector bias). Note that the continuum above threshold which approaches zero remains nearly flat over a wide range and the relative strength of single-photon resonances improves with a different buffer gas composition

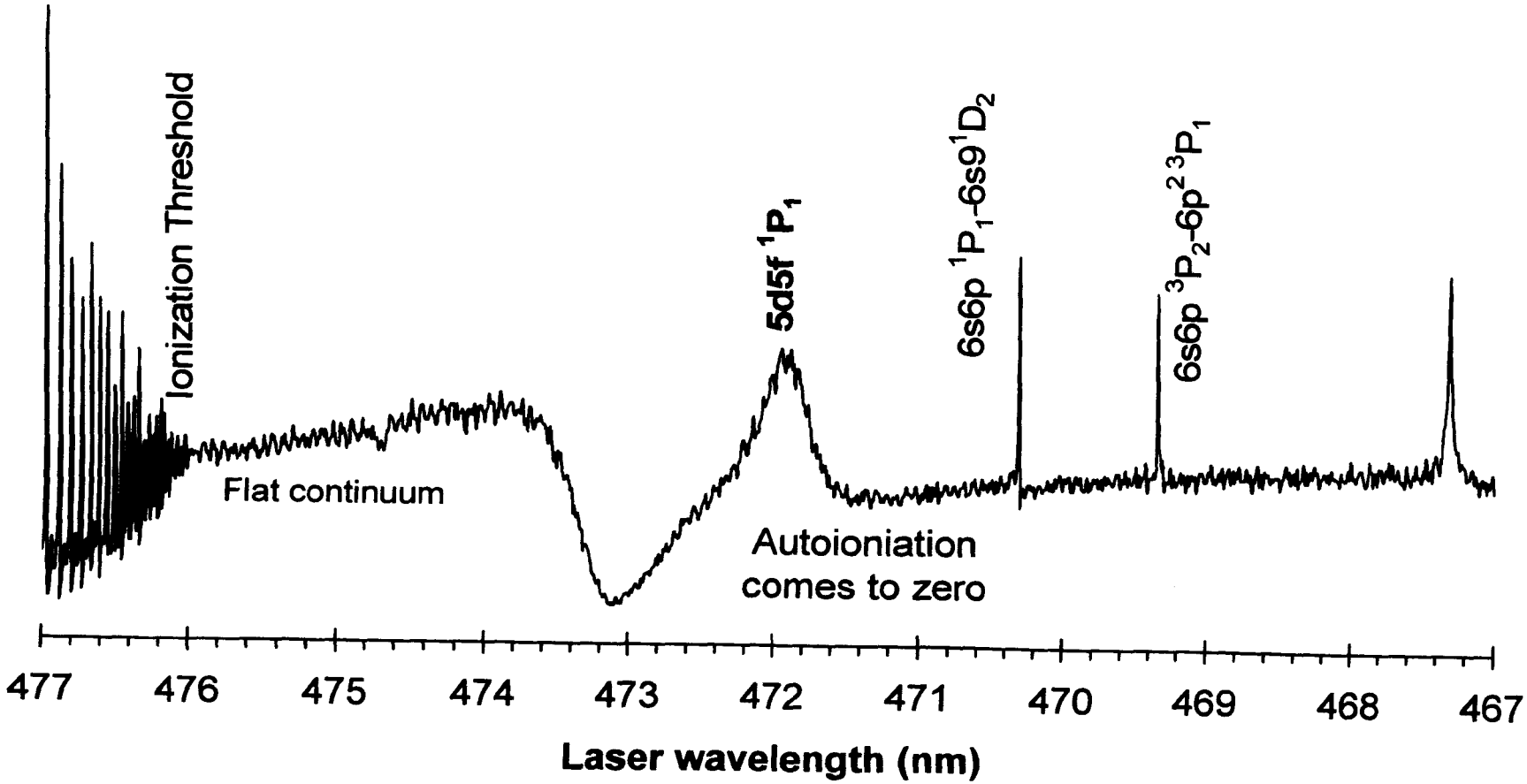

Fig. 3.39 Two-photon spectrum of Ba I showing the ionization threshold and the autoionizing level labeled as 5d5f $^1P_1$. Single-photon resonances also are observed which are due to sequential excitation from the 6s6p $^1P_1$ intermediate level. (This is the same spectrum shown in Fig. 3.25 in Page 126 of the Thesis. Because of its relevance it is repeated here).

3.10 Time evolution of Rydberg atoms probed by the Gated Pulsed Field Technique (GPT)

The lifetime is one of the fundamental properties of the excited states of an atom and provides information about the wave function of the excited state as well as testing theory for the calculation of oscillator strengths and polarizabilities. Rydberg states are characterized by very long radiative decay time (well-known $(n^*)^3$ scaling law for pure, unperturbed states, where n^* is the effective principal quantum number) and large Stark shifts occur due to the large dipole moments. In alkaline-earth atoms due to series perturbations by configuration mixing between Rydberg series and doubly excited configurations (mp^2, $[m\text{-}1]d^2$, where m = 5 and 6 for Sr and Ba respectively) the radiative lifetimes of Rydberg states are found to depart significantly from the $(n^*)^3$ relation. Since the wave function of a perturbed level consists of a short-lived component with typical life-time values (~10 ns) of valence states and a long-lived component with life-time value (several μs) corresponding to pure Rydberg states, the Rydberg character of a perturbed state can be probed by lifetime and Stark shift measurements. Accurate life-time measurements of excited states are also important for reliable level designations and to refine the analysis of atomic structure. Since MQDT calculations of the lifetime are for free atoms only, and do not give values measured in the presence of buffer gas collisions, external fields and black body radiation, experimental data must be appropriately corrected or extrapolated to zero pressure for comparison with theory. Recently the determination of the radiative lifetimes of the 5s5p ^3P_J (J = 1,2) metastable levels of strontium have attracted great interest for frequency standards and atomic clocks (Courtillot *et al* 2005) and for atom cooling and trapping (Derevianko 2001) etc.

A comprehensive review of various experimental techniques for measurement of lifetimes of atomic excited states is given by Imhof and Read (1977). The 'Time-delayed Field ionization Detection' technique (Aymar *et al* 1981) and the time resolved 'Laser Induced Fluorescence' (LIF) technique (Aymar *et al* 1982, Bowers *et al* 1996) are well-recognized as reliable methods of determination of the radiative lifetimes. The delayed coincidence method was used by Jonsson *et al* (1984) to determine the radiative lifetime of the $4p^2$ configuration in calcium. Radiative lifetimes have also been determined from time- and wavelength-resolved fluorescence emission measurements (Smedley and Marran 1993). Fluorescence decay lifetime measurements are reliable for atomic beams where collisions are kept very low.

Using two-step laser excitation and time-resolved field ionization technique Aymar *et al* (1981) measured the lifetimes of barium 6s*n*d $^1D_2$ (n = 17 - 35) and 6s*n*d $^3D_2$ (n = 17-28) in the vicinity of the perturbing 5d7d $^1D_2$ level. They observed a shortening of the lifetime due to configuration mixing between the long-lived Rydberg states and the short-lived perturber. Gallagher *et al* (1981) also reported lifetime measurements of barium 6s*n*d $^{1,3}D_2$ Rydberg series in the vicinity of 5d7d $^1D_2$ perturber state. Aymar *et al* (1982) also employed the Pulse Modulated Laser Spectroscopy (PUMLOS) technique for barium 6s*n*s $^1S_0$ Rydberg series and observed a strong decrease in the lifetime values due to the presence of the short-lived doubly excited state 5d7d $^3P_0$. Grafstrom *et al* (1983) measured the radiative lifetimes of strontium 5s*n*d $^{1,3}D_2$ Rydberg series, by stepwise excitation using the $5s^2$ $^1S_0 \rightarrow$ 5s5p $^1P_1$ intermediate stage, and reported a decrease in lifetimes for the $^1D_2$ series around n = 15, where singlet-triplet mixing takes place. Deviations from the predicted $\tau_{0(n)} \sim (n^*)^3$ relation for the radiative lifetime are also expected in field

ionization detection schemes, due to contributions to the ionization signals by fields E ~ Ecr , where $E_{cr} = 1/16(n^*)^4$ is the critical field in atomic units.

This thesis presents a novel experimental technique, the gated pulsed field detection technique (GPT for short), employed for the first time in a heat-pipe setup, with considerable advantages of simplicity, to examine the time decay of the Rydberg atom population. In this method, unlike in the high voltage pulsed field scheme used to determine lifetime of the cold Rydberg atoms in magneto-optical traps (Nascimento *et al* 2006), very low field (1.5- volt cm^{-1}- 4 volt cm^{-1}) is sufficient for the time-resolved state selective detection of Rydberg atoms. After excitation by the laser, Rydberg atoms are detected by a low voltage pulse with a variable delay in a thermionic diode detector. As the classical Kepler period, $\tau_{k(n)} \sim 1.5 \times 10^{-16} n^3$, is much shorter than (for example, for $n = 40$, $\tau_{k(n)} \sim 10$ps) the duration of the applied pulsed electric field (0.5ms), the atoms behave as in a DC field.

The lifetime τ_{eff} of an excited state is related to the sum of the partial lifetimes τ_i of the various allowed processes given by,

$$\frac{1}{\tau_{eff}} = \sum_i \frac{1}{\tau_i} \qquad (3.26)$$

Considering different processes of decay, the effective decay rate of a Rydberg state can be expressed as,

$$\Gamma_{effective} = C_1\Gamma_{radiative} + C_2\Gamma_{perturber} + C_3\Gamma_{collision} \qquad (3.27)$$

$\Gamma_{radiative}$ is the pure Rydberg level decay rate with $(n^*)^3$ dependence and $\Gamma_{perturber}$ is the decay rate induced by the interloper which perturbs the series. For levels far

away from a perturber the Rydberg level has a decay rate (which is the reciprocal of the lifetime)

$$\Gamma_{effective} = \frac{a\gamma_{radiative}}{(n^*)^3} + b\gamma_{collision} \qquad (3.28)$$

The constants 'a' and 'b' can be obtained from fitting experimental data taken with several collision parameters.

Khan *et al* (1994) reported a considerable increase in τ_{eff} due to collisions. For a pure Rydberg state, the radiative lifetime $\tau_{0(n)}$ of a level with principal quantum number n and effective principal quantum number n^* obeys the scaling law :

$$\tau_{0(n)} = \frac{1}{\gamma_n}(n^*)^k \qquad (3.29)$$

The exponent $k \approx 3$, and γ_n is the atomic transition rate corresponding to the excited state.

In GPT involving the time-resolved detection of the ionization signal following laser excitation, the instantaneous population of a particular state after a time delay t measured from the instant of the excitation pulse (assumed to be very short in comparison) can be written as:

$$N(t) = N(0)\exp\left[-\frac{t}{\tau_{eff}}\right] \qquad (3.30)$$

Where, $N(0)$ is the initial population ($t = 0$) and τ_{eff} is the effective lifetime.

Since the ionization signal is proportional to the population of the state considered, the ionization signal $I(t)$ as a function of time follows the decay curve for the Rydberg state n yielding the lifetime $\tau_{eff(n)}$ from the relation,

$$I(t) = I_0 \exp\left[-\frac{t}{\tau_{eff(n)}}\right] \qquad (3.31)$$

The experimental setup for the present study involves resonant two-photon transverse excitation of an atomic jet (Philip 2007) in a heat-pipe setup using a tunable dye laser with a scheme discussed in the study for strontium (Philip and Connerade 2007). A nearly collimated rectangular (0.2 mm x 12 mm) atomic jet exiting vertically upward from a disposable cartridge filled with 99.99% pure strontium (Goodfellow metals LS13622) located inside the hot zone of a stainless steel heat-pipe (31 cm long, 38 mm internal diameter) sealed with quartz optical windows was intercepted orthogonally by the narrow bandwidth (0.18 cm^{-1}) tunable dye laser (Lambda Physik LPD 3002CES) pumped by the XeCl excimer laser (Lambda Physik LPX 210i). The central hot zone of the heat-pipe was maintained at a suitable temperature (range 750 ^{0}C - 950 ^{0}C). The 436 nm - 444 nm section of the tuning range of the coumarine-120 dye (LC- 4400) at 2.6 μJ energy / pulse and at 13Hz pump laser rep rate with linear polarization (Π-geometry for exciting only |m| = 0 states) was used to excite the $J = 0$ and $J = 2$, 5s*n*s $^1S_0$ and 5s*n*d $^{1,3}D_2$ Rydberg members of neutral strontium from the ground state $5s^2\ ^1S_0$.

The schematic of the experimental geometry for the gated pulsed field detection is shown in Fig. 3.40(a) and the timing sequence is shown in Fig. 3.40(b). A pulsed electric field with a variable delay was applied to the thermionic diode using a pulse and delay generator (SRS DG 535) which also served as the basic timing trigger

pulse generator. The exciting laser pulse was monitored using a fast photodiode which was used to externally trigger SRS DG 535. Time resolved state selective ionization signals following excitations by the laser beam were obtained by setting a variable delay (0-12 μs) with a pulse duration of 500 μs and a pulse height of 1.5 - 3 volts (to avoid saturation) in DG 535. The rise time of the field pulse is 100 ns which is much shorter than the effective lifetime of the Rydberg state investigated. The signals are processed by a gated (with gate width set at 2 ns) boxcar averager/integrator assembly (Stanford Research Systems SR 250) and a personal computer.

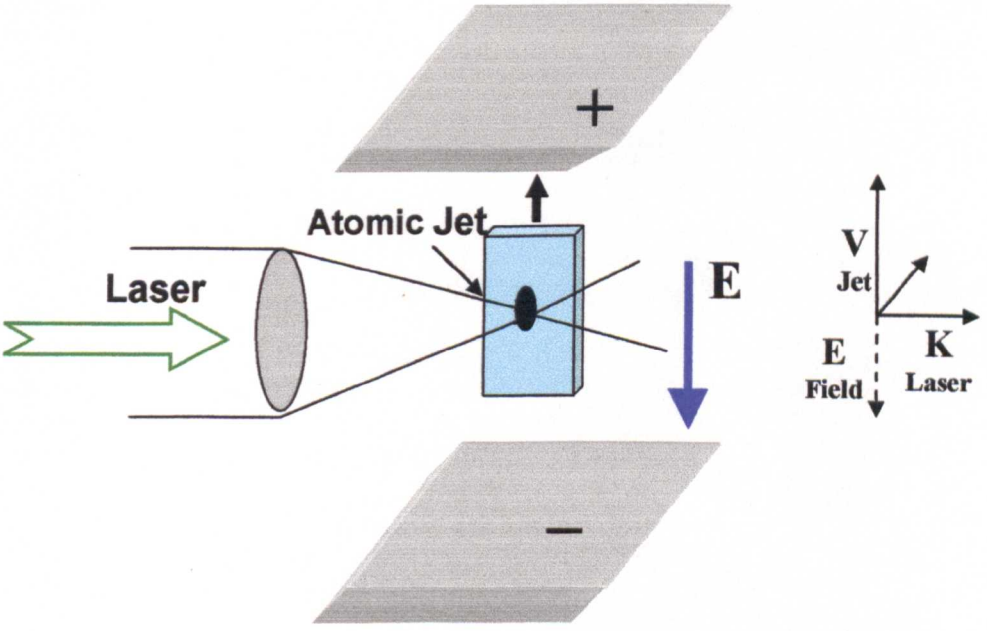

Fig. 3.40(a) Schematic of the experimental geometry for transverse excitation of an atomic jet

In GPT, lifetime measurement is not affected by black body radiation and radiation trapping effects which can occur in optical detection. Besides the lifetime measurement, GPT can also provide a relatively simple alternate method to determine the quenching field (Karapanagioti *et al* 1999) for high-lying Rydberg states.

The validity of the GPT was established by recording as in figure 3.41(a) a two-photon spectra of the even-parity 5s*n*s $^1S_0$ and 5s*n*d $^{1,3}D_2$ states of Sr I for the range $14 < n < 28$ with 2.5 V pulse height, 0.5 ms pulse width , 100 ns rise time and 0.1 μs delay τ_D.

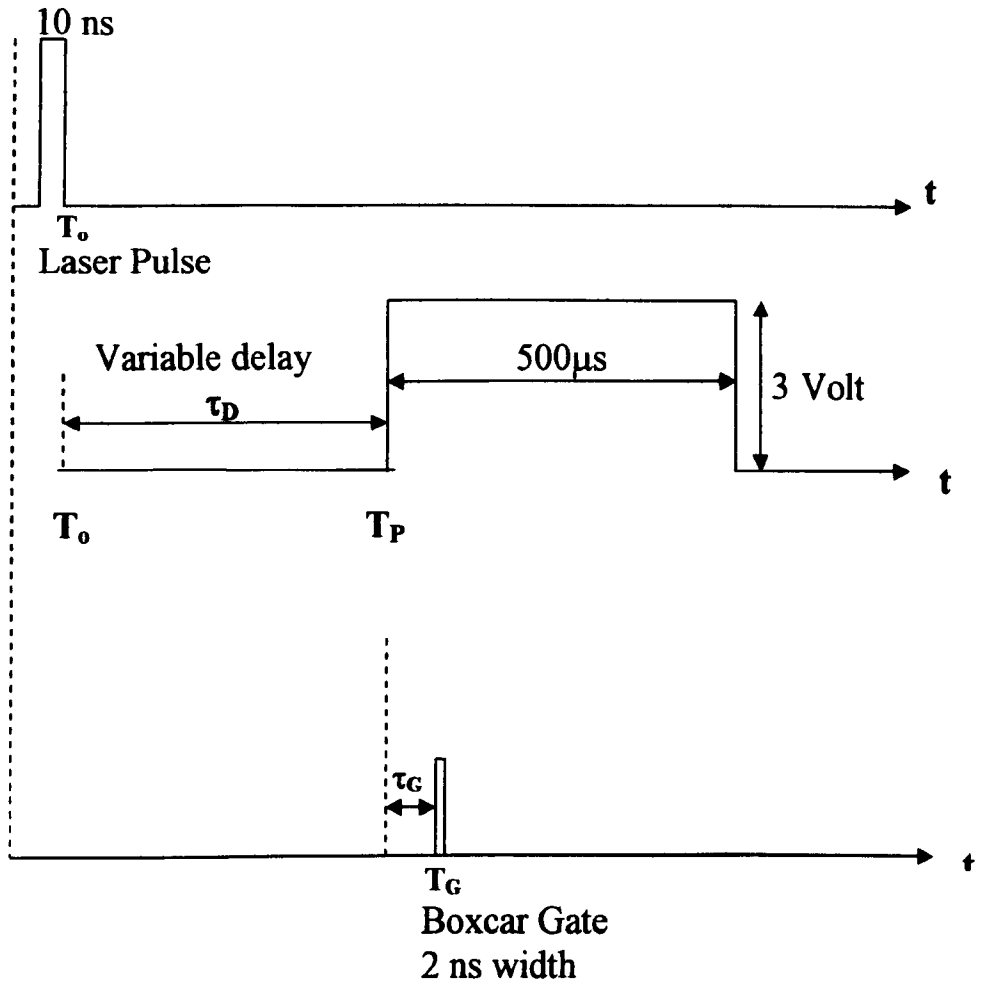

Fig. 3.40(b) Schematic of the Timing Sequence for GPT

A similar spectrum, but taken with static field (+9 volt applied to the thermionic diode) detection and with 20 mbar Ar buffer at 2.1 μJ energy/pulse is presented in Fig. 3.41(b) for comparison. All the features specific of the static field spectrum are reproduced in the pulsed field spectrum in Fig. 3.41(a).

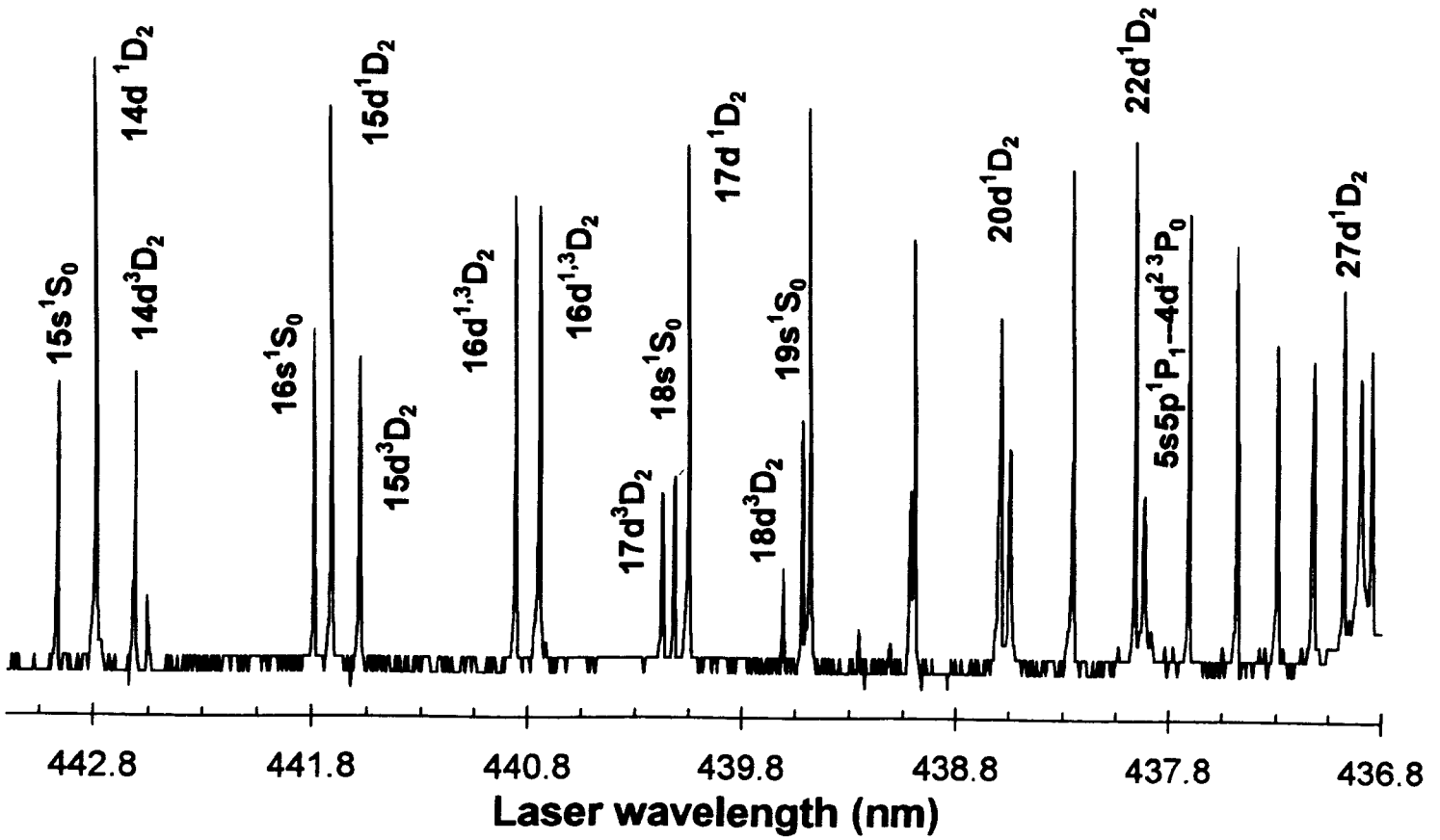

Fig. 3.41 (a) Two-photon spectrum of Sr I taken with the GPT with +2.5 V pulse height, 0.5ms width

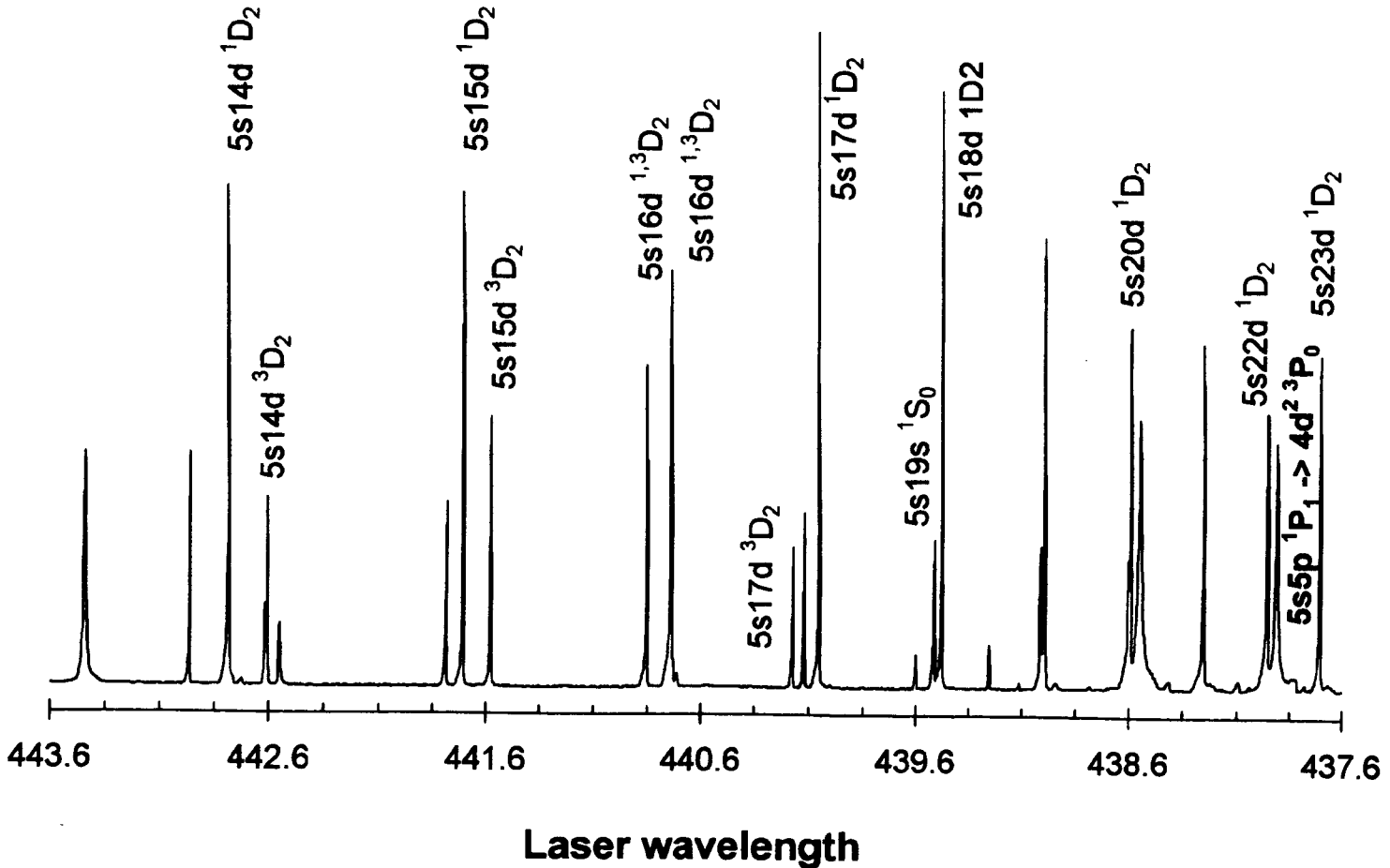

Fig. 41 (b) Two-photon spectrum of Sr I taken with a thermionic diode detector biased with a DC voltage

The features reproduced by GPT include, for example the singlet-triplet swap-over around $n \approx 16$ for the 5s*n*d $^{1,3}D_2$ sequence and the interloper appearing adjacent to 5s22d $^1D_2$, a single-photon excitation to the doubly excited state $4d^2\ ^3P_0$ from the resonance level 5s5p $^1P_1$. However, interestingly, the singlet-triplet mixing coefficient around $n = 16$ in Fig. 3.41(a) is observed to be somewhat different from that in Fig. 3.41(b). The baseline drift seen in figure 3.41(a) is due to the high sensitivity of the signal detection used in GPT.

Fig. 3.41(c) shows the reproduction of the two-photon spectrum of higher members of the 5s*n*d $^1D_2$ Rydberg sequence including the emergence of a remarkable perturbation appearing at $27 < n < 28$. It has been observed that this broad interloper is completely wiped out with a delay $\tau_D \geq 11$ μs while neighboring Rydberg members survive to much longer time delays.

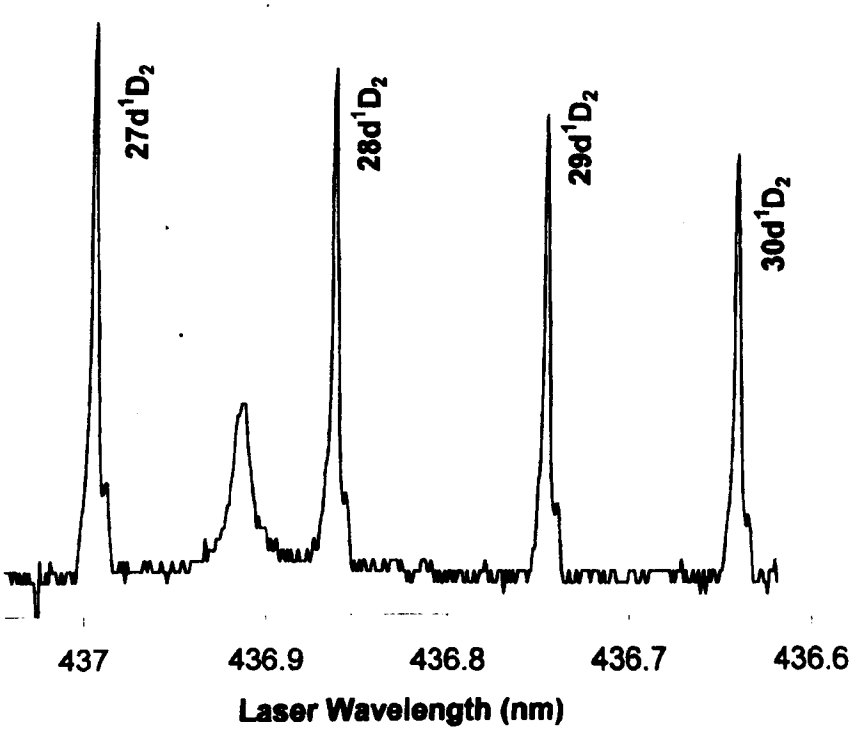

Fig.3.41(c) Two-photon spectrum of Sr I 5s*n*d $^1D_2$ Rydberg series with GPT showing $4d^2\ ^1G_4$ interloper

Also reproduced by GPT are the excitations to the parity forbidden states 5s(n+2) $^3P_2$ merging with the 5snd $^1D_2$ members on the blue wing side (Philip and Makdisi 2006) using themionic detection with static field.

In Fig. 42(a) the intensity ratio of the adjacent Rydberg members, $I_{(5s16s)} / I_{(5s15s)}$ of the $^1S_0$ series is plotted as a function of the time delay between the excitation and detection field pulse. The signal strength is found to increase towards higher n because of the $(n^*)^3$ dependence on the lifetime. The temporal evolution of the intensity ratio $I(^3D_2) / I(^1D_2)$ is also seen in Fig. 3.42(a).

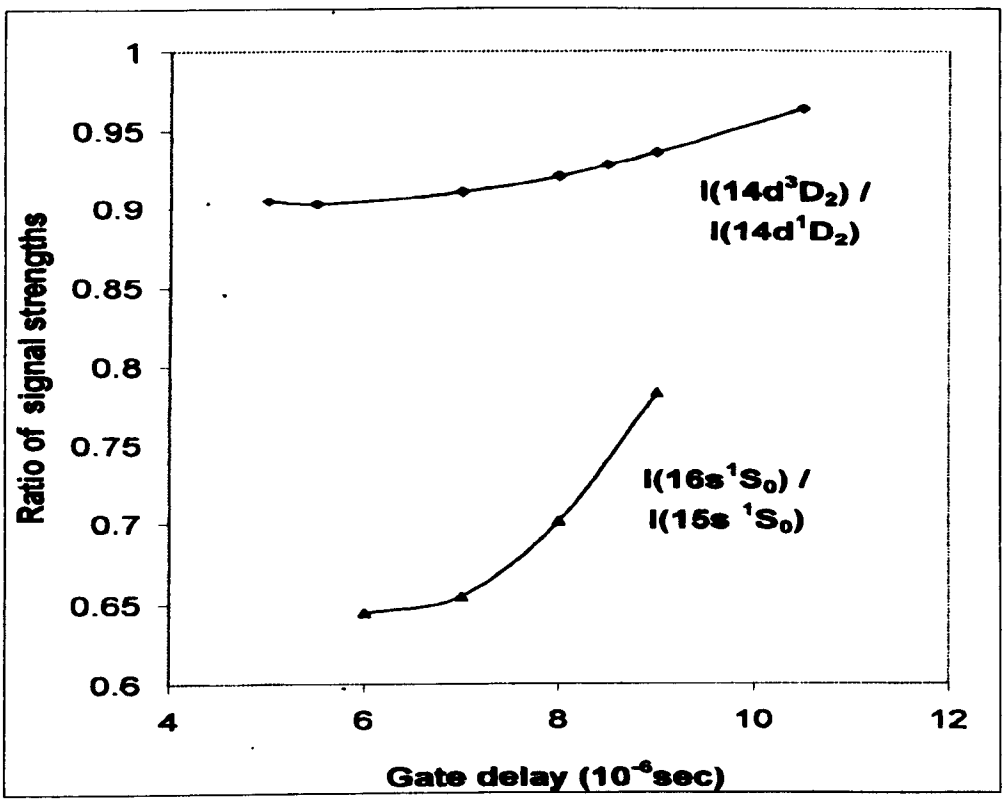

Fig. 3.42 (a) Growth of intensity ratio of adjacent Rydberg members as a function of gate delay time establishing GPT

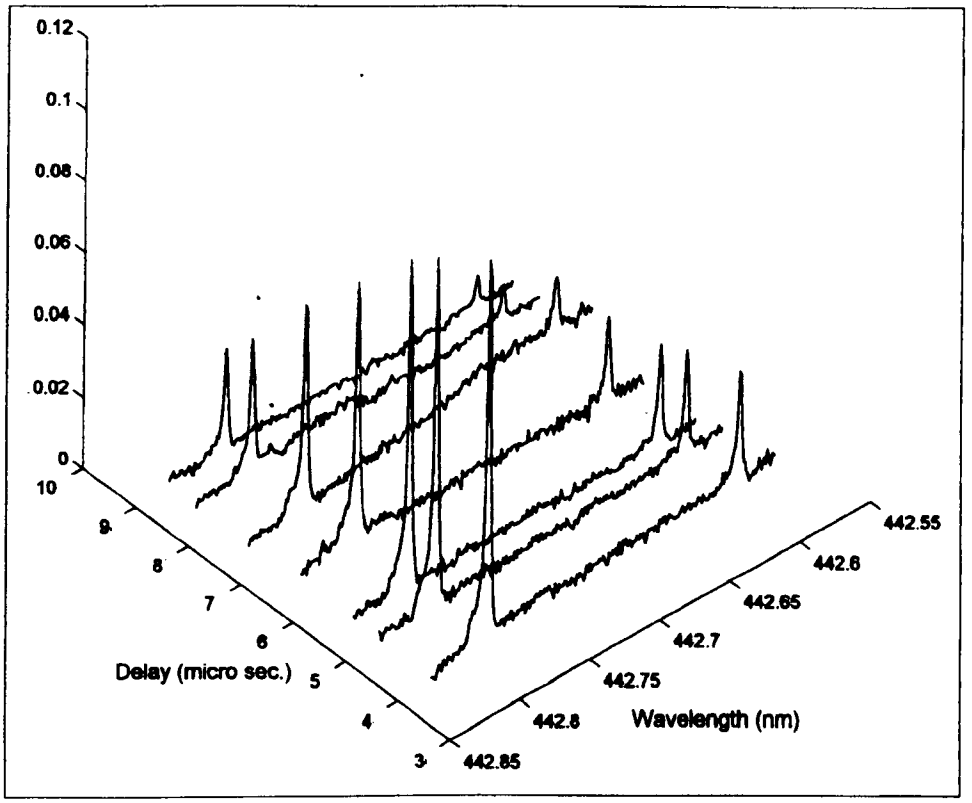

Fig. 3.42 (b) Time evolution of Sr I, 5s14d $^{1,3}D_2$ Rydberg states probed using GPT

Figure 3.42(b) shows a spectrum covering the 0.3nm wavelength region (442.55 nm-442.85 nm), indicating the temporal evolution of the 5s14d $^1D_2$ and 5s14d $^3D_2$ members of Sr I taken with a variable gate delay of 3μs -10μs.

In figures 3.43(a) and 3.43 (b), the time decays of the members of the 5s*n*s $^1S_0$ and 5s*n*d $^1D_2$ sequence for the n = 15 - 20 are plotted after adding helium to bring the buffer gas pressure to 40 mbar and by applying a pulsed field of (height +3 V, width 0.5 ms) and 100 ns rise time for the thermionic diode.

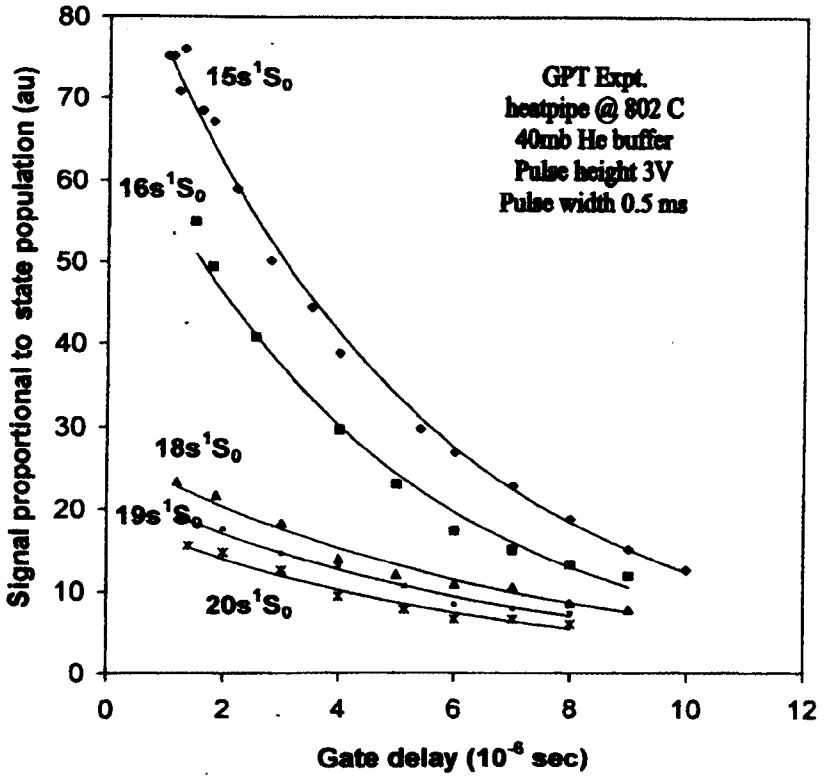

Fig. 3.43 (a) Time decay of Sr I 5s*n*s $^1S_0$ states probed by GPT. Continuous curves are the exp($-t/\tau_{eff}$) fit to the experimental data

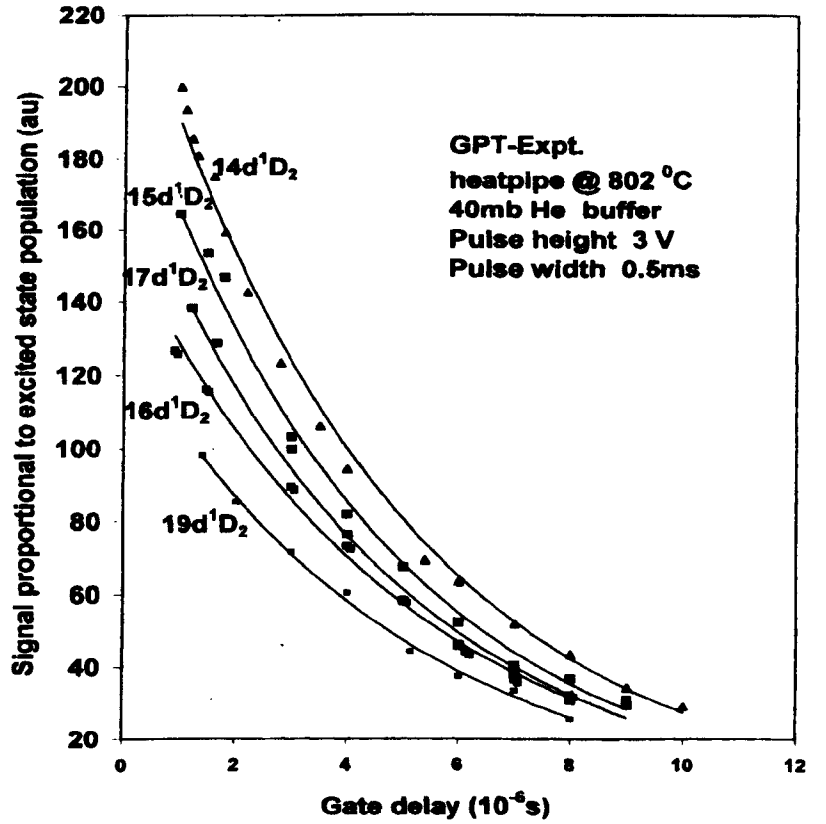

Fig. 3.43 (b) Time decay of Sr I- 5s*n*d $^1D_2$ states probed by GPT. Continuous curves are the exp($-t/\tau_{eff}$) fit to the experimental data

The effective lifetimes of the Rydberg states determined by an exponential fit to the experimental data are presented in Tables 3.13 - 3.15 and are compared with data in the literature (Gallgher *et al* 1981). The effective lifetime values in presence of buffer gas collisions and external electric field are well above the lifetime values given by Grafstrom *et al* (1983) for the $J = 2$ sequence using the pulse modulated laser spectroscopy (PUMLOS) technique.

Table 3.13

Experimental effective lifetime τ_{eff} of the 5s*n*s $^1S_0$ Rydberg series of Sr I from GPT

State	Effective lifetime GPT Expt... 40mbar He τ_{eff} (μs)	Effective lifetime GPT Expt... 40 mbar He +60mbar Ar τ_{eff} (μs)	Radiative lifetime Grafstrom *et al** τ_0 (μs)
5s15s $^1S_0$	4.97		1.145
5s16s $^1S_0$	4.72	15.08	1.424
5s17s $^1S_0$	-----		-----
5s18s $^1S_0$	6.93		-----
5s19s $^1S_0$	6.72		-----
5s20s $^1S_0$	6.37		-----

*Grafstrom *et al* *Phys. Rev.* A **27**, 947 (1983)

Table 3.14

Experimental effective lifetime τ_{eff} of the 5s*n*d $^1D_2$ Rydberg series of Sr I from GPT

State	Effective lifetime GPT Expt... 40mbHe τ_{eff} (μs)	Effective lifetime GPT Expt... 40 mbar He +60mbar Ar τ_{eff} (μs)	Radiative lifetime Grafstrom *et al* * τ_0 (μs)
5s14d $^1D_2$	4.67		0.408
5s15d$^1D_2$	4.54	7.813	0.340
5s16d $^1D_2$	4.86		0.365
5s17d$^1D_2$	4.58		0.517
5s18d$^1D_2$	-------		0.640
5s19d$^1D_2$	4.98		0.738

*Grafstrom *et al* *Phys. Rev.* A **27**, 947 (1983)

Table 3.15

Experimental effective lifetime τ_{eff} of the 5s*n*d $^3D_2$ Rydberg series of Sr I from GPT

State	Effective lifetime GPT Expt. 40mbHe τ_{eff} (μs)	Effective lifetime GPT Expt. 40 mbar He +60mbar Ar τ_{eff} (μs)	Radiative lifetime Grafstrom *et al* * τ_0 (μs)
5s14d $^3D2$	5.56		0.247
5s15d $^3D2$	4.52	6.76	0.282
5s16d $^3D2$	-----		0.286
5s17d$^3D2$	7.02		0.319

*Grafstrom *et al* *Phys. Rev.* A **27**, 947 (1983)

The effective lifetimes of the high-lying members of the 5s*n*d $^1D_2$ series covering the principal quantum number range n = 27 - 30 are given in Table 3.16.

Table 3.16

Experimental lifetime τ_{eff} of the high-lying members of the 5s*n*d $^1D_2$ Rydberg series of Sr I from GPT

State	Effective lifetime GPT Expt. 40 mbar He τ_{eff}(μs)
5s27d $^1D_2$	9.48
5s28d $^1D_2$	10.86
5s29d $^1D_2$	11.42
5s30d $^1D_2$	12.19
5s31d $^1D_2$	14.66

Only limited experimental data are known in the literature for the lifetimes of high members of Rydberg series of Sr I. Grafstrom *et al* (1983) give experimental natural radiative lifetimes in the 5s*n*d $^1D_2$ (n = 13 - 22), 5s*n*d $^3D_2$(n = 14 - 17) and 5s*n*s $^1S_0$, (n = 15 - 16) series. The data presented herein are, therefore, new extensions to the existing lifetime data on the even-parity, J = 0,2, $^1S_0$, $^1D_2$ Rydberg series of strontium. For the 5s*n*d $^{1,3}D_2$ series, the lifetime values around n = 15 - 16 are decreased noticeably due to strong singlet-triplet mixing. It is observed that the lifetimes of the $^1S_0$ Rydberg members are longer than those of the $^1D_2$ members reported by Grafstrom *et al* (1983) in strontium and by Aymar *et al* (1982) in barium. However, it is also noted that the lifetimes of the $^3D_2$ series are longer than those of the $^1D_2$ series in strontium, an observation similar to the one in barium by

Aymar *et al*, but opposite to the observation reported by Grafstrom *et al* in strontium.

In Fig. 3.44 the measured lifetime values for the 5s*n*s $^1S_0$ and 5s*n*d $^{1,3}D_2$ sequences are plotted versus effective principal quantum number. The experimental data are fitted to yield a relation of the form given by equation (3.29) to give an effective lifetime:

$$\tau_{eff(n)} = \frac{1}{\gamma_{eff}}(n^*)^k$$

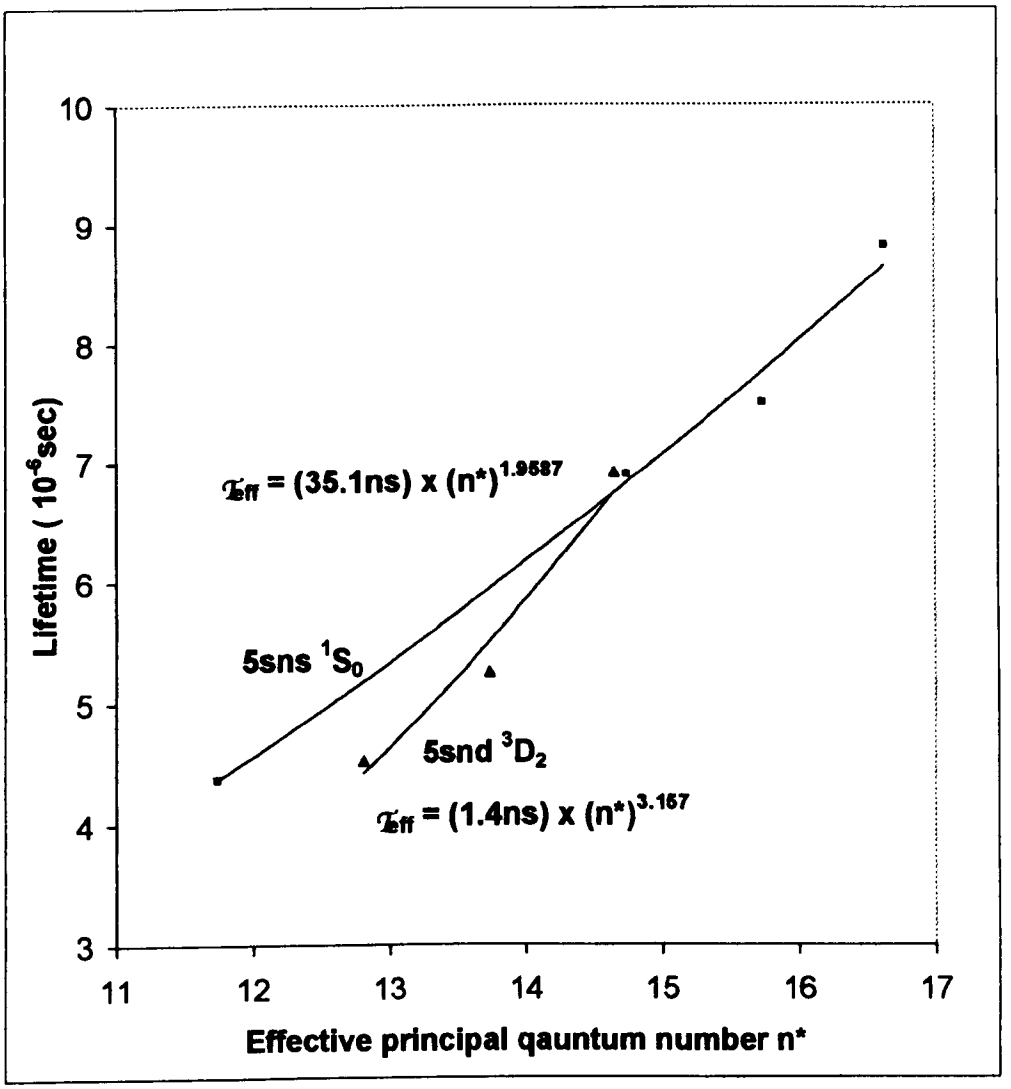

Fig. 3.44 Power law fit for experimental data of lifetime of heavily perturbed 5s*n*s $^1S_0$ and 5s*n*d 3d $^3D_2$ Rydberg series of Sr I.

The deviation of the exponent k from the expected value 3 for Rydberg members can be attributed to effects arising from collisions and heavy series perturbations induced by configuration mixing. The lifetimes of the lower members of the $5snS$ $^1S_0$ series are found to be quite vulnerable to these effects since the experimental value for the power law exponent is 1.96. However the $5snd$ $^3D_2$ series is much less affected as indicated by the power law exponent value of 3.157.

In Fig.3.45 the decay curves are plotted for three different Rydberg members after adding 60 mbar argon to 40 mbar helium buffer in the previous heat-pipe operation. It is observed that the effective lifetime values for the members of all the three different Rydberg series are enhanced by increasing the buffer gas pressure with an addition of 60 mbar argon to make the total buffer gas pressure 100 mbar around 802 ^{0}C. Interestingly, the decay curves indicate that the crossing point in time for the signal intensities can be controlled by changing the buffer gas pressure and composition, thereby modifying the Rydberg atom decay behaviour.

The GPT technique, offers several advantages over other methods in time-resolved decay measurements of Rydberg atoms, particularly those accessed by resonant two-photon excitation in which heavy perturbations, configuration mixing and collisions can occur. The GPT can be used, with considerable simplicity and remarkable reliability, in situations where optical methods such as laser induced fluorescence (LIF) detection techniques, delayed coincidence etc are not suitable, especially in heat-pipe setups where collisions are always present. Also, in controlled excitation to states otherwise forbidden by parity and selection rules, using collisions complemented by external fields, the temporal decay of atoms can be studied with remarkable ease using the new technique. Furthermore, GPT is a unique, and

probably also the fastest, experimental method to yield decay data for all members of a Rydberg series simultaneously.

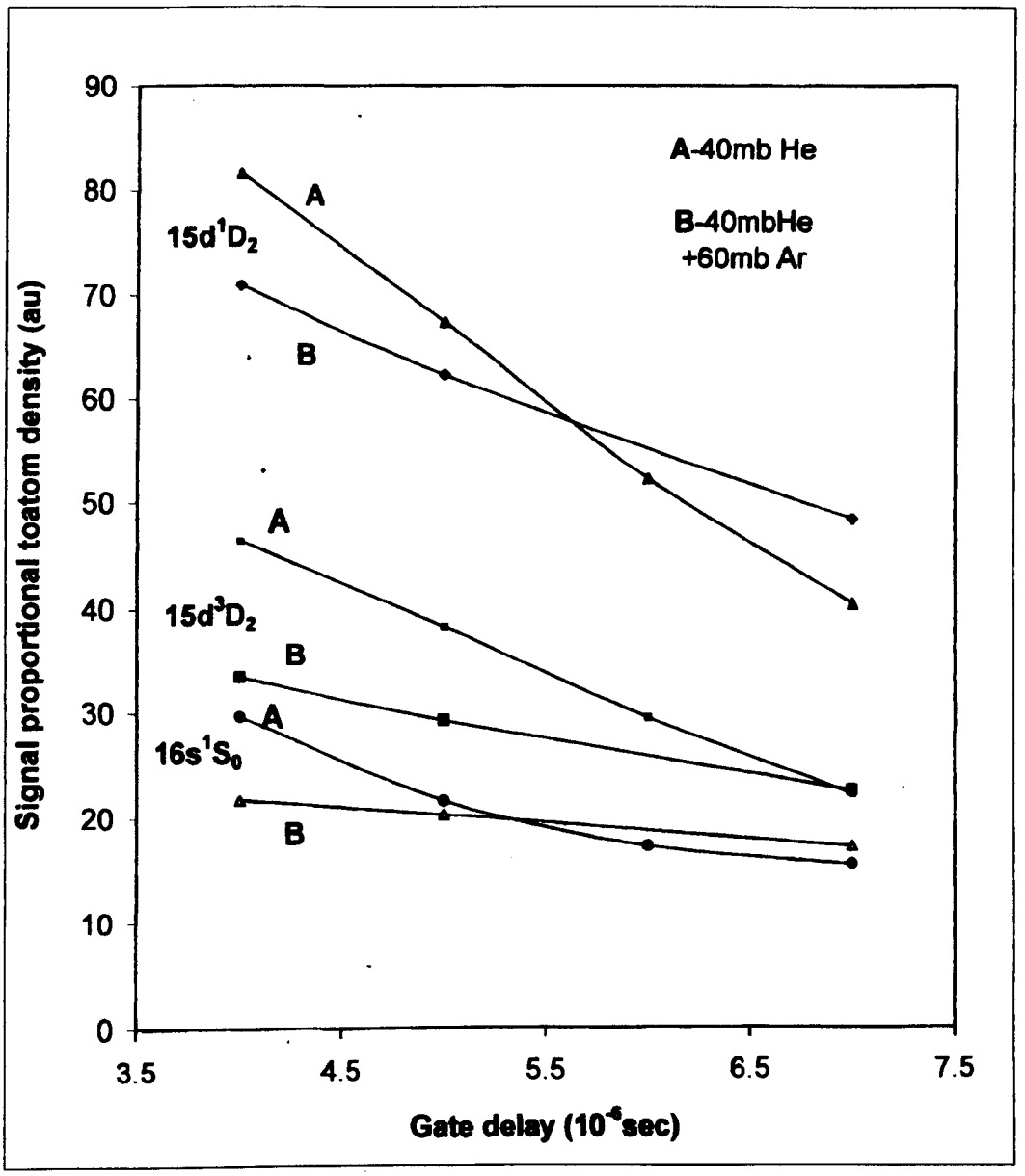

Fig. 3.45 Effect of buffer gas collisions on time evolution of Sr I Rydberg states

Conclusion

In this chapter I have attempted to give a broad survey of the historical development of the multi-photon spectroscopy of Rydberg states of atoms after introducing the essential theoretical concepts involved in the description of the bound and autoionizing series in alkaline–earth atoms. Presented are the concepts like the quantum defect, MQDT, spectroscopic selection rules for one-photon and two-photon transitions. Also given are discussions about the autoionization process and the special features of the Beutler-Fano resonance used to theoretically fit the autoionization profile. Energy level diagrams for both strontium and barium constructed for all relevant levels below the first ionization thresholds from the known energy level data are presented. Possible two-photon and other excitation processes to the bound states are indicated in the level diagram for strontium as a representative for both alkaline-earth atoms. Energy level and possible excitation schemes are also provided for autoionization process exploiting the concepts of the well-established ICE technique for the excitation of autoionizing series in strontium and barium (typically $5p_{3/2}\,ns$ in strontium and $5d_{5/2}\,ns$, $6p_{3/2}\,ns$ series in barium).

Extensive results from the two-photon spectroscopy of strontium and barium are given with representative spectra and the energy level data for all important transitions observed. The results reported include the following:

For **strontium**, energy level data for the bound even-parity, $J = 0$, 2 Rydberg series are presented (for the wavelength range 460 nm - 428 nm of the single dye used):

(i) for the $5sns\ {}^1S_0$ series improved energy level values are presented for the range $\mathbf{12 < \mathit{n} < 46}$ which gives an original extension of the level values for

the range **41 < *n* < 46** reported for the first time in the literature by two-photon excitation from the ground state;

(ii) for the $J = 2$, **5s*n*d $^3D_2$** Rydberg series new and original level data are presented for the range **9 < *n* < 47** which is also an extension from the previously published data by me and others;

(iii) for the $J = 2$, **5s*n*d $^1D_2$** Rydberg series new and original level data are presented for the range **9 < *n* < 82** thereby extending the previous experimental energy level data for this series for the range **74 < *n* < 82**.

Also observed are the excitation to the two-photon forbidden transitions from the ground state $5s^2\ ^1S_0$ to the $J = 1,3$ odd parity $5snp\ ^1P_1$ and $5snf\ ^3F_3$ states by Stark field-induced 'ℓ' mixing complimented by collisions. These forbidden transitions are observed as under:

(i) $5s^2\ ^1S_0 \rightarrow$ **5s*n*p $^1P_1$** for the range **32 < *n* < 46**

(ii) $5s^2\ ^1S_0 \rightarrow$ **5s*n*f $^1F_3$** for the range **29 < *n* < 44**

The forbidden transitions are observed to be dependent on the strength of the electric field and the pressure and composition of the buffer gas used in the heat-pipe setup, thereby, establishing a novel technique, for the first time reported in the literature in such experiments, for the controlled excitation of two-photon forbidden Rydberg states with a novel identification criterion distinct from two-photon allowed transitions.

Another important observation reported in this chapter is the collisional evolution of a remarkable highly compact doubly-excited broad resonance (tentatively labeled as

$4d^2\ ^1G_4$) which intrudes in to the even-parity spectrum of strontium $5snd\ ^{1,3}D_2$ Rydberg series at $27 < n < 28$. Also observed are the sequential excitation $5s5p\ ^1P_1 \rightarrow 4d^2\ ^3P_J$ (J = 0,1,2 doubly-excited configuration) by collision-induced dissociation of the Sr_2 dimers. New original energy level values are presented for these doubly-excited states in neutral strontium.

For **barium** also extensive energy level data for the bound even-parity, J = 0, 2 Rydberg series are presented from measurements in two-photon spectra:

(i) for the $6sns\ ^1S_0$ series improved energy level values are presented for the range $13 < n < 68$ which extends the level values for the range $62 < n < 68$, thereby reporting for the highest n accessed by two-photon excitation in such setups;

(ii) for the $6snd\ ^3D_2$ Rydberg series original level data are presented for the range $11 < n < 46$ which is also an extension for $n \geq 40$ for the previously published data by others in similar experiments;

(iii) for the J = 2, $6snd\ ^1D_2$ Rydberg series new and original level data are presented for the range $11 < n < 88$ thereby extending the previously published experimental energy level data for this series for the range $82 < n < 88$. **This is believed to be the highest level reported in the literature for barium two-photon spectra.**

Two-photon spectra of the autoionizing resonances just above the ionization limit both in strontium and barium also have been presented. In strontium the autoionizing resonance $(4d^2+5p^2)\ ^1D_2$ intrudes in to the J = 2, $5snd\ ^{1,3}D_2$ Rydberg series. Due to

this perturbation intensity variation among the members of the even-parity spectra is observed. In strontium two-photon spectra a strong configuration mixing and the breakdown of *L-S* coupling is observed with the singlet-triplet swap over around n = 16. In barium, the 5d7d configuration is a strong perturbation to the even-parity spectrum. 5d7d $^1D_2$, next to 6s26d $^1D_2$ at the two-photon wavelength in air 477.858 nm, produces intensity fluctuations and deviation from the $f \propto (n)^{-3}$ scaling law. 5d7d $^3P_2$ observed at the two-photon wavelength in air at 477.556 nm perturbs the 6s*n*d $^3D_2$ Rydberg series.

Interesting two-photon spectra recorded without biasing of the thermionic diode detector with such sensitivity as to preserve all features of the spectra are also presented for the first time in the literature.

Finally, in this chapter I have presented the results of a novel experimental technique involving time-resolved pulsed field thermionic diode detection employed for the first time in a heat-pipe setup to examine the time decay of high-lying Rydberg states of atoms yielding their effective lifetimes. Results are presented for the effective lifetime of some members in the highly perturbed region of the J = 0, 2 Rydberg series in strontium. The novelty of the gated pulsed-field technique **(GPT)** lies in the finding that this technique is attractive for states with very long lifetimes in presence of collisions and perturbations, with a unique possibility of simultaneous measurement for all members of a sequence which is not possible by other techniques.

References -Chapter 3 (alphabetical order)

1. Abutaleb M., de Graaff R .J., Ubachs W. and Hogervorst W
Phys. Rev. A **44**, 4187(1991)

2. Allegrini M., Arimondo E., Menchi E., Burkhardt C.E., Ciocca M., Garver W.P., Gozzini S and Leventhal J.J
Phys. Rev. A, **38**, 3271 (1988)

3. Amin N., Mahmood S., Saleem M., Kalyar M.A. and Baig M.A
Eur. Phys. J. D **40**, 331 (2006)

4. Armstrong J.A., Wynne J.J. and Esherick P
J. Opt. Soc. Am. **69**, 211 (1979)

5. Armstrong J.A., Esherick P. and Wynne J.J
Phys. Rev. A **15**, 180 (1977)

6. Aymar M.
J. Phys. B At. Mol. Opt. Phys.**20**, 6507(1987)

7. Aymar M.
J. Phys. B At. Mol. Opt. Phys.**23**, 2697 (1990)

8. Aymar M., Camus P., Dieulin M. and Morillon C
Phys. Rev. A **18**, 2173 (1978)

9. Aymar M , Camus P. and El Himdy A
J Phys. B At. Mol. Opt. Phys **15**, L759 (1982)

10. Aymar M., Champeau R.J., Delsart C. and Keller J.C
J. Phys. B At. Mol. Opt. Phys.**14**, 4489(1981)

11. Aymar M., Grafstrom P., Levinson C., Lundberg H. and Svanberg S
J. Phys. B At. Mol. Opt. Phys **15**, 877 (1982)

12. Aymar M., Greene C.H. and Luc-Koenig E
Rev. Mod. Phys. **68**, 1015 (1996)

13. Aymar M. and Lecomte J.M
J. Phys. B At. Mol. Opt. Phys **22,** 223(1989)

14. Aymar M., Luc-Koenig E. and Watanabe S
J. Phys. B At. Mol. Opt. Phys **20**, 4325 (1987)

15. Aymar M. and Robaux O
J. Phys. B At. Mol. Opt. Phys **12**, 531 (1979)

16. Aymar M. and Telmini M
J. Phys. B At. Mol. Opt. Phys **24**, 4935 (1991)

17. Baig M.A., Yasseen M., Ali Raheel, Nadeem Ali. and Bhatti S.A
The Eur.Phys. Jl. **D6**, 201(1999).

18. Baig M.A. and Connerade J.-P
J. Phys. B At. Mol. Opt. Phys. **17**. L271 (1984)

19. Bartschat K., Mc Laughlin B.M. and Hoversten R. A
J. Phys. B At. Mol.Opt. Phys. **24**, 3359 (1991)

20. Bates K.A., Msae J., Vasilescu C. and Schumacher D
Phys. Rev. A **64,** 033409(2001)

21. Beigang R. and Schmidt D
Phys. Scripta. **27**, 172(1983)

22. Beigang R., Lucke K., Timmermnn A. and West P.J
Opt. Commun.**42,** 149 (1982)

23. Beigang R., Lucke K.,Schidt D.,Timmermann A. and West P. J
Phys. Scripta **26**, 183 (1982)

24. Bente E.A.J.M. and Hogervorst W.
J. Phys. B At. Mol. Opt. Phys. **22**, 2679 (1989)

25. Bente E.A.J.M. and Hogervorst W
J. Phys. B At. Mol. Opt. Phys. **23**, 1403 (1990)

26. Bethe H.A. and Jackiw R.
"*Intermediate Quantum Mechanics*" 2nd Edn (W.A. Benjamin, NY 1968)

27. Beutler H
Zeit. Phys. **91**, 132 (1934)

28. Bhatti S.A., Cromer C.L. and Cooke W.E
Phys. Rev. A **24**, 161(1981)

29. Bohr N and Wentzel M
Z. Phys. **24**, 106 (1923)

30. Bokor J., Freeman R.R. and Cooke W.E
Phys. Rev. Lett. **48**, 1242 (1982)

31. Bowers C.J., Budker D., Commins E.D., De Mille D., Freedman S.J., Nguyen A.T.and Shang S.Q
Phys.Rev. A **53**, 3103 (1996)

32. Bradley D.J., Ewart P., Nicholas J.V. and Shaw J.R.D
J. Phys. B At. Mol. Opt. Phys. **6**, 1594 (1973)

33. Brode R.B.
Rev. Mod. Phys. **5**, 257 (1933)

34. Burgess A
Astrophys. J. **139**, 776 (1964)

35. Burkhardt C.E., Libbert J.L., Jian Xu, Leventhal J.J. and Kelley J.D
Phys. Rev. A. **38**, 5949 (1988)

36. Camus P., Cohen S., Pruvost L. and Bolovinos A
Phys. Rev. A **48**, R9 (1993)

37. Camus P., Dieulin M and El Himdy A
Phys. Rev. A **26**, 379 (1982)

38. Camus P., Dieulin M., El Himdy A. and Aymar M
Phys. Scripta **27**, 125 (1983)

39. Camus P., Gallagher T.F., Lecomte J.M, Pillet P., Pruvost L. and Boulmer J
Phys. Rev. Lett. **62**, 2365 (1989)

40. Camus P., Kompitsas M., Cohen S., Nicolaides C., Aymar M., Crance M. and Pillet P
J. PhysB At. Mol. Opt. Phys. **22**, 445 (1989)

41. Camus P. and Morillon C
J. Phys. B At. Mol. Opt. Phys. **10**, L133 (1977)

42. Carre B., d' Oliveira P., Fournier P. R., Gounand F. and Aymar M
Phys. Rev.A **42**, 6545 (1990).

43. Chin S.L. and Lambropoulos P
"*Multiphoton Ionization of Atoms*" eds. (Acad. Press, NY 1984)

44. Chupka W.A.
Jl. Chem .Phys.**98**, 4520 (1993)

45. Cohen S., Aymar M., Bolovinos A., Kompitsas M., Luc-Koenig E., Mereu H. and Tsekeris P
The Eur.Phys.Jl. **D13**, 165(2001)

46. Cohen S., Camus P. and Bolovinos A
J. Phys. B At. Mol. Opt. Phys. **38**, S1 (2005)

47. Connerade J._P,
"*Highly Excited Atoms*" (Cambridge University Press 1998)

48. Connerade J._P., Baig M.A, Garton W.R.S. and Newsom G.H
Proc. Roy . Soc. Lond A, **371**, 295 (1980)

49. Connerade J.P. and Mansfield M.W.D
Proc. Roy. Soc. Lond. A **346**, 565 (1975)

50. Connerade J. P
J. Phys. B. At. Mol. Opt. Phys. **11**, L381 (1978)

51. Connerade J.-P., Farooq W.A., Ma H., Nawaz M., and Shen N
J. Phys. B At. Mol Opt. Phys. **25**, 1405(1992)

52. Cooke W.E. and Gallagher T.F
Phys. Rev. A **17**, 1226 (1978)

53. Cooke W. E. and Gallagher T. F
Phy.Rev. A **21**, 588 (1980)

54. Cooke W.E. and Bhatti S.A
Phys. Rev. A **26**, 391 (1982)

55. Cooke W.E., Gallagher T.F., Edelstein S.A. and Hill R.M
Phys. Rev. Lett. **40**, 178 (1978).

56. Courtillot I., Quessada-Vial A., Brusch A., Kolker D.and Rover G.D
Eur. Phys. Jl. D. **33**, 161 (2005)

57. Cowan R.D
"*Theory of Atomic Structure and Atomic spectra*"
(University of California – Berkeley, Calif 1981)

58. Dai C.J. and Zhao X.A
J. Qaunt. Spectrosc. Radiat. Transfer. **54,** 1019 (1995)

59. Dai C.J
Phys. Rev. A **52**, 4416 (1995)

60. Dai C.J., Schinn G.W. and Gallagher T.F
Phys. Rev. A **42**, 223(1990)

61. Dai Z., Li Z.S.and Zhankui J
Phy.Rev. A **65**, 022510 (2002)

62. de Graaff R.J., Ubachs W., Hogervorst W. and Abutaleb M
Phys.Rev. A **42**, 5473 (1990)

63. Derevianko A
Phys.Rev. Lett. **87**, 023002 (2001)

64. Dethlefs Muller K., Sandner M. and Schlag E.W
Chem. Phys. Lett. **112**, 291 (1984)

65. Eichmann U., Lange V. and Sandner W
Phy. Rev. Lett. **68**, 21 (1992)

66. Eichmann U., Lange V. and Sandner W.
Phys.Rev. Lett. **64**, 274 (1990)

67. Esherick P
Phys. Rev. A **15**, 1920 (1977)

68. Ewart P. and Purdie A.F
J. Phys. B **9**, L 437(1976)

69. Fano U
Phy. Rev. **124**, 1866 (1961)

70. Fano U
J. Opt. Soc. Am. **15**, 979 (1975)

71. Farooqi S.M, Connerade J.-P. and Aymar M
J. Phys. B **25**, L219 (1992)

72. Feldmann D. and Welge K.H
J. Phys. B **15**, 1651 (1982)

73. Feldmann D., Krautwald J., Chin S.L., von Hellfeld A. and Welge K.H
J. Phys. B: At. Mol. Opt. Phys. **15**, 1663 (1982)

74. Friedrich H
"*Theoretical Atomic Physics*"(Springer-Verlag Berlin 1991)

75. Friedrich H. and Triest J
Phys. Rev. A **54**, 1136 (1996)

76. Gallagher T.F., Safinya K.A. and Cooke W.E
Phys. Rev. A **24**, 601 (1981)

77. Gallagher T.F., Sandner W and Safinya K.A
Phys. Rev. A **23**, 2969 (1981)

78. Gallagher T.F, Safinya K.A. and Cooke W.E.
Phys. Rev. A **21**, 148 (1980)

79. Gallagher T.F
"*Ryberg Atoms*" (Cambridge University Press 1994)

80. Garton W.R.S. and Codling K
Proc. Phys. Soc. **75**, 87 (1960)

81. Garton W.R.S., Grasdalen G.L., Parkinson W.H. and Reeves E.M
J. Phys. B: (Proc. Phys. Soc.) **1**,114 (1968)

82. Garton W.R.S. and Tomkins F.S
Astrophys. J. **158**, 1219 (1969)

83. Garton W.R.S. and Codling K
Proc. Phys. Soc. **75**, 87 (1960)

84. Garton W.R.S. and Codling K
J. Phys. B: At. Mol. Opt. Phys. **1**, 106 (1968)

85. Gomez E., Aubin S., Orozo L.A. and Sprouse G D
J. Opt. Soc. Am. B **21**, 2058 (2004)

86. Goppert-Meyer M
Ann. Phys. **9**, 273 (1931)

87. Gouanand F., Carre B., Fournier P.R., d' Oliveira P. and Aymar M
J. Phys. B:At. Mol. Opt. Phys. **24**, 1309 (1991)

88. Gounand F., Gallagher T.F., Sandner W., Safinya K.A. and Kachru R
Phys.Rev. A**27**, 1925 (1983)

89. Goutis S., Aymar M., Kompitsas M. and Camus P
J. Phys.B. At. Mol. Opt. Phys. **25**, 3433(1992)

90. Grafstrom P., Zhan-Kui J., Jonsson G., Levinson C., Lundberg H and Svanberg S.
Phys Rev. A **27**, 947 (1983)

91. Griesmann U., Esser B. and Baig M.A
J. Phys. B: At. Mol. Opt. Phys. **25**, 3475 (1992)

92. Greene C.H. and Aymar M
Phys. Rev. A **44**, 1773 (1991)

93. Greene C.H
Phys. Rev.A **32**, 1880 (1985)

94. Griesmann U., Esser B. and Baig M.A
J. Phys. B: At. Mol. Opt. Phys. **25**, 3475 (1992)

95. Griesmann U, Esser B and Hormes J
J. Phys. B: At. Mol. Opt. Phys **27**, 3939(1994)

96. Gutzwiller M.C
Rev. Mod. Phys. **70**, 589 (1998)

97. Haq S.U., Mahmood S., Amin N., Jamil Y., Ali R. and Baig M.A
J. Phys. B: At. Mol. Opt. Phys. **39**, 1587 (2006)

98. Haq S.U., Mahmood S., Kalyar M.A., Rafiq M., Ali R. and Baig M.A
Eur. Phys. J. D **44**, 439 (2007)

99. Hieronymus H., Neukammer J. and Rinneberg H
J. Phys. B At. Mol. Opt. Phys: **25**, 3463 (1992)

100. Hudson R.D., Carter V.L. and Young P.A
Phys.Rev. **180**, 77 (1969)

101. Imhof R.E.and Read F.H
Rep. Prog. Phys. **40**, 1 (1977)

102. Jacobs V.L., Davis J. and Kepple P.C
Phys.Rev. Lett. **37**, 1390 (1976)

103. Jaffe S.M., Kachru R., van den Heuvell van Linden H.B.
and Gallagher T.F
Phys.Rev. A**32**, 1480 (1985)

104. Jones R.R., Dai C.J. and Gallagher T.F
Phys. Rev. A **41**, 316 (1990)

105. Jones R.R., Lynos B.J., Baig M.A., Djambova S.T. and Gallagher T.F
Phys. Rev. A **62**, 033408 (2000)

106. Jones R.R. and Gallagher T.F
Phys.Rev. A**38**, 2846 (1988)

107. Jones R.R. and Gallagher T.F
Phy. Rev. A **42**, 2655 (1990)

108. Jones R.R., Fu P. and Gallagher T.F
Phys. Rev. A **44**, 4260 (1991)

109. Jonsson G., Levinson C. and Svanberg S
Physics Scripta **30**, 65 (1984)

110. Kachru R., Tran N.H, Pillet P. and Gallagher T.F
Phys.Rev. A **31**, 218 (1985)

111. Kalyar M.A., Mahmood S., Haq S.U, Amin N. and Baig M.A
Eur. Phys. J. D **41**, 229 (2007b)

112. Kalyar M.A., Rafiq M. and Baig M.A
J. Phys. B At. Mol. Opt. Phys: **40**, 4317 (2007a)

113. Kalyar M.A., Rafiq M., Haq S.U and Baig M.A
J. Phys. B: At. Mol. Opt. Phys **40**, 2307 (2007c)

114. Karlsson H. and Litzen U
Phys. Scripta **60**, 321 (1999)

115. Karapanagiotti N.E., Connerade J._ P., Bhatia K.S., Makdisi Y.Y.
and Philip G
J. Mod. Opt. **46**, 1549 (1999)

116. Katori H., Ido T., Isoya Y and Gonokami M.K
Phys. Rev. Letts.**82**, 1116 (1999)

117. Khan M A., Gondal M.A. and Rais M.H
J Phys. B: At. Mol. Opt.Phys. **27**, 2889 (1994)

118. Kim L. and Greene C.H
Phys.Rev. A **36**, 4272(1987)

119. Kim Y.S. and Lambropoulos P
Phys. Rev. Letts. **49**, 1698 (1982)

120. Kompitsas M., Cohen S., Nicolaides C.A., Robaux O., Aymar M. and Camus P
J. Phys. B: At. Mol. Opt. Phys. **23**, 2247 (1990)

121. Kompitsas M., Goutis S., Aymar M. and Camus P
J. Phys. B: At. Mol. Opt. Phys. **24**, 1557 (1991)

122. Lagadec H., Carre B., Porterat D., Fournier P.R. and Aymar M
J. Phys. B: At. Mol. Opt. Phys. **29**, 471 (1996)

123. Lambropoulos P., Tang X., Agostini P., Petite G. and L'Huillier A
Phys.Rev. A **38**, 6165(1988)

124. Lange V., Aymar M., Eichmann U. and Sandner W
J. Phys. B: At. Mol. Opt. Phys. **24**, 91 (1991)

125. Lange V., Eichmann U. and Sandner W
J. Phys. B: At. Mol. Opt. Phys **22**, L245 (1989)

126. Langer R.M
Phys. Rev. **35**, 649 (1930)

127. Leeuwen K.A.H., van, Hogervorst W. and Post B.H
Phys. Rev. A **28**, 1901(1983)

128. Lu K.T and Fano U
Phys. Rev. A **2**, 81 (1970)

129. Liu Y., Anderson M., Brage T., Zou Y. and Hutton R
Phys. Rev. A **75**, 014502 (2007)

130. Lu J., Dai C.J., Li C.Q., Xu X.H., Liu Z.D. and Tang J.C
J. Quant. Spectrosc. Rad. Transfer **61**, 339 (1999)

131. Madden R.P. and Codling K
Phys. Rev. Lett. **10**, 516 (1963)

132. Madden R.P. and Codling K
Astrophys. J. **14**, 364 (1965)

133. Maeda K., Ueda K., Aymar M., Matsui T., Chiba H. and Ito K
J. Phys. B: At. Mol. Opt. Phys. **33**, 1943 (2000)

134. Makdisi Y., Philip G., Bhatia K.S. and Connerade J.-P
J. Phys. B: At. Mol. Opt. Phys. **34**, 521 (2001).

135. Matthias E., Zoller P., Elliott D.S., Piltch N.D., Smith S.J. and Leuchs G
Phys. Rev. Lett. **50**, 1914 (1983)

136. Mende W. and Kock M
J. Phys. B: At. Mol. Opt. Phys. **29**, 655 (1996)

137. Mende W., Bartschat K. and Kock M
J. Phys. B: At. Mol. Opt. Phys. **28**, 2385 (1995)

138. Moore C.E
"Atomic energy Levels," NBS Circular No. 467, vol. **2** (Washington DC US Govt. Printing Office-1949)

139. Mullins O.C., Zhu Y. and Gallagher T.F
Phys. Rev. A **32**, 243(1985)

140. Nascimento V.A., Caliri L.L, de Oliveira A.L, Bagnato V.S and Marcassa L G
Phys. Rev. A **74**, 054501 (2006)

141. Nawaz M., Farooq W.A. and Connerade J.-P
J. Phys. B: At. Mol. Opt. Phys. **25**. 1147 (1992)

142. Neukammer J. and Rinneberg H
J. Phys. B At. Mol. Opt. Phys. **15**, 3787 (1982)

143. Neukammer J., Jonsson G., Konig A., Vietzke K., Hieronymus H. and Rinneberg H
Phys.Rev. A **38**, 2804(1988)

144. Neukammer J., Rinneberg H., Vietzke K., Konig A., Hieronymus H, Kohli M. and Grabka H.J
Phys. Rev. Lett. **59**, 2947 (1987)

145. Parkinson W.H., Reeves E.M. and Tomkins F.S
J. Phys. B At. Mol. Opt. Phys. **9**, 157 (1976)

146. Percival I.C
Proc. Roy. Soc. London A **353**, 289 (1977)

147. Philip G. and Connerade J.-P
Opt. Commun. **279,** 141(2007)

148. Philip G. and Makdisi Y
Opt. Commun. **266,** 253 (2006)

149. Philip G
Rev. Sc. Instr. **78**, 113101 (2007)

150. Philip G
Appl.Phys. **B 90**, 407 (2008)

151. Philip G. and Connerade J._ P
(to be published)

152. Post B.H., Hogervorst W. and Vassen W
Phys. Rev. A **29**, 2989 (1984)

153. Post B.H., Vassen W., Hogervorst W., Aymar M. and Robaux O
J. Phys. B: At. Mol. Opt. Phys. **18**, 187 (1985)

154. Post B.H,. Vassen W. and Hogervorst W
J. Phys. B: At. Mol. Opt. Phys **19**, 511(1986)

155. Rinneberg H., Neukammer J., Jonsson G., Hieronymus H., Konig A. and Vietzke K
Phys.Rev.Lett. **55**, 382 (1985)

156. Rubbmark J.R. and Borgstrom S.A
Physica Scripta **18**, 196 (1978)

157. Rubbmark J.R., Borgstrom S.A and Bockasten K
J. Phys.B: At. Mol. Opt. Phys. **10**, 421 (1977)

158. Russel H.N and Saunders F.A
Astrophys. J. **61**, 38 (1925)

159. Saleem M., Hussain S., Rafiq M. and Baig M.A
J. Phys. B: At. Mol. Opt. Phys. **39**, 5025 (2006)

160. Sandner W., Safinya K.A and Gallagher T.F
Phys. Rev. A **33**, 1008 (1986)

161. Saunders F.A
Astrophys . J., **56**, 73 (1922)

162. Schlag E.W
"ZEKE Spectroscopy" (Cambridge University Press, Cmbridge 1998)

163. Schumacher D.W., Lyons B.J. and Gallagher T.F
Phys. Rev. Lett **78**, 4359(1997)

164. Seaton M.J
Proc. Phys. Soc. (London) **88**,801 (1966)

165. Seaton M.J
Rep. Prog. Phys. **47**, 167(1983)

166. Seng M., Halka M., Heber K.D. and Sandner W
Phy. Rev. Lett. **74**, 3344 (1995)

167. Shenstone A.G and Russel H.N
Phys. Rev. **39**, 415, (1932)

168. Shenstone A.G
Phys. Rev. **38**, 873 (1931)

169. Shuman E.S., Nunkaew J. and Gallagher T.F
Phys. Rev. A **75**, 044501 (2007)

170. Smedley J.E and Marran D.F
Phys. Rev. A **47**, 126 (1993)

171. Stebbings R.F. and Dunning F.B (eds)
"Rydberg states of atoms and molecules" (Cambridge University Press 1983)

172. Story J.G., Yap E.G. and Cooke W.E
Phys.Rev. A **39**, 5127 (1989)

173. Tanner Gregor, Richter Klaus and Rost Jan-Michael
Rev. Mod. Phys. **72**, 498(2000)

174. van Leeuwen R., Ubachs W., Camus P. and Hogervorst W
Phys. Rev. A **54**, R17(1996)

175. Vaeck N., Godefroid M. and Hansen J.E
Phys. Rev. A **38**, 2830 (1988)

176. Waligorski G., Zhou L. and Cooke W.E
Phys. Rev. A **55**, 1544 (1997)

177. Wannier G.H
Phys. Rev. **90**, 817(1953)

178. White H.E.
Phys. Rev. **38**, 2016 (1931)

179. Willke B. and Kock M
J. Phys. B At. Mol. Opt. Phys **26**, 1129 (1993)

180. Xu E.Y., Zhu Y., Mullins O.C. and Gallagher T.F
Phys. Rev. A **35**, 1138(1987)

181. Xu E.Y., Zhu Y., Mullins O.C. and Gallagher T.F
Phys. Rev. A **33**, 2401 (1986)

182. Yasuda M. and Katori H
Phys. Rev. Lett.**92**, 153004 (2004)

183. Zhu Y., Xu E.Y and Gallagher T.F

Phys. Rev. A **36**, 3751(1987)

Chapter 4

Collisions involving Rydberg Atoms with Rare Gas Atoms

4.1 Introduction

Experimental studies of collisions involving Rydberg atoms date back to the investigation of pressure broadening and shift of Rydberg levels by rare gases by Amaldi and Segre in 1934. The theory of collision between Rydberg atoms and neutral rare gases was first formulated by Fermi (1934) who considered pressure shift alone and later developed by several others (Rinsberg 1937, Alekseev and Sobel'man 1966) to include pressure broadening and by Omont (1977) and Kaulakys (1984) to give dependence of shift and broadening on the principal quantum number n. Early work in this area was reviewed by Chen and Takeo (1957) which was followed by several others -Allard and Kielkopf (1982), Sobel'man *et al* (1981), Biegman and Lebedev (1995). The theory was further improved and generalized by Kaulakys (1984), Herman *et al* (1984) and Herman (1988) to include the spectral features resulting from modification of interaction potential by taking in to account the finite range and anisotropy in the interaction potentials. The collisional perturbation on Rydberg states by neutral perturbing atomic species reflect as several distinctive observable features including asymmetric broadening and shift in frequency from the unperturbed values evidencing two nearly-independent interactions: short-range interaction of the perturber with the nearly free Rydberg electron and the long-range polarization interaction of the perturber with the ionic core. The shift and width of the atomic transitions which depend linearly

on the number density of the perturber atom is referred to as 'pressure shift' and 'pressure broadening'. Measurement of pressure broadening and shift allows an efficient technique for investigating the interactions of the highly excited atoms with foreign gases and determination of atomic polarizabilities and low-energy electron-scattering lengths (cross section) for the Rydberg states. Pressure broadening and shift measurements are used in precision spectroscopy for the determination of temperature and number density and can also be used as probes in extreme conditions like in stellar atmosphere and in ultra cold traps (Bose-Einstein Condensation). Furthermore, Rydberg atoms are well suited for low-energy electron scattering experiments and most of the experimental studies in collisional processes involving Rydberg atoms emerged since the development efficient tunable dye lasers.

4.2 Theoretical Considerations

The theory which was first developed for the alkali metal Rydberg atom colliding with noble gases is satisfactory for systems where inelastic collision cross section is negligible. However, in alkaline-earth atoms where there are important perturbations by doubly excited states the variation of the elastic collision cross sections with principal quantum number n cannot be neglected like in alkali Rydberg atom-noble gas collisions. This makes the line broadening and line shift in alkaline-earth atoms much more complex than in alkali-metal atoms and the theoretical formulation becomes much more challenging for accurate description of various observations, especially anomalies in shift and broadening at intermediate principal quantum numbers. Multi-channel quantum defect theory (Seaton 1966, Fano 1970, Lu and Fano 1970) has been used by Sun *et al* (1991) to explain the observed irregular line shift and line broadening of Rydberg-alkaline-earth- rare gas collisions.

Collisional process involving a Rydberg atom A* and a neutral perturber atom B in the ground state or low excited state differs from the collision between two ground state atoms or atoms in lower states. For highly excited atoms, a three-body interaction has to be considered- outer electron e, ionic core A^+ and the perturber atom B with two independent processes: the scattering of the neutral colliding particle by the highly excited valence electron (short-range interaction e-B) and the scattering by the ionic core A^+(long-range polarization interaction A^+-B). Because of the large size of the Rydberg atom (as illustrated in Fig.4.1 (a)) with the outer electron and the ionic core far away from each other, these two interactions can be treated as independent as shown in Fig. 4.1(b-c). The cross section of the Rydberg atom-neutral atom collision is of the order of geometrical cross section of the Rydberg atom which scales as n^4 for moderate principal quantum numbers. The theoretical treatment of the three-body problem is simplified on the assumption that the perturbing atom does not interact simultaneously with both the valence electron and the ion core for a wide range of the principal quantum numbers because of the fact that the orbital radius of the Rydberg atom is much larger than the characteristic interaction lengths of the electron-perturber ($\rho_{e\text{-}B}$) and the ion core–perturber ($\rho_{A^+\text{-}B}$). The cross section for the Rydberg atom-neutral collision is obtained as a combination of the electron-perturber and core-perturber scattering processes (Lebedev and Siegman 1998) with, in many situations, the scattering by the highly excited electron being the predominant. This led Fermi to the idea of the scattering by 'quasi-free-electron model' to explain the spectral line shift of Rydberg atoms due to collisions with rare gas atoms in measurements by Amaldi and Segre.

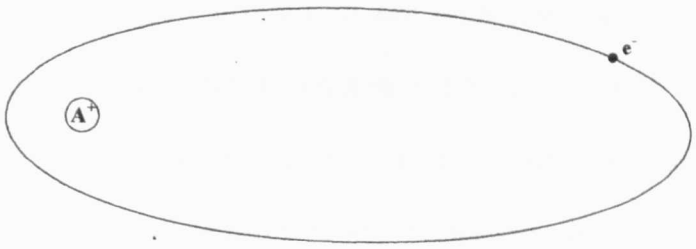

(a) Rydberg atom illustrated

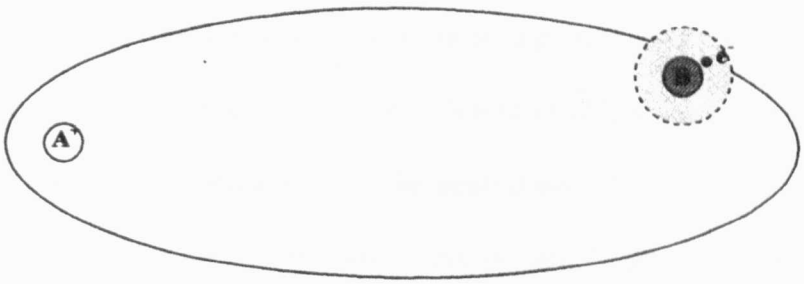

(b) Rydberg electron scattering: e--B Interaction

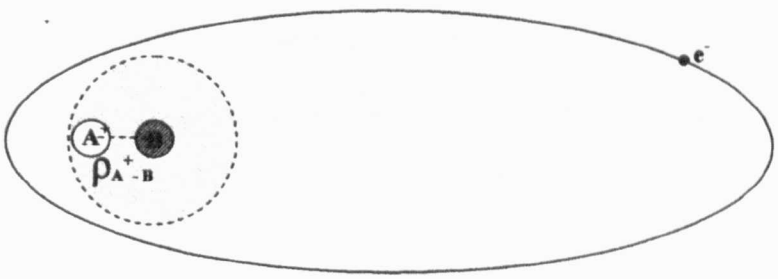

(c)Polarization interaction A^+- B

Fig. 4.1 (a-c) Collision between a Rydberg atom and a neutral rare gas perturber atom treated as two independent interactions:
(b) Scattering of Rydberg electron by the perturber;
(c) Long-range Polarization Interaction
between Rydberg atom core A^+ and the perturber B

The quasi-free-electron model essentially treats the collision of the Rydberg atom A* with the neutral perturber as a two-body collision between the nearly free valence electron and the neutral projectile while the ionic core A^+ remains as a spectator with negligible interaction with the perturber and decides the electron momentum distribution function for the Rydberg state involved through the Coulomb interaction.

Theoretical formulation for pressure shift and broadening within the ambit of the well-known "impact approximation" (Allard and Kielkopf 1982) can be applied to give reliable results under the experimental conditions of importance in two-photon laser spectroscopy of alkaline-earth atoms. Fermi considered the motion of the Rydberg electron essentially that of a free ultra slow electron through the perturber gas and the shift of a spectral line due to collision by a perturber as scattering of the valence electron by the perturber atom. It was Omont (1977) who pointed out that the broadening was due to polarization of the neutral perturber atom by the ionic core. A Rydberg atom, due to its very large size, is capable of containing several perturber atoms in its orbital envelope forming a very large molecular complex called "Fermi Complex" through the polarization field of the electron-ionic core system. The contributions to the line shift (Δ) from these two independent effects (scattering and polarization effects) are written as (Gounand and Berlande 1983):

$$\Delta_{sc} = \pm(\pi\sigma_0)^{1/2} N \qquad (4.1)$$

$$\Delta_{pol} = -10\alpha N^{4/3} \qquad (4.2)$$

Total shift, $\Delta = \Delta_{sc} + \Delta_{pol}$ (4.3)

Where the suffices 'sc' and 'pol' refer to scattering and polarization contributions respectively and σ_0 is the zero-energy elastic scattering cross section for a free electron and α is the polarizability of the perturber atom, N is the perturber atom number density.

Assuming the 'Diffusion Length' approximation the scattering cross section,

$$\sigma_0 = 4\pi L^2 \qquad (4.4)$$

Where, L is the scattering length of the perturber.

According to the impact theory the width (Γ / N) and shift (Δ/N) rates of a transition are given by (Gallagher 1994)

$$\Gamma = 2N\langle\sigma^b v\rangle \tag{4.5}$$

$$\Delta = 2N\langle\sigma^s v\rangle \tag{4.6}$$

Where σ^b and σ^s are respectively the broadening and shift cross sections, v is the relative collision velocity and N is the perturber atom number density. The averaging $\langle\rangle$ is taken over the relative velocity distribution.

For collisions involving Rydberg atoms, the collisional perturbation of the ground state is neglected. Three important processes can be considered contributing to the line broadening:

i Elastic collision of the Rydberg electron with the perturber resulting in phase change in the Rydberg electron wavefunction and;

ii Inelastic collision of the Rydberg electron with the perturber;

iii Collision of the ion core with the perturber (long-range polarization interaction between the ionic core and the perturber).

The cross sections for the elastic collisions are given by Kaulakys (1984)

$$\sigma^b = 2\pi\int[1-\cos\eta(\rho)]\rho d\rho \tag{4.7}$$

$$\sigma^s = 2\pi\int[1-\sin\eta(\rho)]\rho d\rho \tag{4.8}$$

Where ρ is the 'impact parameter' and η is the phase shift due to the interaction with potential V(R) between the perturber and the Rydberg atom.

The phase shift is given by the formula,

$$\eta(\rho) = -\frac{2}{v}\int_{\rho}^{\infty}\frac{V(R)}{\left[1-\rho^2/R^2\right]^{1/2}} \tag{4.9}$$

Where, R is the inter-nuclear distance.

The interaction potential V(R) for Rydberg atom neutral perturber contains two terms: an attractive polarization term and a short-range interaction between the

Rydberg electron and the perturber. The polarization part of the potential is given by,

$$V_{pol} = -\frac{\alpha E^2}{2} \qquad (4.10)$$

Where α is the polarizability of the perturber and E is the electric field due to the Rydberg atom core and the Rydberg electron. The short-range part of the potential arises from the interaction between the Rydberg electron and the dipole moment of the perturber induced by the ionic core due to polarization attraction between the ionic core and the perturber. For collision with heavy perturber the broadening is small for low principal quantum number n and gradually increases to a maximum value at intermediate values of n and subsequently decreases to approach constant value at large values of n where the broadening is determined by contribution from the polarization interaction between the core and the perturber. At intermediate n the observed large broadening is mainly due to the contribution from the Rydberg electron-perturber contribution. For accurate determination of the interaction potential, adequate experimental data for line broadening are required.

Alekseev and Sobel'man (1966) extended Fermi's formulation and expressed the shift and broadening of the spectral lines in terms of elastic scattering of a free electron by the perturber and the broadening and shift cross sections can be expressed in terms of the phase shift due to the interactions. The shift and broadening due to collision with neutral rare gas atoms consist of the contributions from scattering of the Rydberg electron by the rare gas perturber and the polarization of the rare gas atom due to the ionic core of the Rydberg atom. Alekseev and Sobelman (1966) have shown that these two contributions are independent and add up to make the total shift (Δ) and broadening (Γ) given by the relations:

Total shift $\Delta = \Delta_{sc} + \Delta_{pol}$ (4.11)

And, total broadening $\Gamma = \Gamma_{sc} + \Gamma_{pol}$ (4.12)

The above theory assumes the following conditions (Heber *et al* 1988)

1 The collision time is short compared to the time between collisions leading to the condition that the interaction radius for electron-perturber atom ρ_e is such that,

$$\rho_e \ll a_0 n^2 \tag{4.13}$$

Where a_0 is the Bohr radius and n is the principal quantum number

$$\rho_e = \left[\frac{\pi e c}{4\hbar c v_e}\alpha\right]^{1/3} \tag{4.14}$$

2 For the collision between the ionic core and the perturber atom the range of polarization interaction ρ_{pol} should be such that:

$$\rho_{pol} \ll a_0 n^2 \tag{4.15}$$

$$\rho_{pol} = \left[\frac{\pi e c}{4\hbar c v_{c.m}}\alpha\right]^{1/3} \tag{4.16}$$

Where, ρ_{pol} is called the Weisskopf radius (Allard and Kielkopf 1982)

3 The number density N of the perturber should not exceed so that,

$$\rho_{pol} N \ll 1 \tag{4.17}$$

Defining the shift rate ($K^{\Delta} = \Delta/N$) and broadening rate ($K^{\Gamma} = \Gamma/N$) where Γ is the line width (FWHM) these rate constants are expressed in terms of the electron-scattering length L and the dipole polarizability α of the perturber atom (Heber, *et al* 1988, Gounand and Berlande 1983).

$$K^{\Delta}_{sc} = 2\pi L \tag{4.18}$$

$$K^{\Delta}_{pol} = -6.22(\alpha^2 v_{c.m})^{1/3} \tag{4.19}$$

$$K_{sc}^{\Gamma} = \frac{8L^2}{n} \qquad (4.20)$$

$$K_{pol}^{\Gamma} = 7.18\left(\alpha^2 v_{c.m}\right)^{1/3}, \qquad (4.21)$$

Here $v_{c.m}$ is the relative velocity in the centre of mass system. The scattering length approximation in which the elastic scattering cross section $\sigma_0 = 4\pi L^2$, independent of the electron energy, is most valid for collision with He atoms for which the scattering length is positive. However, for collisions with heavier rare gas atoms Ar, Kr and Xe which exhibit the Ramsauer-Townsend effect for the energy range 0.1 eV-1 eV have negative values of the scattering lengths. The above equations predict a constant value for the shift rate, independent of the principal quantum number n and angular momentum (asymptotic behaviour for high-n). Furthermore, for high values of n the pressure broadening also remains constant, except for the inelastic scattering effect at intermediate-n values which explains the experimentally observed irregularities (Kaulakys 1984). For values of the principal quantum number, $n > 30$, the above formulation describes the Rydberg atom collisions with the rare gases with good accuracy as reported by Heber *et al* (1988). A measurement of the shift and broadening for a given principal quantum number provides a means of measurement of scattering length L_n which gives the collision cross section and the atomic polarizability α_n for that state.

Thermal collisions between neutral perturber and the Rydberg atoms are possible at small electron energies. For all practical purposes, the electron energies $E = \frac{(\hbar k)^2}{2\mu}$ in the range 0.1-1 eV ($<< R_y$) for which the $ka_0 < 0.1$- 0.3 are important. Here k is the wave number which depends on the principal quantum number n and the energy ΔE transferred to the valence electron in the e-B collision process. In pure elastic

collision (ΔE = 0) the characteristic wave numbers are in the range of the orbital wave number of the Rydberg electron $k_n \approx 1/na_0$, a_0 is the Bohr radius. For inelastic collisions (n-changing, ionization etc. processes) in which large energy ΔE is transferred to the translational motion of the colliding atoms much larger values of k (such that $\hbar k >> 1/na_0$) than the electron orbital momentum are involved. In such processes the values of k, for medium range principal quantum numbers, also satisfy the condition $kr_0 << 1$ where r_0 is the effective radius of the short-range interaction of the electron with the collision partner B (Lebedev and Biegman 1998).

For highly excited ultra-slow electrons the de Broglie wavelength 1/k is much larger compared to the effective radius r_0 of e-B interaction. In this case the electron scattering is described by the scattering amplitude of the long-range polarization, dipole or quadrupole interaction and the short-range interaction ($r < r_0$) is described in terms of the scattering parameters, scattering length L and the effective radius r_0. The scattering amplitude and the scattering cross section are given as $f_{e\text{-}B} = -L$ and $\sigma_{e\text{-}B} = 4\pi L^2$. Due to its simplicity the scattering length approximation was extensively used for theoretical description on collisions involving Rydberg atoms with neutral atomic targets. But this theory fails to satisfactorily explain the thermal collisions, of highly excited atoms with ground state heavy rare gas atoms, especially the inelastic collisions involving large energy transfer. This theory could not be applied for collisions with neon atom having very low value of the scattering length and for collisions involving large atomic polarizabilities like the alkali atoms and large permanent dipole moments (polar molecules) leading to the observation of anomalous electron-atom scattering processes by such species which are intensively studied in recent years (Biegman and Lebedev 1995). The scattering length L

obtained by extrapolation of the electron-perturber cross section to zero energy are found to be in reasonable agreement with experimental results reported by Moley (1964) for pressure shift of Rydberg levels by noble gases. Table 4.1 shows the polarizability α and electron scattering length L of the ground state of rare gas atoms (Lebedev and Biegman 1998).

Table 4. 1 Polarizability and Scattering length *
He, Ne, Ar and Xe

Atom	Polarizability α (in unit of a_0^3)	Electron scattering length L (in units of a_0)
Helium	1.383	1.19
Neon	2.67	0.214
Argon	11.08	-1.7
Xenon	27.29	-6.5

* Lebedev and Biegman and (1998)

For collision involving Rydberg atoms the spectral line broadening and shift are estimated from impact-parameter ρ and relative velocity v of the Rydberg atom and the perturber atom, assuming the straight-line trajectory and binary interaction with the nearest perturbing atom. Impact approximation (Baranger 1958, Fano 1963) has been widely used for treating pressure shift and broadening of spectral lines. In the impact approximation only binary collisions are important and the spectral process and spectral features are described on the basis of the model of a classical oscillator with an intensity distribution function I(ω). In a collision in which the collision duration is much shorter than the mean time between collisions, the perturbation of the oscillator can be treated as an induced phase change leading to the Lorentzian shape for the intensity distribution function given by (Lebedev and Biegman 1998):

$$I(\omega) = \frac{1}{\pi} \frac{(\Gamma/2)}{(\omega - \omega_0 - \Delta)^2 + (\Gamma/2)^2} \qquad (4.22)$$

Where Γ is the full line width (FWHM) which is the width of the above distribution at half height and is called the impact width. The peak of the distribution is shifted from the line centre ω_0 (unperturbed frequency) by an amount Δ. Lorentzian distribution is characteristic of the impact broadening and the features of the interaction decide the values of the impact width Γ and shift Δ and do not change the form of distribution.

The analytical relations (4.18)-(4.21) give the broadening and shift in terms of important physical quantities like the principal quantum number n, relative velocity of collision, the electron scattering length L and polarizability α of the perturber etc. For experimental applications, collisions at thermal energies corresponding to slow collisions are important. If the principal quantum number is not too small, the total broadening and shift cross sections can be given in terms of the sum of the scattering contributions by the perturber on the quasi-free electron and the ionic core (Lebedev and Biegman 1998). The broadening and shift for the polarization effect (A^+-B scattering) are independent of the principal (n) and the orbital (ℓ) quantum numbers and the shift is negative (towards the longer wavelength) with a value nearly equal to the impact width.

The alkaline-earth atoms with two valence electrons outside the 2^+ closed core have singlet and triplet configurations and doubly excited and autoionizing states. These lead to configuration mixing and the single-electron excitation spectra of these atoms exhibit strong perturbation by doubly excited configurations. The variation of collision cross section with n for the alkaline-earth atoms is not as regular as in alkali-rare gas collision processes. Adequate experimental data are required for refinement of the theoretical treatment of the collisions involving the Rydberg states

of these atoms. Therefore, it is interesting to study the line broadening and line shift of the Rydberg states of the alkaline-earth atoms in the highly perturbed region in the intermediate range of the principal quantum numbers using different rare gas atoms. Broadening and shift rates of neutral strontium and barium Rydberg states with low and intermediate values of the principal quantum number n where strong series perturbation occurs have been investigated and the results are presented in this thesis.

4.3 Experimental Aspects

Experimental studies of the impact broadening and shift of the Sr I 5sns $^1S_0$ and 5snd $^{1,3}D_2$ Rydberg series perturbed by rare gases have been carried out by Weber and Niemax (1982) and Heber *et al* (1988) for a wide range of the principal quantum numbers and reported strong perturbations in the spectra. Collisional shift is positive for He and Ne and the shift gradually becomes negative for the heavier rare gases Ar, Kr and Xe for which the Ramsauer effect takes place and the scattering lengths are negative. (The sign of the pressure shift is decided by the sign of the scattering length L). The above measurements reported the asymptotic behaviour for the impact broadening and shift at high principal quantum numbers by the polarization effect due to the scattering contribution of the perturber by the Rydberg atom core (A^+-B interaction) thereby experimentally confirming the theoretical predictions by Fermi (1934), Reinsberg (1937) and Alekseev and Sobel'man (1966) for the asymptotic behaviour (constant values independent of n and ℓ) of the impact broadening and shift of the Rydberg series in rare gases.

For lower values of the principal quantum number Heber *et al* (1988) found irregularities on the dependence on the principal quantum number n for the impact broadening and shift for the SrI 5sns $^1S_0$ and 5snd $^{1,3}D_2$ Rydberg series resulting from inelastic transitions induced by the collision with the rare gas atoms as reported by Weber and Niemax (1982). Heber *et al* (1988) also observed a remarkable difference between the shift rates for the singlet and triplet states. The pressure shift of the 5s18d $^3D_2$ state is found to be extremely large and for n = 20, the $^3D_2$ states are found to have less broadening and shift rates compared to the $^1D_2$ states, suggesting that the electron spin also has to be considered in the theory. Sun *et al* (1991) explained the irregular broadening behaviour of the Sr I 5sns $^1S_0$ Rydberg series in xenon using the multi-channel quantum defect theory.

Collisional angular momentum (ℓ) mixing of Rydberg states by foreign gas atoms have been investigated by several groups (Kachru *et al* 1983, Wu *et al* 1990). In the presence of a noble gas, the collisional angular momentum mixing cross section is found to increase with the principal quantum number n at low n and to decrease at high n. Mende and Kock (1997) observed parity-forbidden transitions in strontium principal series due to collision with argon buffer gas in a heat-pipe setup with thermionic diode detection. Recently Philip and Connerade (2007) have demonstrated the feasibility of controlled excitation to transitions in violation of parity and spectroscopic selection rules by varying the pressure and composition of the buffer gas in presence of externally applied electric field in a two-photon experiment using π-excitation of a high density atomic jet. This method has allowed new extensions up to n = 44 for the two-photon forbidden J = 3 odd-parity 5snf $^1F_3$ Rydberg series of neutral strontium. In this study it was also possible to extend the

term values of the $J = 0$, even-party $5sns\ ^1S_0$ Rydberg series up to $n = 46$ for the first time by controlled collision and electric filed.

The experimental set up for the study of collisions involving Rydberg atoms with neutral rare gases was essentially the same as discussed in detail in Chapter 2. The heat-pipe (Philip 2007) was operated using the disposable cartridge filled with the alkaline-earth metal samples (strontium and barium) one at a time at a suitable temperature range according to the vapour pressure requirement. The high density atomic jet (Philip 2008) was excited by the linearly polarized dye laser beam as described in Chapter 2. Due to an anomaly in frequency shift observed recently by Philip and Makdisi (2006) in the two-photon spectra of strontium, the measurements in line shift and broadening reported were carried out with a residual helium buffer to compensate the anomalous frequency shift and the wavelength calibration was done using the published data for the term values by Makdisi *et al* (2001) for strontium. For barium new results by Philip and Connerade (2008) which are compared with the published energy level data by Aymer *et al* (1978) have been used. Controlled admission of noble gases (He, Ar and Xe) as buffers was achieved using a vacuum station and gas handling system fitted with vacuum and pressure gauges.

Since the even-parity spectra of strontium are heavily perturbed the pressure shift and broadening study was focused chiefly to obtain new experimental data for the spectra of strontium in the heavily perturbed region involving low and intermediate values of the principal quantum number. Also investigated extensively are the noble gas collisions on the broad resonance which intrude in to the two-photon spectrum of neutral strontium. Furthermore, the autoionizing state of strontium and the low-

lying Rydberg states of neutral barium were investigated. As not much experimental data are available in the literature, a comparison with previous experimental data is, somewhat, limited. The experimental accuracy was limited by the bandwidth of the dye laser which is 0.18 cm^{-1}. Wavelength scanning was kept at the maximum resolution of the dye laser scan controller which is 0.001 nm/sec. The boxcar averager gate scanner and channel setting were adjusted to get sufficient data in a steady operating condition without signal jitter for different spectral regions. These settings were optimized for each experiment. Since xenon has the highest value for polarizability among the noble gases used as buffer, most experimental data was obtained using xenon. In experiments involving collisional effects on the two-photon spectra of barium, low lying Rydberg members were selected for investigation because of its special interest due to strong series perturbations. For convenience the spectra are presented with laser wavelength in air for two-photon excitation which is noted directly from the dye laser scanner controller. These values are converted in to wavenumbers after vacuum correction and the frequency shift and line width are given in the conventional unit, cm^{-1}. Results presented are limited for new observations in selected spectral regions of strontium where not much previous investigation has been reported in the literature. The results obtained are based on the theoretical formulation outlined in the beginning of this chapter within the frame work of impact approximation as adopted by Heber *et al* (1988).

4.4 Experimental Results and Discussion

4.4.1 Collisional shift and broadening of the bound, even-parity Rydberg series of strontium

Figure 4.2 is a portion of the two-photon absorption spectrum of strontium showing the low lying members of the even-parity 5s*n*s $^1S_0$ and 5s*n*d $^{1,3}D_2$ Rydberg series. Due to the configuration interaction, the triplet and singlet series swap over at n =16. The relative strengths of the series members are observed to depend strongly on the environment in which the Rydberg atoms are placed.

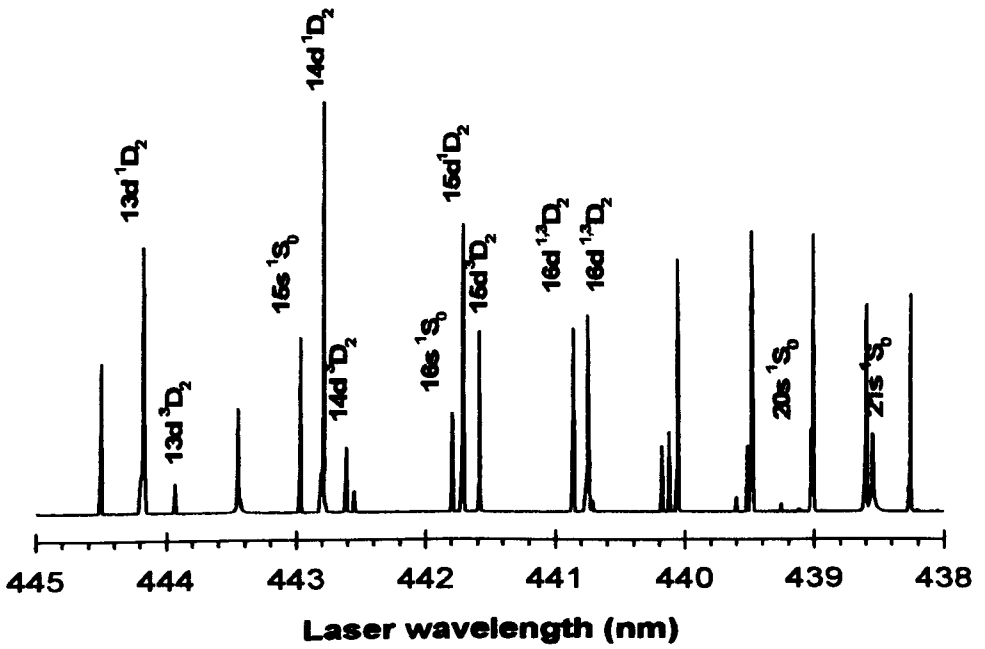

Fig. 4.2 Two-photon spectrum of SrI showing low lying members of 5s*n*s $^1S_0$ and 5s*n*d $^{1,3}D_2$ Rydberg series

Figures 4.3 (a-c) show the two-photon spectra of neutral strontium, covering the 437 nm - 435.5 nm wavelength range of the dye, with He buffer gas at three different values of pressure (10 mbar, 40 mbar and 100 mbar respectively).The interlopers emerging with collisions at 27< n < 28 and at 30 < n <31 result from the resonance level 5s5p $^1P_1$ following dissociation of Sr_2 dimers (Philip and Makdisi 2006).

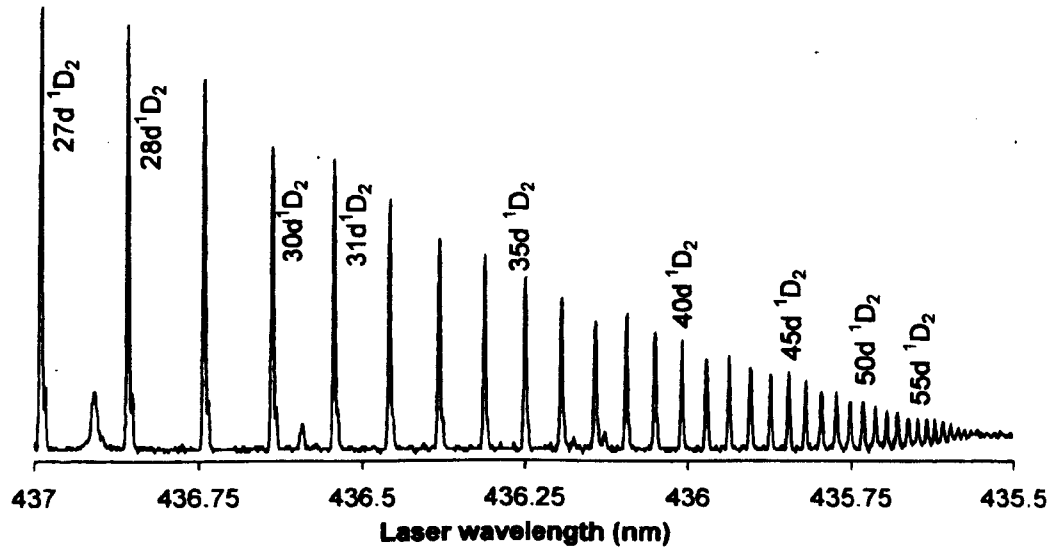

Fig. 4.3(a) Two-photon spectrum of Sr I showing the growth of perturbers for 5s*n*d $^1D_2$ Rydberg series at 10 mbar He

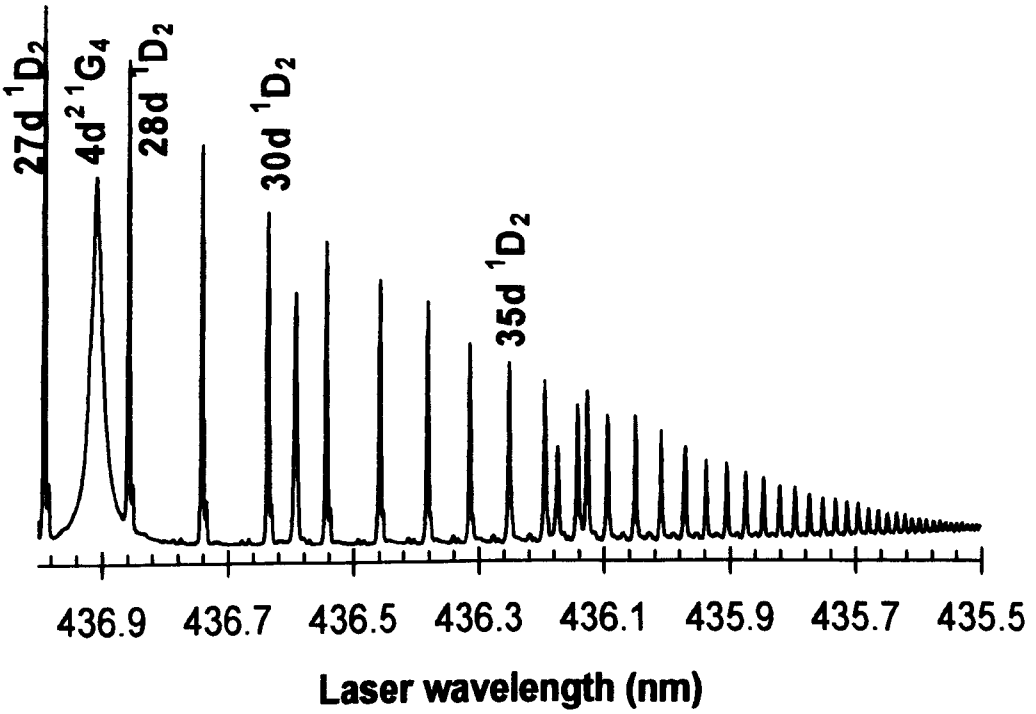

Fig. 4.3(b) Two-photon spectrum of Sr I at 40 mbar He

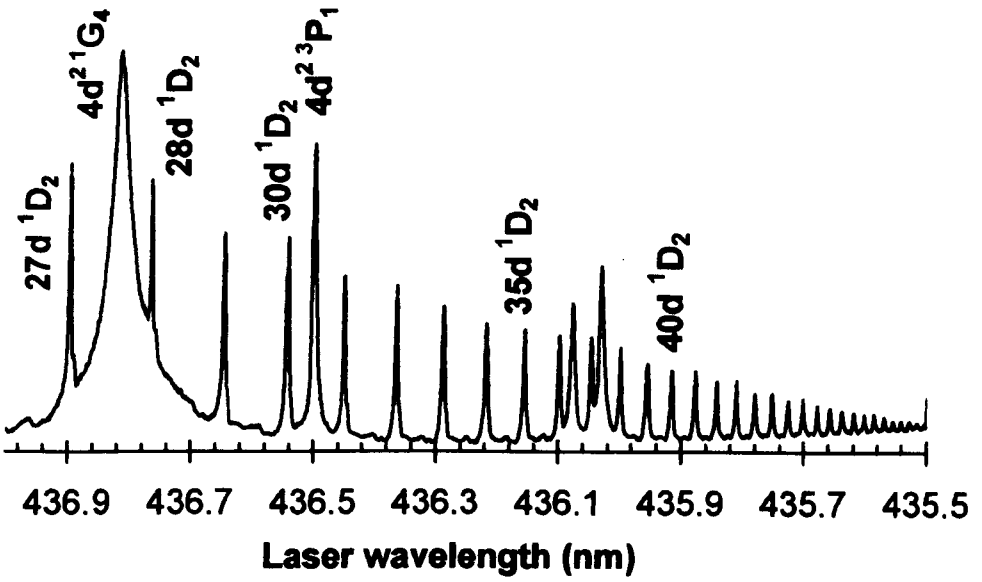

Fig. 4.3(c) Two-photon spectrum of Sr I showing the growth of perturbers for 5s*n*d $^1D_2$ Rydberg series at 100 mbar He

The spectrum in figure 4.4 taken with He buffer at 300 mbar illustrates the growth of the remarkable non-Rydberg interloper with buffer gas collisions at $27 < n < 28$.

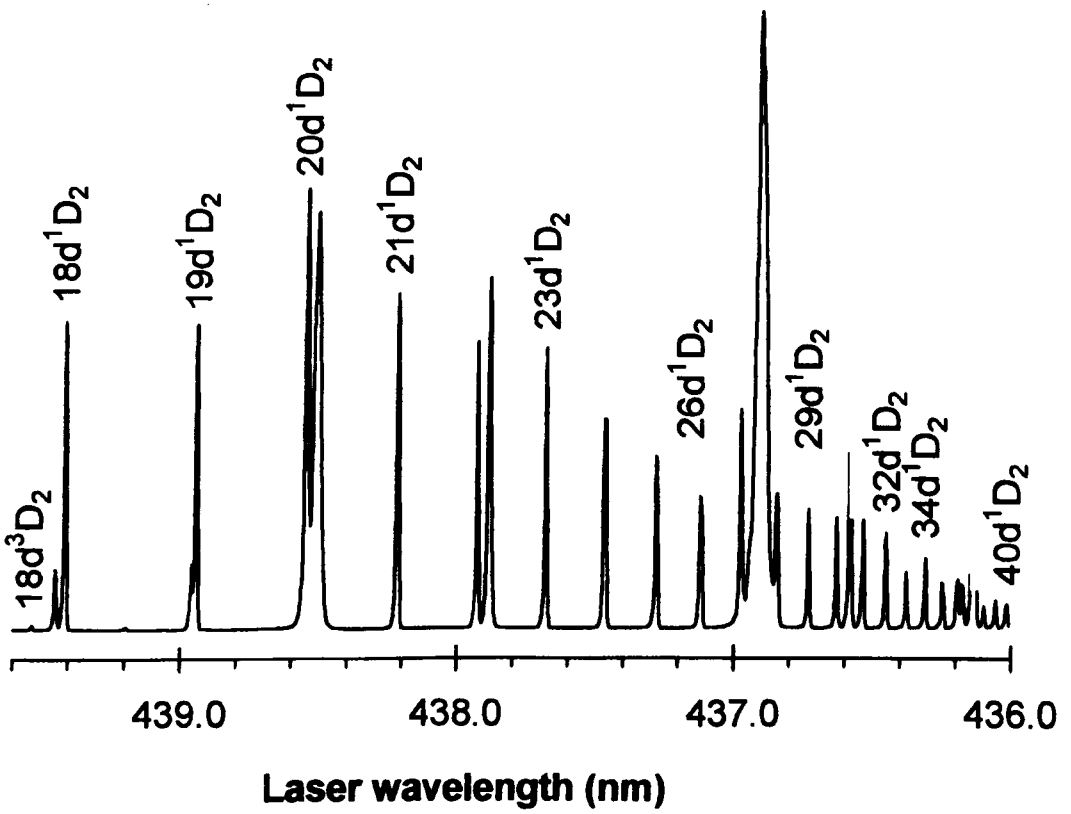

Fig. 4.4. Two-photon spectrum of Sr I showing the growth of perturbers for 5s*n*d $^1D_2$ Rydberg series at 300 mbar He

Quasi-molecular processes following the dissociation collision induced Sr_2 dimers and Sr*-rare gas complex leading to transitions exhibiting the break down of the ΔJ selection rule and parity are also observed as reported by Philip and Makdisi (2006).

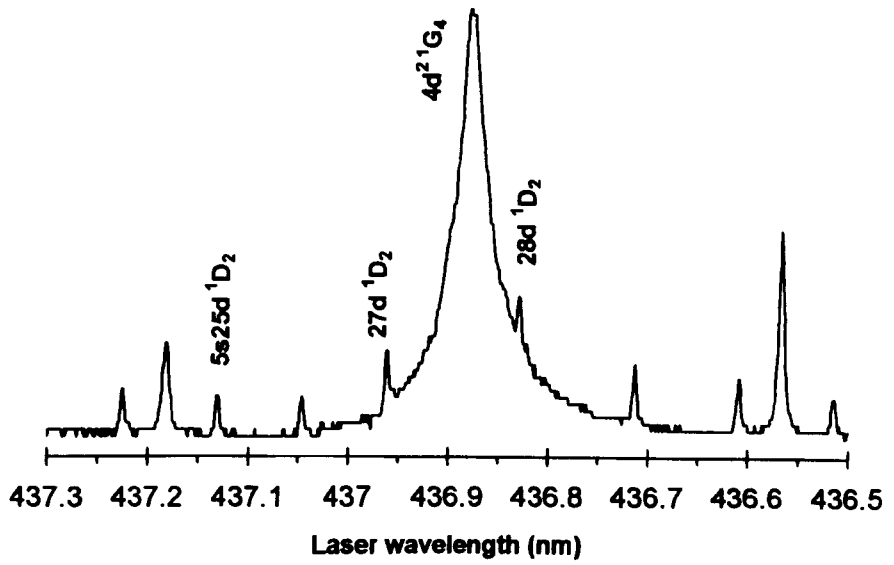

Fig. 4.5 Quenching of Rydberg series and growth of intruders due to collision with Ar (300 mbar) in two-photon spectrum of Sr I

The survival of the interlopers in the presence of enhanced buffer gas collisions confirms the highly localized character by orbital contraction effects (Connerade 1998) of these interlopers. The broad intruder resonance tentatively labeled as $4d^2\ ^1G_4$ has two 4d electrons in highly compact state. It is also interesting to note that strong fluorescence signals are observed from compact excited states while Rydberg states are quenched (Khan *et al* 1994). Forbidden transitions to odd-parity Rydberg states induced by *l*-mixing also are found to be wiped out as the buffer gas pressure is substantially increased. Figure 4.5 shows the growth of the intruder and the quenching of the Rydberg members with argon buffer. In figure 4.6 the relative strengths of the intruders in strontium are compared with an adjacent Rydberg transition and the remarkable effect of buffer gas collision is observed.

The relative strengths of the transitions are determined by an initial calibration with ionization signal due to a Rydberg transition away from a perturber and at a residual buffer gas pressure of 10 mbar He which gives minimum collisional and field-induced perturbation. All signal data are compared to this to obtain relative signal strengths.

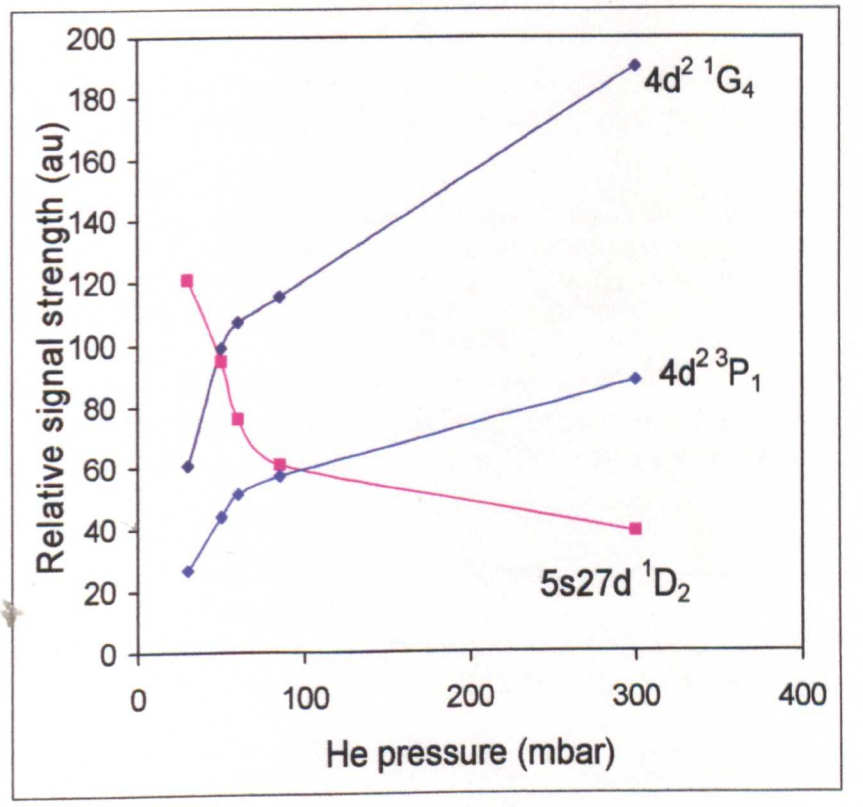

Fig. 4.6 Relative strength of a Rydberg member compared to the nearby intruders as a function of He pressure

Figure 4.7 shows the two-photon absorption spectrum taken with 3 different values (100 mbar, 200 mbar and 300 mbar) of pressure of argon. Due to Ramsauer effect exhibited by Rydberg atoms, collisional shift is found to be positive (blue shift) for helium and negative (red shift) for heavier rare gases like argon and xenon with xenon giving the maximum shift and broadening rates. The non-Rydberg excitation $5s5p\ ^1P_1 \rightarrow 4d^2\ ^3P_1$ is shifted to the opposite of the Rydberg transitions.

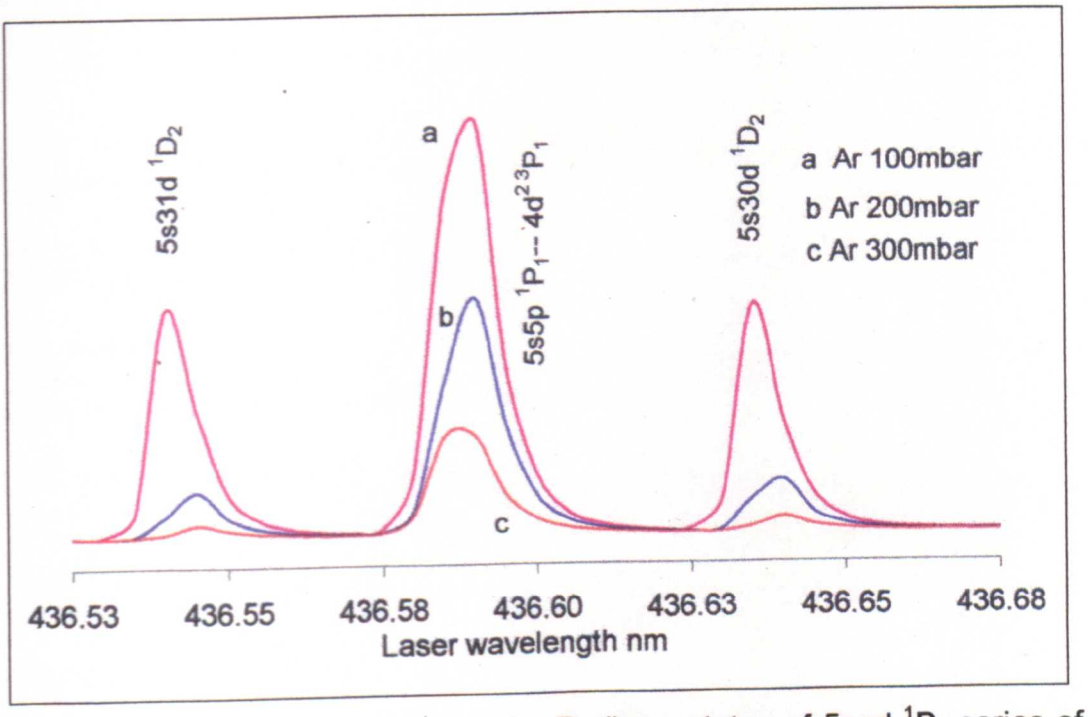

Fig. 4.7. Ramsauer effect in argon for Rydberg states of 5s*n*d $^1D_2$ series of Sr I. A Rydberg member is red-shifted while the interloper is blue shifted

The direction of frequency shift as seen in figures 4.7 and 4.8 can be used (Philip and Connerade 2007) to test whether the transitions are Rydberg or otherwise.

However, interestingly, unlike other non-Rydberg excitation the remarkably broad resonance at $27 < n < 28$ in the 5s*n*d $^1D_2$ Rydberg series of strontium exhibits Ramsauer effect like a Rydberg transition with negative shifts in argon and xenon.

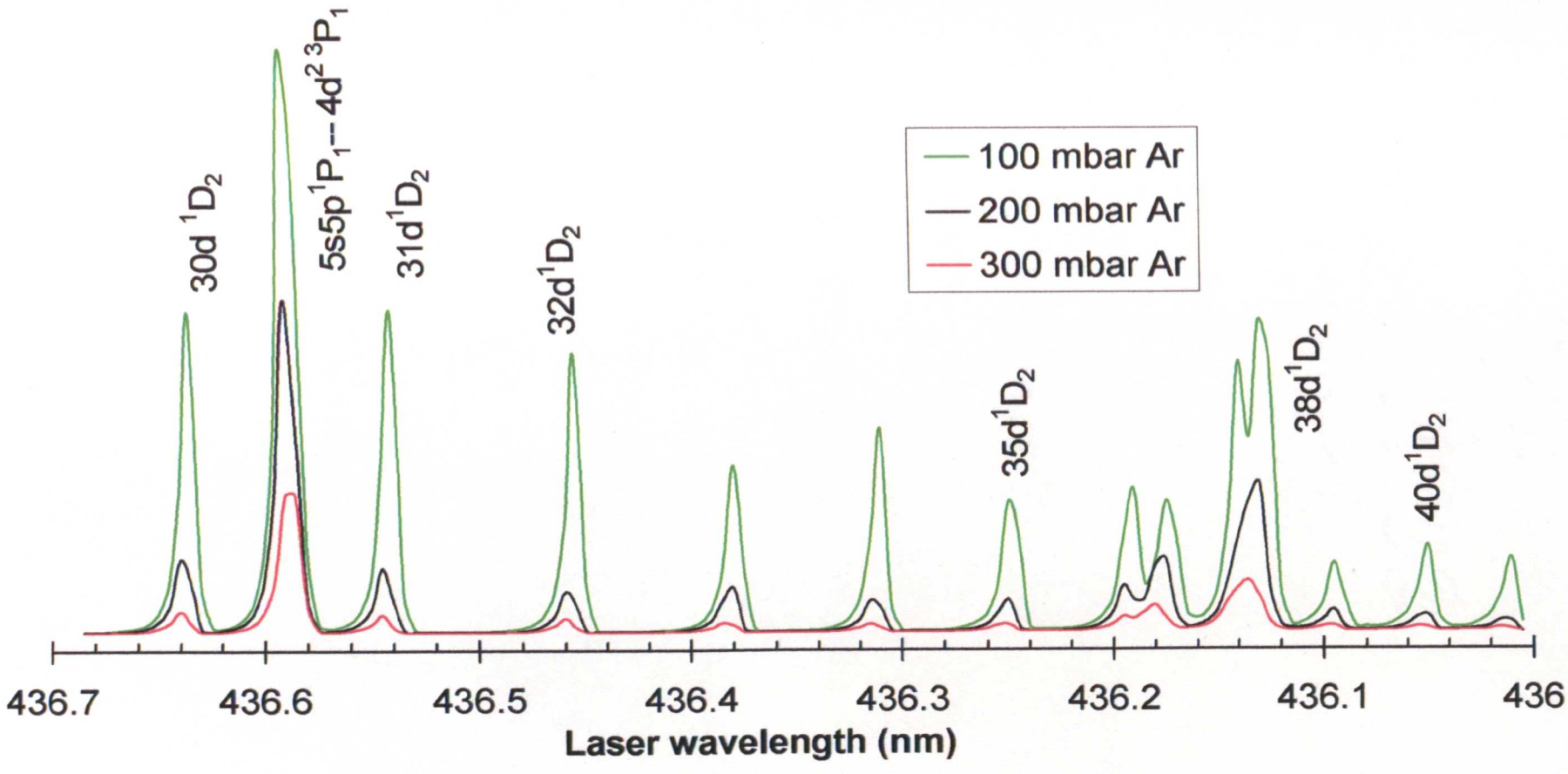

Fig. 4.8 Collisional broadening and shift of high members of 5s*n*d $^1D_2$ Rydberg series of Sr I with Ar buffer at 100 mbar, 200 mbar and 300 mbar. A Rydberg member is red-shifted while the interloper is blue shifted

In figure 4.9 the intensity ratios between a few low lying states [$5s^2\ ^1S_0 \rightarrow 5s\ (n+1)s\ ^1S_0$] / [$5^2\ ^1S_0 \rightarrow 5snd\ ^1D_2$], at 3 values of the buffer gas pressure (100 mbar, 200 mbar and 300 mbar argon) are plotted (Philip and Connerade 2007).

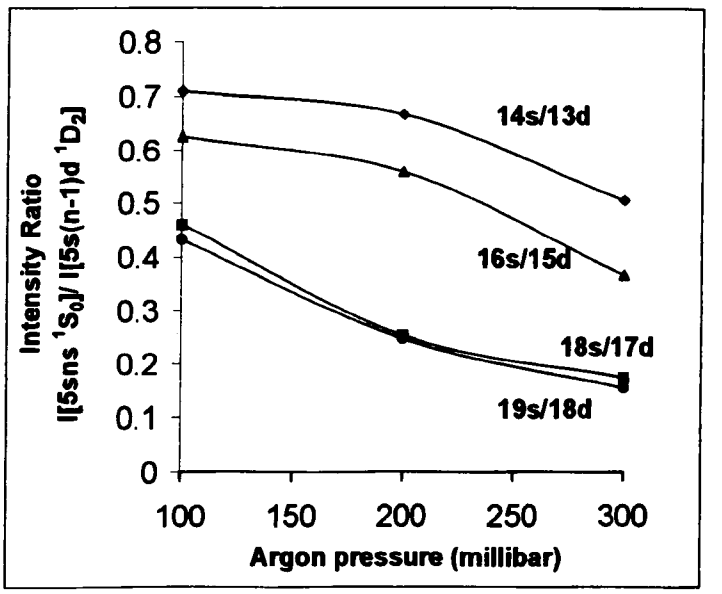

Fig.4.9 Relative strengths of Rydberg members

Extensive analysis is presented here for pressure shift and broadening in xenon along with selected results for helium and argon. Broadening is calculated from the full width at half maximum (FWHM) and shift is taken from the unperturbed frequency. All data are presented corresponding to relative density unit (1 amagat = 2.69×10^{19} cm^{-3}) at 273 K.

$$\text{Relative density} = \frac{P(mbar) \times 273}{1000 \times T(K)} \qquad (4.23)$$

4.4.2 Pressure shift in strontium due to xenon

In strontium, due to configuration mixing, 5s*n*d $^1D_2$ and 5s*n*d $^3D_2$ Rydberg series are found swapping over at n ~16 as seen in Fig. 4.2 Therefore, it is important to study the collisional shift and broadening of these series where they cross over. To have negligible shift from the line centre all measurements are taken with the heat pipe operated with a residual pressure of 20 mbar He to compensate for the Stark shift induced by the effective field inside the thermionic diode detector. The measurements reported for strontium with xenon as the buffer gas are taken with an applied electric field of 4.7 volt-cm^{-1} and the heat-pipe was operated at a temperature of 812 ± 1 ^{0}C and xenon pressure was varied from 30 mbar to 170 mbar.

Frequency shifts for the 5s*n*s $^1S_0$, 5s*n*d and $^3D_2$ and 5s*n*d $^1D_2$ Rydberg series are plotted in Fig. 4.10, Fig. 4.11 and Fig. 4.12 respectively. For these Rydberg series the pressure shifts due to xenon are negative and are proportional to the buffer gas pressure, as expected.

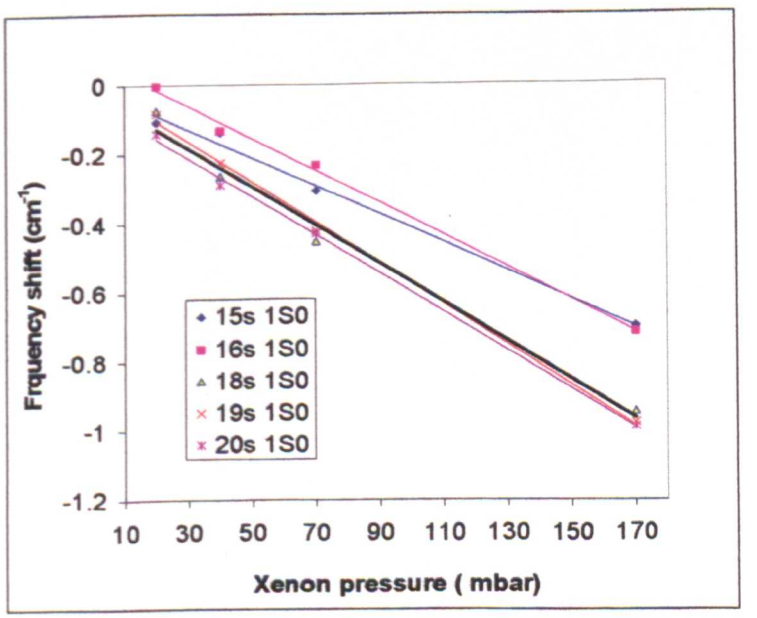

Fig. 4.10 Negative frequency shift for 5s*n*s $^1S_0$ Rydberg members of Sr I due to collision with Xe

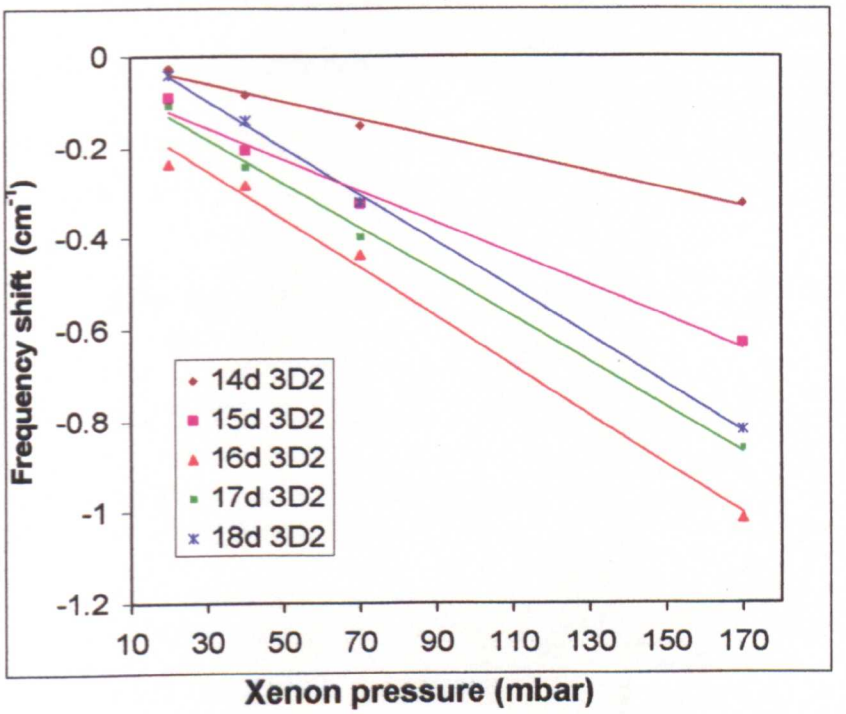

Fig. 4.11 Negative frequency shift for the 5s*n*d $^3D_2$ Rydberg members of Sr I due to Xe

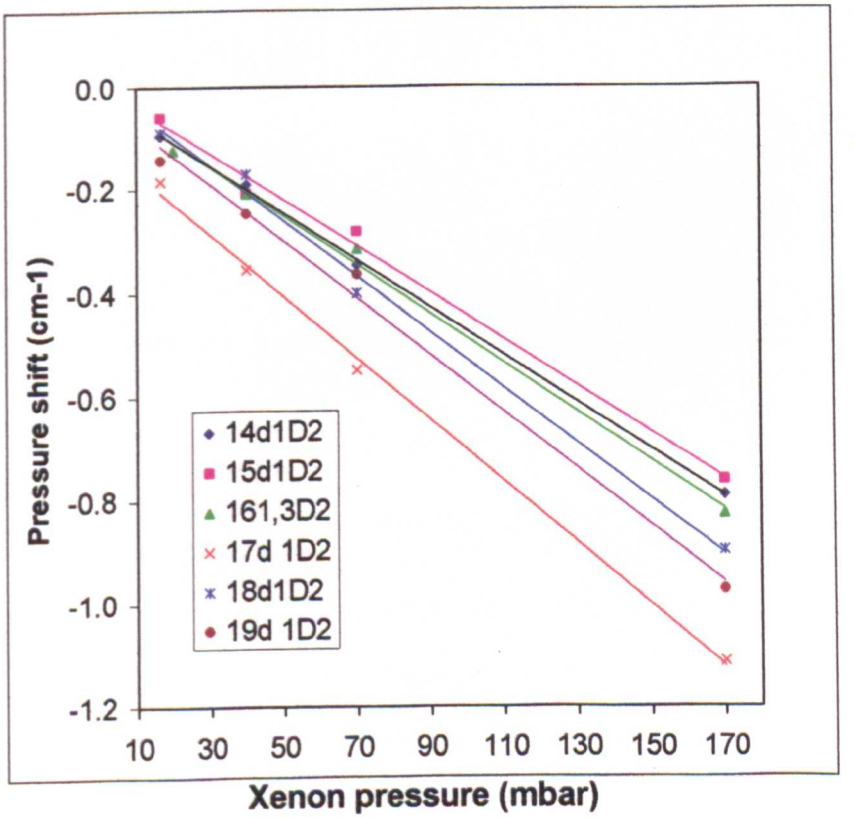

Fig. 4.12 Negative frequency shift for 5s*n*d $^1D_2$ Rydberg members of Sr I due to collision with Xe

Collisional shift rates for the 5s*n*s $^1S_0$, 5s*n*d $^3D_2$ and 5s*n*d $^1D_2$ Rydberg series are given in Table- 4.2, Table- 4.3 and Table- 4.4 respectively. Also given are the experimental values reported by Heber *et al* (1988) after converting to cm^{-1}/amagat.

Table 4. 2 Pressure shift rates - Xe
Sr I 5s*n*s $^1S_0$ (15 < *n* < 20)

Pressure shift rates K^{Δ} for the transition **$5s^{21}S_0 \rightarrow 5sns\ ^1S_0$** in Sr I due to **xenon** as a function of principal quantum number *n* given at reduced pressure and temperature **273 K** in **cm^{-1}/ amagats** (1 amagat = 2.69x 10^{19} atoms /cm^3)

Principal Quantum Number *n*	Pressure shift Rate K^{Δ} cm^{-1}/ amagat
15	-16.66
16	-18.25
18	-20.23
19	-22.61
20	-21.42

Table 4. 3 Pressure shift rates - Xe
Sr I- 5s*n*d $^3D_2$ (14 < *n* < 18)

Pressure shift rates K^{Δ} for the transition **$5s^{21}S_0 \rightarrow 5snd\ ^3D_2$** in Sr I due to **xenon** as a function of principal quantum number *n* given at reduced pressure and temperature **273 K** in **cm^{-1}/ amagat** (1 amagat = 2.69x 10^{19} atoms / cm^3)

Principal Quantum Number *n*	Pressure shift Rate K^{Δ} cm^{-1}/ amagat
14	-9.92
15	-21.82
16	-16.26
17	-24.99
18	-24.98

Table 4.4 Pressure shift rates - Xe
Sr I- 5s*n*d $^1D_2$ (14 < *n* < 19)

Pressure shift rates K^{Δ} for the transition **$5s^{21}S_0 \rightarrow 5snd\ ^1D_2$** in Sr I due to **xenon** as a function of principal quantum number *n* given at reduced pressure and temperature **273 K** in **cm^{-1}/ amagat** (1 amagat = 2.69x 10^{19} atoms / cm^3)

Principal Quantum Number *n*	Pressure shift Rate K^{Δ} cm^{-1}/ amagat	Pressure shift rate K^{Δ} from previous study (Marafie *et al.** 2003) cm^{-1}/ amagat
14	-18.81	-19.4
15	-18.20	-18.6
16	-19.40	-21.0
17	-23.80	-19.8
18	-21.80	-20.3
19	-22.60	-18.8

* Marafi M., Bhatia K.S., Makdisi Y.Y.and Philip G
J. Phys. B: At. Mol. Opt. Phys. **36**, 1835 (2003)

Heber *et al* (1988) reported an experimental confirmation of the theoretical prediction of an asymptotic value for both pressure shift and broadening rates for high principal quantum numbers. Also, these authors reported deviation from the theoretical values for shift and broadening rates below *n* = 35. Due to heavy series perturbations, oscillations in frequency shift are observed for low lying Rydberg members of Sr I.

4.4.3 Pressure shift for the Sr I 5s*n*d $^1D_2$ Rydberg series for the region 27< *n* <31

In the region of intermediate values (27-31) of the principal quantum number *n*, the 5s*n*d $^1D_2$ Rydberg series of strontium is heavily perturbed by the doubly excited $4d^2$ configurations. A highly compact state, tentatively labeled as $4d^2\ ^1G_4$ with an asymmetric line profile is found to evolve with pressure. (Philip and Makdisi 2006).

Also, an interloper emerging with collision at $30 < n < 31$ results from the resonance level 5s5p $^1P_1$ following the molecular dissociation of Sr_2 dimers. Collisional shift of the 5s*n*d $^1D_2$ Rydberg series for this intermediate range of the principal quantum number is plotted in Fig. 4.13. Similar to the observation reported in a recent paper (Philip and Makdisi 2006) an anomaly in frequency shift for the 5s*n*d $^1D_2$ Rydberg series is observed with a frequency shift reversal as seen in Fig. 4.13.

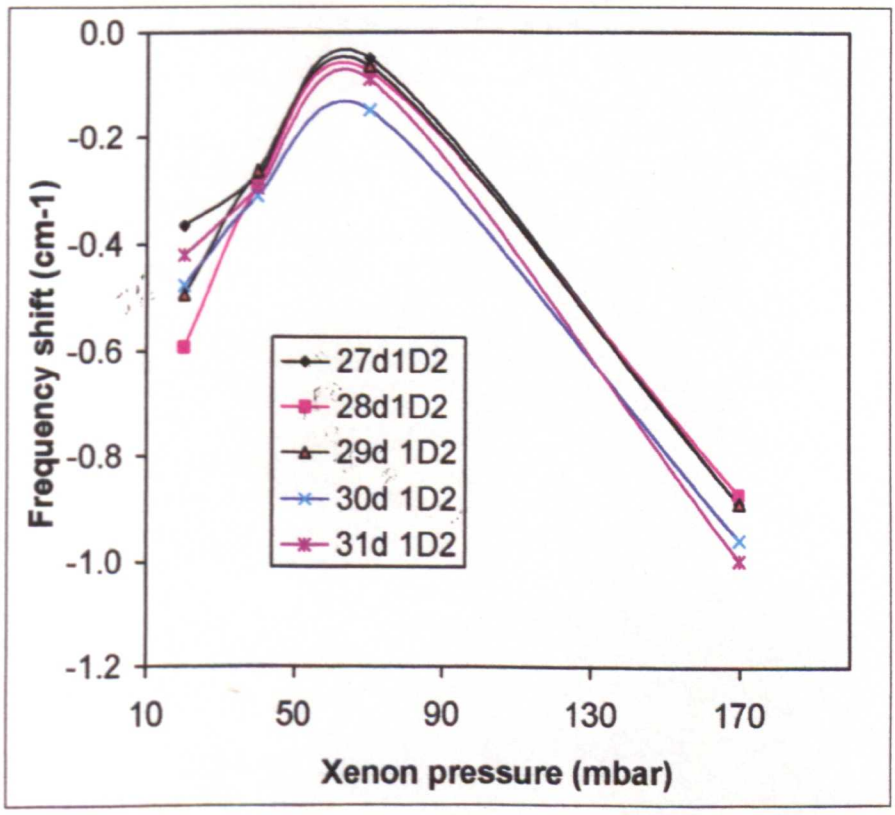

Fig. 4.13 Anomalous frequency shift for the highly perturbed 5s*n*d $^1D_2$ Rydberg members of Sr I due to collision with Xe

When the buffer gas pressure is gradually increased redshift gradually decreases up to around 60 mbar xenon and thereafter the shift increases. It may be considered that such anomalies occur due to the very special environment in which the Rydberg atoms are bathed inside a heat-pipe where electric field and collisions coexist. In TABLE- 4.5 the shift rates for the 5s*n*d $^1D_2$ Rydberg series for $27 < n < 31$ are plotted beyond the reversal point.

Table 4. 5 Pressure shift rates - Xe
Sr I- 5s*n*d $^1D_2$ (27< *n* < 31)

Pressure shift rates K^{Δ} for the transition **$5s^2\ ^1S_0 \rightarrow 5snd\ ^1D_2$** in Sr I due to **xenon** as a function of principal quantum number *n* given at reduced pressure and temperature **273 K** in **cm^{-1}/ amagat** (1 amagat = 2.69x 10^{19} atoms / cm^3)

Principal Quantum Number *n*	Pressure shift Rate K^{Δ} cm^{-1} / amagat
27	-33.32
28	-31.73
29	-32.92
30	-32.13
31	-36.09

4.4.4 Collisional broadening of Sr I- 5s*n*s $^1S_0$, 5s*n*d $^1D_2$ and 5s*n*d $^3D_2$ Rydberg series for the region 14< *n* <20

Collisional broadening (FWHM) of the lower members of the Sr I, 5s*n*s $^1S_0$ Rydberg series is plotted in Fig. 4.14 for the principal quantum number range 15 < n < 20. In Fig. 4.15 the square of the line width is plotted as a function of the square of the buffer gas pressure. Neglecting natural broadening and Doppler broadening the observed line width Γ (FWHM) can be approximately written as,

$$\Gamma = \left(\Gamma^2_{laser} + \Gamma^2_{collision}\right)^{1/2} \qquad (4.24)$$

Using a value Γ_{laser} = 0.18 cm^{-1} for the laser bandwidth (FWHM) and extrapolating the observed line width for xenon pressure = 0 one gets the collisional line width corresponding to the residual buffer gas, 20 mbar He, which is approximately 0.087 cm^{-1}.

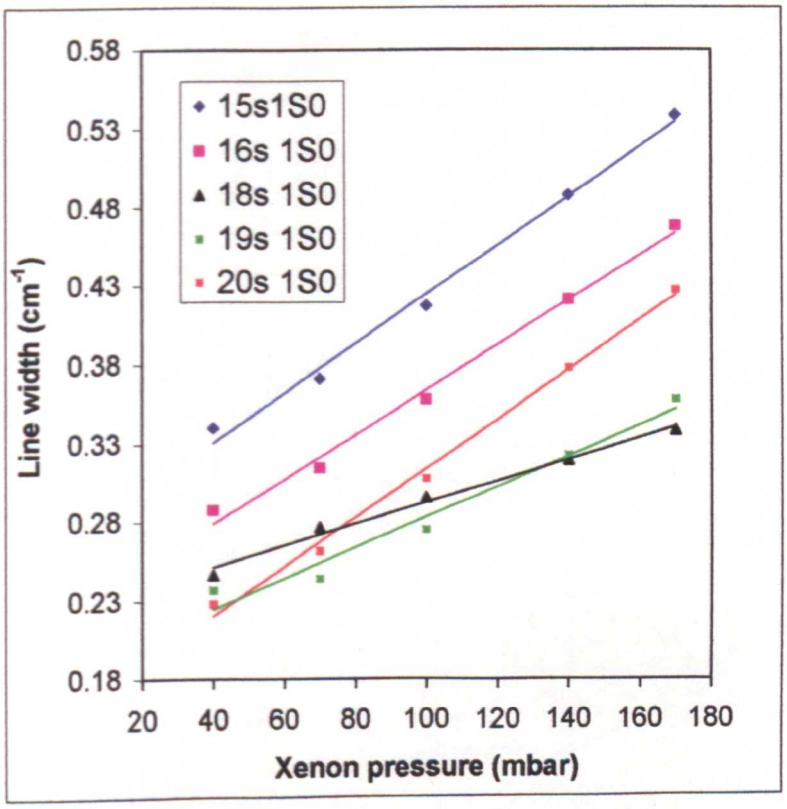

Fig. 4.14 Spectral line width (FWHM) of low-lying 5s*ns* $^1S_0$ Rydberg members plotted against Xe pressure

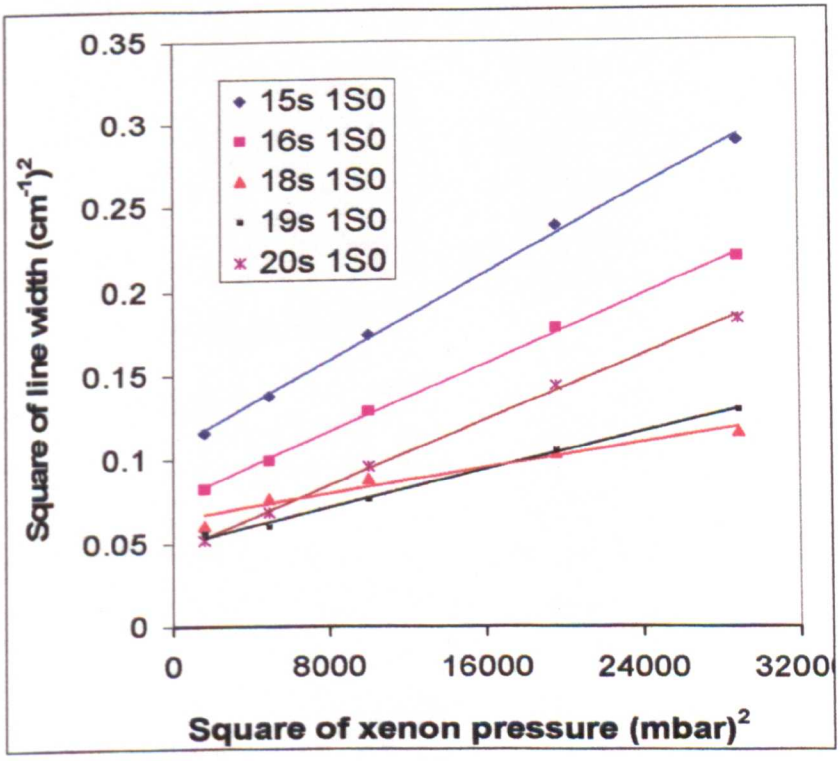

Fig. 4.15 Square of line width (FWHM) of low-lying 5s*ns* $^1S_0$ Rydberg members plotted against square of xenon pressure

Table 4. 6 Pressure broadening rates - Xe
Sr I- 5s*n*s $^1S_0$ (15 < *n* < 20)

Pressure broadening rates K^{Γ} for the transition **$5s^2\ ^1S_0 \rightarrow 5sns\ ^1S_0$** in Sr I due to **xenon** as a function of principal quantum number *n* given at reduced pressure and temperature **273 K** in **cm^{-1}/ amagat** (1 amagat = 2.69x 10^{19} atoms / cm^3)

Principal Quantum Number *n*	Level Energy cm^{-1} (Philip and Connerade 2007) *	Broadening Rate K^{Γ} cm^{-1}/ amagat
15	45135.01	6.30
16	45255.02	5.55
18	45426.67	2.78
19	45488.66	3.97
20	----	6.30

* Philip G. and Connerade J.-P. *Opt. Commun.* **279**, 141 (2007)

For the range of xenon pressure (0-200 mbar), collisional line width is found to be linear with xenon pressure. The collisional broadening rates (K^{Γ}) for xenon for the spectral transitions involving the above members of the 5s*n*s $^1S_0$ Rydberg series of Sr I are given Table 4.6.

Fig. 4.16 presents collisional width of the lower members of the Sr I 5s*n*d $^3D_2$ Rydberg series plotted against xenon pressure. In Fig. 4.17 the square of the width is plotted against the square of the buffer gas pressure. The corresponding quantities for the 5s*n*d $^1D_2$ Rydberg series are plotted in Fig 4.18 and Fig. 4.19 respectively. The square of the line width is found to have a linear relation with the square of the buffer gas pressure in all cases. Pressure broadening rates for the two sequences in the region of low *n* are presented in Table 4.7 and Table 4.8.

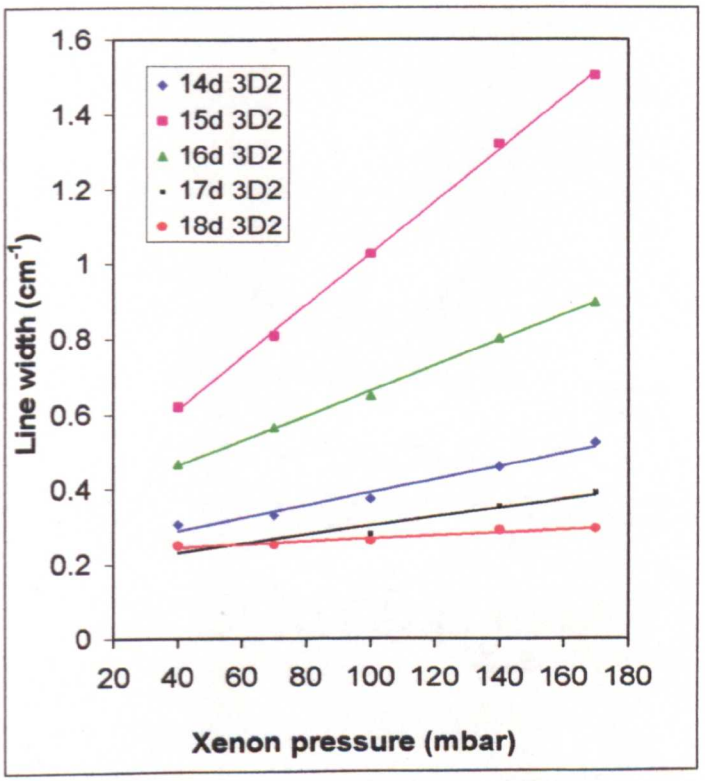

Fig. 4.16 Spectral line width (FWHM) of low-lying- 5s*n*d $^3D_2$ Rydberg members plotted against xenon pressure

Table 4.7 Pressure broadening rates - Xe Sr I-Sr I-5snd $^3D_2$ (14 < n < 18)

Pressure broadening rates K $^{\Gamma}$ for the transition $5s^2\ ^1S_0 \rightarrow 5snd\ ^3D_2$ *in Sr I* due to **xenon** as a function of principal quantum number *n* given at reduced pressure and temperature **273 K** in **cm^{-1}/ amagat** (1 amagat = 2.69x 10^{19} atoms /cm^3)

Principal Quantum Number *n*	Level Energy cm^{-1} (Philip 2008)*	Broadening Rate K $^{\Gamma}$ cm^{-1}/ amagat
14	45171.2	6.74
15	45276.62	27.36
16	45350.01	13.08
17	45420.98	4.76
18	45479.86	1.59

* Philip G., 2008 (*to be published*)

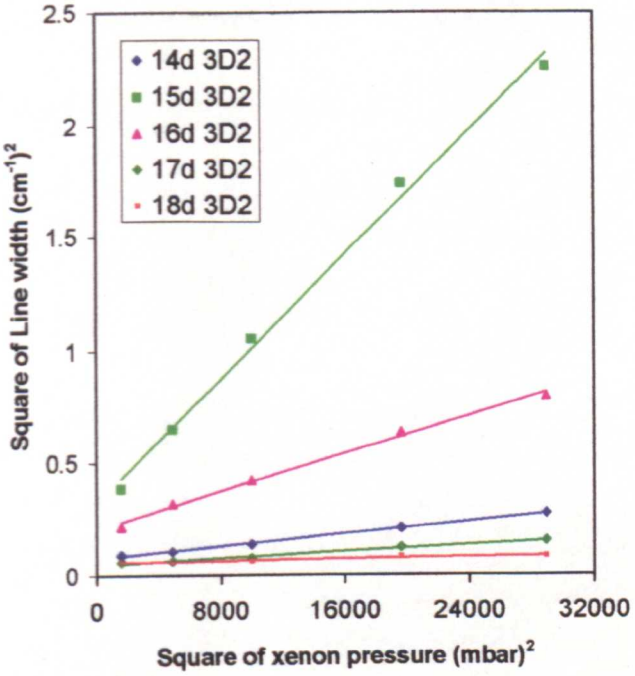

Fig. 4.17 Square of line width (FWHM) of low- lying 5s*n*d $^3D_2$ Rydberg members plotted against square of xenon pressure

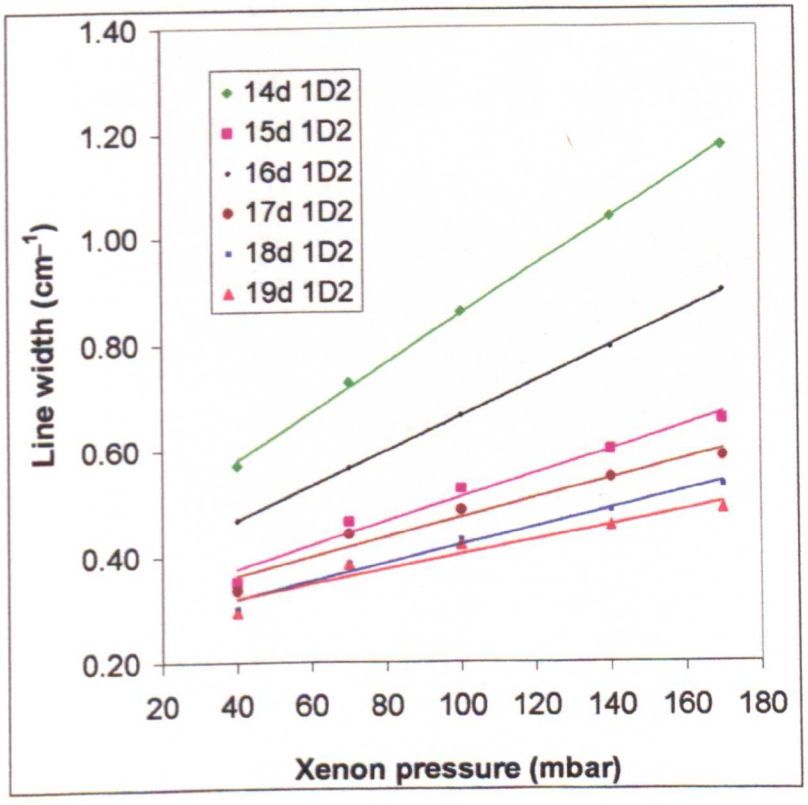

Fig. 4.18 Spectral line width (FWHM) of low lying 5s*n*d $^1D_2$ Rydberg members plotted against xenon pressure

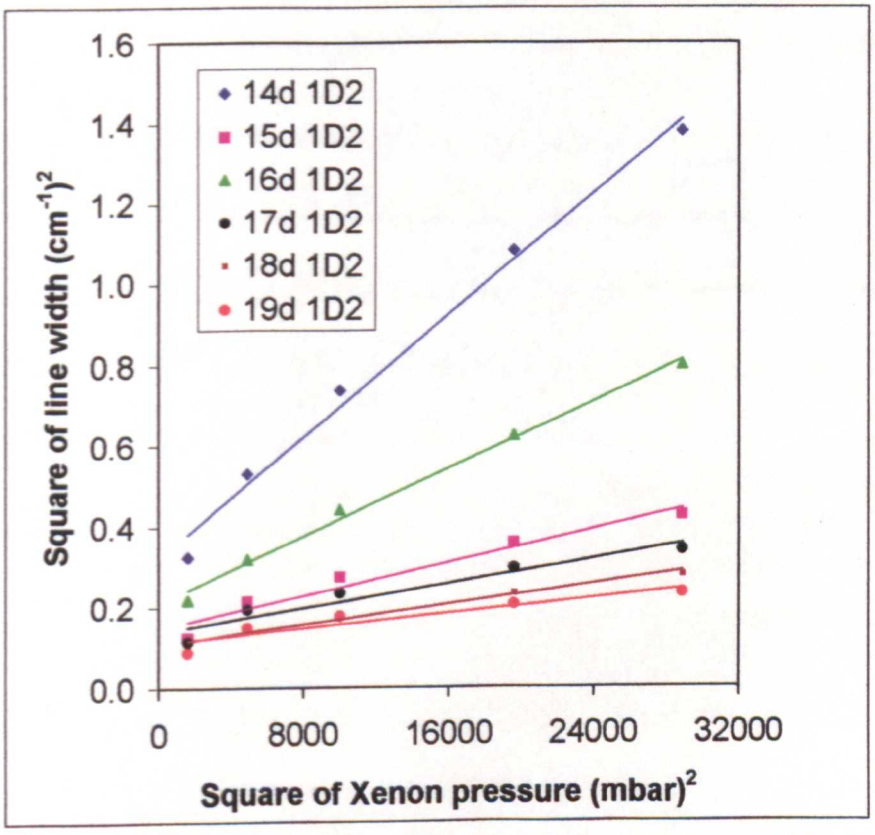

Fig. 4.19 Square of line width (FWHM) of low lying 5s*n*d $^1D_2$ Rydberg members plotted against square of xenon pressure

Table 4.8 Pressure broadening rates – Xe
Sr I- 5s*n*d $^1D_2$ (14 < *n* < 19)

Pressure broadening rates K^{Γ} for the transition **$5s^2\ ^1S_0 \rightarrow 5snd\ ^1D_2$** in Sr I due to **xenon** as a function of principal quantum number *n* given at reduced pressure and temperature **273 K** in **cm^{-1}/ amagat** (1 amagat = 2.69x 10^{19} atoms / cm^3)

Principal Quantum Number *n*	Level Energy cm^{-1} (Philip 2008*)	Broadening Rate K^{Γ} cm^{-1}/ amagat
14	45152.84	18.24
15	45263.72	8.72
16	45361.8	13.02
17	45433.38	7.14
18	45492.28	6.74
19	45542.01	5.55

* Philip G.2008 (*to be published*)

4.4.5 Collisional broadening of Sr I, 5s*n*d $^1D_2$ Rydberg series for the region 27 < n < 31

In the region of intermediate range of the principal quantum number (27< n < 31) the even-parity, $J = 2$, 5s*n*d $^1D_2$ Rydberg series of strontium are heavily perturbed by the $4d^2$ configurations and therefore this region of the two-photon spectrum has several interesting features. These peculiarities are reflected also in the collisional effects of the two-photon excitation spectra.

In Fig .4.20 the line width (FWHM) of the Sr I, 5s*n*d $^1D_2$ Rydberg members are plotted for the heavily perturbed region 27 < n < 31 as a function of xenon pressure. Also, the square of the line width as a function of the square of the buffer gas pressure is plotted in Fig. 4.21.

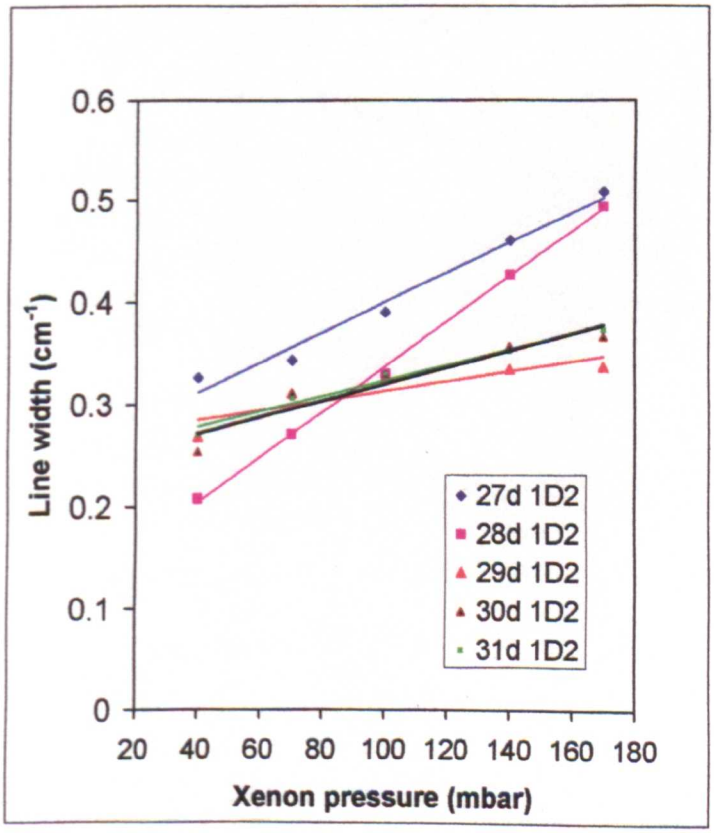

Fig. 4.20 Spectral line width (FWHM) of 5s*n*d $^1D_2$ Rydberg members plotted against xenon pressure

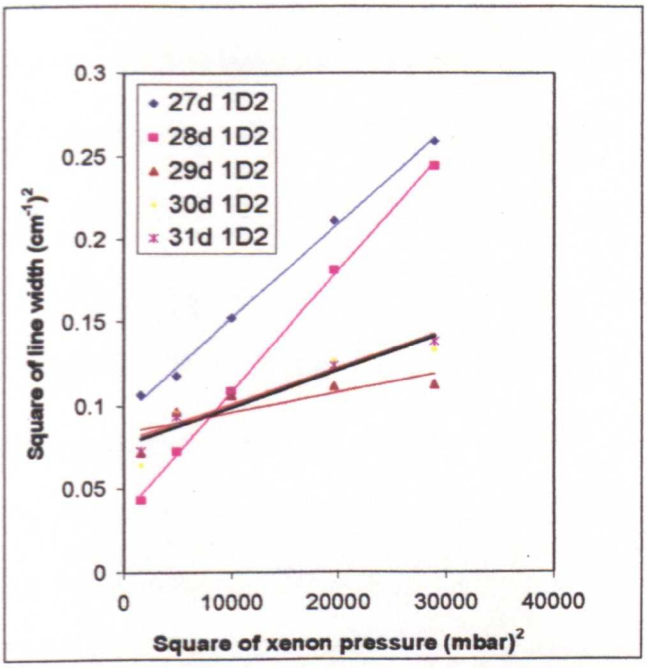

Fig. 4.21 Square of line width (FWHM) of low-lying 5s*n*d $^1D_2$ Rydberg members plotted against square of xenon pressure

The broadening rates in xenon for these members of the Rydberg series is given in Table 4.9. Due to heavy perturbations oscillations in the broadening rate in this region of the principal quantum number are observed.

Table 4. 9 Pressure broadening rates – Xe

Sr I-5snd $^1D_2$ (27< *n* < 31)

Pressure broadening rates K $^\Gamma$ for the transition **5s^2 $^1S_0$ → 5s*n*d $^1D_2$** in Sr I due to **xenon** as a function of principal quantum number *n* given at reduced pressure and temperature **273 K** in **cm^{-1}/ amagat** (1 amagat = 2.69x 10^{19} atoms / cm^3)

Principal Quantum Number *n*	Level Energy cm^{-1} (Makdisi *et al* 2001)*	Broadening Rate K $^\Gamma$ cm^{-1}/ amagat
27	45752.03	5.95
28	45765.75	8.72
29	45777.90	1.98
30	45788.90	3.17
31	45798.76	2.78

* Makdisi Y., Philip G., Bhatia K. S. and Connerade J.-P. *J. Phys. B: At. Mol. Opt. Phys.* **34**, 521 (2001)

4.4.6 Collisions involving low-lying Rydberg members

Fig. 4.22 illustrates the collisional shift and broadening due to argon for the two-photon excitation $5s^2\ ^1S_0 \rightarrow 5s15d\ ^1D_2$ in neutral strontium. As mentioned previously the laser wavelength in the figure indicates the air wavelength for two-photon excitation. As the argon buffer gas pressure is increased the transition is shifted towards the longer wavelength (redshift) with an asymmetry of the line profile gradually increasing on the low frequency side as observed in Fig. 4.22. A similar observation is made for the collision broadened one-photon resonance $5s5p\ ^1P_1 \rightarrow 5s13\ s\ ^1S_0$ due to sequential excitation as indicated in Fig. 4.23.

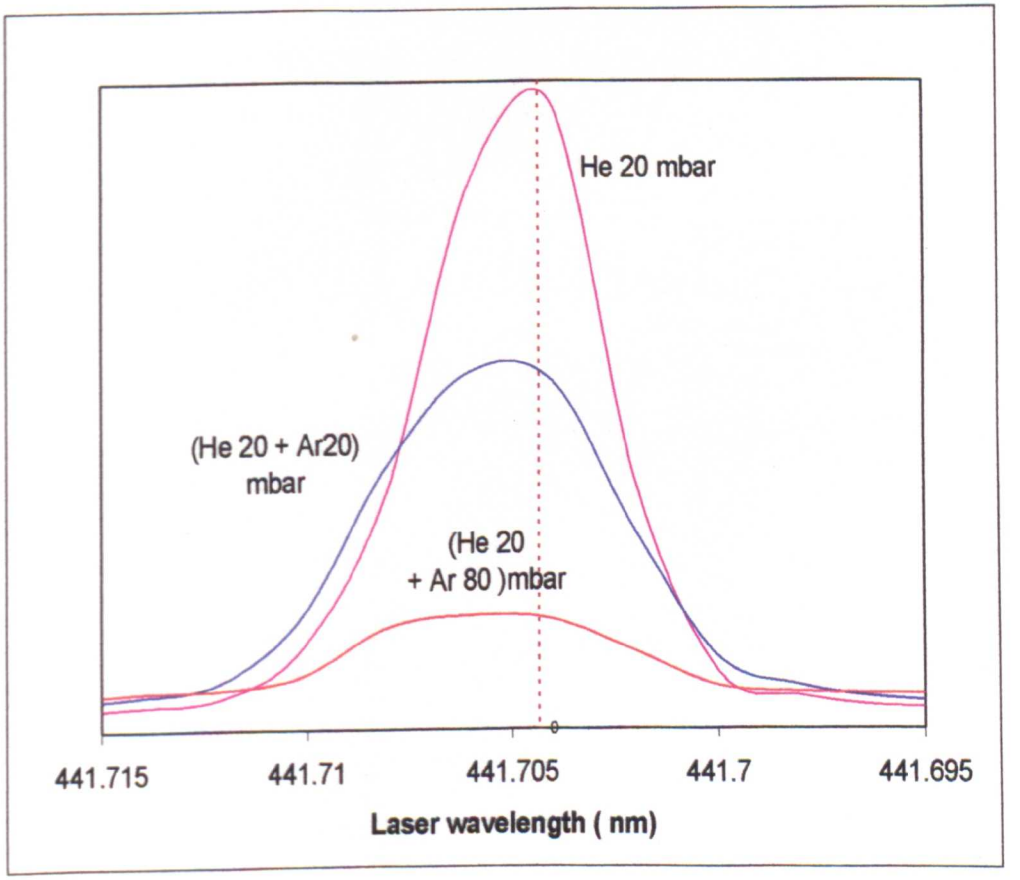

Fig. 4.22 Collisional red shift and broadening in argon for 5s 15d $^1D_2$ Rydberg state of Sr I

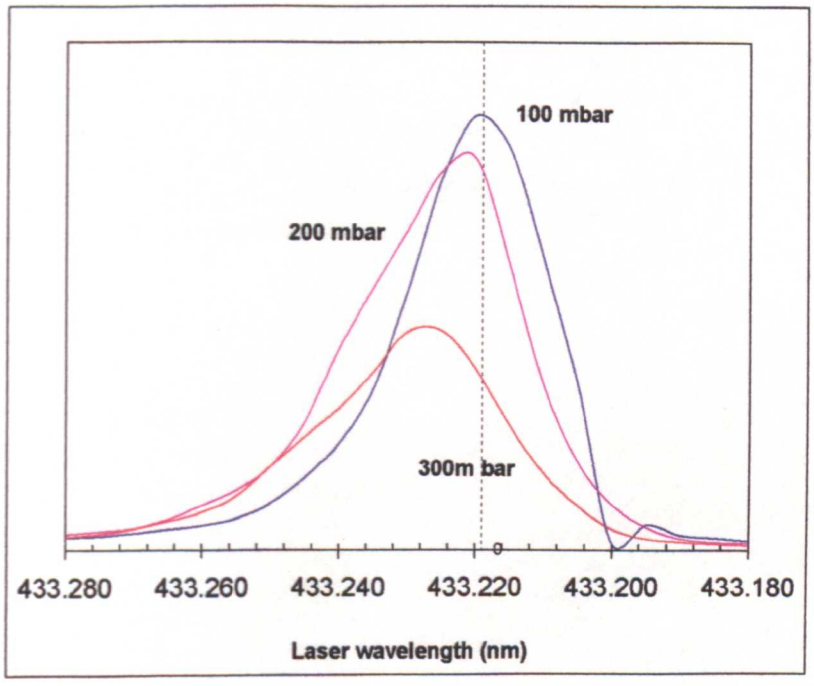

Fig. 4. 23 Collisional red shift and broadening of Sr I single-photon resonance 5s5p $^1P_1 \rightarrow$ 5s13 s $^1S_0$ in argon

Figures 4.24 (a-b) show effect of argon collisions in the highly perturbed region of the $J = 2$, even-parity Rydberg series where the singlet and triplet series cross.

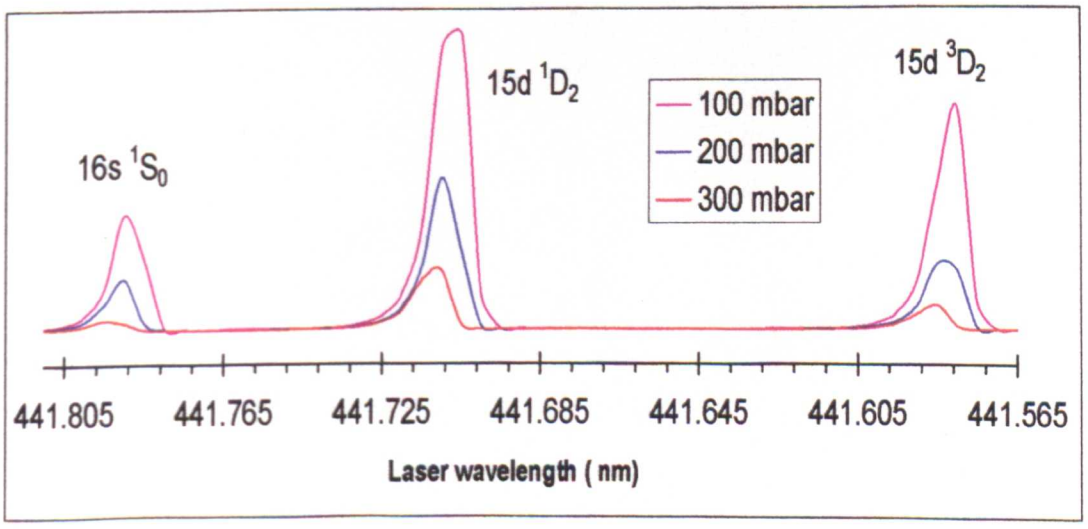

Fig. 4.24 (a) - Shifts and broadening of the low lying members of the 5s*n*s $^1S_0$ and 5snd $^{1,3}D_2$ Rydberg series of Sr I in argon.

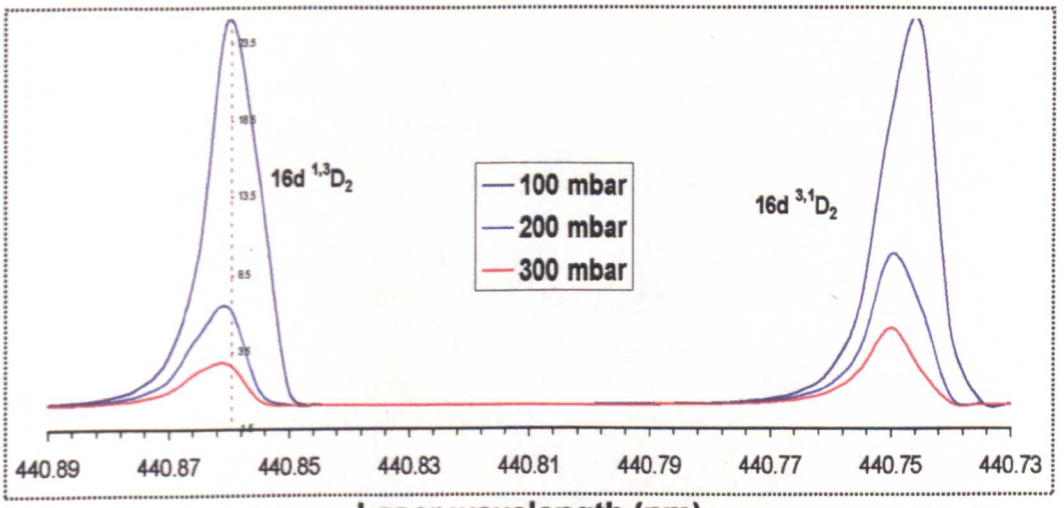

Fig. 4.24 (b) at n = 16, where $^1D_2$ and $^3D_2$ series swap, large oscillation in broadening rates and line profile asymmetry occur

Experimental values of the pressure broadening rates for the lower members of the 5s*n*s $^1S_0$, 5s*n*d $^3D_2$ and 5s*n*d $^1D_2$ Rydberg series of strontium in the region of singlet-triplet mixing are given in Table 4.10, Table 4.11 and Table 4.12 respectively.

Table 4. 10 Pressure broadening rates - Ar
Sr I-5s*n*s $^1S_0$ (16 < *n* < 20)

Pressure broadening rates K^{Γ} for the transition **$5s^2\ ^1S_0 \rightarrow 5sns\ ^1S_0$** in Sr I due to **argon** as a function of principal quantum number *n* given at reduced pressure and temperature **273 K** in **cm^{-1}/ amagat** (1 amagat = 2.69x 10^{19} atoms /cm^3)

Principal Quantum Number *n*	Broadening Rate K^{Γ} cm^{-1} / amagat
16	2.47
18	1.64
19	5.90
20	2.40

Table 4. 11 Pressure broadening rates - Ar
Sr I-5s*n*d $^3D_2$ (15 < *n* < 17)

Pressure broadening rates K^{Γ} for the transition **$5s^2\ ^1S_0 \rightarrow 5snd\ ^3D_2$** in Sr I due to **argon** as a function of principal quantum number *n* given at reduced pressure and temperature **273 K** in **cm^{-1}/ amagat** (1 amagat = 2.69x 10^{19} atoms /cm^3)

Principal Quantum Number *n*	Broadening Rate K^{Γ} cm^{-1} / amagat
15	2.51
16	0.66
17	2.41

Table 4. 12 Pressure broadening rates - Ar
Sr I-5s*n*d $^1D_2$ (15 < n < 19)

Pressure broadening rates K^{Γ} for the transition **$5s^2\ ^1S_0 \rightarrow 5snd^1D_2$** in Sr I due to **argon** as a function of principal quantum number *n* given at reduced pressure and temperature **273 K** in **cm^{-1}/ amagat** (1 amagat = 2.69x 10^{19} atoms /cm^3)

Principal Quantum Number *n*	Broadening Rate K^{Γ} cm^{-1} / amagat
15	1.44
16	2.39
17	2.23
18	2.61
19	2.74

4.4.7 Collisional evolution of the broad resonance intruding on the 5snd $^1D_2$ Rydberg series at $27 < n < 28$

As mentioned previously, in the experiments involving the effects of noble gas collisions on the two-photon excitation of the neutral strontium from the ground state $5s^2\ ^1S_0$ to the even–parity $5snd\ ^1D_2$ Rydberg states, a non-Rydberg single-photon transition to a highly localized doubly excited state (exhibiting orbital contraction- Connerade 1998) intruding upon the spectrum with a strong perturbation at principal quantum number $27 < n < 28$ was observed, with strong sensitivity on the pressure and nature of the foreign gas collision partner and the vapour pressure of strontium. As reported by Philip and Makdisi (2006) the non-Rydberg excitation to this remarkable resonance is the collisional formation of quasi-molecular Sr_2 dimers by two ground state atoms. The high density atomic jet used supports the formation of strontium dimers more efficiently than a low density atomic beam or a cloud of strontium vapour used by other investigators who were not able to investigate this perturbation. Extensive investigation of this broad resonance with an asymmetric profile with strong dependence on pressure and nature of gas used has been carried out with the three noble gases(He, Ar and Xe) and the results are summarized in this section.

Figures 4.25 (a-c) show the evolution of the $5s5p\ ^1P_1 \rightarrow 4d^2\ ^1G_4$ resonance due to collision with helium atoms. Unlike other non-Rydberg excitation, this perturbation exhibits Ramsauer effect in argon and xenon like a Rydberg state (with blue shift in He and red shift in Ar and Xe) as in figures 4.26-4.27.

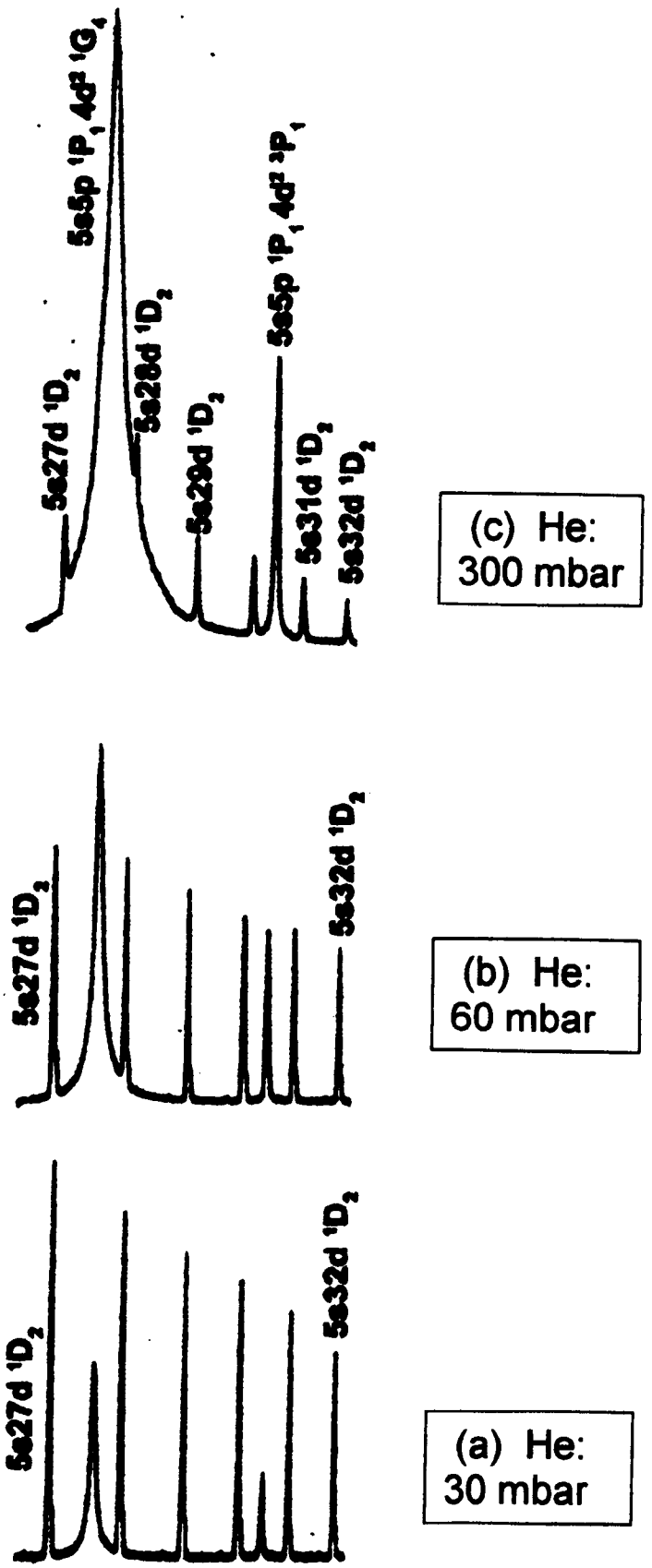

Fig 4.25 (a-c) Collisional evolution of $4d^2\,{}^1G_4$ interloper in the $5snd\ {}^1D_2$ Rydberg series of Sr I

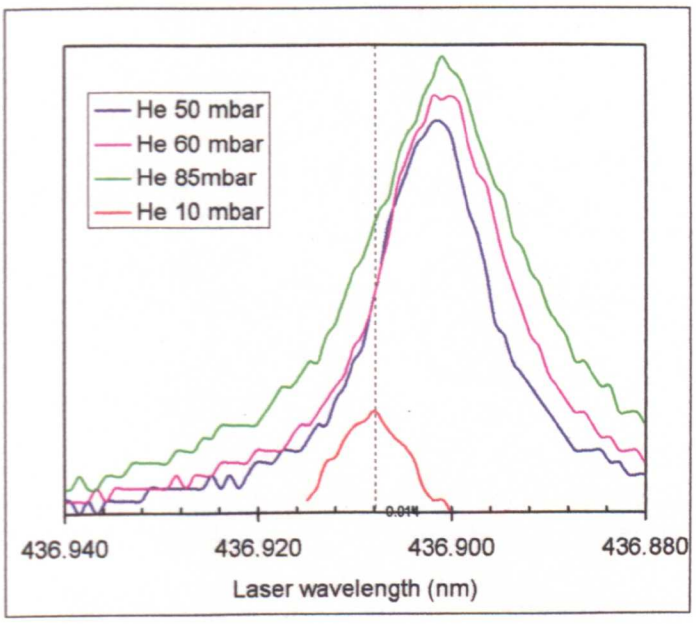

Fig 4.26 Collisional blue shift of $4d^2\,{}^1G_4$ with He buffer

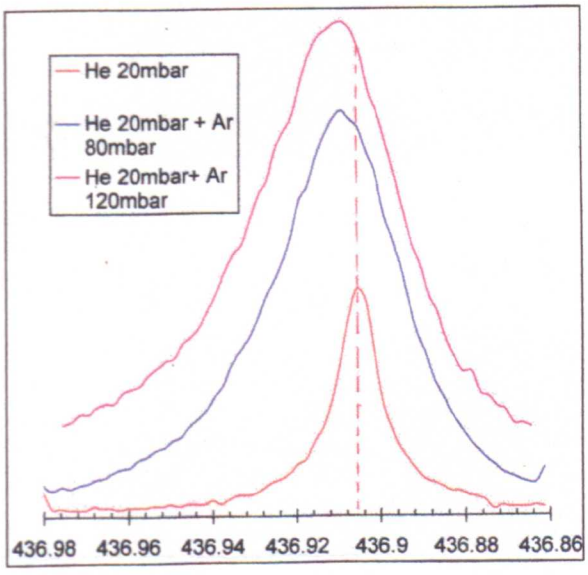

Fig. 4.27 Collisional red shift of $4d^2\,{}^1G_4$ due to Ramsauer effect in Ar buffer

Observed frequency shifts for $4d^2\,{}^1G_4$, resulting from collisions with the 3 different noble gases are plotted in Fig. 4. 28. Ramsauer effect with positive shift for collisions with helium atoms and red shifts for argon and xenon exhibited by the doubly excited state $4d^2\,{}^1G_4$ is evident in Fig. 4.28,

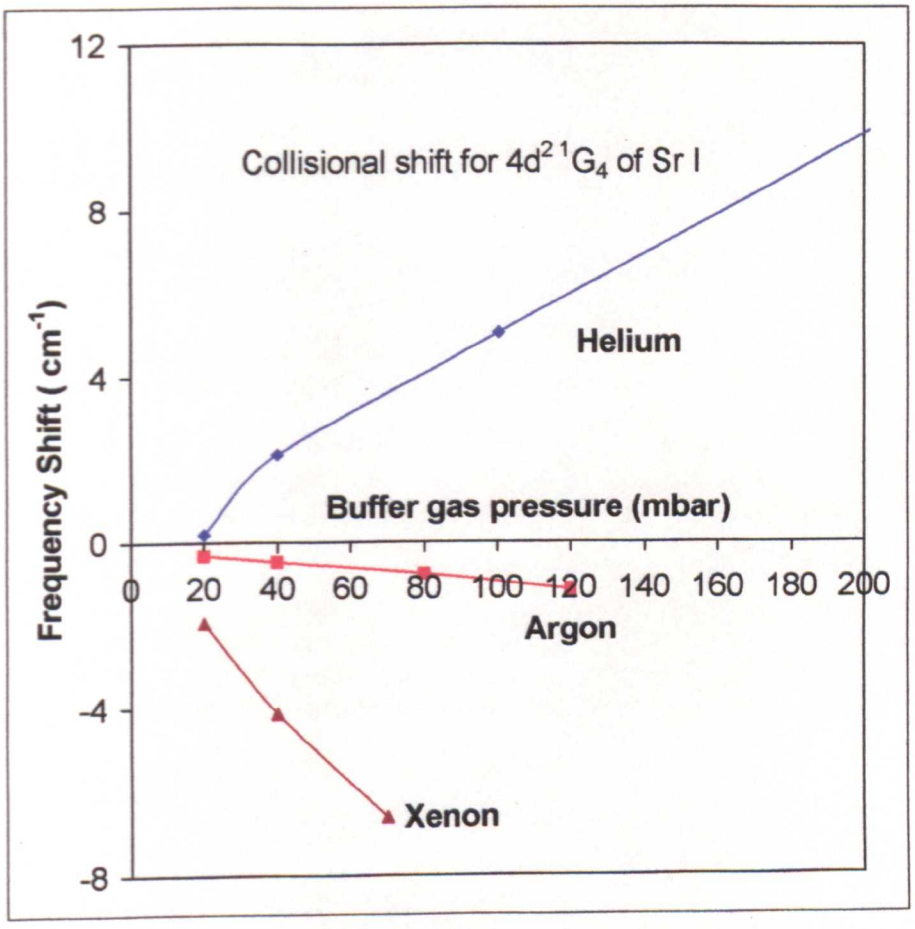

Fig. 4.28 Frequency shifts for $4d^2\,{}^1G_4$ for collisions in different noble gases

Lower shift for argon in figure 4.28 may indicate that the residual helium buffer used to compensate the Stark shift of the Rydberg states has a profound influence on the blue shift of the $4d^2\,{}^1G_4$ interloper. Figures 4.29 (a-b) present, respectively, the collisional line width and square of the line width in helium. Pressure shift rates and broadening rates for this excitation are presented in Tables 4.13 and 4.14.

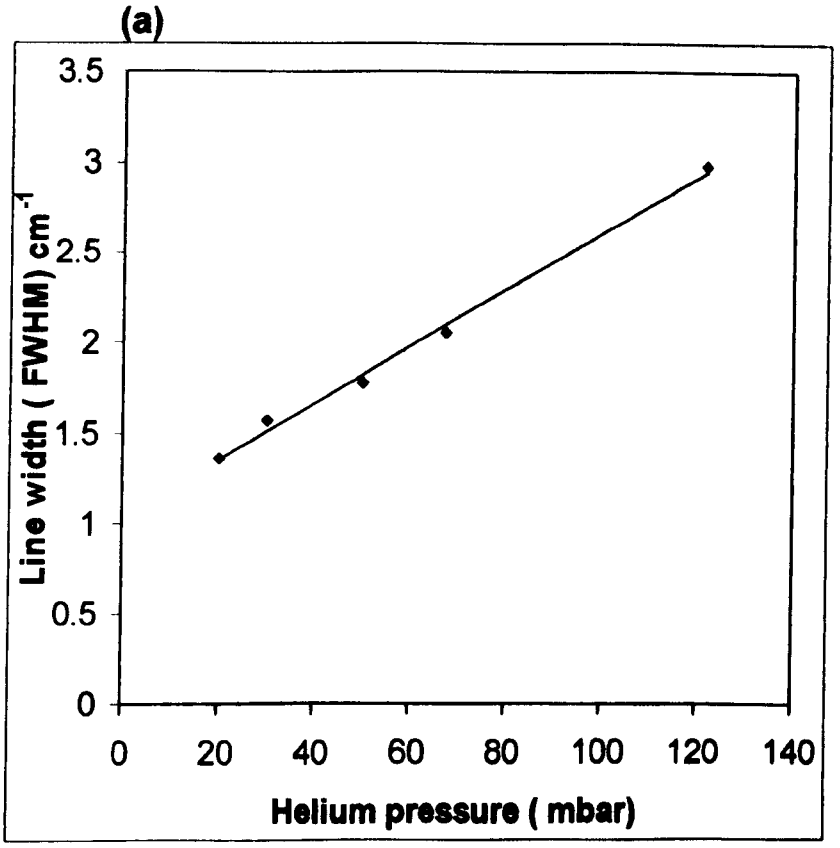

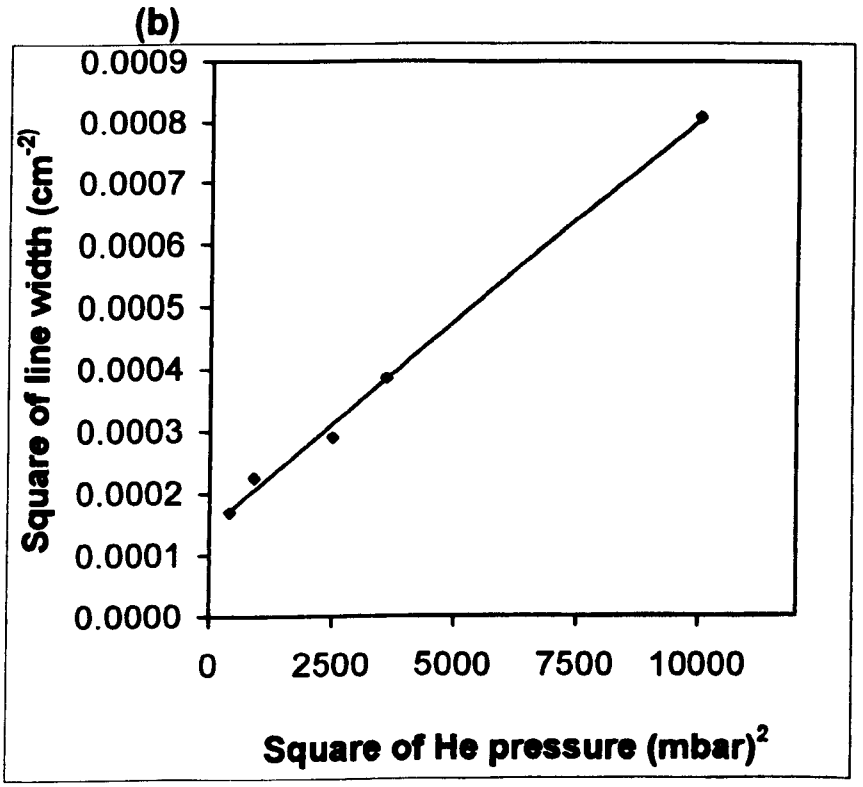

Fig. 4.29 (a-b) Line width and square of the line width for $4d^2\,{}^1G_4$ interloper in Sr I

Table 4. 13 Pressure shift rates – $4d^2\ ^1G_4$

Pressure shift rates K^{Δ} for the $4d^2\ ^1G_4$ intruder in Sr I due to **different noble gases** given at reduced pressure and temperature **273 K** in **cm^{-1}/ amagat** (1 amagat = 2.69×10^{19} atoms / cm^3)

Noble gas	Broadening Rate K^{Γ} cm^{-1} / amagat
Helium	+198.79
Argon	- 32.94
Xenon	-366.3

Table 4. 14 Pressure broadening rates – $4d^2\ ^1G_4$

Pressure broadening rates K^{Γ} for the $4d^2\ ^1G_4$ intruder in Sr I due to **different noble gases** given at reduced pressure and temperature **273 K** in **cm^{-1}/ amagat** (1 amagat = 2.69×10^{19} atoms /cm^3)

Noble gas	Broadening Rate K^{Γ} cm^{-1} / amagat
Helium	21.24
Argon	.....
Xenon	37.70

The asymmetry for the spectral line of the interloper $4d^2\ ^1G_4$ emerging from collision is found to be largely dependent on the size of the noble gas atoms with xenon giving the maximum asymmetry. For quantification purposes the asymmetry of the collision broadened spectral line can be defined by the asymmetry index ξ defined as,

$$\xi = 1 - \frac{\Gamma_{-1/2}}{\Gamma_{+1/2}} \qquad (4.25)$$

Where $\Gamma_{-½} = \omega_0 - \omega_{-½}$ and $\Gamma_{+½} = \omega_{+½} - \omega_0$ are the half widths on lower frequency and higher frequency half–points (½ of FWHM - Γ) from the line centre ω_0. The ratio of the two half widths on either side of the line centre gives the asymmetry parameter $\varepsilon = (\Gamma_{-½} / \Gamma_{+½})$. Figure 4.30(a) illustrates the growth asymmetry of a Loretzian profile with the asymmetry parameter ε which depends on the pressure and nature of the foreign gas as observed in the experiment and given in figure 4.30(b).

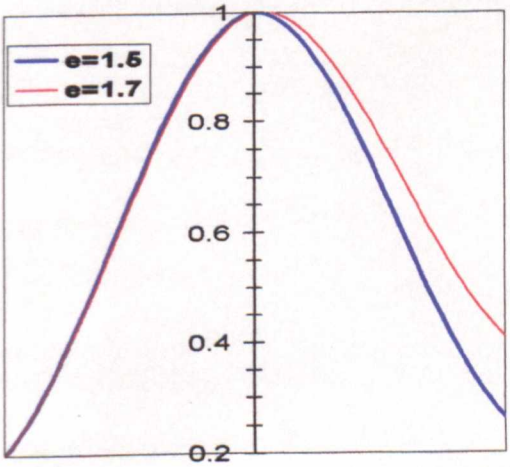

Fig. 4.30(a) Spectral line asymmetry on parameter ε

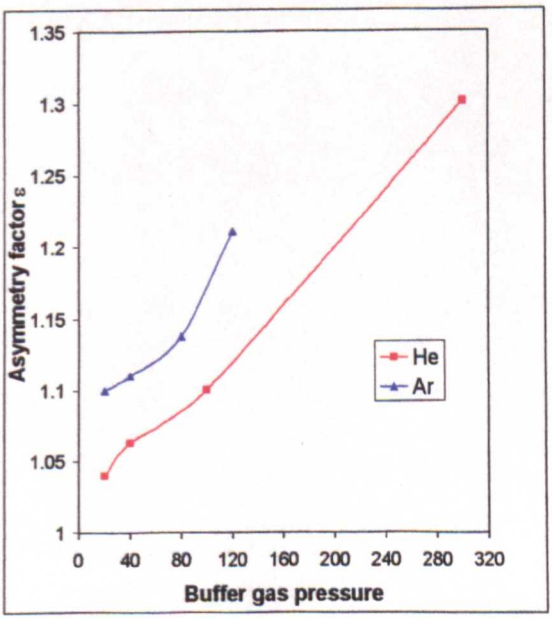

Fig. 4.30(b). Dependence of Line asymmetry parameter ε on the type and pressure of the buffer gas used

4.4.8 Effect of Collisions on highly excited states of Sr I

At high n ($35 \leq n \leq 100$), impact broadening and shift of the Rydberg series in rare gases is expected to show asymptotic behaviour (constant value independent of n and ℓ) due to elastic scattering contributions of the perturber atom by the ionic core of the Rydberg atom (polarization interaction) as predicted by Fermi. For large values of the principal quantum number n, accurate measurements of collisional shift and broadening become increasingly difficult due to fast quenching of Rydberg states and collisional mixing of nearby states of opposite parity ('ℓ'- mixing) and nearly degenerate states. Figures 4.31(a-b) show the pressure shift rates and broadening rates of Rydberg members of Sr I due to xenon plotted against the principal quantum number n.

Fig. 4.32 shows the two-photon spectra of the high-lying states of strontium taken at 3 different values of argon pressure. Controlled excitations to forbidden transitions using collisions complimented by electric field have been established using different buffer gases (Philip and Connerade 2007). Fig. 4.33 shows the two-photon spectra taken at three different values of argon pressure. This spectrum indicates the redshift for the single-photon resonances appearing in the 434 nm - 432 nm wavelength region.

Another interesting spectral region to explore experimentally is the autoionizing region using two-photon spectroscopy. The autoionizing resonance around 431 nm wavelength region of the laser for two-photon excitation also has a line profile with asymmetry evolving with buffer gas pressure and exhibiting Ramsauer effect both in argon and xenon.

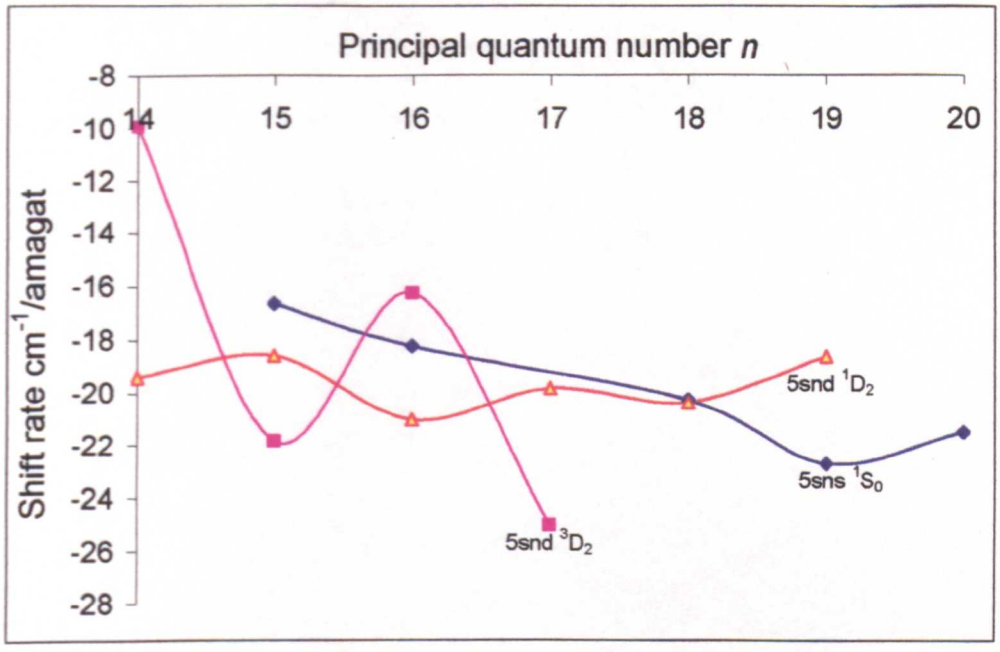

(a)

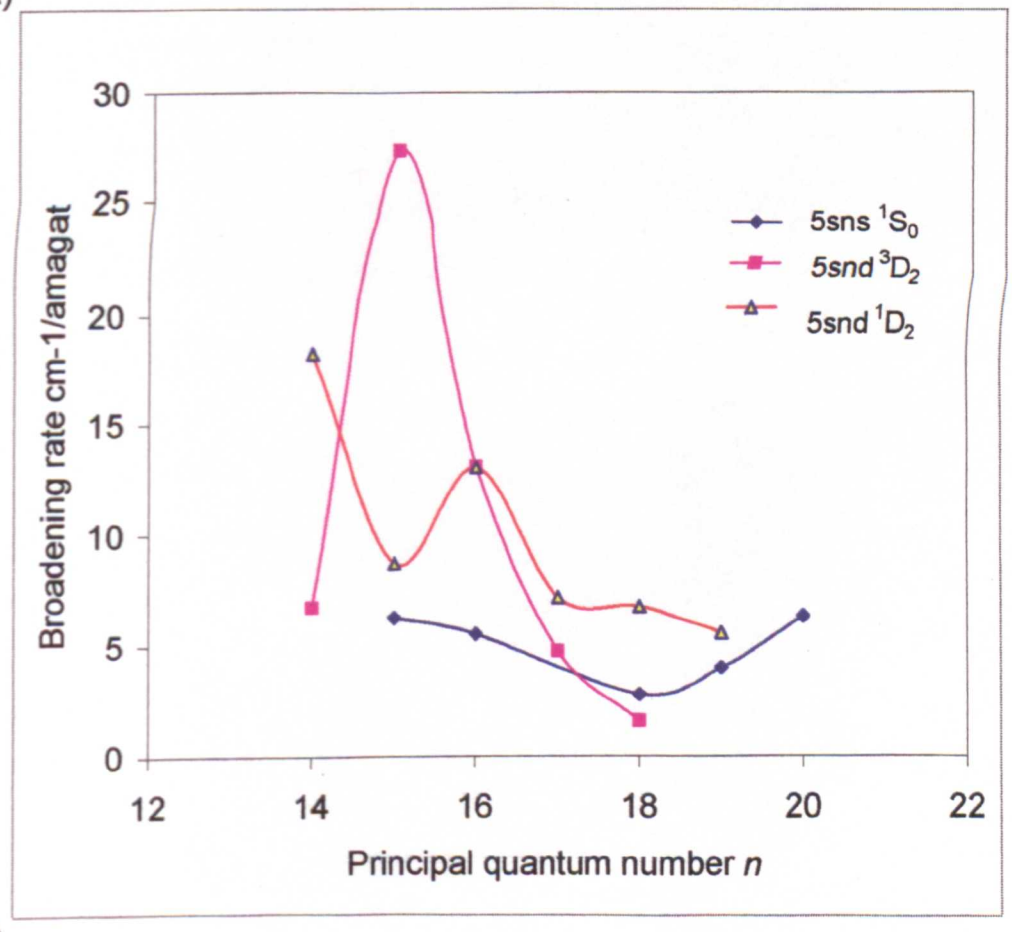

(b)

Fig. 4.31(a-b) Pressure shift rates (a) and broadening rates (b) of low–lying Rydberg members of Sr I due to xenon plotted against the principal quantum number *n*. Large irregularities are observed in this region.

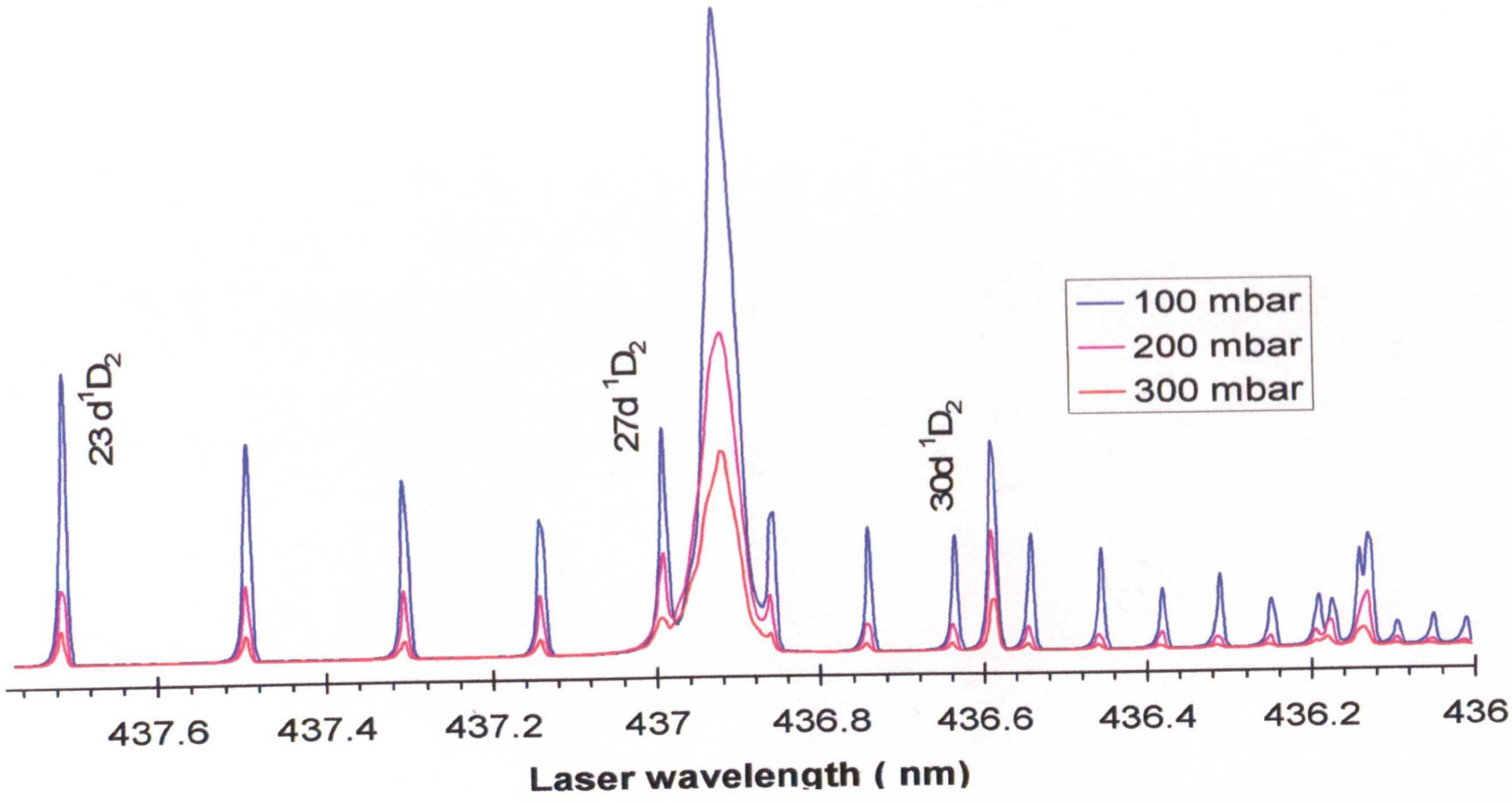

Fig. 4.32 Shift and broadening of intermediate Rydberg states of Sr I. Due to Ramsauer effect all Rydberg members are red shifted. Rydberg member is quenched. A non-Rydberg member survives collision and exhibits blue shift.

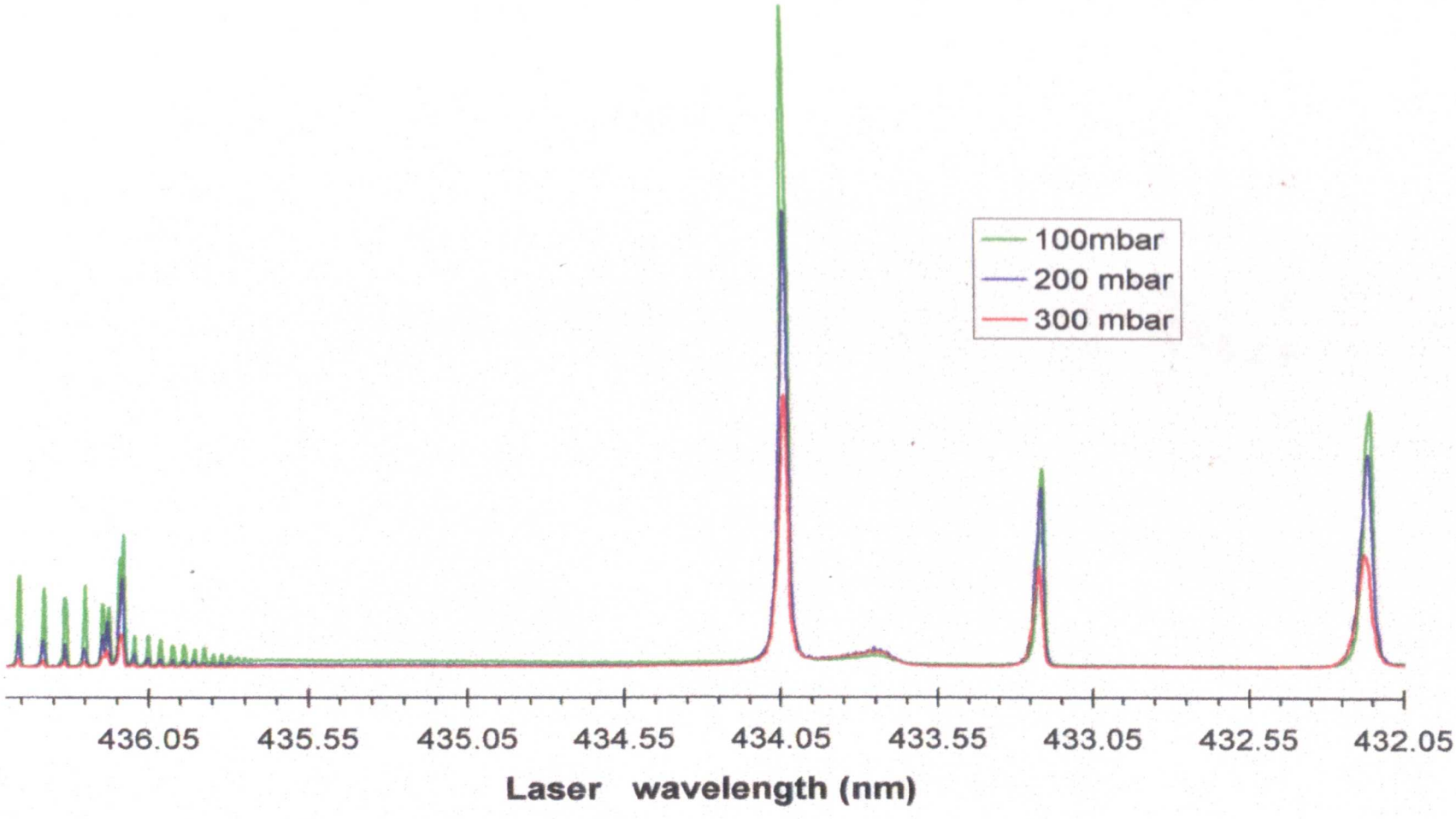

Fig. 4.33 Effect of foreign gas collisions on the highly excited states of Sr I including single-photon excitations. Two-photon excitation wavelength in air is indicated.

4.4.9 Collisional broadening of barium Rydberg states with xenon

Collisional broadening rates have been experimentally determined for neutral barium for the principal quantum number range $14 < n < 21$. Large oscillations in the broadening rates are observed for the region perturbed by 5d7d $^3P_0$ and 5d7d $^1S_0$ interlopers and configuration interaction. Reported work by other authors on noble-gas broadening of barium levels involves the 6s 5d ^3D_J metastable levels and does not offer results for comparison with the results presented in this study involving two-photon excitation to the 6s*n*d $^1D_2$ Rydberg states from the ground state $6s^2\ ^1S_0$. The experimental arrangement used is the same as in strontium two-photon spectroscopy with the atomic jet target with disposable sample cartridges and laser and associated instrumentation.

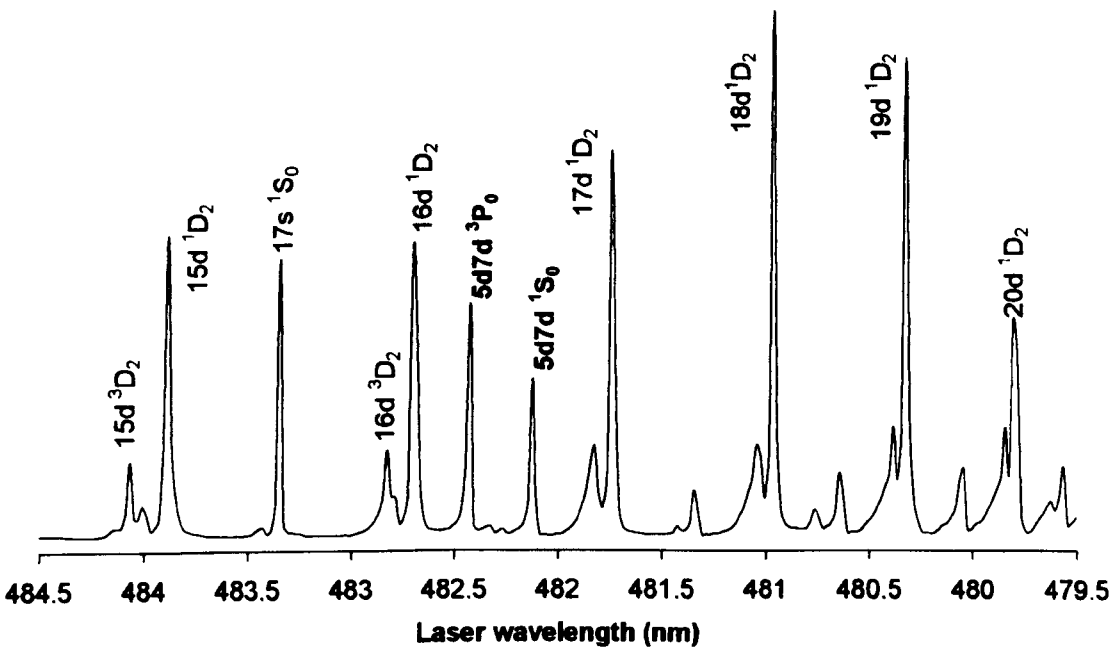

Fig.4.34 Part of the barium two-photon spectrum showing the low-lying Rydberg states and perturbers

Fig. 4.34 is a part of the spectrum showing the lower states of the 6s*n*d $^1D_2$ Rydberg series whose collisional broadening has been investigated using xenon buffer gas. Table-4.14 gives the broadening rates of these members by collision in xenon.

Table 4. 15 Pressure broadening rates – Xe
Ba I- 6s*n*d $^1D_2$ (14< *n* < 20)

Pressure broadening rates K^{Γ} for the 6s*n*d $^1D_2$ Rydberg members of Ba I due to **xenon** given at reduced pressure and temperature **273 K** in **cm^{-1}/ amagat** (1 amagat = 2.69x 10^{19} atoms /cm^3)

Principal Quantum Number *n*	Broadening Rate K^{Γ} cm^{-1} / amagat
14	8.68
15	10.19
16	9.44
17	10.95
18	7.17
19	4.91
20	3.40

Conclusion

In the present chapter, I have reviewed the subject of collisions involving Rydberg states of the alkaline-earth atoms from a general point of view and presented new and original data obtained in the experiments which were performed in Kuwait. Extensive study of the spectral line shift and broadening of the bound even-parity Rydberg series of strontium due to collision with neutral inert gases (helium, argon and xenon) had been carried out following two-photon excitation from the ground state. Among many results presented in this thesis, specially brought out are those for the frequency shift rates and broadening rates of members of the Sr I series: 5s*n*s $^1S_0$ ($15 < n < 20$), 5s*n*d $^3D_2$ ($14 < n < 18$) and 5s*n*d $^1D_2$ ($14 < n < 19$) due to collision with xenon. Also presented are the pressure broadening rates of the members of the Sr I series: 5s*n*s $^1S_0$ ($16 < n < 20$), 5s*n*d $^3D_2$ ($15 < n < 17$) and 5s*n*d $^1D_2$ ($15 < n < 19$) due to collision with argon. The observations in strontium had clearly established the "Ramsauer effect" exhibited by Rydberg members with positive frequency shift (blue shift) in helium and negative frequency shift (red shift) in argon and xenon.

Collisional evolution of the interloper, tentatively labeled as $4d^2\ ^1G_4$, which is a dominant perturber for the $J = 0,2$ even-parity Rydberg series was extensively investigated using the neutral rare gases (He, Ar and Xe). This remarkable perturber also exhibits Ramsauer effect in argon and xenon with negative frequency shift. New results for pressure shift rates for this doubly-excited state are presented here. Also, the pressure broadening rates for barium 6s*n*d $^1D_2$ Rydberg series are presented for the principal quantum number range $14 < n < 20$ due to collision with xenon.

The most intriguing feature of the Rydberg atom-neutral perturber collision is that during the collision the ionic core of the Rydberg atom and the outer electron act as independent scattering targets for the perturber, as predicted by Fermi. From the spectral data it is clearly understood that the electron-perturber atom (e-B) interaction is more dominant than the ionic core-perturber (A^+-B) interaction particularly at high n values. The new observation of collision and external electric field-induced anomalies also indicates scope for further investigation of the collision of Rydberg atoms in presence of strong electric fields, especially the variation of the collision cross section and the collisional decay of the Rydberg state as a function of the field strength.

Normally one expects a reduction in the lifetime due to collision with the buffer gas atoms because of enhanced decay channels for Rydberg atoms. However, in the actual experiment with perturbed Rydberg series it was found the other way round. This could be, perhaps, because the collisions lead to a two-channel exponential decay for the Rydberg atoms with a fast component and a slow component (with transitions to long-lived states such as metastable states). This suggests that two independent measurements, (both optical and electrical to compliment each other) would be necessary for accurate determination of the lifetime of Rydberg atoms at high pressures.

References -Chapter 4 (alphabetical order)

1 Alekseev V.A. and Sobel'man I.I
Sov. Phys.-JETP **22**, 882 (1966)

2 Allard N. and Kielkopf J
Rev. Mod. Phys. **54**, 1103(1982)

3 Amaldi E. and Segre E
Nuovo Cimento**11**, 145 (1934)

4 Aymar M., Camus P., Dieulin M. and Morillon C
Phys. Rev. A **18,** 2173 (1978)

5 Baranger M
Phys. Rev. **111**, 481(1958)

6 Biegman I.L and Lebedev V.S
Phys. Rep. **250**, 95 (1995)

7 Chen S. and Takeo M
Rev. Mod. Phys. **29**, 20(1957)

8 Connerade J.-P.
"*Highly Excited Atoms*"- (Cambridge University Press, 1998)

9 Fano U
Phys. Rev. **131**, 259(1963)

10 Fano U
Phys. Rev. A **2**, 353(1970)

11 Fermi E
Nuovo Cimento **11**, 157 (1934)

12 Gallagher T.F
"*Rydberg Atoms*"– (Cambridge University Press, 1994)

13 Gounand F. and Berlande J
"*Rydberg states of atoms and molecules*" (Eds.) R. F. Stebbings and F.B. Dunning, (Cambridge University Press, 1983)

14 Heber K.D, West P.J. and Matthias E
Phy. Rev. A **37**, 1438 (1988)

15 Herman G
Phys. Lett A **133**,225(1988)

16 Herman G., Kaulakys B., Lasnitschka G., Mahr G and Scharmann A
J. Phys. B: At. Mol. Opt. Phys. **25**, L407(1992)

17 Kachru R., Gallagher T.F., Gounand F., Safinya K.A. and Sandner W
Phys. Rev. A **27**, 795(1983)

18 Kaulakys B
Phys. B: At. Mol. Opt. Phys. **17**, 4485 (1984)

19 Khan M.A , Connerade J.-P. and Rafique M
J. Phys. B: At . Mol. Opt. **27** L 563 (1994)

20 Lebedev V.S and Beigman I.L
"*Physics of Highly Excited Atoms and Ions*" (Springer, 1998)

21 Lu K.T. and Fano U
Phys. Rev. **A2**, 81(1970)

22 Makdisi Y., Philip G., Bhatia K.S. and Connerade J. _ P
J. Phys. B: At. Mol. Opt. Phys. **34,** 521 (2001)

23 Marafi M., Bhatia K.S., Makdisi Y.Y. and Philip G
J. Phys. B: At. Mol. Opt. Phys. **36,** 1835 (2003)

24 Mende W. and Kock M
J. Phys. B: At. Mol. Opt. Phys. **30**, 5401 (1997)

25 O'Malley T.F
Phys. Rev. A **13 4**, 1188 (1964)

26 Omont A
J. Phys. (Paris) **38**, 1343(1977)

27 Philip G
Rev. Sc. Instrum. **78**, 113101(2007)

28 Philip G
Appl. Phys. B **90**, 407 (2008)

29 Philip G. and Connerade J._ P
Opt. Commun. **279**, 141 (2007)

30 Philip G. and Connerade J.-P.
(to be published 2008)

31 Philip G and Makdisi Y
Opt. Commun. **266**, 253 (2006)

32 Reinsberg C
Z. Phys. **105**, 460 (1937)

33 Seaton M.J
Proc. Phys. Soc. London **88**, 801 (1966)

34 Sobel'man I.I., Wainshtein L.A and Yukov E .A
"*Excitation of Atoms and Broadening of Spectral Lines*"(Springer – Berlin 1981)

35 Sun J.Q., Matthias E., Heber K.D., West P. J. and Gudde J
Phys. Rev. A **43**, 5956 (1991)

36 Weber K.H. and Niemax K
Z. Phys. A **309**, 19(1982)

37 Wu. Dong-hong., Yang Yu-fen. and Lu K.T
J. Phys. B: At. Mol. Opt. Phys. **23,** L 149(1990)

Chapter 5

Rydberg atoms in external electric fields

5.1 Introduction

Spectroscopic measurements based on Stark effect (field-dependent shift and splitting of a transition in to the Stark manifold) in Rydberg states of neutral atoms give information about atomic wave functions which can be represented by a superposition of different angular momentum states with the same principal quantum number. Hydrogen atom exhibits linear Stark effect (energy shift scales linearly with the electric field strength) even at low fields as a consequence of the degeneracy of the states of different angular momentum states with the same principal quantum number. Unlike hydrogen atom, the alkaline-earth atoms exhibit quadratic Stark effect (Cole *et al* 1980, Sandner *et al* 1981, van Leuwen *et al* 1983) with clear 'avoided crossings' because of the non-degeneracy at zero fields. In these atoms, the high principal quantum number states with low 'ℓ' ($\ell \leq 2$) undergo quadratic Stark shift while high 'ℓ' ($\ell \geq 3$) states having negligible quantum defect undergo linear shift, at low fields; 'ℓ' is the orbital angular momentum quantum number. At very high field strength, high 'ℓ' and low 'ℓ' states mix together with linear Stark shift. High angular momentum states not directly accessible from the ground state or low lying states may be populated by electric field-induced mixing (Luc- Koenig *et al* 1979, Lahaye *et al* 1989).

The Stark effect in alkaline-earth atoms has been a well-investigated topic for several years (Gallagher *et al* 1977, Zimmerman *et al* 1978, Lahaye *et al* 1987,

Rinneberg *et al* 1985 and Robicheaux *et al* 1999) and, recently, there has been a tremendous revival of interest in the study of the Rydberg atoms in external electric fields (Elliott *et al* 1995) and in combined electric and magnetic fields due to its emerging importance in quantum chaos (Connerade 1997), quantum computing (Ryabtsev *et al* 2005) etc. High-lying Rydberg states of atoms in static external fields form an important area of study for both theory and experiment for investigating classical chaos in a three dimensional quantum system (Elliott *et al* 1995, Connerade 1997, Connerade *et al* 1999, Rao *et al* 2001, Abdulla *et al* 2004, Connerade *et al* 2005). Also, one and two electron atoms have been under extensive investigation in static electric fields, especially for atomic states with large orbital angular momentum which are not accessible by optical excitation. Delande and Gay (1988) suggested that crossed-field could be used to prepare atomic states with large n, ℓ and m quantum numbers for atoms whose Stark manifold can be selectively populated.

The n-scaling properties of Rydberg atoms make them ideal candidates to study the influence of external fields- for example the quadratic Stark effect scales as $(n^*)^7 F^2$, n^* is the effective principal quantum number and F is the electric field strength and the diamagnetic effect (zero electric field) scales as $B^2 n^4$, the fourth power of the principal quantum number in a magnetic field of strength B. For Rydberg states of very high principal quantum numbers small external fields including earth's magnetic field become important and measurements should compensate for external stray fields (Rinneberg *et al* 1985). Neukammer *et al* (1987) could observe barium Rydberg states with principal quantum number up to n = 520 which allowed a sensitive measurement of small electric fields and their spatial distribution.

5.2 Effect of static electric field on Rydberg atoms

For very high-lying Rydberg states near the ionization threshold the behavior of the atom is hydrogenic where an electron moves in a Coulomb potential plus the potential due to the external field. But for low-lying states there is a significant deviation from this due to core effects which modify the hydrogenic wavefunctions observed as quantum defects. Also, the external field has different effects on Rydberg states and doubly excited states. Alkaline-earth atoms are ideal candidates to study these effects. In the absence of external electric field, the Rydberg electron may be thought of moving in an elliptical orbit of semi major axis $a = n^2 a_0$ (a_0 is the Bohr radius and n is the principal quantum number) with focal point at the atomic nucleus. When an external static electric field is applied both eccentricity and the orientation of the plane of the classical elliptical orbit in a $1/r$ Coulomb potential will be modified with an orbital speed determined by the strength of the electric field. In a static electric field F, the time scales (in atomic units) are:

(i) The classical Kepler period $\tau_K = 2 \pi n^{*3}$ which is the period of motion of electron in the Keplerian elliptical orbit. n^* is the principal quantum number corrected for quantum defect;

(ii) The Stark period $\tau_S = 2 \pi / 3nF$ which is associated with the precision of the orbital angular momentum in the field F. (The torque $\boldsymbol{\tau} = \mathbf{d} \times \mathbf{F}$ experienced by the electric dipole $\mathbf{d}$ when a Stark field $\mathbf{F}$ is applied produces the precision)

Figures 5.1 (a-b) illustrate the effect of application of a static electric field to a Rydberg atom. In figure 5.1 (a) without the external electric field, the potential well due to the Coulomb force on the electron due to the core is symmetrical .When a

static electric field is applied (figure 5.1 (b)) the Coulomb potential gets modified and the electron energy level is split as a result of Stark effect. If field is sufficiently large the electron will have enough energy to escape from the potential well by quantum tunneling. The potential experienced by the Rydberg electron in the combined Coulomb field and an electric field F applied in the z direction can be written in atomic units as:

$$V_F(r) = -\left(\frac{1}{r}\right) + Fz \qquad (5.1)$$

This potential has a saddle point maximum at $z = -1/F^{1/2}$ given by:

$$V_{sp} = -2F^{1/2} \qquad (5.2)$$

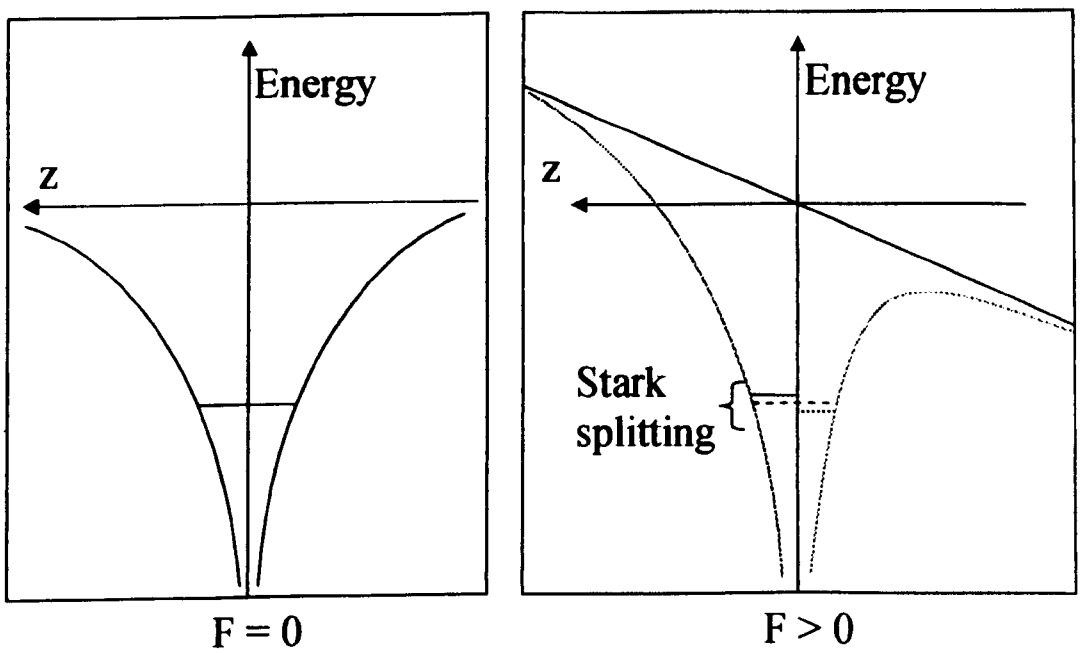

(a). Zero electric field (b). Applied electric field F

$$V_F(r) = -\left(\frac{1}{r}\right) + Fz$$

Fig.5.1 (a-b) Effect of static electric field on the Rydberg atom

For a state to be bound its energy must be below the saddle-point potential V_{sp} and the threshold energy E_{th} for ionization, therefore, becomes:

$$E_{th} = -2F^{1/2} \tag{5.3}$$

Thus, if the field applied is above a critical field F_{cr}^{*}, the atom will be ionized.

The critical field is:

$$F_{cr}^{*} = \frac{E^2}{4} \tag{5.4}$$

Neglecting Stark effect, approximately, the threshold (critical) field for ionization can be written in atomic units as (Bethe and Salpeter 1957):

$$F_{cr}^{*} = \frac{1}{16n^{*4}} \text{ in atomic units} \tag{5.5}$$

In laboratory units the critical ionizing field F_c^* (Kleppner *et al* 1983) is:

$$F_{cr}^{*} = \frac{3.2\times10^{8}}{n^{*4}} Voltcm^{-1} \tag{5.6}$$

For $n = 20$, $F_{cr}^{*} \approx 2$ KV/cm, and for $n = 40$ the field reduces to $Fcr^{*} \approx 125$ volt/cm.

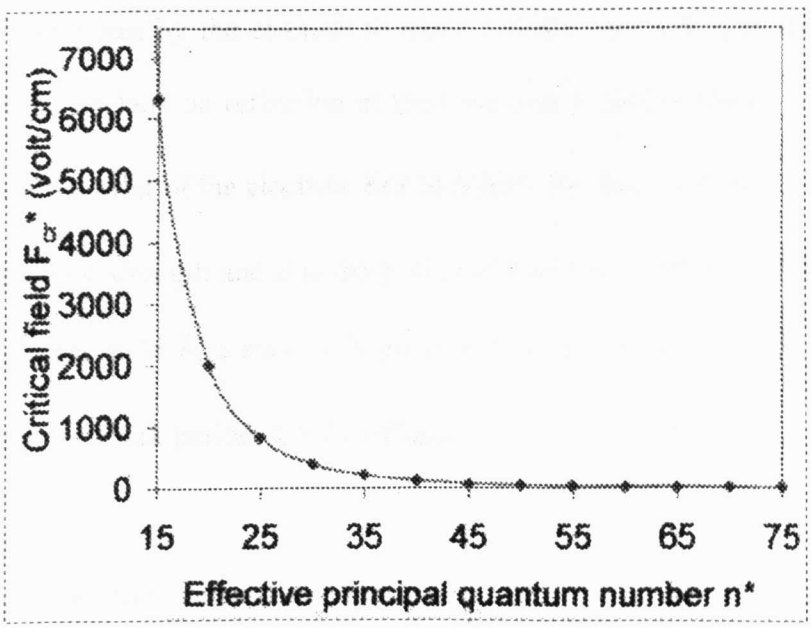

Fig. 5.2 Estimated critical (threshold) field F_{cr} plotted against effective principal quantum number n^*

In figure 5.2 the critical (threshold) field is plotted against the effective principal quantum number. Deviations from this value for the critical field become significant due to energy shift arising from Stark effect and collisional effects. The ionization rate increases with the applied electric field F so rapidly that, it is almost zero for $F < F_{cr}^{*}$ and infinite for $F > F_{cr}^{*}$. Field ionization may be used for detecting Rydberg atoms (Karapanagioti *et al* 1999).

5.3 Stark effect in alkaline-earth Rydberg atoms

Whereas the theory is accurate only for the hydrogen atom in external field, only approximate solutions are available for a many-electron Rydberg atom. The wavefunctions for the Rydberg electron can be approximated to the eigen functions of the hydrogen atom with a Coulomb field. An electric field is considered to be weak if its magnitude is small compared to the internal effective Coulomb field experienced by the electron and the energy of the electron does not change considerably during a Kepler period. Classically, the Kepler period is approximately equal to the time taken by the electron to move radially outward from the nucleus and return to the nucleus on reflection at the Coulomb potential barrier or it is the period of the radial orbit of the electron. For hydrogen the Stark period $\tau_S = 2\pi / 3nF$ where F is the field strength and n is the principal quantum number. In linear Stark effect in an electric field F, a state with given n will split with a spacing $\Delta E_{Stark} = 3nF$. Therefore, the Stark period $\tau_S = 2\pi / \Delta E_{Stark}$.

In a Rydberg atom the bound outer electron is far away from the nucleus and, therefore, even weak external fields can modify the motion of the electron and its wavefunctions. The Stark effect modifies the time scales like the Kepler time, time

for spin-orbit interaction (departure from normal zero-field scaling laws) leading to transitions forbidden under selection rules and parity via field-induced mixing of degenerate states. The ratio of the intensities of the forbidden to the allowed transitions can provide a measure of the electric field strength. The splitting of a particular state in to several eigenstates in a Stark manifold with shift proportional to the field strength F is called the "linear Stark effect". As explained in section 5.1, for hydrogen and similar atoms the splitting of the spectral terms with $\ell \neq 0$ scales linearly with the field because of the degeneracy of different angular momentum states with the same principal quantum number n. For the alkaline-earth atoms the splitting and frequency shift are proportional to the square of the electric field. This is called the "quadratic Stark effect". The applied electric field produces an electric dipole moment $\mathbf{p} = \alpha\mathbf{F}$, where α is the polarizability which depends on the electronic configuration and quantum number of the state. The electric field introduces an interaction energy $V_{electric} = \frac{1}{2}\,\mathbf{p}.\mathbf{F} = \frac{1}{2}\,\alpha F^2$, and hence, the shift is proportional to the square of the applied electric field strength. Unlike hydrogen atom these atoms exhibit clear avoided crossings as shown in figure 5.3 because of non-degeneracy at zero fields. The second order Stark shift for a transition between the ground state $|i\rangle$ and an excited state $|j\rangle$ can be written as:

$$\Delta\nu = KF^2 \tag{5.7}$$

Where K is the Stark shift rate given by,

$$K = -\frac{\left[\alpha_0(|j\rangle) - 2\alpha_2(|j\rangle) - \alpha_0(|i\rangle)\right]}{2} \tag{5.8}$$

Here α_0 and α_2 are the scalar and tensor polarizabilities respectively.

For the single-photon transition, $^1S_0 \rightarrow {}^1P_1$ the quadratic Stark shift rate becomes:

$$K = -\frac{\left[\alpha_0(^1P_1) - 2\alpha_2(^1P_1) - \alpha_0(^1S_0)\right]}{2} \tag{5.9}$$

$^1S_0$ states having $J = 0$ will have only shift whereas states with $J \geq 1$ will have both shift and splitting in to more than one component. Quadratic Stark effect may be used to determine the polarizabilities of the alkaline-earth atoms (Li and van Wijngaarden 1996). van Leeuwen and Hogervorst (1983) used Stark effect calculations combined with MQDT analysis for the description of the highly perturbed barium 6s*n*d $^1D_2$ Rydberg series. Robicheaux *et al* (1999) also investigated the strongly perturbed Stark states of barium 6s*n*d $^{1,3}D_2$ series for the range $n = 25$ - 28 in static electric field. The polarizability can be calculated from the quadratic Stark shift using the relation,

$$\alpha = -\frac{\Delta(MHz)}{F^2(volt/cm)^2} \qquad (5.10)$$

Deviations from the expected quadratic Stark effect have been observed for barium 6s*n*d $^1D_2$ Rydberg series due to hyperpolarizabilities (Kulina and Rinkleff 1985).

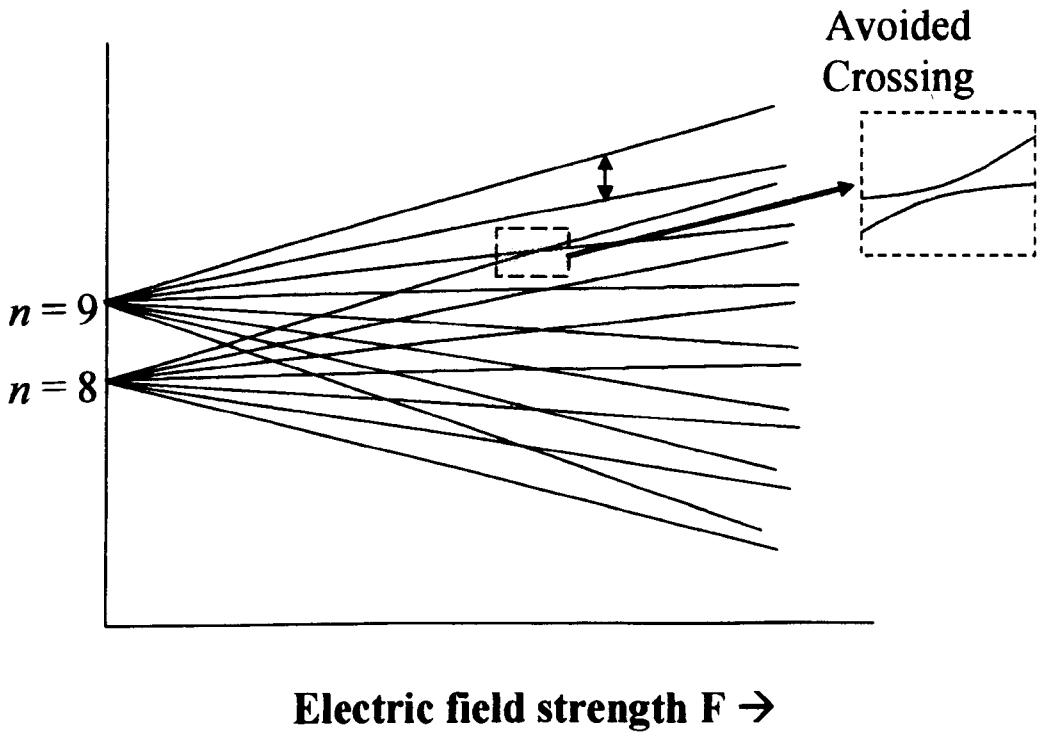

Fig.5.3 Stark splitting in to *n*k manifold with avoided crossing for |*m*| = 1 states

When an electric field is applied 'ℓ' is no more a good quantum number and the zero field '$n\ell$' states evolve in to 'nk' Stark manifold. Also, the autoionization rates in the '$n\ell$' state get distributed among the 'nk' manifold, thereby, increasing the autoionization rates. In presence of an external electric field (in the z-direction) which causes a perturbation of the Rydberg energy levels and mixing between states of different 'ℓ', the Hamiltonian becomes,

$$H = H_0 + eFz \tag{5.11}$$

Where H_0 is the zero-field Hamiltonian and F is the external electric field strength in the z direction and e is the electronic charge. As m is well-defined, we can define a set of parabolic quantum numbers n_1 and n_2 such that:

$$m + n_1 + n_2 + 1 = n \tag{5.12}$$

Since n_1 and n_2 are not independent, they can be replaced by the new quantum number

$$k = n_1 - n_2; \qquad 1 < k < n-m \tag{5.13}$$

which represents the nodes in the wavefunction in the parabolic co-ordinates ξ and η defined by:

$$\xi = r + z \tag{5.14}$$

$$\eta = r - z \tag{5.15}$$

And $$\varphi = \tan^{-1}\left(\frac{x}{y}\right) \tag{5.16}$$

For non-hydrogen atoms, at zero fields, low 'ℓ' states are not degenerate due to non-zero quantum defects. At low field strengths the states are very weakly mixed with nearby states and at high field strengths mixing become stronger. Also, the states behave like in hydrogen above the "Inglis-Teller limit" which is the field at which the width of a Stark manifold becomes equal to the Rydberg state splitting.

5.3.1 Anomalous Stark shift due to space charge effects in the excitation region

Anomalies in Stark shift as reported by Philip and Makdisi (2006) were observed with departure from the quadratic Stark effect at very low field strengths including a well-defined shift reversal with a broad antiresonance for perturbed 5s*n*d $^1D_2$ Rydberg states of strontium due to space charge-induced effects in the thermionic diode detection. In Fig.5.4 the observed frequency shift for Sr I 5s*n*d $^1D_2$ Rydberg series in the range n = 27 - 42 is plotted as a function of the square of the applied electric field.

The frequency shift of the line centre ($\delta\nu = \nu - \nu_0$) is measured relative to the field strength with +1.2 volt biasing on the ionization detector which produces negligible Stark shift and asymmetry in line profile. As the electric field strength is increased the 5s*n*d $^1D_2$ states are red-shifted with a maximum frequency shift of approximately 0.38 cm^{-1} around 9.5 -10 volt/cm for the n = 42 state. Further increase in the electric field reverses the frequency shift and a blue shift is observed beyond a broad anti-resonance region (figure 5.5). For the electric field strengths used in the present study (much below the Inglis-Teller limit $F_{I-T} = 1/(3n^5)$ in atomic units) Stark broadening is negligible. The dipole allowed transitions are observed to be blue shifted with nearly quadratic dependence on the electric field while the forbidden transitions are red shifted beyond the anti-resonance region.

Electric field reversal is an important phenomenon in glow discharges due to ion flux and due to fluctuation in pressure and species composition. It indicates that, to obtain electric dipole polarizabilities which depend not only on the wave functions and energies of the states but also on the electric field induced mixing between states, detailed Stark shift measurements are required with excitation region free

from external fields. Simple estimates ($\Delta E_n = -1/2\ \alpha_d F^2$) is inaccurate for heat-pipe setups to determine the dipole polarizability α_d of the Rydberg states due to the space charge effects.

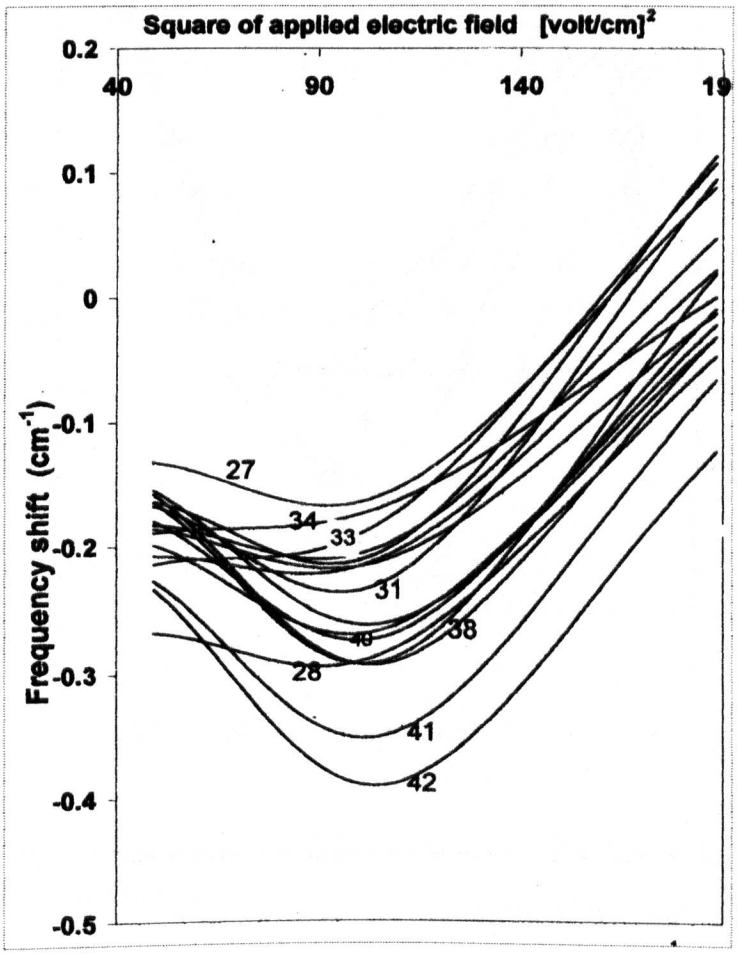

Fig. 5.4 Stark shift for high (n = 27 - 42) members of Sr I-5snd $^1D_2$ Rydberg series as a function of the square of the field. Frequency shift reversal with "quadratic Stark" effect is observed beyond the saddle point. (*Opt. Commun.* **266**, 253, 2006)

The microscopic field present in the space charge region inside the thermionic diode produces a repulsive potential causing a blue shift beyond the saddle point as observed in this study. The effect of the resultant field due to the applied field and the field produced by the local charge distribution in the laser interaction region produces varying energy level perturbations as observed by Armstrong and Greene (1994).

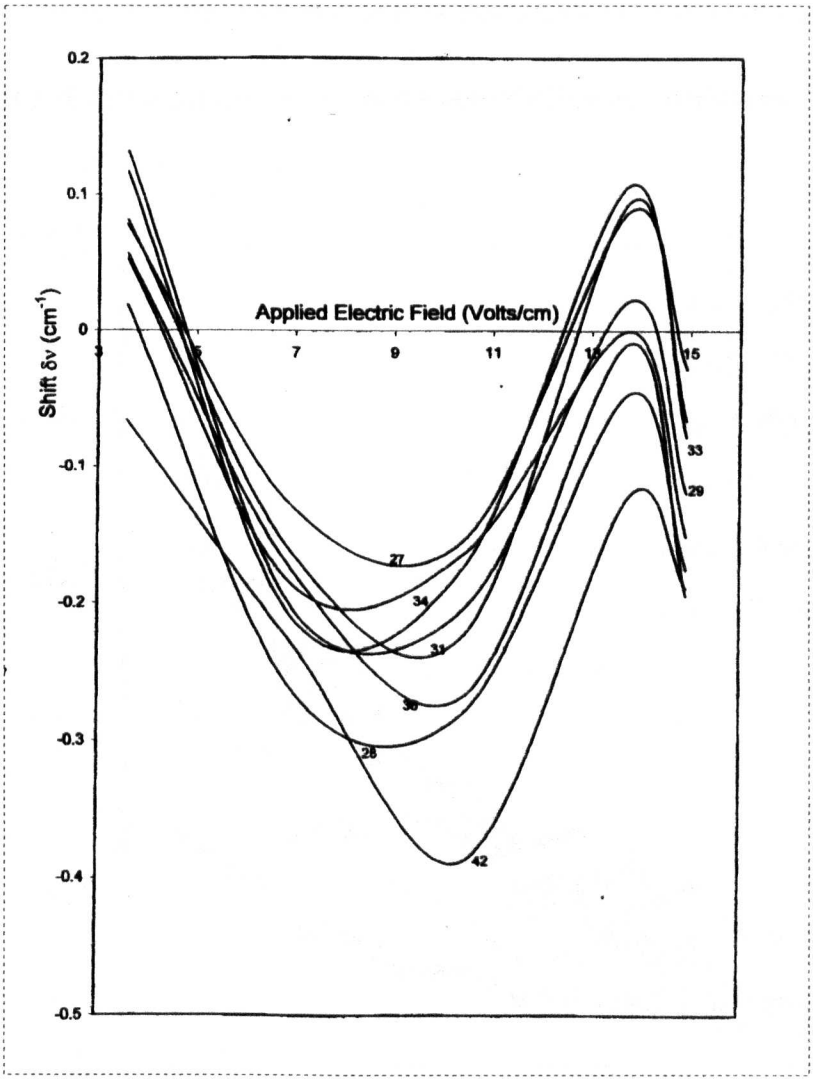

Fig. 5.5 Stark shift of high members of SrI, 5s*n*d $^1D_2$ Rydberg series

The anomalous shift reversal effect suggests gradual breakdown of coupling between Rydberg electron and the external field at low field strengths where the space charge effects are comparable or more dominant. Also, it was observed that the forbidden transitions show opposite behaviour in frequency shift as compared to the two-photon allowed transitions, beyond the region of the anti-resonance, with a linear Stark shift. Such observations can be used to estimate the effective electric field inside the excitation region. Figure 5.6 shows the two-photon absorption signals detected by the thermionic diode detector with varying biasing voltage. As expected the intensity of the photoabsorption signal decays approximately following

the $(n^*)^{-3}$ law. However field-induced intensity fluctuations are observed as in figure 5.6 besides intensity fluctuations due to series perturbation by interlopers.

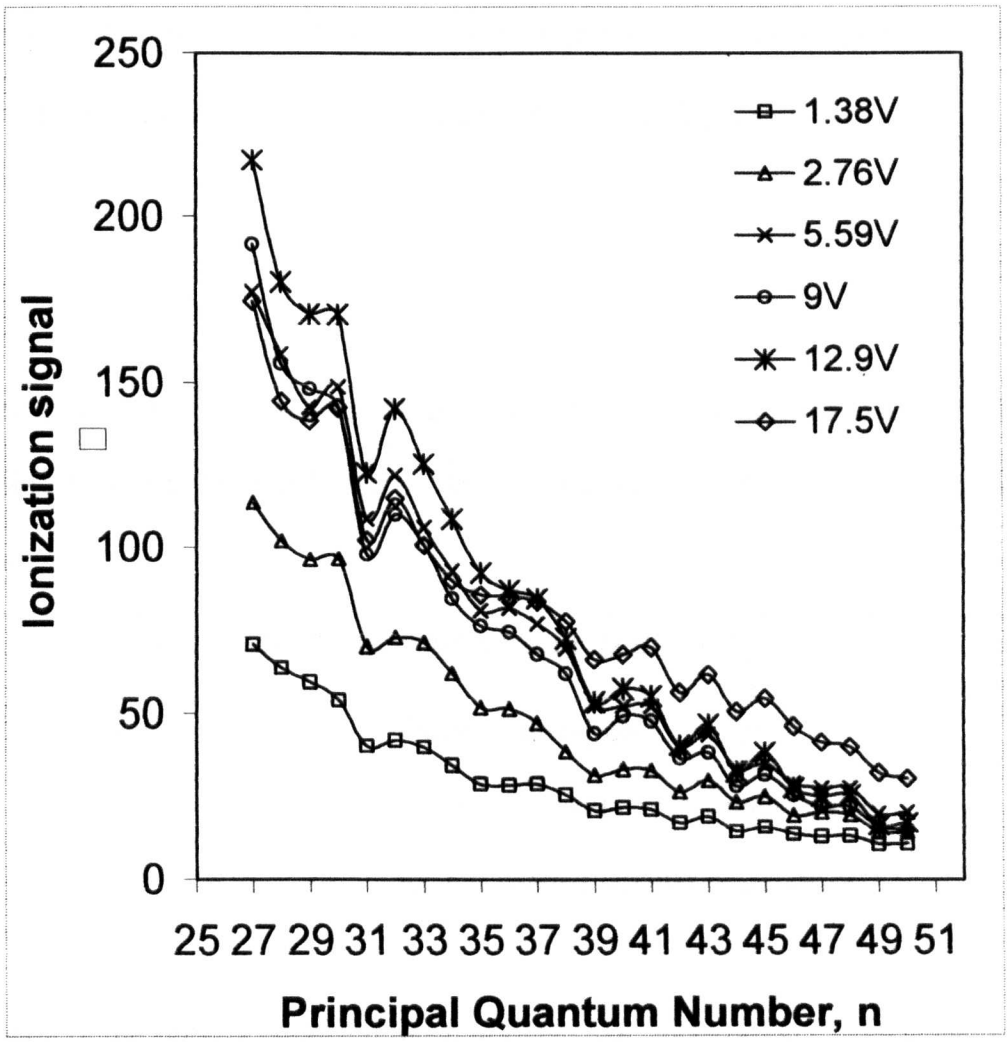

Fig. 5.6 Effect of thermionic diode bias voltage on the ionization signal

5.3.2 Importance of the laser beam polarization

For atoms in external electric and combined electric and magnetic fields, the angular momentum (m_ℓ) is a good quantum number and the angular momentum of the final state is determined by the polarization of the exciting laser beam and experimental geometry: The Stark shift $\Delta\nu$ of an m-sublevel with total angular momentum J is given by (Li and van Wijngaarden 1996):

$$\Delta\nu = -\frac{1}{2}\left[\alpha_0 + \alpha_2\left(\frac{3m^2 - J(J+1)}{J(2J+1)}\right)\right]F^2 \qquad (5.17)$$

Where α_0 and α_2 are the scalar and tensor polarizabilities and J is the total quantum number F is the electric field strength. For laser beam polarized parallel to the electric field F, only $|m| = 0$ states are populated. So, that Stark shift becomes:

$$\Delta\nu = -\frac{1}{2}\left[\alpha_0 - \alpha_2\left(\frac{J+1}{2J+1}\right)\right]F^2 \qquad (5.18)$$

By using a circularly polarized light beam traveling parallel to the magnetic field it is possible to excite both σ^+ and σ^- spectra by selecting the sense of circular polarization.

The angular momentum change is given by:

Δm_ℓ	=	0	linear polarization
Δm_ℓ	=	+1	for right handed circular polarization
Δm_ℓ	=	-1	for left handed circular polarization

Conversion of the linearly polarized beam in to circular polarization can be achieved by using a Glan-Thomson polarizer in combination with a Soleil-Babinet compensator. In a crossed field set up the electric field can be applied perpendicular to both the magnetic field and the direction of propagation of the laser beam and the evolution of both σ^+ and σ^- Stark spectra can be obtained by varying the electric field strength. Since the diamagnetic effect scales as n^2 B^4 the strength of magnetic field for breaking the symmetries and hence to remove degeneracy can be significantly reduced at high principal quantum numbers. Also, reduced electric field strength can be used at high principal quantum numbers.

5.4 Scaled Energy Spectroscopy in external fields

Atomic spectroscopy for which the scaling parameter $\varepsilon = \frac{E}{\sqrt{F}}$ held constant is called "scaled energy spectroscopy". Here E is the energy of the state and F is the externally applied electric field. The Hamiltonian for hydrogen atom in an electric field can be scaled by transforming in to scaled variables (r, p, t) such that:

$$r = r \times (F)^{1/2} \tag{5.19}$$

$$p = p \times (F)^{-1/4} \tag{5.20}$$

The Hamiltonian in atomic units, $\left(H = \frac{p^2}{2} - \frac{1}{r} + Fz \right)$ becomes in scaled variables as:

$$H(r, p, F) = (F)^{1/2} \times H(r, p, F = 1) \tag{5.22}$$

The Hamiltonian does not depend on E or F, but on the scaling parameter, ε. Therefore, if the scaling parameter is held constant the classical motion becomes invariant (orbit shapes, orbital periods etc remain constant) in scaled co-ordinates. This is an extremely interesting result. Scaled photo-excitation spectrum of the hydrogen atom in crossed electric and magnetic field was calculated by Rao *et al* (2001).

5.5 Atomic circular states in external fields

Atoms in external fields have also received tremendous attention especially for the large angular momentum circular states which are difficult to access by optical excitation. In external fields (electric and magnetic) localization of the wavefunction takes place which can be controlled by varying the relative strengths of the electric and magnetic fields (Bivona *et al* 2005). "Stark switching technique" was first used by Cooke *et al* (1978) to populate Sr 5s*nl* states of l up to 7. Jones and Gallagher

(1988) produced states of $\ell \geq 4$ in Ba 6s$n\ell$ states. In this technique, at electric field strength strong enough for Stark levels to be well-resolved, a single Stark level is excited with a laser. The field is then adiabatically switched off and subsequently the Stark level is allowed to evolve in to a zero field angular momentum state.

An alternative technique, proposed by Delande and Gay (1988) is the "adiabatic switching technique" which has been used by Delande *et al* (1988), Hansen *et al* (1993) and several others to prepare atomic circular states with $\ell = m = n\text{-}1$ which involves collision with oriented atomic states. In this scheme a well-defined ($m = 0$) Rydberg state is created by multi-photon pulsed laser excitation in presence of a parallel electric field which is adiabatically switched off in the presence of a perpendicular magnetic field and collisions of the type: Sr (5snd $^1D_2$) + Xe$\rightarrow$ Sr (5s(n+1)p $^1P_1$) + ΔE + Xe. Here "collision energy defect" ΔE depends on the projectile-target relative velocity (v_r) which can be adjusted by proper choice of the electric and magnetic field strengths.

5.6 Forced Autoionization in electric field

In a double excitation process if the total energy of both the electrons exceeds the binding energy, one of the electrons may undergo autoionization (Chapter3, Thesis) resulting in an ion plus an electron. But, if the total energy is less than the binding energy, the doubly excited state couples to bound Rydberg states. However, in the presence of an external electric field the bound Rydberg state couples to a field-induced continuum leading to forced autoionization (Sandner *et al* 1986). Forced autoionization is an important process for the Ba 5d7d doubly-excited state in electric field investigated by Wesdrop *et al* (1999). They reported Stark-induced

modulation in autoioniation. Freeman and Bjorklund (1978) reported modification of the auotionizing resonance profiles by the influence of the electric field on the bound part of the autoionizing state. Kelleher *et al*(1985) studied the effect of electric field for strontium autoionizing states and Safinya *et al* (1980) investigated the effects of electric field on the doubly-excited 6p*n*l autoionizing state of barium for $n^* = 12$.

5.7 Electric field-induced *ℓ*-mixing

Electric field-induced mixing between Rydberg states which are lying close to each other in energy, but differing in angular momentum quantum number '*ℓ*' has been observed in strontium, in violation of selection rules for two-photon excitations. Stark mixing was reported also in calcium (Armstrong *et al* 1977) and in barium (Rubbmark *et al* 1977, Rinneberg *et al* 1985). Mixing of states of opposite parity at high electric field causes broadening effect, as in the case of strontium 4d5d $^1D_2$ autoionizing resonance (Kelleher *et al* 1985) and drastically enhances the polarizabilities (Li and van Wijngaarden 1996). In two-photon excitations in strontium (Philip and Makdisi 2006, Philip and Connerade 2007) certain weak Rydberg series (5s*n*p $^1P_1$, 5s*n*f $^1F_3$) have been observed by electric field-induced angular momentum mixing in violation of normal parity and selection rules. This field-induced '*ℓ*'-mixing is observed to be highly sensitive on the electrical discharge characteristics of the thermionic diode governed by the nature and composition of the buffer gas used.

Figures 5.7(a-c) indicate the electric field induced mixing between states of opposite parity and different angular momenta along with collisional quenching of high

members of strontium 5s*n*d $^1D_2$ Rydberg series. In (a) the two-photon forbidden, odd-parity 5s(n+1)p $^1P_1$ states emerge as weak satellites with 5s*n*d $^1D_2$ ($47 < n < 73$) series by 'ℓ'-mixing in the electric field.

When 20 millibar xenon is added, (Figure 5.7 (b) with 20 times higher signal amplification than in figure 5.7(a)) these forbidden transitions are wiped out (quenching by collisions) from the spectrum. However, at higher electric field strength (Figure 5.7(c)) the odd-parity satellites re-emerge, confirming the excitation by Stark mixing. Stark effect leads to a breakdown of the angular momentum selection rules for the electric dipole transitions ($\Delta L = \pm 1$ for one- and $\Delta L = 0, \pm 2$ for two-photon transitions), thereby leading to transitions which are otherwise forbidden.

While the intensity of a dipole –allowed transition decreases as $(n^*)^{-3}$, the forbidden line intensity grows rapidly with an enormous dependence on the effective principal quantum number n^* as can be seen in figure 5.8.

At low field strengths the intensity of a parity forbidden transition depends quadratically on the electric field strength while at high field the dependence is nearly linear.

Perturbed Rydberg states at high 'n' get rapidly mixed with nearly degenerate '$n\ell$' states and the electric field assists in the redistribution of the states. The large value of Stark mixing coefficient for high principal quantum number ($n \geq 60$) makes the intensities of the forbidden transitions becoming comparable to those of the allowed transitions even at fields as low as 5volt-cm^{-1} (as observed in this thesis research).

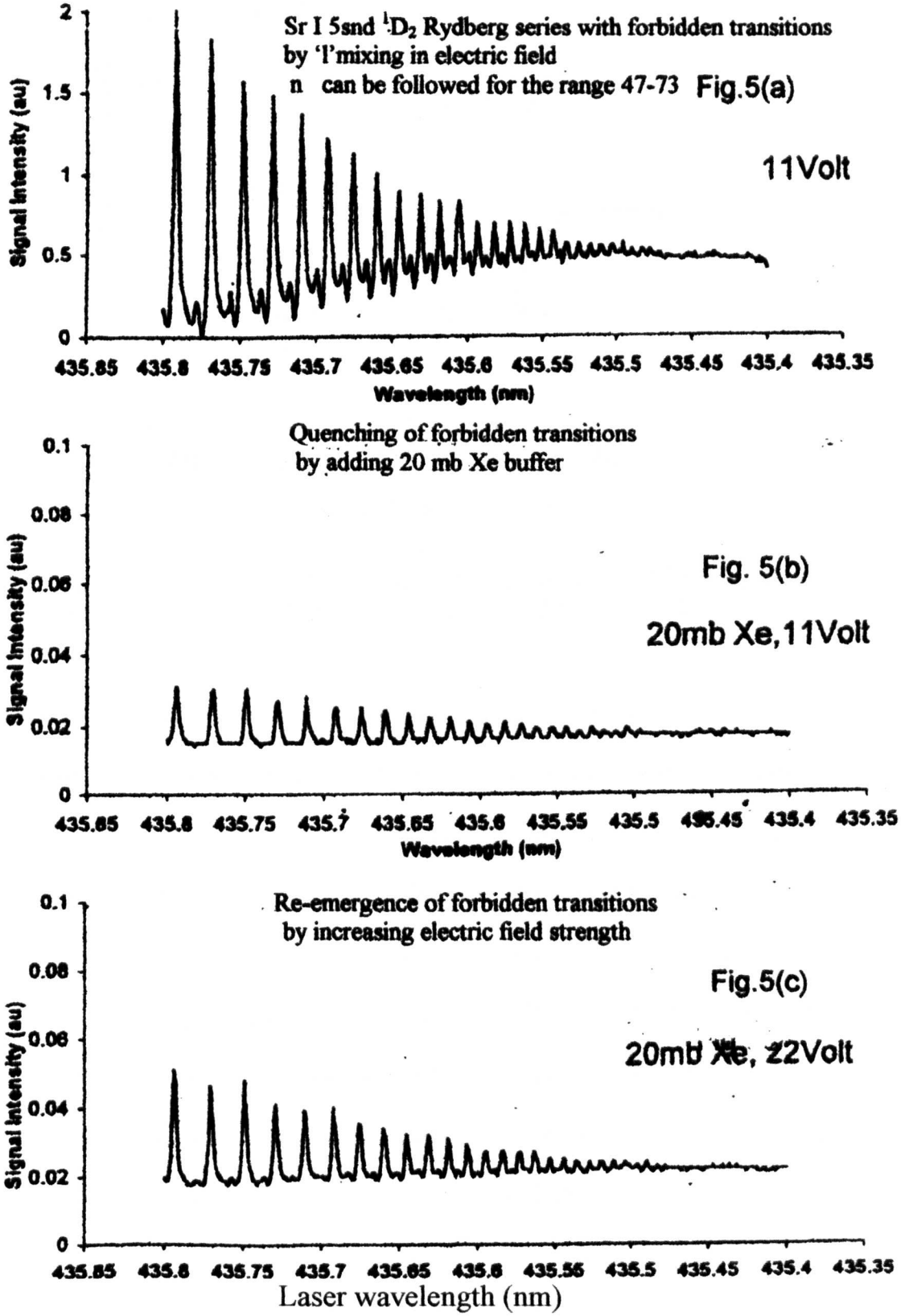

Fig. 5.7 (a-c) Two-photon spectra Sr I 5s*n*d $^1D_2$ Rydberg series (a) field –induced 'ℓ'-mixing, (b) collisional quenching with 20 mbar Xe buffer and (c) re-emergence at high field strength (*Opt. Commun* **266**,253, 2006)

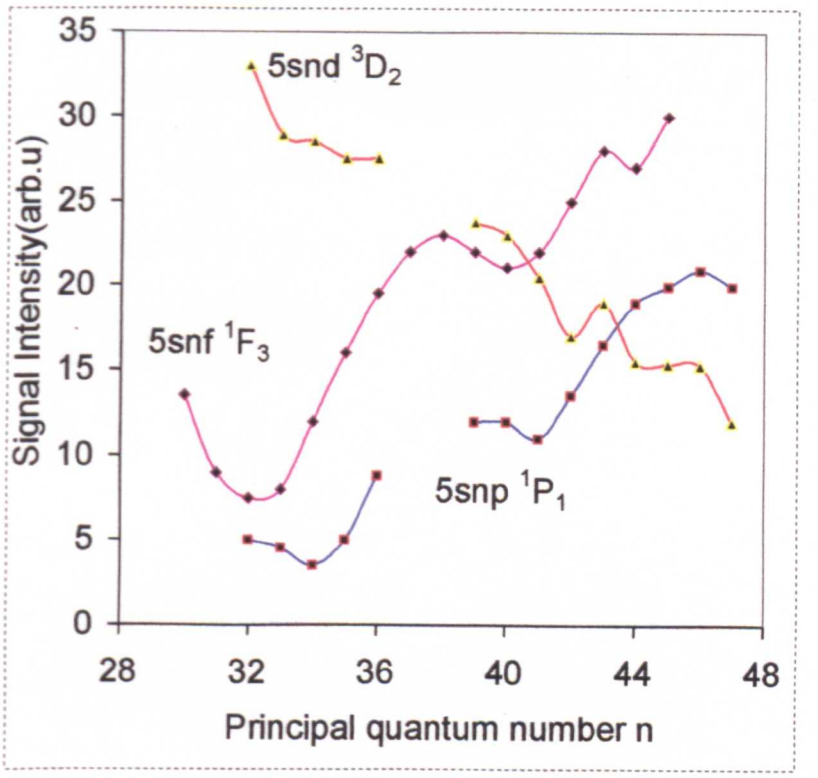

Fig. 5.8 Fast growth of forbidden transitions and $(n^*)^{-3}$ decay of allowed transitions in Sr I (*Opt. Commun.* **279,** 141, 2007))

Forbidden transitions due to Stark mixing were also reported by Borgstrom and Rubbmark (1977) in calcium and by Littman *et al* (1976) in barium. Electric field-induced mixing between adjacent states of opposite parity was also reported in strontium by Vidolova *et al* (1996). Whereas the dipole-allowed line intensity decreases as $(n^*)^{-3}$, the forbidden line intensity grows with an enormous dependence on the effective principal quantum number. This makes the Stark mixing spectroscopy of forbidden transitions (Zimmermann *et al* 1979) a sensitive probe for the measurement of weak electric fields in systems where ideally, pure '*J*' assignments and level designations are important and in systems requiring field-free conditions. The present study in strontium showed that the oscillator strengths of the forbidden transitions due to field-induced '*l*'-mixing could be controlled by the spatial distribution of the electric field and the ratio of the electric field to pressure (E / *p*) and polarizability of the buffer gas used (Philip and Connerade 2007).

5.8 Effect of Electric field on the autoionizing resonance $(4d^2+5p^2)\ ^1D_2$ in strontium

The effect of applied electric field on the broad autoionizing resonance $(4d^2 + 5p^2)$ $^1D_2$ just above the first ionization threshold in Sr I was examined in the study reported here by varying the thermionic diode detector bias voltage in the heat-pipe setup.

Increasing the electric field strength produces broadening besides the emergence of field-induced weak satellite transitions on the wings of the autoionizing resonance as seen in figure 5.9. Also observed are the one-photon transitions from 5s5p $^1P_1$ level.

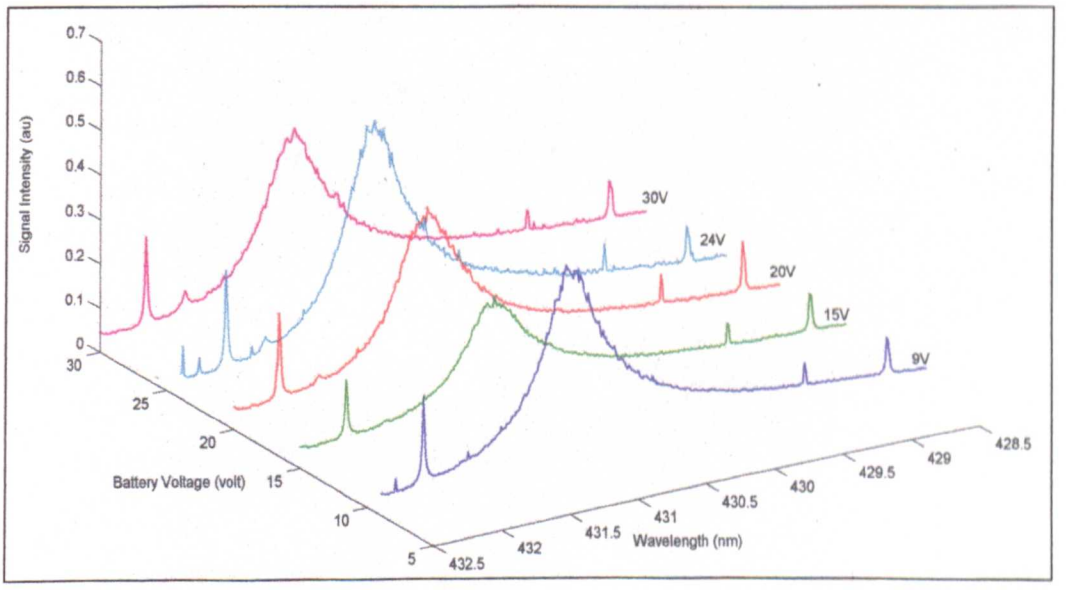

Fig. 5.9 Effect of electric field on $(4d^2+5p^2)\ ^1D_2$ autoionizing resonance in strontium. Evolution of field-induced states and broadening can be seen. Spectrum taken with 40 mbar Ar buffer

Salomon *et al* (1985) studied electric field-induced interference in barium autoionizing resonances above the first ionization threshold. As the dielectronic recombination rates get substantially increased, the effect of an electric field on autoionizing states is very important (Armstrong *et al* 1993).

Figure 5.10 presents the two-photon spectra for the strontium $(4d^2+5p^2)^1D_2$ autoionizing resonance taken at 20 mbar argon buffer with the bias on the thermionic diode varied from 0 - 24 volts.

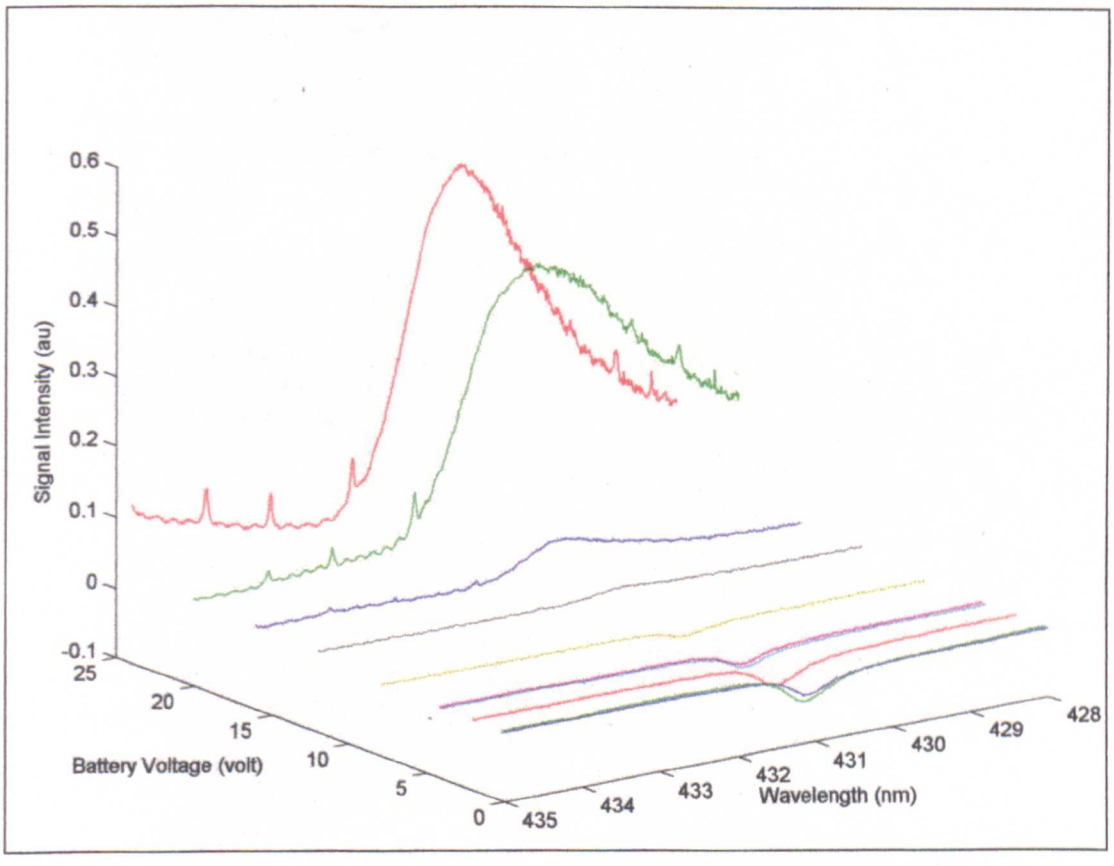

Fig.5.10 Evolution of $(4d^2+5p^2)\ ^1D_2$ autoionizing resonance in strontium. Spectrum taken with 20 mbar Ar buffer shows the reversal of signal polarity and profile asymmetry indicative of a possible field-induced q-reversal effect besides broadening effect.

Unlike in the spectra taken at 40 mbar argon buffer shown in figure 5.9 the autoionization process gives negative signals gradually decreasing and reversing the polarity at biasing voltage ≥ +14 volts. Moreover, the asymmetry of the autoionizing resonance profile is observed to be significantly modified indicative of a possible electric field-induced "q-reversal effect" besides broadening and shift. For an autoionizing transition the shape index 'q' defined in the Fano formula is reversed: the so-called q-reversal effect first discovered by Connerade (1978) in presence of

perturbation by an interloper. Also, the symmetry of the profile of an autoionizing resonance can be in modified in a controlled manner by coupling the bound excited states of an atom with the continuum by the use of a laser-a possibility to control the Beutler-Fano profile (Connerade 1998).

It is interesting to note that the behaviour of bound Rydberg state is different from the observation cited above for the autoionizing state. The profile and symmetry of all members of the bound Rydberg series are preserved as observed in two specific cases presented here. Figure 5.11 shows the low-lying Rydberg members taken with a positively biased detector. By setting the detector bias voltage to zero, negative signals are detected and all specific features in the spectrum in figure 5.11 are reproduced in the zero-field spectrum shown in figure 5.12. The interloper appearing past the 5s20d $^1D_2$ (transition 5s5p $^1P_1 \rightarrow$ 5s12s $^1S_0$) in Fig. 5.11 is completely absent in Fig. 5.12 indicating that it is due to an excitation process supported by external electric field.

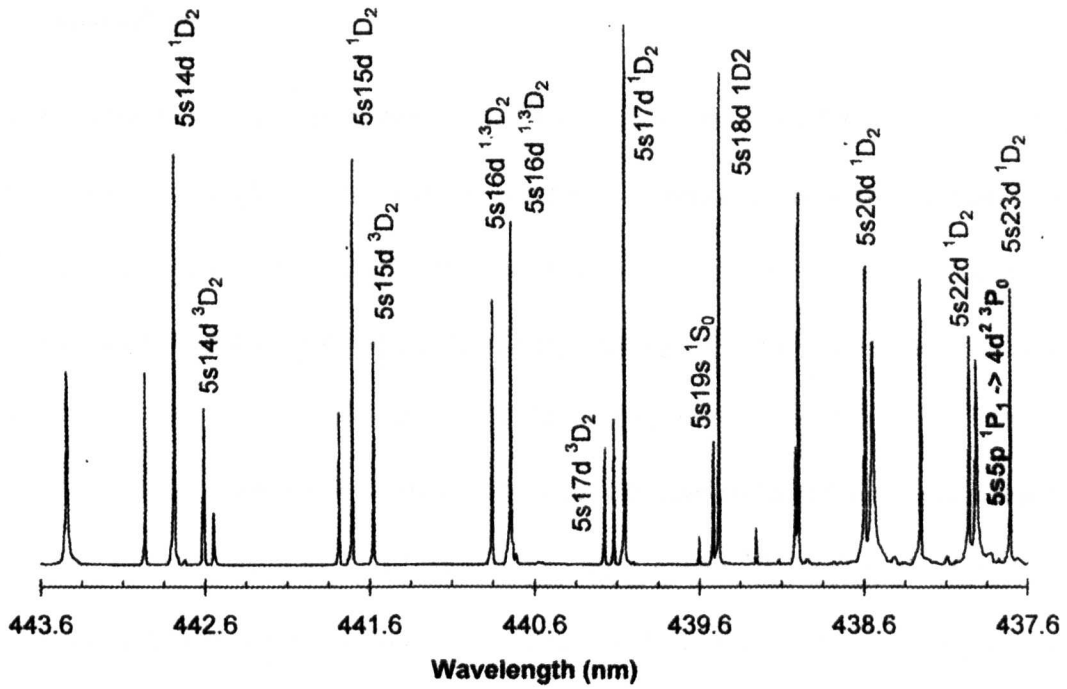

Fig. 5.11 Two-photon spectrum of low members of Sr I , J = 0 and 2 even-parity Rydberg series taken with positively biased (+9 volt) detector (*Opt. Commun.* **279**, 141, 2007))

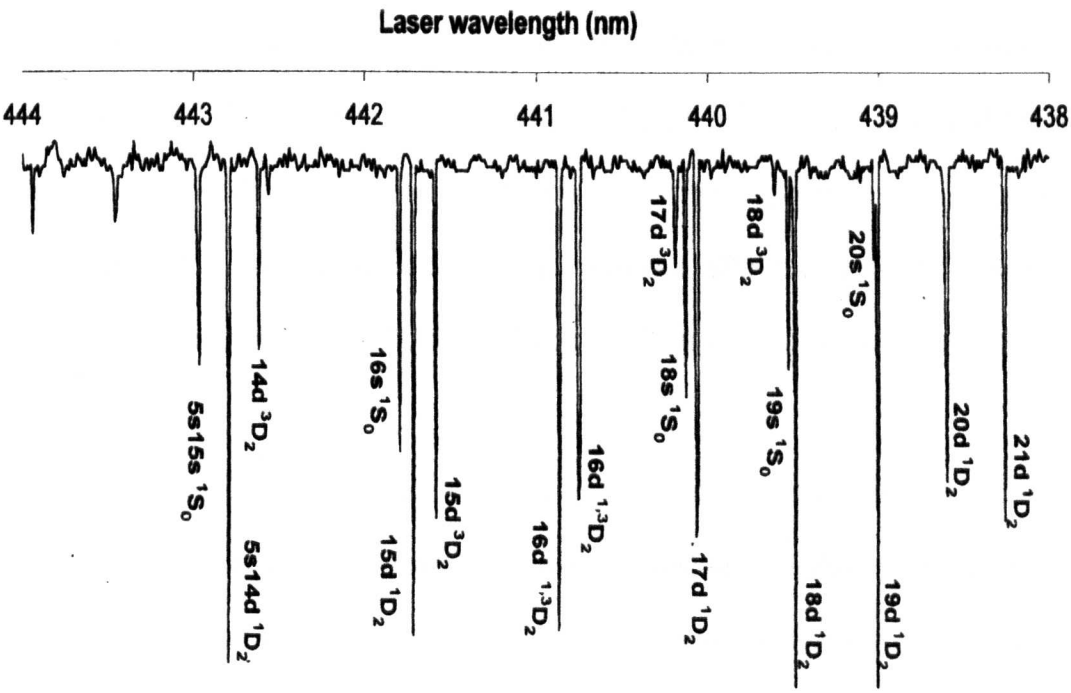

Fig. 5.12 Two-photon spectrum of Sr I, J = 0, 2 even-parity series with detector bias set to zero. Electric field-induced forbidden transitions are absent in this spectrum. All features of the spectrum in Fig. 5.11 are preserved. (*Opt. Commun.* **279**, 141, 2007)

Conclusion

In this section I have attempted to make a cursory survey of the effects that are important when Rydberg atoms are subjected to external weak static electric fields- the peculiarities based on Stark effect such as change in energy level structure and field-induced angular momentum (ℓ) mixing leading to forbidden transitions. Hence the study reported in this section involving two-photon excitation of $5snd\ ^1D_2$ Rydberg series of neutral strontium in a weak external electric field has established the field-induced excitation of odd-parity states ($5snp\ ^1P_1$ and $5snf\ ^1F_3$) at high principal quantum numbers which are otherwise forbidden according to parity and selection rules for two-photon transitions. The oscillator strengths of such forbidden transitions can be controlled by suitable manipulation of the electric field strength and its spatial distribution. Also, this study of Rydberg atoms in external electric field has helped to observe certain anomalies in the spectra in the midrange of principal quantum numbers. The observed frequency shift reversal effect suggests the existence of field gradients inside the heat-pipe with space charge detection setup. The forbidden transitions are found to exhibit opposite behaviour with a linear Stark shift as compared to the two-photon allowed transitions above a threshold value of the electric field which is a saddle point for frequency shift.

Effect of electric field on the $(4d^2 + 5p^2)\ ^1D_2$ autoionizing resonance just above the first ionization threshold in strontium which indicates, probably a forced "q-reversal" effect in electric field also has been presented. This study also indicates a convenience and flexibility in the choice of excitation schemes with the participation of external electric fields and collisions to compliment laser excitation to access various high-lying states.

References -Chapter 5 (alphabetical order)

1. Abdullah A.M., Hogan S., Zhan M.S. and Connerade J.-P
J. Phys. B: At. Mol. Opt. Phys. **37**, L147 (2004)

2 Armstrong D.J., Greene C.H., Wood R.P. and Cooper J
Phys. Rev. Lett. **70**, 2379(1993)

3 Armstrong D.J and Greene C.H.
Phys. Rev. A **50**, 4956(1994)

4 Bethe H.A. and Salpeter E.E
"Quantum Mechanics of One- and Two-Electron Atoms"
(New York Academic Press, 1957)

5 Bivona S., Burlon R., Ferrante G. and Leone C
J. Phys. B: At. Mol. Opt. Phys. **38**, S131 (2005)

6 Borgstrom S.A. and Rubbmark J.R
J. Phys. B: At. Mol. Opt. Phys. **10**, 3607 (1977)

7 Cole B.E., Cooper J.W. and Solomon E.B
Phys. Rev. Lett. **45**, 887 (1980)

8 Connerade J._P
Proc. Roy. Soc. (London) **A 362**, 361 (1978)

9 Connerade J._P
J. Phys. B: At. Mol. Opt. Phys **30**, L31 (1997)

10 Connerade J._P
"*Highly Excited Atoms*" (Cambridge Univ. Press, Cambridge, 1998)

11 Connerade J._P., Zhan M.S., Rao J. and Taylor K.T
J. Phys. B: At. Mol. Opt. Phys. **32**, 2351 (1999)

12 Connerade J._P., Hogan S.D. and Abdullah A.M
J. Phys. B: At. Mol. Opt. Phys. **38**, S141 (2005)

13 Cooke W.E., Gallagher T.F., Edelstein S.A. and Hill R.M
Phys. Rev. Lett. **40**, 178 (1978)

14 Delande D. and Gau J.C
Europhys. Lett. **5**, 303 (1988)

15 Elliott R.J., Droungas G. and Connerade J._P
J. Phys. B: At. Mol. Opt. Phys. **28**, L 537(1995)

16 Feldman P. and Novick R
Phys. Rev. **160**, 143 (1967)

17 Freeman R.R and Bjorklund G.C
Phys. Rev. Lett. **40**, 118 (1978)

19 Gallagher T.F., Humphrey L.M., Cooke W.E., Hill R.M. and Edelstein S.A
Phys.Rev. A **16**, 1098 (1977)

20 Hansen S.B., Ehrenreich T., Horsdal- Pedersen E., Mac Adam K.B. and Dube L.J
Phys. Rev. Lett. **71**, 1522 (1993)

21 Jones R.R. and Gallagher T.F
Phys. Rev. A **38,** 2846(1988)

22 Karapanagioti N.E., Connerade J.P., Bhatia K.S., Makdisi Y. and Philip G
J. Mod. Opt. **46**, 1549 (1999)

23 Kelleher D.E., Delpech J.F and Weiner J
Phys.Rev. A **32**, 2230 (1985)

24 Kleppner D., Littman M.G and Zimmermann M.L
"Rydberg states of Atoms and Molecules"
Eds. R. F. Stebbings and F. B. Dunning (Cambridge University Press 1983)

25 Kulina P. and Rinkleff R-H
J. Phys. B: At. Mol. Opt. Phys **18**, L245 (1985)

26 Lahaye C.T.W., Hogervorst W. and Vassen W
Z. Phys. **D 7**, 37 (1987)

27 Lahaye C.T.W. and Hogervorst W
Phys. Rev. **A 39**, 5658 (1989)

28 Li J. and van Wijngaarden W.A
Phys. Rev. **A 53**, 604 (1996)

29 Littman M.G., Zimmerman M.L., Ducas T.W., Freeman R.R. and Kleppner D
Phys. Rev. Lett.**36**, 788 (1976)

30 Liu X.J., Cao J.W., Zhan M.S. and Connerade J._P
J. Phys. B: At. Mol. Opt. Phys **35**, 2069 (2002)

31 Luc-Koenig E., Liberman S. and Pinard J
Phys. Rev. A **20**, 519 (1979)

32 Neukammer J., Rinneberg H., Vietzke K., Konig A., Hieronymus H., Kohl M. and Grabka H.J
Phys. Rev. Lett. **59**, 2947(1987)

33 Philip G. and Makdisi Y
Opt. Commun. **266**, 253(2006)

34 Philip G. and Connerade J._ P
Opt. Commun. **279**, 141(2007)

35 Rao J., Delande D. and Taylor K.T
J. Phys. B: At. Mol. Opt. Phys **34**, L391 (2001)

36 Rinneberg H., Neukammer J., Jonsson G., Hieronymus H., Konig A. and Vietzke K
Phys. Rev. Lett. **55**, 382 (1985)

37 Robicheaux F. and Pindola M.S
Phy. Rev. Lett. **79**, 2237 (1997)

38 Robicheaux F., Wesdrop C. and Noordam L.D
Phys. Rev. A, **60**, 1420 (1999)

39 Rubbmark J.R., Borgstrom S.A. and Bockasten K
J. Phys. B: At. Mol. Opt. Phys **10**, 421 (1977)

40 Ryabsev I.I, Tretyakov D.B. and Beterov I.I
J. Phys. B: At. Mol. Opt. Phys **38**, S421 (2005)

41 Safinya K.A., Delpech J.F. and Gallagher T.F
Phys. Rev. A **22**, 1062 (1980)

42 Sandner W., Safinya K.A. and Gallagher T.F
Phys. Rev. A **23**, 2448 (1981)

43 Sandner W., Safinya K.A. and Gallagher T.F
Phys. Rev. A **33,** 1008 (1986)

44 Soloman E.B., Cooper J.W. and Kelleher D.E
Phys. Rev. Lett. **55**, 193 (1985)

45 van Leeuwen K.A.H, Hogervorst W. and Post B.H.
Phys.Rev. A **28**, 1901(1983)

46 van Leeuwen K.A.H. and Hogervorst W
J. Phys.B: At. Mol. Opt. Phys **16**, 3873(1983)

47 Vidolova Angelova E., Baharis C., Roupakas G. and Kompitsas M
J. Phys. B: At. Mol. Opt. Phys **29**, 2453(1996)

48 Wesdrop C., Noordam L.D. and Robicheaux F
Phys. Rev. A, **60**, R 3377 (1999)

49 Zimmermann M.L., Litmann M.G., Kash M.M. and Kleppner D
Phys. Rev. A **20,** 2251 (1979)

50 Zimmermann M.L, Ducas T.W, Littmann M.G and Kleppner D
J. Phys. B: At. Mol. Opt. Phys **11**, L11 (1978)

Chapter 6

Conclusion

Inspired by the contemporary revival of interest and the need to further extend and improve the understanding of the spectra of Rydberg atoms I had embarked on this Ph.D project to experimentally study the two-photon spectra of alkaline-earth atoms, strontium and barium (especially strontium), using laser-based techniques and, thereby, extend the previously published observations in the high Rydberg states of these atoms placed under a variety of test conditions such as external electric field, collisions with foreign gases etcetera. As a unique feature of this experimental study, I had designed and established novel experimental schemes (Philip- Appl. Phys. B 90, 407-2008) and developed highly efficient and sensitive diagnostic techniques (ionization complimented by optical detection) for obtaining original and new experimental data. A novel atomic jet in a purpose-built heat-pipe setup (Philip- Rev. Sc. Instrum 78, 113101-2007) which combines the advantages of both atomic beam geometry for polarization selective orthogonal photo-excitation and the high sensitivity of space-charge ionization in thermionic detection was used in different configurations for various measurements reported in this dissertation.

Rydberg atoms are very sensitive to collisions with cross section scaling as n^4 for low n, but decreasing as n increases because very large Rydberg atoms become transparent. I have carried out an intensive study of the effect of foreign gas (helium, argon and xenon) collisions on the bound and autoionizing doubly excited states of strontium. Interesting effects like the evolution of highly localized doubly-excited

states uncovering orbital contraction effects of high angular momentum states in the two-photon spectra were observed. Effect of collisions with different buffer gas composition and static electric field strength on the evolution of a broad remarkable resonance (tentatively assigned the label $4d^2\ ^1G_4$) which intrudes in to the even-parity spectrum of Sr I $5snd\ ^{1,3}D_2$ Rydberg series at $27 < n < 28$ has been examined. Controlled excitations to both Rydberg and non-Rydberg states were achieved by weak electric fields complimented by collisions (Philip and Connerade: Opt. Commun. 279, 141-2007). This process opens up a new class of experiments with flexibility in the choice of excitation schemes to study highly excited states which cannot otherwise be accessed from the ground state due to parity and spectroscopic selection rules (for example the autoionizing states converging to the $5p_{1/2}$ and $5p_{3/2}$ limits in strontium can be accessed by two-photon excitation from the intermediate $5s5p\ ^1P_1$ level populated by sequential excitation as observed in the present study). Revised experimental data were also obtained for the collisional shift and broadening rates of strontium Rydberg members in the highly perturbed region. Interesting peculiarities of the spectra like the Ramsauer effect exhibited by a Rydberg state which gives an additional identification criterion without ambiguity in a highly perturbed spectrum in which both Rydberg and non-Rydberg members are present have been observed. Field-induced frequency shift and an anomalous shift reversal with a quadratic Stark effect has been observed for strontium Rydberg series perturbed by space charge produced field gradients (Philip and Makdisi- Opt. Commun. 266, 253-2006). Interesting effects in intensity distribution of the members of the series which reflect on the environment in which the atoms are placed and the series perturbation have also been observed. Strong spin-orbit interaction and the breakdown of parity and selection rules and field-induced 'ℓ' mixing also have been observed.

Controlled configuration mixing in two-photon spectroscopy by exploiting electric field and collisions has allowed new extensions in the literature for high members of the two-photon forbidden $J = 3$ odd-parity $5snf\ ^1F_3$ up to $n = 44$ and the $J = 1$ $5snp\ ^1P_1{}^0$ series up to $n = 46$ in strontium. Two-photon excitations to Sr I doubly-excited states belonging to the $4d^2\ ^3P_J$ configuration have been observed besides single-photon resonances to these states via sequential excitation from the $5s5p\ ^1P_1$ level populated by dissociation of Sr_2 dimers. There are still discrepancies in the labeling of certain doubly excited states such as $4d^2\ ^1D_2$, $5p^2\ ^1D_2$ in strontium. My study has also attempted to assign these levels without ambiguity.

Much improved two-photon absorption spectra and original new energy values on the even-parity $J = 0$ and $J = 2$ levels of the Rydberg series of both strontium and barium have been obtained, thereby, substantially extending the spectral data for these atoms beyond those reported hitherto by others in the literature in similar experiments. Experimental term values are presented for the members of the strontium Rydberg series: $5sns\ ^1S_0$ up to $n = 46$, $5snd\ ^3D_2$ for the range $9 < n < 47$ and for $5snd\ ^1D_2$ for the range $9 < n < 82$. Also, energy level data are presented for the members of barium Rydberg series: $6sns\ ^1S_0$ (for the range $13 < n < 68$ with new extension $62 < n < 68$), $6snd\ ^3D_2$ (for the region $11 < n < 46$) and $6snd\ ^1D_2$ (for the range $11 < n < 88$ with new extension $82 < n < 88$).

The lifetime is one of the fundamental properties of the excited states of an atom and accurate lifetime measurements are important for reliable level designations and to refine atomic structure. The Rydberg states are characterized by very long radiative decay time (well-known $(n^*)^3$ scaling law for unperturbed states). In alkaline-earth

atoms series perturbations are significant due to channel or configuration interaction between a Rydberg series converging to the first ionization limit and doubly excited configurations (mp^2, $[m-1]d^2$, where m = 5 and 6 for Sr and Ba respectively). Due to these interactions the lifetimes of Rydberg states are found to depart significantly from the $(n^*)^3$ scaling law. Since not much experimental data are available in the literature for lifetime measurements of Rydberg states, a novel experimental technique (Gated Pulsed-field Technique, GPT for short) involving time-resolved pulsed field thermionic diode detection was designed and integrated to the atomic jet setup to examine the time decay of the high-lying Rydberg states of strontium yielding their effective lifetimes (Philip and Connerade 2008- to be published). This novel technique which has been incorporated for the first time to a heat-pipe setup offers several advantages over other methods in time resolved decay measurements of Rydberg atoms, particularly accessed by resonant two-photon excitation and under heavy perturbation by configuration mixing and collisions. It can be used, with considerable simplicity and remarkable reliability, in situations where other methods are seldom suitable, especially in heat-pipe setups. Effective lifetime values have been presented for the members of Sr I Rydberg series: $5sns\ ^1S_0$ ($15 < n < 20$), $5snd\ ^3D_2$ ($14 < n < 17$) and $5snd\ ^1D_2$ ($14 < n < 19$ and $27 < n < 31$). The novelty of GPT lies in the observation that this technique is attractive for states with very long lifetimes with the unique possibility of obtaining lifetime data simultaneously for all members of a sequence, normally impossible with other methods.

Outlook for Future Research

This thesis research involving two-photon laser spectroscopy of the two heavy alkaline-earth atoms (strontium and barium) has contributed, to considerable extent, to expand the knowledge of the Rydberg states of these atoms in terms of revised and extended energy level data, interaction between Rydberg series and other important peculiarities. Reliable experimental schemes are established to reveal the perturbations of the Rydberg series by highly compact doubly-excited configurations and external electric field, collisions etc. by observable effects: anomalies in frequency shift, configuration interaction, enhanced lifetime and intensity fluctuations which directly reflect on the oscillator strengths. The data obtained can be of importance in refining the MQDT analysis for deriving reliable wavefunctions and for improving the atomic structure calculations of the two-electron atoms. This thesis research is also hoped to provide motivation for future experimental investigations. Some potential investigations feasible in laboratories equipped with present day tunable lasers are given below.

(i) Two-step photoionization with combined two-photon and single-photon excitation of the atomic jet

In strontium the region between the 1st ionization threshold and the 4d ($4d_{3/2,5/2}$) series limit is dominated by $4dnp\ ^{1,3}P_J$, $4dnp\ ^3D_J$ and $4dnf\ ^{1,3}P_J$, $4dnf\ ^{1,3}D_J$ doubly excited states which are autoionizing. Since the exact assignment of the doubly-excited states are still not free from ambiguity, it will be important to carry out a systematic investigation of these states by two-step laser excitation (involving two-photon combined with single-photon with suitable delay between the pulses) using the atomic jet. Also, two-step photoionization can be applied with the atomic jet

crossed at right angles by two laser beams to excite the $5p_{1/2,3/2}$ np autoionizing states. Corresponding investigations can also be carried out in barium.

(ii) Simple method for measurement of photoabsorption cross section using interferometry integrated to the atomic jet

Improvement on the experimental data for photoabsorption cross section which in turn provides experimental values for the oscillator strengths of the transitions will be an important extension to the present study. Very few reliable measurements are reported in the literature for oscillator strengths of strontium and barium. The atomic jet facility offers a convenient setup for Mach-Zender interferometry to determine absorption cross section based on the following well-known principle:

$$I(\lambda) = I_0(\lambda) \exp[-\sigma(\lambda) N L]$$

Where $I_0(\lambda)$ is the incident intensity, $I(\lambda)$ is the transmitted intensity and NL is the column density along the line of laser beam propagation in the atomic jet. Using known data for the absorption cross-section $\sigma(\lambda)$ for a few marker transitions, the column density can be calculated from the ratio $I(\lambda)/I_0(\lambda)$. An arrangement like the Mach-Zender type interferometer with atomic jet embedded in one arm can be used to obtain interferogram corresponding to the transitions involved by scanning across the wavelength region.

(iii) Electric discharge controlled ICE for autoionizing states

Using the atomic jet facility 5s5p $^1P_1$ and 5s5p ^3P_J states of Sr I can be preferentially excited with arbitrary relative strengths by controlling the electric discharge inside the thermionic diode. These intermediate states can be used for ICE (inner core excitation) to the autoionizing states. Moreover, these intermediate states are suitable for exciting 5snd $^{1,3}D_2$ Ryderg series by single-photon transitions. The

relative strengths of these transitions also can be controlled. Other Rydberg series which can be excited using one-photon absorption using the above intermediate states are 5s*n*s $^1S_0$ series which appear in the middle region between two successive 5s*n*d $^1D_2$ states and 5s*n*s $^3S_0$ states appearing at midway between two successive 5s*n*d $^3D_2$ states. Corresponding excitations are also possible in barium.

As an alternative to the ICE scheme it could be possible to use the crossed heat-pipe setup (Philip- Appl. Phys. B 90,407-2008) incorporating a DC electric discharge to populate the metastable states, 5s5p ^3P_J and the resonance level 5s5p $^1P_1$ in Sr I as intermediate stages for further stepwise two-photon excitation using two laser beams to generate the $5p_{1/2}$ and $5p_{3/2}$ autoionizing states. Furthermore, it will be interesting to investigate the lower members of the autoionizing series both in strontium and barium such as Sr 5p*n*s (odd) and Sr 5p*n*p (even) or 5p*n*d (odd) series using resonant two-photon excitation and the intermediate states.

(iv) The photoionization cross-section measurements by direct two-photon excitation from ground state

Despite extensive studies there are still uncertainties to be cleared like accurate assignment of certain series members, irregularities in quantum defects, oscillator strengths and auotionization widths. Since the photo-absorption spectrum of barium from the ground state $6s^2\ ^1S_0$ is strongly influenced by the 5d8p $^1P_1$ autoionizing resonance just above the first ionization threshold, the photoionization cross-section is enhanced at the first threshold for excitation from 6s6p $^1P_1$ state. Photo-absorption above the first threshold is very complex due to the presence of the 5d7d $^1D_2$ perturber. The photoionization cross-section measurements by direct two-photon excitation from the ground state $6s^2\ ^1S_0$ of Ba I using different wavelength dyes (480 nm- 440 nm range for different states such as 5d*n*p $^{1,3}P_1$, 5d*n*f $^{1,3}P_1$ etc.) would be

very challenging using narrow bandwidth dye laser. Also, if the excitation of the 5d8p $^1P_1$ autoionization resonance is from the parity-forbidden 6s6p $^3P_1$ state smooth absorption cross-section across the discrete to continuum border can be experimentally observed.

(v) Temporal evolution of autoionization decay and pulsed autoionization using ultrafast GPT

In two-electron atoms, the number of interacting channels can be tuned by the energy and intensity of the exciting laser photon. Excitation just above the first ionization threshold produces relatively simple spectra. But the excitation just below the second ionization threshold generates highly complex spectra due to coupling between decay channels via bound and autoionizing channels. By using extremely short pulse excitation, time-resolved autoionization decay can be studied with control on autoionization events to proceed stepwise with temporal delay between events. This possibility is provided by the coupling between the two doubly-excited configurations, one which has a very short life-time for autoionization while the other has an extremely long lifetime for decay. Switching between these two configurations results in to pulsed autoionization effect (Story and Ereifej 2001) and the oscillation frequency could be controlled by the application of an external static field. Since not much experimental data are available in the literature, it will be interesting to study the pulsed autoionization effect with a fast gated pulse detection technique (an advanced GPT) for detection and ultrafast lasers for excitation.

(vi) Experiments in search of electron correlation: Wannier and planetary states in barium

Atomic states in which two electrons with the same value of the principal quantum number n (Wannier states) have highly correlated motion and hence the structure,

coupling and wavefunctions of these states are quite different from those of the conventional atomic states and a proper description and understanding of such states still constitute a major challenge in atomic physics. Three-body Coulomb states in alkaline-earth atoms with both valence electrons excited to high ℓ- orbitals have emerged as an important electron correlation effect (Donke *et al* 1995). Such a study of the correlated motion of the two electrons in strontium and barium (one valence electron excited to a Rydberg state followed by selective excitation of the second electron to a bound state) and determination of the evolution of the three-body Coulomb system will also be an experimental challenge which can be undertaken using the present atomic jet facility and the ionization detection complimented by optical detection with barium as the preferred candidate to search for planetary states by selective excitation using combination of tunable dye lasers.

(vii) Probing the wavefunctions of excited states using collision and electric fields

For low-lying states the core penetration by the valence electron is large and consequently these states will have large quantum defects. However, the large angular momentum states are prevented from large core penetration due to the centrifugal barrier term in the potential (ℓ (ℓ +1) / $2\mu r^2$). Penetration of the core by the Rydberg electron can cause oscillations in the wave functions as suggested by Wang and Cooke (1993). Probing the wavefunctions of the excited states by controlled buffer gas collisions and electric field also would be experimentally very challenging.

(viii) Use of the atomic jet for high resolution spectroscopy

Theoretical treatment of the even-parity J = 2 bound spectrum of barium is substantially more demanding than the corresponding spectrum of strontium because

of the more severe departure from L-S coupling in Ba than in the lighter alkaline-earths and because of the presence of many more bound perturbers in barium. Additional measurements, such as lifetime and hyperfine structure measurements are also important besides accurate term values for deduction of accurate wavefunctions and atomic structure of this heavy alkaline-earth element. One such measurement can be a high resolution measurement of the hyperfine splitting of the $6snd\ ^1D_2$ and $6snd\ ^3D_J$ levels using two counter propagating laser beams in the crossed heat-pipe set up with atomic jet and improved bandwidth of the dye laser with a pressure-tuned intra-cavity etalon.

(ix) Looking for q- reversal effect in strontium

It will also be interesting to examine a possible q-reversal effect in strontium and barium involving a flip in asymmetry in Rydberg series when traversing a perturber, caused by static external electric field and using the atomic jet facility.

References- Chapter 6 (alphabetical order)

1 Connerade J.-P. and Farooqi S.M.
J. Phys. B. At. Mol. Opt. Phys. **24**, L331 (1991)

2 Domke M, Schul K., Remmers G., Gutierrez A., Kaindl G. and Wintgen D
Phys. Rev. A **51**, R 4309 (1995)

3 Story J.G. and Ereifej H.N
Phy Rev Lett **86**, 612(2001)

4 Wang X. and Cooke W.E
Phys. Rev. A **47**, 4955(1993)